NASA CONTRACTOR REPORT

STUDY AND DEVELOPMENT OF TURBOFAN NACELLE MODIFICATIONS TO MINIMIZE FAN-COMPRESSOR NOISE RADIATION

Volume IV - Flightworthy Nacelle Development

Prepared by
THE BOEING COMPANY
Seattle, Wash. 98124
for Langley Research Center

NATIONAL AERONAUTICS AND SPACE ADMINISTRATION • WASHINGTON, D. C. • JANUARY 1971

1. Report No.	2. Government Accession No.	3. Recipient's Catalog No.
NASA CR-1714		

4. Title and Subtitle	5. Report Date
STUDY AND DEVELOPMENT OF TURBOFAN NACELLE MODIFICATIONS TO MINIMIZE FAN-COMPRESSOR NOISE RADIATION. VOLUME IV - FLIGHTWORTHY NACELLE DEVELOPMENT.	January 1971
	6. Performing Organization Code
7. Author(s)	8. Performing Organization Report No.
	10. Work Unit No.
9. Performing Organization Name and Address The Boeing Company Seattle, Washington 98124	11. Contract or Grant No. NAS 1-7129
	13. Type of Report and Period Covered Contractor Report May 1, 1967 to November 1, 1969
12. Sponsoring Agency Name and Address National Aeronautics and Space Administration Washington, D.C. 20546	14. Sponsoring Agency Code

15. Supplementary Notes

16. Abstract A flightworthy configuration of the treated inlet and fan exhaust duct resulted from further development of acoustic, aerodynamic, and structural design of the nacelle concept developed and tested during the boilerplate/prototype phase of the contract. Both the design and manufacturing processes that were developed placed performance goal achievement above minimum weight considerations. The estimated airplane empty weight increase of a weight-oriented production design is 3140 lb. Four nacelles were fabricated and each was subjected to ground calibration testing. Compared to baseline ground test results of an existing 707 airplane nacelle, static takeoff thrust of the flightworthy nacelle was shown to be essentially unchanged, with 2 percent less fuel consumption at cruise. Attainment of the 15-PNdB reduction in perceived noise level set as a program goal for flight operations was indicated. A Boeing 707-320C airplane was modified to accommodate the flightworthy nacelles. A comprehensive flight test program was run on the airplane prior to modification and after modification. These comparison tests provided data showing suppression at approach power of 16 PNdB with a 3PNdB reduction at takeoff power, 6.5 PNdB at cutback power and 330 000 lb gross weight, and 7.5 PNdB at 250 000 lb gross weight. No deviations were indicated in flight operating procedures nor in operational restrictions except for a 200 n. mi. loss in maximum cruise range with international reserves.

17. Key Words (Suggested by Author(s))	18. Distribution Statement
707 airplane Noise, aircraft Flight tests Propulsion Performance	

19. Security Classif. (of this report)	20. Security Classif. (of this page)	21. No. of Pages	22. Price*
Unclassified	Unclassified	190	$3.00

*For sale by the National Technical Information Service, Springfield, Virginia 22151

STUDY AND DEVELOPMENT OF TURBOFAN NACELLE MODIFICATIONS TO MINIMIZE FAN-COMPRESSOR NOISE RADIATION

OVERALL REPORT ORGANIZATION

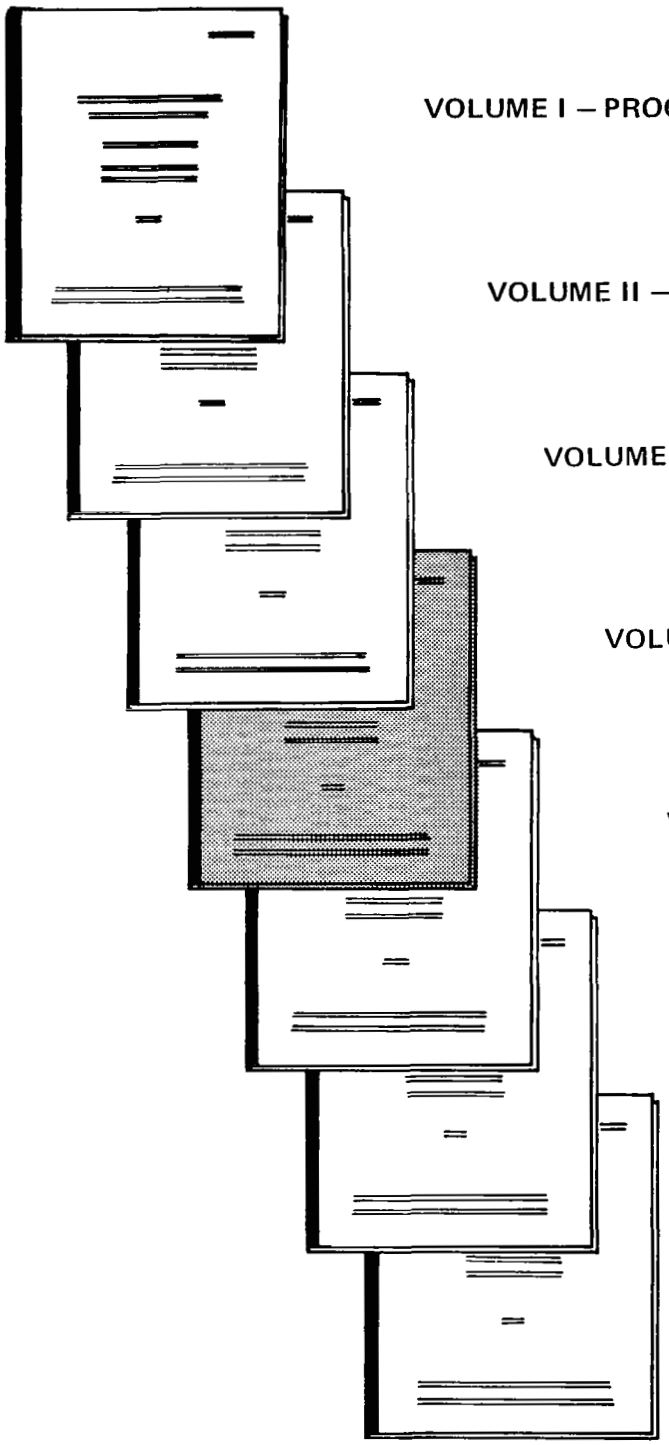

VOLUME I – PROGRAM SUMMARY

VOLUME II – ACOUSTIC LINING DEVELOPMENT

VOLUME III – CONCEPT STUDIES AND GROUND TESTS

VOLUME IV – FLIGHTWORTHY NACELLE DEVELOPMENT

VOLUME V – SONIC INLET DEVELOPMENT

VOLUME VI – ECONOMIC STUDIES

VOLUME VII – SUBJECTIVE EVALUATION TESTS

CONTENTS

TABLES

FIGURES

FIGURES—Continued

FIGURES—Continued

FIGURES—Continued

FIGURES—Continued

FIGURES—Continued

FIGURES—Continued

FIGURES—Continued

FIGURES—Continued

FIGURES—Concluded

STUDY AND DEVELOPMENT OF TURBOFAN NACELLE MODIFICATIONS TO MINIMIZE FAN-COMPRESSOR NOISE RADIATION

VOLUME IV

FLIGHTWORTHY NACELLE DEVELOPMENT

The Boeing Company
Seattle, Washington

SUMMARY

A flight test program has been completed using a Boeing 707-320C airplane equipped with JT3D-7 engines (1) in a baseline existing production configuration and (2) as modified by incorporation of acoustically treated nacelles. Program goals were to determine the comparative acoustic and engine/airplane performance of the two configurations. Acoustic and performance data were acquired during ground runup, takeoff, climbout, power cutback, cruise, landing approach, and steady state flyovers. Results established by the flight program for the treated nacelle configuration were:

- A noise suppression at landing approach power of 15.5 EPNdB 1 n. mi. from threshold.
- A reduction of 3.5 EPNdB 3.5 n. mi. from brake release at takeoff power and 330 000-lb gross weight.
- A reduction of 4.5 EPNdB with cutback power to a 6-percent climb gradient at 330 000-lb gross weight and 6.5 EPNdB at 260 000-lb gross weight.
- An increase of approximately 135 ft in takeoff distance to a 35-ft altitude.
- A reduction in climbout altitude at the 3.5 n. mi. point of approximately 120 ft.
- A 200 n. mi. loss in maximum range due primarily to displaced fuel equivalent to the predicted 3140-lb increase in treated nacelle weight.
- No deviations in flight operating procedures nor in operational restrictions except as they may be affected by range degradation.

Prior to the flight tests, ground tests were performed to calibrate each nacelle by comparing acoustic and propulsion performance to that of a baseline nacelle. These tests indicated that available static takeoff thrust of the treated nacelle was essentially the same as for the baseline nacelle, whereas at the cruise condition the thrust specific fuel consumption was 2 percent less than for the baseline nacelle. The tests also indicated that the goal of 15-PNdB noise suppression under flight approach power conditions would be met.

Development of the acoustically treated flightworthy nacelles for the ground and flight test part of the program required translation of the technology developed during concept studies and boilerplate ground tests into detail designs. These detail designs were drawn to production flight component standards for structural integrity, safety, reliability, anti-icing, and cooling. Simplified prototype construction was used. Considering the experimental nature of the nacelles, the limited time for design and fabrication, and the use of prototype soft tooling, weight was treated as subordinate to achieving acoustic, aerodynamic, and structural performance goals. It was estimated that if this experimental design were converted to a weight-conscious production treated nacelle design, the airplane empty weight with retrofit would increase 3140 lb.

INTRODUCTION

The purpose of this volume is to describe the design development and testing of flightworthy acoustically treated nacelles for the 707-320B/C airplane. The design of these nacelles was based on an evaluation of the program model work and the boilerplate/prototype testing that are presented in volume III. The design, fabrication, and testing of the flightworthy nacelles represent the final phases of the treated nacelle development program. The ground and flight test portion of the program provided data necessary to compare the treated airplane with the existing airplane in the areas of acoustics, propulsion, and airplane performance. These data are presented in this volume of the report.

In addition, a brief description of the nacelle fabrication and the aerodynamic, acoustics, and structural design considerations for both the inlet and duct necessary to provide a flightworthy nacelle are presented. The flightworthy nacelle makes use of polyimide resin fiberglass reinforced honeycomb for structural components as well as for acoustic material in the engine ducts and inlets. Use of the material in this manner represents a new technology. Some of the material maintainability studies that were conducted on the polyimide-fiberglass structure are therefore described. These studies were not designed to provide a nacelle for airline in-service operation, but they did provide a trouble-free test nacelle design.

SYMBOLS

C_D	drag coefficient
C_{gf}	fan gross thrust coefficient
dB	decibel
EPNdB	unit of effective perceived noise level
EPNL	effective perceived noise level, EPNdB
F_g	gross thrust, pounds
F_n	net thrust, pounds
Hz	hertz (cycles/second)
K	Mach number effect parameter
L	length, inches
M	Mach number
N_1	low-pressure compressor rotor speed, rpm
N_2	high-pressure compressor rotor speed, rpm
n. mi.	nautical mile
OASPL	overall sound pressure level, dB re 2×10^{-4} μbar
P	pressure, pounds/inch^2
PNdB	unit of perceived noise level
PNL	perceived noise level, PNdB
PNLM	maximum perceived noise level, PNdB
PNLT	tone-corrected perceived noise level, PNdB
q	dynamic pressure, pounds/inch^2

R	flow resistance, gas constant
rayl (cgs)	unit of acoustic resistance, centimeter-gram-second
SPL	sound pressure level, dB re 2×10^{-4} μbar
st. mi.	statute mile
T	temperature, °F or °R
U	velocity, feet/second
u_s	velocity through porous media, centimeters/second
V	true airspeed, feet/second or knots
V_s	velocity at initial buffet of stall, knots
V_2	aircraft minimum climb velocity, knots
W	gross weight of aircraft, pounds
W_A	inlet or engine airflow, pounds/second
δ	pressure ratio, P/P_o
γ	ratio of specific heats
θ	temperature ratio, T/T_o
ϕ	angle from inlet centerline, degrees
μbar	microbar
Subscripts:	
amb	ambient
F_4	fan duct exit plane
ℓ	lip anti-icing air
rs	ring and strut anti-icing air
S	static

T	total
th	throat
w	model wake
x	distance or location, inches
o	sea level standard
1	inlet entrance station
2	engine entrance station
2.5	fan duct entrance station
7	turbine discharge station

FLIGHT TESTS

The flight test program was run to evaluate the acoustic and operational performance of a 707-320B/C airplane equipped with four acoustically treated nacelles. The performance was evaluated by comparing data obtained with the acoustically treated nacelles installed on the airplane to data obtained with baseline nacelles installed. Tests were performed at Grant County Airport, Moses Lake, Washington, during February through May of 1969.

Test Plan

The flight test program was conducted in two phases. The first phase established a baseline for the program, using the 707-320C airplane equipped with production nacelles. The second phase was conducted after installation of acoustically treated nacelles on the aircraft. Each phase included a ground runup and a series of flight tests at takeoff, climb, approach, cruise, and flyby conditions.

The ground runup tests were conducted to measure engine-nacelle performance and to determine the noise levels around the airplane with one outboard engine operating over the full range of power settings.

Airplane approach conditions were run using a 3° glide slope and maintaining constant thrust settings of 5000 and 6500 lb. Takeoffs were made at airplane gross weights of 330 000 lb and 260 000 lb. Maximum power settings were used, and the climbout was made at

velocities equivalent to V_2 + 10 kn. Tests were also made in which takeoff power was cut back to the power required to maintain a 6-percent climb gradient when the aircraft reached a 700-ft altitude. In these tests the takeoff conditions were simulated by making flybys at low altitude to a point where a normal climb path would be intercepted and then making the climbout at takeoff power until the power cutback altitude was reached. Noise data for level flyby conditions were obtained for thrust settings corresponding to approach, maximum takeoff, and cutback power. The airplane was flown at a 400-ft altitude and at approximately 160 kn for all flyby conditions.

All the acoustic test conditions were run three times, and data were averaged for each condition. An aircraft-tracking radar measured the airplane space position during the acoustic tests. All ground and airplane data recordings were time correlated. The tests were carried out only during the following weather conditions:

- No rain or other precipitation
- Relative humidity not higher than 90 percent or lower than 30 percent
- Airfield winds not above 10 kn at 10 m above the ground
- Ambient temperature below International Standard Atmosphere (I.S.A.) plus 15° C

Weather conditions were monitored using three meteorological stations situated near the acoustic range. The effects of atmospheric conditions on the noise measurement were determined by recording limited acoustic data for the flyby conditions over the Puget Sound area where atmospheric conditions are more stable and similar to a standard day.

Airplane performance and propulsion performance were determined from takeoff data recorded concurrently with acoustic data and during additional tests at cruise conditions. The takeoff performance was calculated using time-correlated runway distances and altitudes obtained from airplane-mounted theodolite cameras and basic airplane and engine data. Airplane cruise drag tests were run at constant values of W/δ (gross weight divided by the ambient to standard pressure ratio) of 0.8, 1.0, and 1.2 x 10^6 for Mach numbers ranging from 0.65 to 0.88. The propulsion performance during cruise conditions was determined at various engine pressure ratios (EPR) from 1.4 to the maximum cruise thrust by varying the EPR of two engines and maintaining the test condition with the other two. Test conditions were at Mach numbers of 0.7 and 0.8 at a 35 000-ft altitude. Static ground tests correlated the propulsion performance to earlier ground calibration tests.

Additional tests were run with the treated nacelles installed to ensure flight safety and to obtain detailed measurements of internal flow in the inlet and fan duct of the number 2 nacelle. Flight safety checks included measurements of flutter characteristics, the nacelle and oil cooling systems' performance and engine operation during maximum sideslip conditions, power-on and power-off stalls, and engine acceleration. The flutter tests were required to (1) evaluate the influence of increased nacelle weight and the attendant shift in center of

gravity on airplane flutter characteristics and (2) extend the initial airplane speed placard from M = 0.7 and 250-kn equivalent airspeed to M = 0.9 and 320-kn equivalent airspeed, and thus enable the programmed performance tests to be conducted. Ground tests of the oil and nacelle cooling systems were required to determine that the systems were safe for flight. In-flight cooling tests were conducted to demonstrate capabilities of the systems under typical flight operational conditions.

Test Configuration

The airplane used in both phases of the flight test program was a long-range, heavy-weight (330 000-lb gross weight) version of the 707 series. A general description of the aircraft is given in figure 1; four Pratt & Whitney (P&WA) JT3D-7 calibrated engines were used.

The airplane contained several minor modifications, including wing tip changes, static electricity discharge probes on each wing, and radar antennas on the upper aft portion of the fuselage that were installed for other tests. Since the configuration was the same for both phases of the test, there would be no measurable effect on the incremental performance between the baseline and treated nacelles.

The airplane was calibrated to obtain accurate airspeed measurements.

Baseline airplane.—The existing 707 nacelles were used as a baseline configuration and were designed to provide minimum weight and cruise drag. The inlets are 36.0 in. long and have a small contraction ratio (highlight-to-throat area) of 1.18. This ratio minimizes cruise drag but requires blow-in doors to provide surge-free engine characteristics during low-speed operation. The inlets were the latest iteration of the basic inlets and used large blow-in doors. A short fan exhaust duct and tightly fitted aft cowl were used to obtain the minimum nacelle cross-section area and thus provide minimum wing-nacelle interference drag (fig. 2).

The primary thrust reverser was replaced with an adapter section to eliminate potential leakage and thus provide consistent results. Existing 707 primary nozzles were used.

Treated airplane.—The acoustically treated nacelles used in the second phase of the test program are shown in figures 3 and 4 and are described in detail in the "Design" and "Fabrication" sections of this report. The treated inlet length was increased to 45 in. to accommodate the two acoustic rings. The lip design used a contraction ratio of 1.25 to provide low-speed operation without the use of blow-in doors. The full-length fan ducts increased the diameter of the nacelles relative to the baseline configuration and thus caused an increased external drag. However, this effect is offset by the elimination of the scrubbing drag caused by the relatively high-velocity fan discharge air blowing over the aft engine cowl of the baseline nacelles. The treated fan duct did not contain a thrust reverser.

The tests with the treated nacelles used the same engines as the baseline tests along with the same primary thrust reverser adapter sections and primary nozzles.

Instrumentation

The basic measurements required to determine aerodynamic and propulsion performance were obtained from instrumentation installed on the aircraft and recorded on the airplane data system. During takeoff performance tests, weather data were also recorded at a ground-based weather station. The acoustic test data were recorded at ground test stations. In addition, engine and airplane data were recorded on the airplane. The ground stations included the acoustic microphone range, a tracking radar for airplane space position data, and the weather stations. The data from the various recording stations were time correlated using calibrated time code generators.

Baseline airplane.—The test airplane contained calibrated instrumentation to measure airspeed, altitude, air temperatures, and longitudinal and normal accelerations. Theodolite cameras accurately determined the space position of the airplane during takeoff performance tests. Measurements of engine parameters, including fuel flow, compressor speeds, nozzle pressure ratios, and temperature, were recorded for all test conditions. The airplane data were recorded on magnetic tape and processed on the Boeing flight test computer using existing computer programs.

Treated airplane.—When the treated nacelles were flight tested, instrumentation was included to evaluate the internal flow in the number 2 nacelle. This instrumentation was the same as that used during ground calibration tests. The inlet performance was measured using the total pressure rakes, static pressure taps, and boundary layer rakes. The fan duct performance was determined using only the static pressure taps located on the inside wall of the duct. Nacelle internal cooling and oil cooling systems were evaluated from temperature measurements.

Acoustic test range.—Ground and flight tests and test support for the acoustic measurements are discussed below.

Ground tests: The static ground test range layout is shown in figure 5. The microphones were in a horizontal plane at the level of the engine centerline. Acoustic signals from the microphones were recorded on multichannel tape recorders for laboratory analysis. These tests differed from the previous ground calibration tests by being conducted over a concrete ground surface using an airplane-mounted engine and flight nacelle.

Flight tests: Acoustic flight test measurements were conducted over a test range of 20 microphones arrayed around the main runway as shown in figure 6. The microphones were mounted 5 ft above local ground level. Nine microphones connected to a multichannel tape recorder in an instrumentation van near the runway threshold were

used to record noise levels during landing approach tests. The remaining microphones were connected to a second instrumentation van at the other end of the runway and were used for takeoff and level flyover tests. At the critical microphone positions of 1 n. mi. from threshold and 3.5 n. mi. from brake release, for landings and takeoffs, respectively, dual microphones were used to ensure noise signal recording.

Test support: To complement acoustic measurements and provide data necessary to correct results to standard conditions, test support was provided by airplane tracking radar and meteorological test instrumentation.

The radar, which was stationed approximately 4760 ft from the brake release point and 570 ft to one side of the runway centerline, recorded the airplane's range, altitude, and sideline position.

The main meteorological station situated near the radar van recorded continually the following weather data: wind velocity and direction 10 m above ground; temperature, pressure, and humidity 1.5 m above ground; and temperature lapse rate between ground level and 10 m above ground. Instrumented weather balloons and an instrumented light airplane recorded weather data profiles up to altitudes of 3000 ft at regular intervals during the acoustic test series. Two automatic, remote weather stations with 3-m towers provided continuous records of wind and temperature at each end of the runway.

Data analysis procedures: Moses Lake static ground test data were analyzed into preferred 1/3-octave bandwidths, with the analysis system providing the average SPL over 6 to 8 sec of data. For each engine power setting, the resulting sets of data were arithmetically averaged. In addition, narrowband analysis was used to resolve spectral components, and SPL versus time analyses were used to study data variability. Flight test data were reduced in 1/3-octave bandwidths with a 1/2-sec integration time. The resultant 1/3-octave band time histories were analyzed using a Boeing Company computer program which calculated time histories of perceived noise levels (PNL) and effective perceived noise levels (EPNL). The computer program is capable of correcting the results for change of airplane altitude, forward velocity, and sideline position. Results are analyzed for measured weather conditions as well as for corrected standard-day conditions of 70-percent relative humidity and 59° F temperature, using the method described in ARP 866 (ref. 1).

During the preliminary analysis of baseline airplane data, it was discovered that due to the limited dynamic range of the recording instrumentation, the high-frequency end of the noise spectrum was quite often masked by the instrument background noise. Under these circumstances, corrections for changes in atmospheric absorption of sound could not be applied since the true acoustic levels at the high frequencies were unknown. Atmospheric corrections applied automatically to data masked by instrument noise caused the time histories to show an increase rather than a decrease in perceived noise with airplane distance. Scrutiny of the results showed that the largest contributors to this overcorrection were the 6.3-, 8-, and 10-kHz 1/3-octave bands, which were expected to have the lowest noise levels in the

spectrum. Consequently, the computer program was modified and atmospheric absorption corrections were applied to all but the last three 1/3-octave bands. This procedure prevented the anomalous situation where PNL increases with airplane distance, and enabled EPNL to be calculated with a reasonable degree of accuracy. Improvement of the dynamic range of the recording and analyses equipment would permit the use of standard analyses techniques for future tests.

Although all flight test conditions were repeated three times, it was found that the climbout profile varied sufficiently due to airplane weight changes during the takeoff phase of the program so that direct averaging of results was not desirable.

Test Results

Acoustics.—A summary of the noise levels and noise reductions achieved during takeoff and landing approach conditions is presented in table I.

Landing approach: The results for landing approach tests, as measured and corrected to standard weather conditions, are shown in figures 7 through 14. Average PNL time histories for an altitude of 370 ft, corresponding to 1 n. mi. from threshold, are shown in figure 15. The maximum perceived noise spectra for the approach condition are shown in figure 16, indicating a noise reduction of 16 PNdB, which exceeds the program goal of 15-PNdB noise reduction during landing approach. The treated airplane spectrum shows a faint, yet audible, fundamental fan tone that is less pronounced than that obtained from the ground static tests.

Takeoff: The results for conventional takeoffs and takeoffs with power cutback at the various power settings, both as measured and corrected to standard weather conditions, are shown in figures 17 through 28. Assuming an airplane altitude of 1000 ft over the 3.5 n. mi. microphone, a pair of average PNL time histories is shown in figure 29. The apparently higher PNL's for the treated airplane as it leaves the observer are attributed to the change in primary jet noise directivity. A noise reduction of approximately 3.5 EPNdB is shown. By examining a pair of measured maximum noise spectra in figures 30 and 31, the effect of correcting results to standard weather conditions is aptly demonstrated. For example, in figure 30 the uncorrected spectrum shows a noise reduction of 2.5 PNdB. In figure 31, because of the strong tonal content, the corrections for humidity and temperature influence the baseline PNL more than the treated PNL, and result in a noise reduction of about 4 PNdB.

For the cutback tests, power settings of 12 400- and 9200-lb thrust per engine were used to approximate two conditions that correspond to airplane gross weights of 330 000 and 260 000 lb, respectively. For these conditions, the test data showed noise reductions of 4.5 and 6.5 EPNdB if the power cutback was initiated just prior to reaching the 3.5 n. mi. microphone station.

Sideline noise measurements were taken 1500 ft to one side of the runway centerline for various airplane altitudes during takeoff. It was found that sideline noise was reduced by approximately 4.5 EPNdB and, on the average, the maximum noise occurred when the airplane was at an altitude of 1000 ft with full takeoff power. The actual variations of sideline noise with airplane altitude for as-measured and corrected to standard weather conditions are shown in figures 32 through 35. The increase in data scatter shown by the corrected results is mainly due to the corrections being applied to ground-affected measurements.

Ground static tests: The average ground test values of PNL's measured for three runs at the same power setting at each microphone station are shown in figure 36. Examples for two engine conditions of N_1 = 4450 and 6200 rpm, corresponding to landing and takeoff power settings, respectively, are shown. A significant change in the directivity of primary jet noise was observed between the baseline and treated engines at the takeoff power settings. The noise from the coplanar jet of the treated nacelle peaked at an angle closer to the jet axis. Figure 36 shows that substantial perceived noise reduction has been achieved at the landing approach power setting at all positions around the airplane. For the takeoff power setting, however, where the primary jet noise predominates, perceived noise reductions have been achieved only at angles forward of 130° from the inlet.

A detailed analysis of the static test results is shown in figures 37 through 40 where the maximum noise spectra are averaged over three runs for the inlet and fan exhaust duct at landing and takeoff power settings. The effectiveness of the acoustic linings can be determined from an analysis of the treated nacelle spectra over the fan noise dominated range of frequencies. In the case of maximum inlet noise at landing power setting, a noise reduction of 13.5-PNdB has been achieved due to the attenuation provided by the acoustic lining over the range of frequencies between 1 and 10 kHz (fig. 37). The apparent reduction in jet noise below 1 kHz is attributed to the change in directivity of the primary jet noise for the treated configuration. It can be seen that due to the semibroadband attenuation characteristics of the inlet lining, not only has the fundamental tone been reduced the desired amount, but the broadband noise has also been reduced to such a low level that the fundamental tone is still present. The maximum fan exhaust noise at landing power setting has been reduced by approximately 14.5 PNdB, with the lining attenuating the fan tones sufficiently so they are not discernible above the broadband noise (fig. 38).

At takeoff power settings, the maximum inlet noise was reduced by approximately 9.5 PNdB as shown in figure 39. Due to the higher jet-broadband noise levels at maximum power and possible near-sonic throat effect in the inlet, the fan tones have been attenuated to the point where they cannot be heard. Similarly, the maximum fan duct noise in figure 40 has been reduced by approximately 9.5 PNdB and the fan tones have been eliminated. Turbine noise at 8 kHz, which radiates from the primary jet exhaust, was still present. These results are similar to those obtained during the ground calibration tests.

The changeover from a JT3D-3B engine, used for boilerplate/prototype evaluations, to JT3D-7 engines for ground calibration and flight test evaluations required that a comparison

of baseline noise for the two engines be made. Unpublished data from both the engine manufacturer and Boeing flight tests of JT3D-3B and JT3D-7 equipped airplanes indicated the noise levels to be the same for both engines (fig. 41). A comparison of static ground test data indicated the two engines had the same noise levels at maximum thrust, but at approach thrust the JT3D-7 engine noise level was 2 to 3 dB higher. The difference in noise levels for ground test engines is considered a result of the particular engines used and not generally representative of the two engine types.

Level flyby tests: The results of the level flyby tests, as measured and corrected to standard weather conditions, are shown in figures 42 and 43 for a range of power settings corresponding to the previously described takeoff and landing tests. It was found that the absolute noise levels measured, as well as the noise reductions obtained with the treated configuration, were in good agreement with the above takeoff and landing results at the same altitude.

Additional level flyover tests of the baseline and treated airplanes were conducted over the open waters of Puget Sound to provide acoustic data taken at near-standard weather conditions. Final analysis of the treated airplane test data, however, indicated that due to some untraceable change in record level or microphone response, the results are lower in noise level than expected by approximately 2 to 6 dB. Since there is no way to correct these errors without rerunning the flight tests, the treated airplane results obtained over Puget Sound will not be considered in this report.

Analyzing the test results for the existing airplane only, a comparison was made between pairs of tests conducted under different weather conditions to establish the need for normalizing test data to a standard weather day and to show that the standardization method used produced acceptable results. Figure 44 shows differences of approximately 4 PNdB and 4 EPNdB between the test results. The lower noise levels recorded at Moses Lake are attributed to the very low relative humidity conditions causing high atmospheric absorption of the noise before it reached the microphone. Standardizing both sets of test data to 70-percent relative humidity and 59°F, it can be seen in figure 45 that the Puget Sound noise levels are raised by approximately 0.5 dB due to the near-standard test conditions of 76-percent relative humidity and 48° F. The Moses Lake data, however, have been raised in level by approximately 2 dB as a result of the applied weather corrections.

Although a difference of up to 2 dB is still shown between the standardized results, it can be seen that many of the data points overlap over the range of data scatter. It is thought that a more accurate knowledge of the weather conditions existing between the noise source and measuring station would reduce the error even further. The need for weather corrections to be applied to acoustic data taken under nonstandard atmospheric conditions is clearly indicated.

Measured noise reduction: The noise curves based on experimental results and presented in the foregoing sections have been summarized in appropriate groups for standard weather conditions of 70-percent relative humidity and 59° F in figures 46 through 49. Ground level noise profiles for maximum gross weight takeoff, takeoff with cutback, and landing approach

were predicted using peak noise spectra recorded during the 400-ft-level flyby tests. The results for both baseline and treated airplanes are shown in figures 50 through 52. Quite good agreement was found between these predicted profiles and values measured in the field at various microphone stations. Finally, a comparison was made between the proposed FAA noise certification levels for new airplanes (ref. 2) and the EPNL's achieved in this test series (fig. 53). For the takeoff condition, the FAA limit is approached to within 5 EPNdB for the maximum gross weight takeoff with power cutback. For landing approach, the treated airplane is approximately 2 EPNdB below the proposed limit, while the maximum sideline noise for the treated airplane is 0.5 EPNdB below. The test series, however, was not conducted in strict accordance with the procedures proposed by the FAA, so the above comparison can only be viewed in general terms.

Performance.—For a 330 000-lb gross weight airplane, the addition of the treated nacelles increased takeoff distance to a 35-ft height by approximately 135 ft (1.6 percent) and reduced airplane altitude by approximately 120 ft at a point 3.5 n. mi. from brake release. Payload range at long-range cruise conditions is approximately 200 n. mi. less for the treated airplane. A production version of the treated nacelle is estimated to increase the airplane operating empty weight by 3140 lb. The resultant displacement of available fuel contributes the major part of the loss of capacity payload range. The effects of nacelle acoustical treatment on airplane and propulsion system performance are evaluated in the following sections.

Propulsion: Engine inlet, fan duct, and overall nacelle modification effects on engine performance are presented separately.

- Treated inlet—The treated inlet performance during takeoff is shown in figure 54. The total pressure recovery is 97.6 percent at zero runway speed and increases asymptotically to 98.2 percent as the forward speed increases.

  The total pressure recovery of the treated inlet at cruise conditions of 35 000-ft altitude and M = 0.8 is shown in figure 55. The inlet total pressure recoveries are 0.988 and 0.979 at inlet airflows of 439 and 489 lb/sec, respectively. The inlet total pressure recovery is 0.987 at a representative cruise inlet airflow of 453 lb/sec.

  The inlet performance was determined from the total pressure measurements in the ring and strut wakes and cowl wall boundary layer in front of the fan face, as shown in figures 56 and 57. The ring wakes appear symmetrical and the cowl wall boundary layer thickness is about 1.2 in. Inlet losses attributed to each inlet component were determined, as shown in figure 58. At reference cruise airflow of 453 lb/sec, the breakdown of inlet losses is presented in table II. The inlet loss due to the rings and struts amounts to 69 percent of the total inlet loss (loss in inlet pressure recovery is 0.009).

Flight and ground test inlet loss measurements are in close agreement, except for the cowl wall. Improved inlet flow conditions during flight results in a lower cowl wall loss. This influence is also evident in the reduced thickness of the cowl wall boundary layer during flight operations.

The static pressures on the cowl wall and centerbody are correlated in figure 59. The difference between the measured and calculated static pressure correlation parameters for the cowl wall is due to the boundary layer development on the cowl wall. For the centerbody, the differences in correlation parameters are believed to be partly due to upflow in front of the airplane wing at cruise.

- Treated duct–Figure 60 shows that the static pressures follow the expected trend throughout the flight conditions. The static pressure ratio (static pressure to duct inlet total pressure [$P_S/P_{T2.5}$]) at all duct stations decreases as the fan duct pressure ratio increases to a value of approximately 2.0. At this duct pressure ratio, the nozzle is choked (exit velocity becomes sonic), and the static pressure ratios are constant up to the maximum duct pressure ratios tested. The static pressures measured up to takeoff conditions agree with the static test-stand data, and the data at cruise conditions are typical of data obtained during model tests.

- Treated nacelle–For flight test conditions, engine thrust was calculated from the engine primary and fan duct thrust coefficients, measured fan and turbine exit pressure, turbine exit temperature, and nozzle exit area. Calculation of the thrust is necessary because equipment to measure thrust directly is not provided on the airplane. The thrust coefficients were determined from full-scale static calibrations on a test stand, where thrust is measured directly, and from model test data. The model test data were used to extrapolate the fan duct thrust coefficients to flight test conditions that are beyond the nozzle pressure ratios obtained at static conditions. As discussed in volume III, the fan duct thrust coefficients for a short baseline duct include the effect of scrubbing drag produced by the high-velocity fan discharge over the aft part of the baseline nacelle. The resulting values of calculated thrust therefore include the scrubbing drag as a thrust loss.

The correlation between measured static thrust on the ground test rig and thrust calculated with the nacelles installed on the airplane is shown in figures 61 and 62. The static takeoff thrust (engine pressure ratio of 1.848) with the baseline nacelles was calculated to be 1.5 percent greater than that measured during the static calibration (fig. 61), while the calculated treated nacelle static thrust agreed with the calibration data (fig. 62). All four treated nacelles used in the flight test program were calibrated on the static test stand. Since the treated nacelles were identical on the test stand and on the airplane, errors in measurement of the nozzle areas and in determination of the thrust coefficient tend to compensate for each other and provide good correlation between measured and calculated thrust values. However, actual baseline flight test nacelles were not available for

calibration, and fan nozzle area and pressure data measured with the fan duct used to define the performance baseline during the static calibration did not agree with previous data. Therefore, it was decided to use previously determined fan duct thrust coefficients to calculate in-flight thrust of the baseline airplane. Since hardware for the static calibration test was different from that of the flight test, errors in the measurement of nozzle areas and the differences in individual nacelle thrust coefficients will compound the error in calculated thrust. Considering this error and applying it to the measurement accuracy of engine parameters, it is estimated the calculated thrust with the baseline nacelles on the airplane is accurate to ±2.5 percent. While small errors in nozzle areas and nozzle pressures may cause a significant error in calculated thrust, the accuracy of the directly measured thrust on the ground test rig would not be affected. For this reason, the relative performance of the treated nacelle at static conditions can best be judged from ground calibration test data.

During takeoff, thrust varies as the inlet performance changes with forward velocity (see fig. 54). Because of the small contraction ratio used with the baseline nacelle, it was expected that the pressure recovery would improve more rapidly than the treated nacelle. Based upon the ground test calibrations, the baseline nacelle was expected to provide about 1.5 percent more thrust than the treated nacelle at 100-kn forward velocity. This results in a degradation in takeoff performance with the treated nacelles, as indicated in the airplane performance section of this report.

At cruise conditions, the calculated thrust values are even less accurate due to the extrapolation of the thrust coefficient with model data. The nacelle performance at cruise, including changes in thrust and external drag, is best determined from the fuel mileage comparisons, presented in the following section on airplane performance.

The nacelle internal performance at cruise was estimated from the static ground tests using measured inlet recoveries and thrust coefficients. At a constant fan pressure ratio, the estimated fan thrust is 3.2 percent higher for the treated duct than for the baseline duct (this calculation eliminates the ground rig to airplane pressure measurement difference). At M = 0.8 and 17 000-lb corrected net thrust, the treated inlet recovery is 1.1 percent less than that of the baseline inlet. Using these values, the cruise thrust specific fuel consumption (TSFC) with the treated nacelles was estimated to be 2.0 percent less than that with the baseline nacelles. From in-flight measurements at M = 0.8 and 17 000-lb corrected net thrust, the specific fuel consumption (SFC) with the treated nacelles was determined to be 0.9 percent less than with the baseline nacelle (fig. 63). These data are subject to the airplane thrust calculation accuracy and to the ±0.5-percent accuracy of measured fuel flow.

Airplane: Airplane takeoff, climbout, cruise, and payload/range test results are given next.

- Takeoff—A total of 15 measured takeoffs were available for analysis: seven for the baseline configuration and eight for the treated nacelle configuration. The uncorrected data are shown for each configuration in figures 64 and 65. These data were then corrected to standard conditions of ambient temperature, zero wind velocity, and takeoff technique. Temperature and wind corrections were obtained from operational data available in the flight manual for the particular airplane model. The resultant corrected takeoff performance is shown in figures 66 and 67. These data indicate that with the treated nacelles installed, total takeoff distance to a 35-ft altitude increases approximately 135 ft. Under conditions where available takeoff field length determines maximum takeoff weight, this degradation of takeoff performance would correspond to an airplane weight reduction of approximately 2500 lb.

- Climbout—Most of the takeoffs were followed by a measured climbout. Airplane position data were obtained from airborne theodolite data (normally used to establish takeoff distance to a 35-ft height), airborne instrumentation, and ground radar data. Airplane climb gradients achieved in the gear-up, takeoff flap configuration were deduced from these data. These gradient data were then corrected to standard atmospheric conditions and correct power settings. The effects of wind shear velocities during climbout were also considered. The effects of incidental test airspeed discrepancies were determined to be negligible and were consequently ignored. Final corrected climb gradient data are presented in figure 68. The corrected climb gradient performance was combined with the corresponding takeoff performance to produce the climbout performance under standard atmospheric and technique conditions shown in figure 69. At 3.5 n. mi. from brake release, the treated nacelle configuration is 120 ft lower in altitude than the baseline configuration for the 330 000-lb gross weight condition.

- Cruise—A total of 41 cruise conditions were investigated: 17 for the baseline configuration and 24 for the treated nacelle configuration. Three discrete values of W/δ—0.8, 1.0, and 1.2 x 10^6—were tested to provide a complete range of operational cruise conditions. The results for normalized fuel mileage are summarized in figures 70 and 71. These results show a loss in fuel mileage due to the nacelle modifications of 0.7 to 2.1 percent over the representative range of Mach numbers 0.80 to 0.83.

  Drag for the cruise configuration was deduced from the installed gross thrust values, with the latter estimated from flight test measurements discussed earlier in this volume. The airplane drag thus deduced is presented in figure 72. The nacelle modifications appear to increase cruise drag at M = 0.8 from 1.55 percent at W/δ = 1.2 x 10^6 to 3.45 x 10^6 percent at W/δ=0.8 x 10^6. It should be noted that this estimate of drag can only be as accurate as the prediction of in-flight thrust.

- Payload/range—The measured fuel mileage values of figure 70 have been used to calculate the effect of nacelle modifications on payload/range. This estimate

assumes the current maximum gross takeoff weight of 327 000 lb and an estimated basic operating weight increment of 3140 lb due to the introduction of a production version (including thrust reversers) of the nacelle modifications. For the purposes of this estimate, all fuel other than that used during the cruise has been assumed to increase by 1.0 percent due to the nacelle modifications.

Figures 73 through 76 show the following range losses due to the nacelle modifications when the airplane is carrying the space-limited payload of 30 545 lb (typically 30 first- and 119 coach-class seats):

Fuel reserves	Cruise technique	Loss of range, n. mi.
Domestic	Maximum range	200
	Minimum cost	225
International	Maximum range	200
	Minimum cost	225

Maximum allowable payload is not affected by the increase in operating empty weight which results from the nacelle modifications. Results of a structural evaluation showed that because of the distribution of the extra weight of the nacelles across the wing span, a corresponding increase in maximum zero fuel weight is permissible.

Structural-mechanical.—The results of preflight and flight tests for the structural and mechanical aspects of the treated nacelle and the airplane as a whole are discussed in the following sections.

Flutter: Airplane flutter tests were run with a takeoff gross weight of 292 600 lb and a flight termination gross weight of 260 000 lb at altitudes of 24 000 to 35 000 ft. All flutter response was completely satisfactory and the airplane was cleared for the full flight program.

Nacelle cooling: Preflight ground test on the airplane indicated satisfactory operation of the nacelle cooling system and alternator constant speed drive (CSD) and turbocompressor (T/C) drive oil cooling systems. The maximum temperatures for all engine components monitored, corrected to a standard plus 41° F day, remained below the maximum allowable limit (fig. 77). Results showed close correlation with ground calibration tests. Nacelle cavity ambient temperatures and wrap cowl inner wall temperatures were satisfactory and about 50° F lower than predicted. Based on the above results, the cooling systems were cleared for flight operations.

Satisfactory performance under typical flight conditions of the nacelle cooling system, as well as the alternator constant speed and turbocompressor drive cooling systems, was demonstrated by the test results. All component temperatures corrected to a standard plus 41° F day were below the maximum allowable limit (fig. 77). Maximum flight temperatures, occurring after cutback from takeoff power to maximum continuous thrust climb, were

the respective flow patterns, it was concluded that a maximum 3° change in angle would exist at the leading edge of the inner ring and that there would be no appreciable angle difference at the outer ring. The leading- and trailing-edge contours of the rings are based on NACA 64 series airfoil sections and the strut contours are based on NACA 0012 airfoil sections. The basic contour for the external lines was selected as an NACA 1 series with a length of 60 in. and a maximum height of 6.40 in. However, because of the noncircular shape of the nacelle exterior and the 3.5° droop of the inlet, only the horizontal profile can comply exactly with this requirement. The remainder of the contour was faired as necessary to account for the diameter variations. The estimated performance of the treated inlet, based on one-dimensional flow analysis, indicated 1.2 percent less pressure recovery at cruise than for the baseline inlet.

Structural-mechanical.—The external cowl structure is of conventional aluminum semimonocoque construction. The internal acoustic treatment is of frame-mounted, load-carrying polyimide resin-reinforced fiberglass sandwich panel construction. (Refer to fig. 79 for the general configuration.)

Design criteria: The basic criteria used in the inlet design were:

- Conservative structural design based on least-cost tooling and fabrication while meeting flight load criteria without the need for substantiation by structural test
- Engine attachment structural design loads, within Pratt & Whitney allowables
- Acoustic ring and strut design based on combined loading including engine surge, aerodynamic drag, and thermal expansion due to anti-icing
- Weight control subservient to meeting performance, least-cost tooling, and fabrication objectives
- Positive retention of all components subject to engine ingestion
- All normal engine environment contaminants with exposure to -65° F and to a 42 000-ft altitude
- Anti-icing under continuous maximum icing conditions while maintaining engine power required for aircraft holding operation
- Positive water drainage from each of the acoustic treatment panels
- A service life goal of 1000 hr of combined ground and flight operation

Inlet mounting adapter ring: The inlet is structurally attached to and supported by the engine at the forward fan face by means of a structural adapter mounting ring. This aluminum ring provides the required 3.5° inlet droop with respect to the engine centerline.

The concept of providing for inlet droop in a separate ring greatly simplifies tooling since it permits all interior surfaces of the inlet from highlight to the adapter ring to be surfaces of revolution.

Outer cowl assembly: The outer cowl assembly of the inlet is an aluminum semi-monocoque structure extending forward from the inlet mounting adapter ring. The external skin, which contains assembly access doors, is supported by an internal structure consisting of two main circumferential frames joined by eight longerons. The cowl lip structure is attached to the forward frame while the aft frame provides the means of attachment to the inlet mounting adapter ring. Secondary stub longerons and intermediate circumferential stiffener intercostals complete the outer cowl structure. Cowl lip anti-icing plumbing is contained within the structure.

Acoustic treatment assembly: The inner and outer rings and the cowl wall acoustic panel are joined by the eight forward and eight aft struts into a subassembly. A circumscribing structural ring, attached to the outer ends of the forward struts by means of pin-ended links, completes the subassembly, herein after defined as the acoustic treatment assembly.

The acoustic treatment assembly is inserted into the aft open end of the outer cowl assembly. Joining of these two major subassemblies is by means of bolted attachments through abutting circumferential rings at the forward strut azimuth locations.

The cowl wall acoustic panel is a circumferential ring consisting of four acoustic sandwich panel ring segments with longitudinal joints at four of the strut azimuth locations. The forward edge of the cowl wall acoustic panel is supported by the circumscribing structural ring of the acoustic treatment assembly. The aft edge of this panel is linked to the trailing edges of the inner and outer rings by means of the eight aft struts, and is supported by the outer cowl structure. The acoustic treatment is of typical polyimide single sandwich, using 3/8-in. hexcell, all-polyimide-fiberglass core of 500-psi shear strength (room temperature).

Water accumulation in the core is prevented by cutting circumferential grooves in the core surface that fays on the nonporous skin. The resulting notch in the cell wall (approximately 1/8 by 1/8 in.) provides a linked cell path to a common collection/drainage groove.

The four-ply, 11-rayl (cgs) polyimide acoustic skin, a six-ply nonporous polyimide outer skin, and solid edge members complete the sandwich construction. Aluminum sheet is used at the edges and joints of the panels to protect edges and permit attachment.

The forward struts are of stainless steel and consist of a machined spar/trailing-edge member and a formed sheet leading-edge cap. These are joined by riveting. The hollow leading edge provides space for ring and strut anti-icing plumbing. The machined strut spar includes fittings for attachment of inner and outer ring leading edges. The aft strut consists

of stainless steel structural links joining the inner and outer rings and the cowl wall acoustic panel by means of pin-connected joints.

Both rings are of similar construction. The ring leading edge is of stainless steel and consists of eight segments structurally joined by a connection through the forward strut. Ring trailing edges are of aluminum sheet construction. Ring acoustic treatment is riveted to the ring leading and trailing edges through a solid laminate edge member. The ring acoustic sandwich panel is similar in construction to that described for the cowl wall acoustic panel except that it consists of two single sandwiches sharing a common non-porous septum.

Centerbody: An existing 707 inlet centerbody design was modified to provide a recessed skin surface in which to inset acoustic treatment panels. The acoustic treatment is typical single sandwich construction provided as two identical half panels. In all other respects these panels are similar to those of the outer cowl wall.

Anti-icing system.—The treated inlet is equipped with thermal anti-icing provisions to prove the feasibility of meeting the requirement for an economically viable design. Additionally, anti-icing provides the necessary safety to flight test operations without weather-imposed test schedule delays. The inlet design includes the following thermal anti-icing subsystems.

Cowl lip anti-icing is essentially identical to that of the baseline airplane. A mixture of 16th-stage engine bleed and ambient air is ducted to a spray ring at the cowl leading edge and exhausted overboard through an exit on the bottom of the cowl.

Centerbody anti-icing is also very similar to that of the baseline airplane. Exhaust air from the engine inlet guide vane anti-icing system is ducted to the inner skin surface of the centerbody. The anti-icing air is exhausted at the aft end of the centerbody into the engine inlet.

The leading edges of the acoustically treated rings and their eight forward support struts are anti-iced by direct 16th-stage engine bleed air. The air is supplied to the inner surfaces being anti-iced by means of spray tubes and is exhausted via surface slots into the inlet airstream (fig. 81). The air supply system is diagrammed in figure 82. In addition to the system shutoff valve, a thermostatically controlled flow-limiting valve is used to minimize engine performance losses yet meet anti-icing airflow requirements. Flow restriction increases to a maximum at approximately 650° F. The ice-protection system airflow requirement is based on the following criteria: evaporating water impinging on the leading edges at 15 000-ft altitude, Mach = 0.4, and 0° F ambient temperature. Cloud liquid water content is taken to be 35 grams per cubic meter, with a water droplet mean diameter of 15 microns. The resulting air bleed requirement at this condition for the rings and struts is about 0.8 lb/sec, which provides the capability to handle all conditions within the continuous maximum-icing envelope as set forth in the Civil Aeronautics Manual. The total nacelle anti-icing air bleed requirement, at the above condition, is approximately 1.5 lb/sec.

Treated Fan Duct

The boilerplate duct tests, discussed in volume III of this report, proved the adequacy of the basic design to meet the overall requirements of the program. However, in the detail design of the flightworthy ducts, a number of changes from the boilerplate design were found to be required to make the ducts suitable for flight testing.

Acoustic.—In volume III it was shown that the boilerplate fan duct lining configuration met the acoustic design requirements. However, subsequent evaluation of this double-layer lining configuration for use in the flightworthy nacelle indicated that it was difficult to maintain the required porosity in the inner acoustic laminate. The variation in the distribution of adhesive bond lines, with core bonding on both sides of the porous inner laminate, results in unacceptable variation in porosity of the laminate. Consequently, single-layer lining designs were considered and evaluated in the flow duct facility. It was found that the acoustic performance of single-layer linings of different core depths facing each other was only slightly inferior to that of the double-layer boilerplate design. Hence, the acoustic treatment selected for the flightworthy fan duct consisted of single-layer linings with 3/8-in. honeycomb core on all treated walls.

Total area of effective acoustic treatment is 267 ft^2, distributed as follows:

Wrap cowl	216 ft^2
Nozzle	51 ft^2

The design flow resistances and core depths are shown in figure 83 and are applicable to all walls and splitters within station zones shown.

Aerodynamic.—The design of the internal contours of the flightworthy ducts was selected to be the same as that of the boilerplate duct except for minor modifications related to the change in thickness of the acoustic material and the selected external contours. In addition, the straight-line segments in the aft section and the abrupt turns at the nozzle exit (used to facilitate the boilerplate fabrication) were changed to smooth faired contours. The extension of the fan duct inner wall, aft of the primary nozzle exit plane, was modified to form a slightly larger diameter and shorter sleeve around the primary discharge. This modification was made to ensure adequate cooling airflow between the engine and fan duct.

The fan duct external contour was selected tc form a boattail radius of curvature equal to six times the maximum diameter of the nacelle and tangent at the maximum diameter.

Structural.—The fan exhaust duct configuration, consisting of four basic components (fig. 84), is similar in design to the boilerplate/prototype configuration reported in volume III. Mounting support for the bifurcation duct is at the engine fan air discharge flange as is

standard practice. All other duct components are supported from the nacelle strut. Metal reinforcement of the strut structure was added at the duct attachment points to accommodate duct support design loads. Neither primary nor fan thrust reversers are included in the design.

Design criteria: All parts were designed for a service life of 1000 engine hours of combined ground and flight testing. In consideration of the experimental nature of the ducts and the limited time for design and fabrication, weight was treated as subordinate to acoustic, aerodynamic, and structural performance goals.

The fundamental environmental criteria used in design of the duct were:

- Flight structural design loads—consistent with production 707-320B/C airplane
- Engine attachment structural design loads—within Pratt & Whitney allowables
- Design ultimate differential pressure loading—40 psi on outer wall and 36 psi on inner wall
- Altitude—sea level to 42 000 ft
- Design temperatures—ambient side, -65° to +160° F; duct internal, -65° to +228° F; engine side, -65° to +400° F (wrap cowl duct) and to +900° F (nozzle duct)
- Relative humidity—100-percent maximum with freezing condensation
- Atmospheric impurities—blowing sand, dust, salt-laden air, and engine exhaust ingestion
- Engine impurities—fuel, lube oil, and hydraulic oil
- Duct leakage—5 lb/min at maximum applied pressure differential

Bifurcation duct: To conserve tooling and fabrication costs, the compound curvature walls and splitters of the bifurcation ducts are constructed of high-temperature (350° F) preimpregnated epoxy resin laminated fiberglass as bonded integral structure. The tension-tie function between inner and outer walls is provided by through-bolts contained within the splitters. The aft flange of the bifurcation section interfaces with the forward edge of the wrap cowl. A pressure-actuated seal is provided at this interface; seals are also provided at the splitters. The forward flange provides the connection interface with the engine fan case rear flange.

Wrap cowl duct: The wrap cowl walls and splitters are completely constructed of polyimide-fiberglass sandwich honeycomb that is designed to meet both acoustic and structural requirements. Polyimide-fiberglass was selected because of its good acoustic

characteristics, including the acoustic requirement for close-tolerance control of porosity and variation in porosity with length that can be achieved in this material, and the fact that the material offers good structural properties, thus obviating the need for a separate duct structure. (See vol. II for further details regarding selection.)

Construction details of the wrap cowl as well as mechanical connections of splitters and wall panels with through-bolts are shown in figures 85 through 88. The type of splitter joint selected approximates a pin connection in that splitter deflection is accomplished without large moment increase. Preloading of splitter bolts, which ensures minimum joint separation with duct pressure increase, is reacted through the bolt sleeves to prevent damage to the polyimide structure. This design also allows disassembly for repair or replacement of polyimide walls or splitters if necessary.

Outer wall thickness was determined by an acoustic cell depth requirement of 0.75 in. (see fig. 83) plus 0.06 in. of nonporous laminate outer skin. The total wall thickness of slightly less than 1 in. was also adequate to carry the 40-psi ultimate design pressure loading, but it required that the porous acoustic laminate be at least five plies thick to resist the resultant 1200 lb/in. of width beam bending loading (see fig. 59, vol. II). The wrap cowl inner wall required an acoustic liner depth of only 0.30 in. (see fig. 83). This was structurally insufficient and necessitated building the wall thickness to a total of 0.70 in., which was accomplished by adding a second core and nonporous laminate structure (see fig. 86). To provide structural capability with the wall thicknesses selected, end fixity of the side cowl was required; therefore, reinforcement frames around both forward and aft ends of the wrap cowl were provided. The duct was supported from the engine strut by mechanical fasteners and was removable for engine access. In a production version of this design, the wrap cowl would be hinged for engine maintenance access as described in volume III.

Nozzle duct: The forward portion of the nozzle duct, called the thrust reverser reserve section (see vol. III), has a stainless steel inner wall with circumferential stiffeners on the engine side. The outer wall is double construction with zee section circumferentials riveted in place between wall sheets. The outer sheet forms the nacelle surface while the inner sheet forms the duct airflow surface. Oil coolers for the turbocompressor and constant speed drives, shown in figure 89, form, in part, the two center splitters. Fins for the coolers extend 0.25 in. into the airstream. A pressure-actuated seal is installed in the forward end of the duct at the wrap cowl interface. This section is supported from the strut and mechanically fastened at the aft end to the rear nozzle section.

The rear nozzle section is composed of two parts: For the forward 30 in., the inner wall is constructed of stainless steel, and the outer wall and splitters are of acoustic/structural polyimide sandwich construction, all structurally similar to the wrap cowl. As stated in volume III, this 30-in. length of outer wall and splitter acoustic material was incorporated as acoustic attenuation backup to the acoustic treatment in the wrap cowl. Boilerplate tests, as previously reported, have indicated that this treatment may not be necessary to meet the 15-PNdB attenuation goal. Elimination of this treatment in a production version of the design could result in weight and cost savings. Construction for the aft 36 in. is aluminum alloy sheet outer wall and stainless steel inner wall, mechanically fastened together.

Fan cowl: The fan cowl provides nacelle interconnecting aerodynamic fairing from the treated inlet at the forward fan face of the engine to the forward end of the wrap cowl. The two fairing halves are supported from the forward nacelle strut structure and are latched at the bottom centerline.

Nacelle cooling.—The objective of the flightworthy nacelle cooling systems was to provide adequate cooling for the turbocompressor and alternator constant speed drive systems as well as other engine accessories during ground and flight test operations. The T/C and alternator CSD oil coolers are oil-to-air heat exchangers, cooled by fan airflow in the duct; see figure 89.

Critical engine accessories are provided with cooling air from individual bleed tubes located in the inner wall of the wrap cowl duct (fig. 90). The cooling air, serving as the heat transport fluid, carries excess heat from the accessory compartment through circulation aft across the engine fire seal and subsequent aspiration discharge at the coplanar fan and primary jet exit nozzles.

Protection of the polyimide duct walls from radiation-induced heating and engine case gas leakage is accomplished by using a stainless steel heat shield and a multiple-layer metallized polyimide thermal insulation blanket.

TREATED NACELLE FABRICATION

Treated Inlet

The treated inlet is fabricated as two major bench subassemblies: the external cowl assembly and the internal acoustic treatment assembly. Detail configuration description was given previously under structural-mechanical design.

External cowl assembly.—Fabrication of the external cowl details utilized conventional sheet metal forming practices. Figure 91 shows the spun-formed aluminum inlet lip and external skin riveted to the structural frame.

Acoustic treatment assembly.—Fabrication of the acoustic treatment panels used in the inlet is typical of the polyimide-fiberglass sandwich panel techniques described in volume II. Achievement of minimum material properties to satisfy structural design requirements was proven by quality control testing of each polyimide skin and sandwich panel produced. Laminate skins and sandwich panels were fabricated with additional material allowance for quality assurance test specimens. A typical plastic tooling surface used in the layup of sandwich panels and the plaster mandrel used to prepare the plastic tool are shown in figures 92 and 93, respectively.

The use of plastic tools in the fabrication of the polyimide-fiberglass sandwich panels and their subcomponents represents a significant tooling economy. This was possible since plastic tools are suitable for use in the 350° F temperature environment during oven curing. Postcuring, which requires temperatures of 500° to 550° F, was accomplished using simple space frames that provided minimum but adequate support and restraint of the sandwich panel in process.

Figure 94 shows acoustical panel assemblies for the outer ring and cowl wall in the assembly process. Centerbody acoustic panels assembled in place are depicted in figure 95. Experimental process development subsequent to completion of the treated inlets has demonstrated the feasibility of fabricating continuous ring-shaped sandwich panels. Elimination of joints for a production design would result in substantial weight and cost savings.

Figure 96 shows bench subassembly of the forward struts, ring leading edges, ring and strut anti-icing plumbing, and the inner acoustical rings. Subassembly of the aft struts with the ring trailing edges is shown in figure 97. Ring leading-edge segments are hammer-die formed of stainless steel sheet, while trailing edges are lathe-turned aluminum rings. Aluminum ring blanks are welded assemblies of formed bar stock. Main elements of both forward and rear struts are machined of stainless steel flat stock. The use of castings or forgings would also represent areas for weight and cost savings in production quantities.

Final assembly and fit check.—The completed acoustic treatment assembly is inserted into the aft end of the external cowl and is bolted to the forward circumferential frame (fig. 98). Addition of the engine mounting adapter ring, which is machined from an aluminum roll forging, completes the assembly.

Fit check of the completed nacelles shown in figure 99 was accomplished at the Boeing Wichita facility prior to shipment. The inlets were installed on the ground test rig and the flight test airplane without further fitup modification.

Treated Fan Duct

The treated fan duct was fabricated as seven major bench subassemblies: left- and right-hand assemblies of fan cowl, of bifurcation duct, and of wrap cowl, and a single nozzle assembly that also incorporates the fan thrust reverser reserve section. Detail configuration description was given under structural design.

Fan cowl assembly.—Fabrication of the left and right fan cowl is of conventional aluminum alloy construction, consisting of rolled sheet and circumferential ring stiffeners.

Bifurcation duct assembly.—Figure 100 shows the left and right halves of the high-temperature fiberglass bifurcation duct section after removal from the mold and prior to assembly of the two halves. Fiberglass layup of each section was accomplished on a water-

soluble mold conforming to the duct inside mold lines. The layup was then cured in an autoclave at 190° F and 15 psi for 30 min, immediately followed by a 90-min cure at 350° F and 45 psi. After cure the mold was dissolved from the fiberglass by use of a jet water stream. The left- and right-hand halves were then bolted together to form the completed assembly.

Wrap cowl assembly.—Fabrication of the wrap cowl consisted essentially of (1) fabrication of inner wall, outer wall, and splitter sandwich panels and (2) assembly of these panels by bolted construction. Basic detailed procedures for sandwich panel fabrication are given in volume II. A condensed sequence of single-core sandwich panel fabrication procedures is: (1) lay up and cure the acoustic laminate sheets, (2) fabricate and cure the sandwich core, (3) bond the core to the acoustic sheet, (4) bond the uncured nonporous layup for the outer skin to the core to complete the sandwich, and (5) postcure the sandwich assembly. Partially completed inner wall and splitter are shown in figures 101 and 102, respectively, which depict bonding of a completed core subassembly to the acoustic skin. A single plastic tool is used for both the acoustic skin fabrication and the sandwich buildup and bonding procedures.

After postcure, the panels were trimmed to size, alined and clamped in the drill and assembly fixture (fig. 103), and drilled for the assembly fasteners. The panels were then removed from this fixture and bolted together on the assembly fixture.

Nozzle assembly.—Fabrication of the thrust reverser reserve section and the aft transition nozzle section uses conventional sheet metal forming practices. Metal sheets are stretch-formed and circumferential stiffeners are rolled or hydropressed, depending on design. Final assembly views are shown in figures 104 and 105. The polyimide-fiberglass acoustic/structural outer wall and splitters were bolted into place after assembly of all metal portions had been completed.

Engine and strut modification.—To install the treated fan duct, it was necessary to modify the nacelle strut structure and to relocate several engine accessories and tubing runs. A mockup of the existing 707 strut and JT3D-3B engine was utilized to resolve these problems. The airplane parts were fabricated to duplicate the mockup installation.

Final assembly, fit check, and installation.—To ensure proper alinement of all duct sections and to ensure resolution of potential interferences with engine components prior to installation on the airplane, an assembly and fit check of the complete nacelle installation was accomplished, using the 707 strut and JT3D-3B engine mockup (fig. 99). Figure 4 shows the treated nacelles installed on the test airplane.

Nacelle Weights

In the following sections, the weight effect on the experimental flight test airplane with the treated inlet and treated fan duct installed is presented. Also discussed is the estimated weight effect on the 707-320B/C airplane should a production design version of the technology development presented herein be incorporated. In evaluating the data, it

must be recognized that, as previously stated, weight economy was not a paramount concern in development of the experimental flightworthy nacelles. Therefore, in estimating what might be done on a production version of a treated nacelle, a preliminary weight saving study was conducted. Some of the salient design improvements considered in estimating production treated nacelle weights were:

- Eliminate 14 heavy fore-and-aft splices in the four circumferential polyimide-fiberglass surfaces of the inlet and centerbody, as has been proven practical (see discussion on treated inlet fabrication).

- Eliminate one-half of the eight steel support struts for the two inlet acoustic rings and change fabrication to production-type forgings. As stated in volume III under treated inlet conceptual studies, the eight struts were recommended by Pratt & Whitney because of concern with possible fan blade excitation. Subsequent information has indicated four struts satisfactory in this regard.

- Change bifurcation duct material from heavy wall, low structural strength epoxy fiberglass to conventional hydropress aluminum alloy construction.

- Develop full allowable structural properties in the polyimide-fiberglass acoustic/structural parts of the wrap cowl and inlet in accordance with data presented in volume II.

- Reduce the excessive use of heavy, solid polyimide-fiberglass edge members of the wrap cowl wall and splitters, and use lighter fabrics proven acceptable.

- Delete or reduce 30 in. of polyimide acoustic/structural wall and splitters in the nozzle duct (see section entitled "Design–Treated Fan Duct–Structural-Mechanical").

- Reduce the gage of the stainless steel used in splitters, inner wall, and circumferentials of the nozzle section, and replace a considerable portion of this construction with aluminum alloy.

- Redesign many heavy machined parts to production forgings and/or castings.

Flightworthy test airplane.–Actual weights per nacelle of the treated inlet and treated fan duct components as installed on the test airplane were:

Component	Weight, lb
Treated inlet, instrumentation, and turbocompressor fairing	540
Treated centerbody	30

Component	Weight, lb
Fan cowls and support structure	76
Bifurcation duct and support structure	123
Wrap cowl ducts plus attachments	758
Fan thrust reverser reserve section	385
Rear nozzle section duct plus attachment	648
Engine and strut modifications	49
Primary thrust reverser adapter	35

Estimated weights per nacelle of components removed from the experimental test airplane in order to install the treated inlet and treated fan duct were:

Component	Weight, lb
Inlet	197
Centerbody	14
Fan cowl and turbocompressor fairing	48
Side cowls	222
Fan thrust reverser	288
Primary thrust reverser, cascades, and sliding sleeve cowl	514
Miscellaneous nacelle structure below strut	52

Treated nacelle production airplane.—Estimated weights per nacelle of a possible production version of a treated nacelle are as follows:

Component	Weight, lb
Treated inlet and turbocompressor fairing	343
Treated centerbody	19
Fan cowls and support structure	50
Bifurcation duct and supports	90
Wrap cowl ducts plus support hinges	480
Fan thrust reverser	325
Sliding rear nozzle section duct	400
Engine and strut modifications	50
Total estimated weight added per nacelle	1757

Estimated weights per nacelle of components to be removed from a standard production-type 707-320B/C airplane in order to install a production treated nacelle are as follows:

Component	Weight, lb
Inlet	197
Centerbody	14
Fan cowl and turbocompressor fairing	48
Side cowls	222
Fan thrust reverser	288
Sliding sleeve cowl	151
Miscellaneous nacelle structure below strut	52
Total estimated weight removed per nacelle	972

The delta operational empty weight (ΔOEW) increase to a 707-320B/C airplane incorporating a production design version of a treated nacelle is estimated as:

$$\begin{aligned} \Delta\text{OEW increase/airplane} &= 4\,(1757 - 972\text{ lb}) \\ &= 4\,(785\text{ lb}) \\ &= 3140\text{ lb} \end{aligned}$$

The above analysis recognizes that the design utilizes an acoustic material new to jet engine environment on production airplanes. As reported in volume II, structural and environmental tests were performed on this polyimide-fiberglass material. These included the laboratory simulation of an equivalent 4000 hr of flight operation. However, it should be recognized that structural integrity tests for long service life in jet engine installations have not been conducted, and that results of such tests could have a small effect on the total weight estimates.

Maintainability

A maintenance analysis of the treated nacelle was prepared to evaluate the influence of the design modification on nacelle hardware maintainability. The analysis was accomplished on a comparative basis, using available data for the present 707 airplane as the baseline. Costs were derived for a treated nacelle in terms of man-hours and materials per flight hour for each ATA system considered significant (ATA 54, 71, and 78 were used for this purpose).

The estimated maintenance costs were based on the flightworthy treated nacelle configuration and with installation of production-type thrust reversers. No estimate was made of ground support equipment revisions that may be required. Items such as durability, cleaning, and susceptibility to damage from foreign objects entering the inlet cowl were considered. For the treated inlet it was assumed that:

- Cleaning would be accomplished once a year.

- Inspection of the treatment would be accomplished at each "C" periodic check (currently varies between operators from 600 to 800 hr).

- Repair of treated areas for sand and dirt erosion, flaking, chipping, and foreign object damage would be necessary once a year for each treated nacelle.

For the treated duct it was assumed that:

- The increased weight of the acoustic treatment would require a corresponding increase in maintenance labor (to hoist and handle).

- The treated duct seals would require increased maintenance and more frequent replacement than seals for the present nacelles.

- Inspection of the acoustic material would be accomplished at each "C" periodic check.

- Cleaning would be accomplished during engine hot section inspection, at least once a year (inspection currently varies between operators from 2000 to 5000 hr).

- Replacement of acoustic panels would be required every 3 yr or 10 000 flight hours, whichever occurs first.

Since operating time with the treated nacelle is quite limited, maintenance analysis estimates are based on judgment rather than experience. Analysis results indicate an increase in maintenance cost from $2.70 per flight hour for each present 707 nacelle to $3.02 per flight hour for each treated nacelle. These values are based on cost levels projected for 1972. These maintenance cost estimates cannot be substantiated without a lengthy service test of treated nacelles under average airline operating conditions.

GROUND CALIBRATION TESTS

Purpose

Static ground tests were conducted to measure the acoustic and propulsion performance of a JT3D-7 turbofan engine with each of the four flightworthy treated nacelles installed. Similar tests were made to obtain comparative performance of a baseline nacelle and a Pratt & Whitney reference configuration. The tests provided data to determine the power settings and thrust coefficients required for the flight tests and served as an operational check of the revised fuel, oil, and cooling systems of the treated nacelles. The ground test also provided a check of the structural integrity and adequacy of the seals between the various sections of the treated nacelles.

Test Plan

The present 707 nacelle served as a baseline to determine the performance changes associated with treated nacelles. The configuration included a large blow-in door inlet, a short fan duct, and an existing primary nozzle. A P&WA reference configuration with a bellmouth inlet and long fan duct was tested at three intervals to determine data repeatability and to establish the basic engine performance.

Tests were also conducted to isolate the propulsion performance of the fan ducts and inlets of the treated and baseline configurations. Fan duct performance was determined from tests with the P&WA bellmouth inlet. This configuration was also used to determine the proper fan duct nozzle discharge area. Acoustic data for the baseline fan duct were obtained using an inlet directionalizer to prevent inlet noise from influencing measurement of noise radiated from the fan ducts. During the treated nacelle tests, acoustic data were recorded only when both the treated inlet and treated fan duct were installed. No attempt was made to isolate the noise radiated from the inlet or duct because the interference from one source to the other will be limited with both sources acoustically treated.

Measurements of the internal flow through the inlet and fan duct were obtained from the first treated nacelle tested. Total pressures were measured in the treated inlet to determine the pressure losses behind the rings and struts and on the cowl wall and centerbody. These data were used to estimate the pressure recovery at the fan face. Static pressures were measured to determine the local velocities and structural loads on the rings, cowl wall, and centerbody. Crosswinds were simulated with a wind machine to investigate the engine surge limits with the inlet installed. Data were recorded during steady state and engine acceleration conditions. A "cruise" bellmouth was installed on the inlet to reduce the lip losses associated with static tests and to provide an estimate of the inlet performance during cruise conditions.

The internal flow through the treated fan duct was evaluated from measurements of the total pressure loss through the duct and local static pressures along the various channels. Operational checks of the fuel, oil, cooling, and anti-icing systems were also made.

The tests of the treated inlet anti-icing systems were conducted to demonstrate the feasibility of meeting the requirements of a viable design and to provide clearance for use of the systems during the flight test program. Measurements of surface temperatures, bleed air temperatures, bleed air surface temperatures, and bleed airflow were obtained to ensure that material allowables and engine bleed limits were not exceeded. Data were recorded after at least 2 min of stabilized running at N_1 speeds of idle, 4100, 5000, 5950, and maximum power rpm.

The nacelle cooling tests were conducted on the first flightworthy nacelle installed on the test stand and demonstrated capability of the system prior to flight. Flight conditions were simulated with the engine operated at various power settings from idle to takeoff with the generator loaded to the maximum test airplane load of 30 kW.

Acoustic and performance tests for all the configurations were run at least three times for each test condition, and the data were averaged for the three runs. Test conditions were set at 13 low-speed compressor speeds that varied from approximately 2000 rpm at idle to 6500 rpm at maximum takeoff thrust. Data were recorded only after proper engine warmup and after the test condition had stabilized. Acoustic data were recorded on magnetic tape for 15 to 90 sec for all microphones in the test range. Acoustic data were not recorded if precipitation occurred, and all test operations were suspended if wind velocity exceeded 10 kn.

The various configurations used for the ground calibration tests are shown in figure 99 and figures 106 through 109.

Instrumentation

Ground calibration test instrumentation consisted primarily of that provided for measurement of treated nacelle acoustic and engine performance and secondarily of that provided to obtain data for the following areas of interest:

- Ambient environmental conditions
- Aerodynamic performance of the treated inlet and fan duct
- Inlet anti-icing systems performance
- Inlet and fan duct vibration measurement
- Nacelle and oil cooling systems performance

Acoustic data were recorded in the far field using microphone arrays on a 200-ft radius in the horizontal plane at engine centerline height and on a 75-ft radius in the vertical plane through the engine centerline. Twenty-four microphone systems were used to record data, and microphones could be situated at any of the locations shown in figure 110.

Instrumentation provided for measurement of engine performance as well as for ambient environmental conditions is typical of that defined in volume III under the boilerplate/prototype treated fan duct test.

One of the airplane sets of four engine inlets was equipped with instrumentation for measurement of inlet flow conditions, internal acoustic sound pressure levels, and anti-icing system performance, as follows:

- Two total pressure rakes, with 33 probes per rake, were located forward of the engine face to define the ring and strut wakes along with the wall and centerbody boundary layers. These rakes were spaced 180° apart.

- Four total pressure rakes, with six probes per rake, were located at the same inlet station as the two previously mentioned rakes and were spaced uniformly between them.

- Thirty-six static pressure pickups were located at various stations on the cowl wall, centerbody, and acoustic rings to determine the local velocity and pressure loads.

- Boundary rakes with six probes per rake were located on the cowl wall 6 and 25 in. downstream from the inlet highlight.

- Three microphone-type pressure transducers were mounted flush with the surface of the cowl wall acoustic panel. Located at intervals in a fore-and-aft line, the transducers provided sound pressure level data within the inlet and measured progressive attenuation along the inlet length.

- Four thermocouples were positioned on the polyimide panel surface just aft of the anti-icing air exhaust slots (see fig. 81). Temperature-indicating paint (Tempilaq), with a range of melting temperatures, was located on ring leading edges and strut surfaces (fig. 111) and on cowl lip surfaces (fig. 112).

Instrumentation for measurement of aerodynamic performance of the treated fan duct is identical to that described in the boilerplate/prototype treated fan duct test section of volume III. The right half of one nacelle fan duct was instrumented as follows:

- A total and static pressure survey at the fan duct exit was obtained with a traversing rake.

- Static pressures were measured at 50 locations spaced at intervals along the length of both inside and outside walls of each flow channel.

To ensure structural integrity of the nacelle hardware and the test instrumentation items, seven accelerometers were attached at locations on the inlet and duct selected to give maximum response level. The output of the accelerometers was monitored during testing to assist in detection of possible hardware failure.

Nacelle cooling was evaluated by thermocouples distributed both forward and aft of the engine firewall station. Temperatures were measured at selected locations on engine

accessories components, the engine case, the inner fan duct wall, and within the air space between the fan duct wall and engine. Static air pressures were measured both forward and aft of the engine firewall to indicate adequacy of cooling airflow.

To evaluate oil cooler performance for the airplane CSD, oil temperatures were measured using temperature probes at both inlets and outlets of the cooler and drive unit. A flowmeter was used to determine oil flow rates, and oil pressures were monitored at the cooler inlet and outlet.

Test Results

Acoustic and propulsion system performance results obtained from ground tests of the baseline and the treated nacelles are presented in this section.

Acoustic.—The noise reduction achieved by the addition of acoustic treatment to the engine nacelle was determined by comparing acoustic data from the baseline nacelle to data from the flightworthy treated nacelles. In the evaluation, emphasis was placed on the SPL in the 1/3-octave band containing the discrete components generated at fan blade passage frequencies. The reduction in level of this fan noise component, the most significant in PNL calculations, provides a good indication of acoustic treatment effectiveness. The acoustic performance of inlet and fan discharge duct treatment are discussed separately.

Four treated nacelles were statically calibrated, and it was found that the acoustic characteristics of the nacelles were similar. For this reason and unless otherwise stated, the results presented are from the first treated nacelle tested. A description of data analysis procedures is given in volume III as are the effects present in sound measurements made close to a ground plane. Data recorded in the horizontal plane during treated nacelle static calibration tests also showed this sound reflection interference phenomenon.

Treated inlet: At approach thrust, comparison was made between the maximum inlet noise spectra for the baseline and treated inlet (fig. 113). In the 1- to 10-kHz frequency range where fan-generated noise predominates, the reductions in 1/3-octave band sound pressure levels varied between 6 and 18 dB. The maximum reduction in SPL was in the frequency band containing the fan blade passage frequency discrete components. Reductions in SPL were similar for both discrete and broadband components. For this reason, the characteristic discrete inlet noise components were still present with the treated inlet. The reduced SPL in frequency bands below 1000 Hz is attributed to the change in jet noise directivity due to the coplanar nozzle configuration of the treated fan ducts. These effects were also observed during tests of the boilerplate/prototype fan ducts (see vol. III).

Typical samples of constant bandwidth (50 Hz) narrowband analysis are shown in figure 114. The fundamental, second, and third harmonic components of the fan blade passage frequency or combination tones of these components are still dominant in the sound

spectrum. The 50-Hz bandwidth analysis shows the relative attenuation of discrete and broadband noise as was indicated in the 1/3-octave band analysis.

Data recorded inside the treated inlet, at the outer wall surface (fig. 115), substantiated the results from far-field data. The attenuation of SPL along the outer wall treatment corresponds closely to far-field SPL reductions obtained by comparison of baseline and treated inlet data.

The directional characteristics of the treated inlet at approach thrust are shown in figure 116. To obtain good definition of the directional characteristics of the fan noise radiated from the treated inlet, a portable microphone was traversed at a 25-ft radius around the inlet. Two distinct sound pressure level peaks were evident at approximately 20° and 40° to the inlet axis.

Comparative inlet noise spectra for the baseline and treated inlet at maximum engine thrust are shown in figure 117 (1/3-octave bandwidth) and figure 118 (50-Hz bandwidth). When compared with approach thrust noise spectra, an increase in the attenuation of inlet-radiated noise was evident. This increase was approximately 2 to 5 dB at fan blade passage frequencies, and up to 10 dB at frequencies above 4 kHz.

The change in attenuation characteristics of the inlet is attributed to the effects of the higher velocity of the inlet airflow at high thrusts opposing the sound propagation. The directional characteristics of inlet-radiated noise at maximum thrust (fig. 119) showed a uniform radiation pattern. This would be expected from a noise source that is essentially broadband.

The maximum SPL of inlet-radiated discrete fan noise is shown as a function of gross engine thrust in figure 120. The inlet treatment provides a substantially constant reduction in peak fan noise level, between 17 and 19 dB, up to a gross thrust of 15 000 lb. Above 15 000-lb thrust, the complementary attenuations due to inlet treatment and increasing inlet flow velocity result in a maximum reduction of approximately 23 dB at takeoff thrust.

Treated fan duct: The acoustic characteristics of the flightworthy treated fan ducts were similar to those of the boilerplate/prototype fan ducts described in volume III. A comparison between the flightworthy and boilerplate fan ducts, based on the SPL in the frequency band containing the fan blade passage frequencies, is shown in figure 121.

Comparative 1/3-octave band spectra for the baseline short fan ducts and flightworthy treated ducts are shown for approach thrust in figure 122. At this thrust the SPL in the frequency band containing the fan passage frequencies was reduced by 20 to 25 dB. Turbine noise was evident in frequency bands above 5 kHz. Narrowband (50-Hz bandwidth) analysis (fig. 123) indicated that the discrete fan-generated noise components were attenuated by up to 30 dB. The discrete component at 3.5 kHz was present during testing of the boilerplate fan ducts (vol. III) and has not been identified. Discrete noise generated by the low-pressure stages of the turbine can be identified at 6, 8.1, and 8.6 kHz.

Comparative spectra for the baseline and treated fan ducts at takeoff thrust are shown in figure 124 (1/3-octave bandwidth) and figure 125 (50-Hz bandwidth). These data show that the duct treatment attenuates discrete fan-generated noise to a level equal to or below the levels set by the primary jet noise.

The reduction of fan noise as a function of gross engine thrust is shown in figure 126. As in the boilerplate fan duct evaluation, fan noise was attenuated by approximately 22 dB up to a thrust of 13 000 lb. At higher thrusts, measured attenuation was limited by the predominance of jet noise. For additional information on the treated fan duct acoustic performance, refer to volume III.

Treated nacelle: Fan noise radiated from the baseline nacelle and the treated nacelles at approach thrust are compared in figure 127. The fan noise was reduced by 16 to 22 dB depending on the angular location considered. The maximum reduction recorded was at 110° to the inlet centerline, which is the angle of maximum duct-radiated fan noise. The treated inlet noise radiation characteristics, described in the treated inlet test results, gave maximum inlet noise levels at angles between 20° and 40° to the inlet at a 200-ft radius.

Comparative fan noise levels at takeoff thrust are shown in figure 128. The maximum reduction in fan noise was in the inlet quadrant, 50° to the inlet axis. For the treated nacelles, the predominance of primary jet noise at takeoff thrust is reflected in the decreasing noise reduction at angles toward the primary jet axis.

Data from the individual nacelles were generally within ±2 dB of the mean established by the four nacelles, as shown in figures 127 and 128. Individual comparison of the treated nacelles did not indicate any consistency in the data variations. Therefore, it was concluded that within the test data limits, the four nacelles had the same acoustic characteristics.

Extrapolation of data from a polar microphone array to corresponding sideline locations enables data to be presented in a form that exists during an airplane flyover. The maximum levels of inlet- and fan-duct-radiated fan noise, on a 200-ft sideline, are shown in figure 129 for both baseline and treated nacelles. The acoustically treated nacelle provides a reduction of maximum sideline fan noise in excess of 20 dB up to a gross thrust of 13 000 lb. Above this thrust, the reduction decreases progressively, to approximately 14 dB at takeoff thrust.

Prediction of flight test results: The in-flight acoustic performance of the airplane equipped with the treated nacelles was predicted using the data obtained during ground calibration of the nacelles. The data, measured at each angular location on a circular arc centered on the geometric midpoint of the engine, were extrapolated radially to sidelines at given distances. The engine noise was assumed to have the characteristics of a point source. These sideline distances were equal to the level flyover altitudes to be used during flight tests (400 and 1000 ft).

Static test data, standardized to atmospheric conditions of 59° F and 70-percent relative humidity, were extrapolated by applying factors for spherical divergence and atmospheric absorption (per ref. 1). Predicted noise levels also include a factor of 6 dB to account for the four engines of the airplane. Due to their complicated nature, no corrections were applied for ground attenuation, reflection, or shielding effects resulting from the presence of the airplane structure, or for Doppler effects on the frequency.

Static test data were measured using microphone arrays at a 200-ft radius in the horizontal plane and at a 75-ft radius in the vertical plane. Predictions for the baseline flight data were made using data from both microphone arrays. Subsequent comparison with measured flight test data indicated that more accurate predictions could be made using data measured at the 200-ft radius. Data from this horizontal plane microphone array were used, therefore, in making the final flight test predictions. However, as stated in volume III, data recorded in the horizontal plane did indicate effects due to ground reflection. As these effects were evident primarily below 1000 Hz, their influence on calculated PNL was small. Predicted in-flight data were corrected using the assumption that sound pressure reinforcement and cancellation exist in the data, as shown in figure 130. Using this type of correction reduces possible errors due to ground reflection and provides a realistic sound spectrum shape below 1000 Hz.

Comparison between static and in-flight data was made with N_1 as the common engine performance parameter. However, use of this parameter does not take into account the effects on jet noise due to the change in relative jet velocity between static and flight conditions. Available static and flight test data have been compared, and indications are that these jet velocity effects are small. For the purposes of PNL predictions, no corrections for the jet velocity effects were included.

Predicted spectra at the instant of maximum PNL during landing approach are shown in figure 131 for both baseline and treated configurations. Figure 132 shows the predicted maximum PNL as a function of jet engine thrust for level flyovers at 400 and 1000 ft. The predicted levels for the treated nacelle show that a PNL of approximately 108 PNdB will be measured at typical approach conditions of 4000- to 6000-lb thrust and 400-ft altitude at the 1 n. mi. reference point. During takeoff, at maximum thrust and at a 1000-ft altitude, a PNL of 113 PNdB is predicted.

The predicted PNL reductions achieved with the treated nacelles installed are shown in figure 133. The results indicate that the target noise reduction, 15 PNdB during landing approach, will be achieved. Also, a reduction of 4 to 5 PNdB is predicted at takeoff.

Propulsion.—The evaluations of the inlet, fan duct, and nacelle modifications on propulsion system performance are discussed in this section. In addition, the measurements of inlet and fan duct flow characteristics are examined and compared to earlier design predictions and tests.

The effects of the four treated inlets on engine performance were determined by comparing engine thrust and thrust specific fuel consumption obtained with the treated inlets and the Pratt & Whitney reference bellmouth inlet installed on an otherwise identical test configuration. A direct comparison of the baseline and treated inlet performance was not possible since similar tests to isolate baseline inlet performance were not conducted.

Treated fan duct performance was evaluated by comparing engine thrust and TSFC measurements to similar measurements made when the P&WA reference ducts and the baseline short fan ducts were installed. A P&WA reference bellmouth inlet was used for this series of tests.

Engine thrust and TSFC measurements with the four treated nacelles and the baseline nacelle installed on the ground test stand were compared to evaluate the overall performance effects of the treated nacelles.

Fan duct exit areas and primary nozzle area were matched prior to the fan duct performance tests. The effective fan duct exit areas were adjusted to provide the same relationship between fan pressure ratio and fan speed as measured with the P&WA reference inlet and fan duct configuration. Aluminum wedges, attached to the outer duct nozzle wall, were used to adjust the duct nozzle area.

When tested with the treated fan ducts, the primary nozzle effective exit area was controlled to 1 percent over area, which agreed with the effective nozzle area for the baseline configuration. This control was accomplished by adjustment of the fan duct inner wall extension downstream of the primary nozzle exit plane.

The engine pressure ratio setting to be used for maximum power operation of the engines installed in the treated nacelles was determined during the ground calibration tests. A maximum EPR of 1.875 was established by Pratt & Whitney for the engine with the reference bellmouth inlet and fan ducts. Adjustment of the EPR is required when the operation is with other inlets and primary nozzles. The EPR is selected to provide the same high-pressure-stage speed (N_2) as measured at the maximum EPR setting with the Pratt & Whitney reference hardware. Fan duct areas were matched prior to selecting the EPR settings for the treated nacelles.

The maximum standard-day EPR setting for the engine with the treated nacelles was 1.828. When the engine was operated with the reference bellmouth inlet, treated fan ducts, and over-area primary nozzle, the maximum EPR was 1.868. Previous tests established a maximum EPR of 1.848 for the engine with the baseline nacelle. The applicable EPR settings were used in the comparisons made of maximum power and TSFC.

Treated inlet: Effects of the treated inlets on engine performance were determined by comparing engine thrust and TSFC, shown in figures 134 through 141. Except for the number 1 treated inlet, no difference in engine thrust was observed for primary nozzle pressure

ratios up to 1.55. At higher primary nozzle pressure ratios, thrust reductions were observed for all the treated inlets. Based on maximum EPR's, takeoff thrust is 18 300 lb for the number 1 treated inlet compared to 19 120 lb for the bellmouth inlet—a 4.3-percent thrust reduction. The average reduction of takeoff thrust for the four treated inlets compared to the bellmouth inlet is 4.1 percent.

The treated inlet loss at takeoff power was also estimated from the difference in pressure recovery between the number 2 treated inlet and the bellmouth inlet. Using the Pratt & Whitney thrust loss coefficient, the estimated thrust loss is 4.4 percent, which is consistent with measured thrust results.

Comparing TSFC values at a nominal cruise condition, where the total engine corrected airflow is 453 lb/sec and the corresponding corrected net static thrust is 17 000 lb, the treated inlet shows an increase of 1.5 to 2.9 percent over the bellmouth inlet. The average increment was found to be 2.2 percent. Tests to simulate cruise conditions using a bellmouth lip on a treated inlet indicated an improvement in inlet pressure recovery of about 0.2 percent. The corresponding estimated change in TSFC is 0.27 percent and indicates that the average increase in TSFC for the treated inlet during the simulated cruise condition would be 1.9 percent. An estimate of TSFC change was also obtained from the measured inlet recovery during the simulated cruise condition and from the Pratt & Whitney loss coefficient. This estimate indicates an increase of 1.4 percent relative to the bellmouth.

Static surge-free engine operation was demonstrated during the inlet tests with a simulated 15-kn, 90° crosswind. Surge-free engine operation was also observed at this crosswind condition during transient conditions of rapid engine acceleration and deceleration.

Inlet total pressure recoveries were obtained by measuring total pressures in ring and strut wakes and boundary layers on the cowl wall and centerbody near the fan face (see figs. 142 and 143). Inlet total pressure recovery at 480 lb/sec airflow is 97.3 percent, which indicates a total pressure loss of 2.7 percent (see fig. 144). With a bellmouth lip installed, total pressure recovery is increased to 98.0 percent, indicating a total pressure loss of 2.0 percent.

The wake shape of the inner ring was symmetrical with respect to the trailing edge. The flow on the outer surface of the outer ring appears to be slightly affected by the thick boundary layer (about 3 in.) on the cowl wall. A thin boundary layer was observed on the centerbody. Installation of a bellmouth lip does not change the symmetry of the ring wakes; however, a thinner boundary layer (about 2.25 in.) was observed on the cowl wall. The strut wakes were symmetrical with respect to the trailing edges for the test configurations both with and without bellmouth lip.

The inlet measurements were also analyzed to obtain inlet total pressure losses attributed to each inlet component. Inlet total pressure losses (inlet lip, cowl wall, rings, and struts) were plotted against inlet airflows as shown in figures 145 through 148. Detailed inlet loss breakdown at 480 lb/sec airflow is tabulated in table IV.

The selected inlet contours apparently result in local laminar flow separation and reattachment forward of the throat at takeoff conditions. The magnitude of the inlet separation is not considered detrimental to engine-inlet compatibility. The lip loss was estimated from boundary layer measurements at the inlet throat. A bellmouth lip was installed to reduce the lip loss and to simulate cruise conditions. Pressure recovery loss changed from 0.0086 to 0.0016 with the bellmouth lip installed. Lip loss will be maximum at static conditions and will reduce rapidly as forward velocity is increased (see discussion on flight test inlet performance). As the inlet airflow decreases, lip loss diminishes. For inlet airflow less than 360 lb/sec, lip loss is comparable to that with a bellmouth lip installed.

The cowl wall loss in total pressure recovery (measured near the fan face) also decreases from 0.0138 to 0.00717 at 480 lb/sec airflow as the bellmouth lip is installed. This difference is inherent from the difference in lip loss. Total pressure losses from the inner ring and struts do not show any appreciable change when the bellmouth lip is installed, whereas the loss from the outer ring shows higher values for the treated inlet without the bellmouth lip. Test data scatter, together with the effect of inlet lip curvature on the cowl wall boundary layer development, are believed to cause this higher loss on the outer ring.

Since the treated inlet was designed using only analytical methods, static pressure measurements obtained during the full-scale tests were compared to the analytical results to evaluate the design procedures. Correlation of the cowl wall and centerbody static pressures is shown in figure 149. The correlation parameter used is based on the Prandtl-Glauert similarity rule for two-dimensional flow using a reference throat Mach number M_{th}.

$$\frac{P_T - P_S}{q_{th}} \sqrt{1 - M_{th}^2} - K(M_{th})$$

where:

$$K(M_{th}) = 2\sqrt{\frac{1 - M_{th}^2}{\gamma M_{th}^2}} \left[\left(1 + \frac{\gamma - 1}{2} M_{th}^2 \right)^{\frac{\gamma}{\gamma - 1}} - 1 \right]$$

M_{th} = inlet throat Mach number based on one-dimensional flow

P_T = total pressure

P_S = surface static pressure

q_{th} = $1/2\ \rho_{th} U_{th}^2$, calculated at M_{th}

γ = ratio of specific heats

Correlation of the measured static pressures on the cowl wall shows acceptable scatter except at 6.5 in. downstream of the inlet lip (near the inlet throat). The difference between the test and analytical results for the inlet lip and throat is the result of viscous effects on the local flow, which were not accounted for in the potential-flow analysis. The difference between the test and analytical results 6.5 in. downstream of the inlet lip is due to boundary layer development on the cowl wall. The pressure gradient on the centerbody is favorable; thus, good correlation between test and analytical results is obtained.

The total pressure and velocity profiles in the boundary layers, determined from the inlet pressure measurements, are shown in figures 150 and 151. In general, the boundary layer thickness increases as inlet airflow increases; however, at the measuring stations, the flow is not separated for the range of conditions tested.

Treated fan duct: The total thrust of the engine with the treated fan duct installed (averaged for the four ducts tested) is compared to that with the Pratt & Whitney reference ducts and baseline ducts in figure 152. The treated duct installation produces approximately 0.5 percent (100 lb) less thrust at takeoff (engine pressure ratio of 1.875) than the Pratt & Whitney reference ducts and 0.5 percent more than the baseline short ducts. Since the fan thrust at takeoff is approximately half the total thrust, the treated duct produces 1 percent more fan thrust than the baseline duct (at the same engine pressure ratio).

At takeoff, engine TSFC with the treated duct is approximately 1.5 percent greater than with the Pratt & Whitney reference ducts (fig. 153), while the baseline duct causes an increase in specific fuel consumption of 2.8 percent over the reference (fig. 154). Thus, the TSFC with the treated duct is approximately 1 percent less than that with the baseline duct.

The total pressure distortion at the fan exit with the treated ducts installed, shown in figure 155, was less than 5 percent, well within the P&WA limit of 14 percent.

The total and static pressures measured at the exit of one of the flightworthy ducts are compared with similar data for the boilerplate in figure 156. Although the flightworthy duct shows a better total pressure recovery, the flow at the nozzle exit plane is not as expanded as that at the boilerplate exit. The circumferential distribution of the total pressure loss is shown in figure 157 and agrees well with the boilerplate and model data (vol. III).

The static pressure trends and values measured on the walls of one of the flightworthy ducts agreed well with the boilerplate data except in the channel next to the bottom, where the static pressure in the flightworthy duct is uniformly higher than that in the boilerplate. However, boilerplate statics in this channel were lower than expected, and the boilerplate data indicated a distorted flow field at the bottom of the duct exit (vol. III). The static pressure will be a constant percentage of the duct inlet pressure when the duct is choked, provided no additional flow disturbances occur at the higher pressure ratios. The exit traverse data indicated that the fan duct will choke at a fan pressure ratio of approximately 2.0. The average flightworthy duct static pressures at each axial station are shown as a

function of inlet pressure in figures 158 and 159. The inside wall static data will be extrapolated and used to monitor the internal duct performance during the flight test. The treated inlet has no influence on the internal duct pressures at a given duct inlet pressure.

A fan thrust coefficient curve was determined for the treated duct from the static calibration and model test data (fig. 160). Comparing this curve to similar data for the baseline duct shows that thrust at cruise with the treated duct is 3.2 percent greater than thrust with the baseline duct. The fan thrust coefficient for the baseline duct includes the effects of duct losses and scrubbing drag discussed previously.

Treated nacelle: The static engine thrusts with the baseline and treated nacelles installed are shown in figure 161. The data indicate the static takeoff thrust with the treated and baseline nacelles will be approximately the same. This comparison considers that the engine is operated at the same high-pressure compressor speed with both nacelles (EPR's of 1.842 and 1.828 for the baseline and treated nacelles, respectively).

Cruise performance cannot be directly obtained from the ground test results because of changes in inlet flow and fan duct pressure ratios at high forward speeds. However, based on the estimated treated inlet and fan duct performance at nominal cruise conditions (airflow of 453 lb/sec, 17 000-lb equivalent static thrust), the nacelle performance was estimated. The estimated inlet performance was based on results of simulated cruise tests with the bellmouth lip installed, which indicated that TSFC with the treated inlet would be approximately 1.2 percent greater than that with the baseline inlet. Based on the fan thrust coefficients obtained from model and full-scale test data, TSFC was estimated to be 3.2 percent less with the treated duct than with the baseline short duct. The combined results indicate that TSFC at nominal cruise conditions with the treated nacelle would be 2 percent less than with the baseline nacelle.

Anti-icing.–In summary, the anti-icing system tests showed adequate distribution of heat to the anti-iced surfaces with no locally overheated areas. Air bleed quantities were within predicted values. The systems were approved and used as required during the flight test program.

Engine air bleed quantities and temperatures for cowl lip and ring/strut anti-icing are shown in figure 162. Engine bleed air temperatures for the cowl lip and ring/strut systems are, for practical purposes, identical and closely approximate baseline inlet cowl lip bleed air temperatures over the full range. Bleed quantities for the cowl lip system also compare closely with those for the baseline inlet over the full engine operating range. Maximum flow of 1.58 lb/sec to the ring and strut system is slightly less than the predicted value. The total bleed is within the engine manufacturer's allowable, which is set at 2 percent of primary airflow or approximately 3.9 lb/sec at takeoff (static) thrust.

Figure 163 summarizes maximum temperature rise above ambient for anti-iced surfaces in the inlet with all anti-icing systems in operation. Temperature rise estimates for the

centerbody were determined from previous test of the baseline inlet. Cowl lip temperature rise of 300° F maximum compares very well with the 305° F temperature rise measured for a baseline inlet. The maximum recorded temperature rise for the polyimide surfaces is 151° F. It has been estimated that for a 120° F day, with inadvertent system operation, the maximum polyimide surface temperature would be approximately 270° F. This value is far below the allowable of 475° F set for the polyimide material. The maximum recorded surface temperature rises for the strut and ring leading edges are 310° and 260° F, well within the capability of the stainless steel material. Figure 164 shows the distribution of ring leading-edge surface temperatures. It is indicated that the outer ring system could be improved by moving the spray tube from 1/2 to 3/4 in. forward, thus increasing the low-temperature 130° F rise at the forward zone while locally decreasing the high-temperature 260° F rise area. Figure 165 shows the equivalent temperature data for the strut.

Nacelle cooling.—The test results demonstrated satisfactory performance of the nacelle cooling and constant speed drive oil cooling systems. The maximum temperature of all engine components corrected to a standard plus 41° F day did not exceed the maximum allowable limits (fig. 77).

Nacelle cavity ambient temperatures and wrap cowl inner wall temperatures forward of the fire seal were satisfactory although 50° to 70° F higher than predicted.

CONCLUDING REMARKS

The results of design development and of ground and flight testing of the treated nacelles are summarized as follows:

- During landing approach 1 n. mi. from threshold, the treated airplane had a noise level 15.5 EPNdB under that of the baseline airplane.

- A noise reduction of 3.5 EPNdB was achieved with the treated airplane 3.5 n. mi. from brake release at takeoff power conditions.

- With power cutback after takeoff, noise reductions 3.5 n. mi. from brake release were 4.5 and 6.5 EPNdB for the treated airplane at gross weights of 330 000 and 260 000 lb, respectively.

- Maximum perceived noise levels at landing approach, and takeoff conditions and the noise suppression achieved during these operations were predicted within 1 PNdB using static test stand data.

- It is estimated that the 707-320B/C airplane operational empty weight would be increased by approximately 3140 lb by incorporation of production-type treated nacelles.

- Cruise performance of the treated inlet and fan duct along with changes in external drag result in a fuel mileage loss for the treated airplane of 0.7 percent at M = 0.8 and 2.1 percent at M = 0.83.

- Change in fuel mileage and the increased weight result in a predicted range loss of 200 n. mi. with the treated nacelle airplane for the international maximum range cruise condition. Displacement of fuel equivalent to the predicted weight increase for production treated nacelles contributes the major part of the range loss.

- Takeoff distance to a 35-ft height with the treated nacelle airplane is approximately 135 ft greater than with the standard production airplane. Where field length establishes takeoff weight, an approximate 2500-lb weight reduction is indicated.

- Climbout to 3.5 n. mi. from brake release results in a 120-ft decrease in altitude of the treated airplane with respect to the baseline airplane.

- Ground calibration test of the treated nacelle indicated that, compared with the baseline nacelle, the available engine static takeoff thrust was approximately the same and the TSFC was approximately 2 percent less at nominal cruise condition.

- Use of polyimide-fiberglass material in the inlet and duct enhances design in that the acoustic desirability for close-tolerance control of porosity and variation of porosity can be achieved, and the good structural properties of the material obviate the need for additional supporting structure.

- For the two-ring inlet selected for design, the target attenuation goal appears to be best satisfied using approximately 71-ft^2 treatment area, equal spacing of rings, treatment depths of 0.3 and 0.6 in. on opposite facing walls, and a nominal flow resistance of 11 rayls (cgs) throughout.

- The fan duct target attenuation goal can be satisfied by acoustically treating all walls of the duct channels for a length of 69 in. (approximately 216 ft^2), with treatment depths of 0.3 and 0.75 in. on opposite facing walls and 0.5-in. on splitter walls, with a nominal flow resistance of 15 rayls (cgs) at the forward end and 26 rayls (cgs) at the aft end.

- Design of the fan duct is compatible with the existing primary thrust reverser, but a new fan thrust reverser design is required.

The Boeing Company
Commercial Airplane Group
Seattle, Washington, September 1969

REFERENCES

1. Standard Values of Atmospheric Absorption as a Function of Temperature and Humidity for Use in Evaluating Aircraft Flyover Noise. Soc. of Automotive Engrs., ARP 866, Aug. 31, 1964.

2. Federal Aviation Administration, Department of Transportation: Noise Standards, Aircraft Type Certification (Notice of Proposed Rule Making 69-1). Federal Register (34 F.R.453), Jan. 11, 1969.

TABLE I.–SUMMARY OF ACOUSTIC TEST DATA

Condition			Baseline	Treated	Reduction
Landing approach 5000-lb thrust 1 n. mi. point	Varied weather conditions	PNdB EPNdB	122 117.5	107.5 104.5	14.5 13
	70% RH; 59° F	PNdB EPNdB	123.5 119.5	107.5 104	16 15.5
Landing approach 6500-lb thrust 1 n. mi. point	Varied weather conditions	PNdB EPNdB	123.5 119	109 105.5	14.5 13.5
	70% RH; 59° F	PNdB EPNdB	124 120	109.5 105.5	14.5 14.5
Takeoff maximum power 3.5 n. mi. point	Varied weather conditions	PNdB EPNdB	114 110.5	111.5 109.0	2.5 1.5
	70% RH; 59° F	PNdB EPNdB	116.5 114	112.5 110.5	4.0 3.5
Takeoff with cutback 12 400-lb thrust 3.5 n. mi. point	Varied weather conditions	PNdB EPNdB	112 108.5	108.5 106	3.5 2.5
	70% RH; 59° F	PNdB EPNdB	115.5 113.0	109 108.5	6.5 4.5
Takeoff with cutback 9200-lb thrust 3.5 n. mi. point	Varied weather conditions	PNdB EPNdB	98.5 96.5	93 93	5.5 3.5
	70% RH; 59° F	PNdB EPNdB	104.0 101.5	95 95	9.0 6.5
Maximum sideline noise takeoff power 1500-ft sideline	Varied weather conditions	PNdB EPNdB	108 107	104.5 104	3.5 3.0
	70% RH; 59° F	PNdB EPNdB	110 110	105.5 105.5	4.5 4.5

TABLE II.—INLET LOSS BREAKDOWN, FLIGHT TESTS

Condition	Inlet components	Loss in inlet pressure recovery, $(P_{T_1}-P_{T_2})/P_{T_1}$	Total loss, percent
Cruise	Cowl wall and lip	0.004	31
35 000-ft alt	Outer ring	0.005	.38
0.8 Mach	Inner ring	0.003	23
	Struts	0.001	8
	Centerbody	0.0	0

TABLE III.—INLET ACOUSTICAL LINING DESIGN PARAMETERS

Item	Outer wall	Outer ring	Inner ring	Centerbody
Acoustic treatment depth, in.	0.6	0.3/0.3	0.6/0.3	0.6
Honeycomb cell size, in.	3/8	3/8	3/8	3/8
Nominal flow resistance, $R_{(nom)}$, rayls (cgs)	11 ± 2	11 ± 2	11 ± 2	11 ± 2
Peak frequency, Hz	2400 to 2800	2400 to 2800	2400 to 2800	2400 to 2800
Area treated, ft^2	30.3	25.0	11.9	4.4
Treatment separation, in.	5 to 6	5 to 6	5 to 6	5 to 6

TABLE IV.—INLET LOSS BREAKDOWN, GROUND CALIBRATION TESTS

Condition	Inlet components	Loss in inlet pressure recovery, $P_{amb}-P_{T_2}/P_{amb}$	Total loss, percent
Ground static test at 480 lb/sec airflow	Cowl wall and lip	0.014	52
	Outer ring	0.007	26
	Inner ring	0.004	15
	Struts	0.002	7
	Centerbody	0.0	0
	Total	0.027	100
Ground static test at 480 lb/sec airflow with bellmouth lip installed	Cowl wall and lip	0.007	37
	Outer ring	0.006	32
	Inner ring	0.004	21
	Struts	0.002	10
	Centerbody	0.0	0
	Total	0.019	100

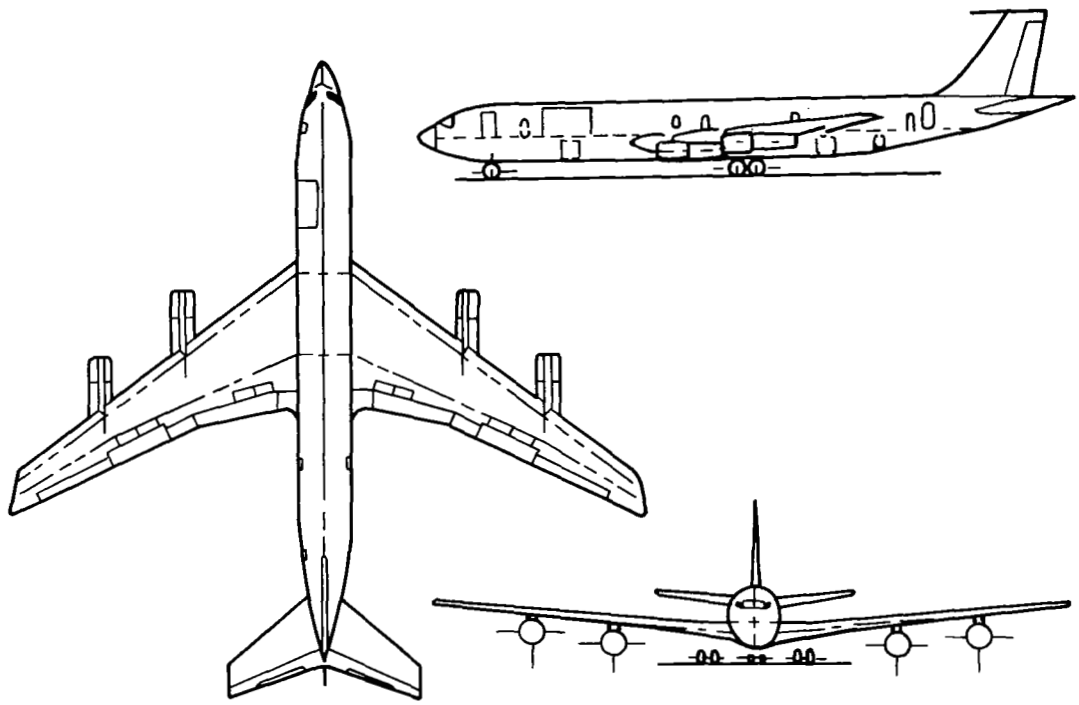

Dimensions	
Body length	145 ft, 6 in.
Wingspan	145 ft, 9 in.
Wing sweepback	35°
Horizontal tail span	45 ft, 9 in.

Engines		
Pratt & Whitney JT3D-7 turbofan		
Takeoff thrust	19 000 lb	to 84° F
Max. continuous thrust	17 200 lb	
Max. cruise thrust	15 500 lb	
Idle thrust	800 lb	

FIGURE 1.—TEST AIRPLANE DESCRIPTION, 707-320B/C SERIES

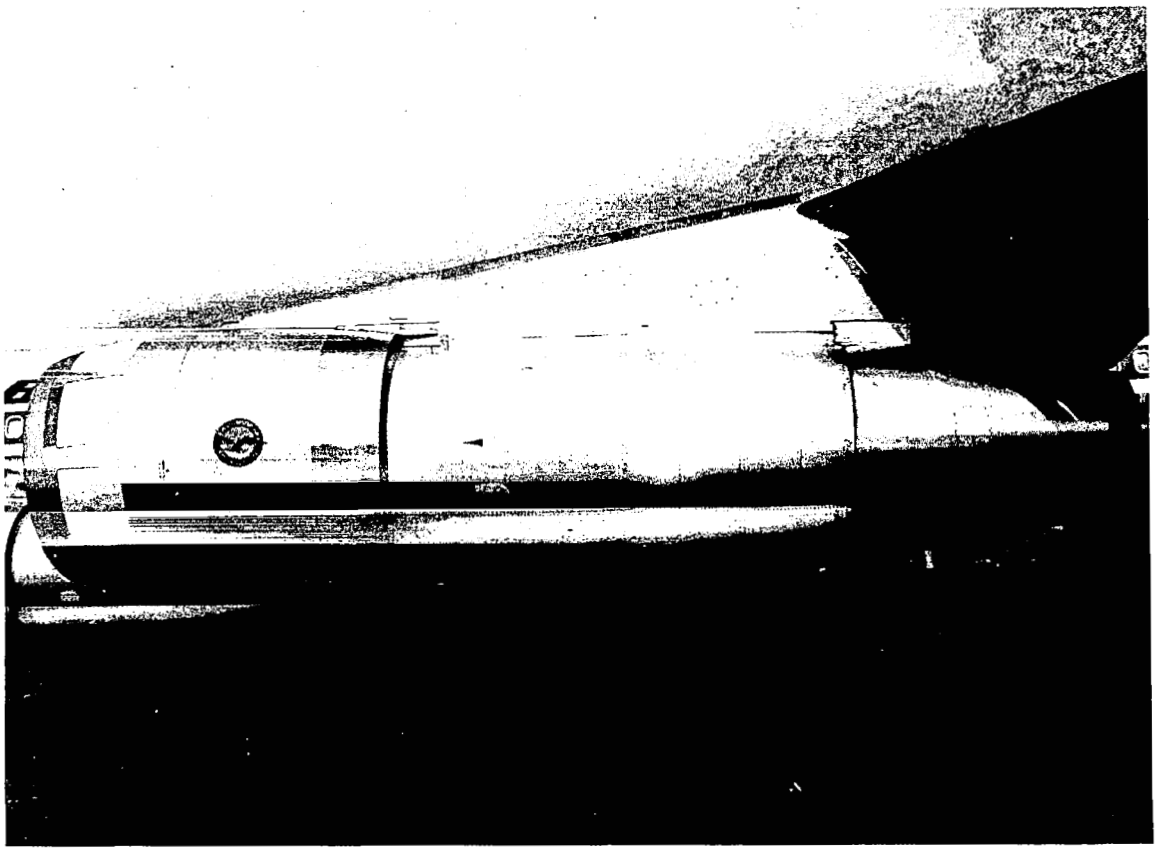

FIGURE 2.—707-320B/C EXISTING NACELLE (BASELINE)

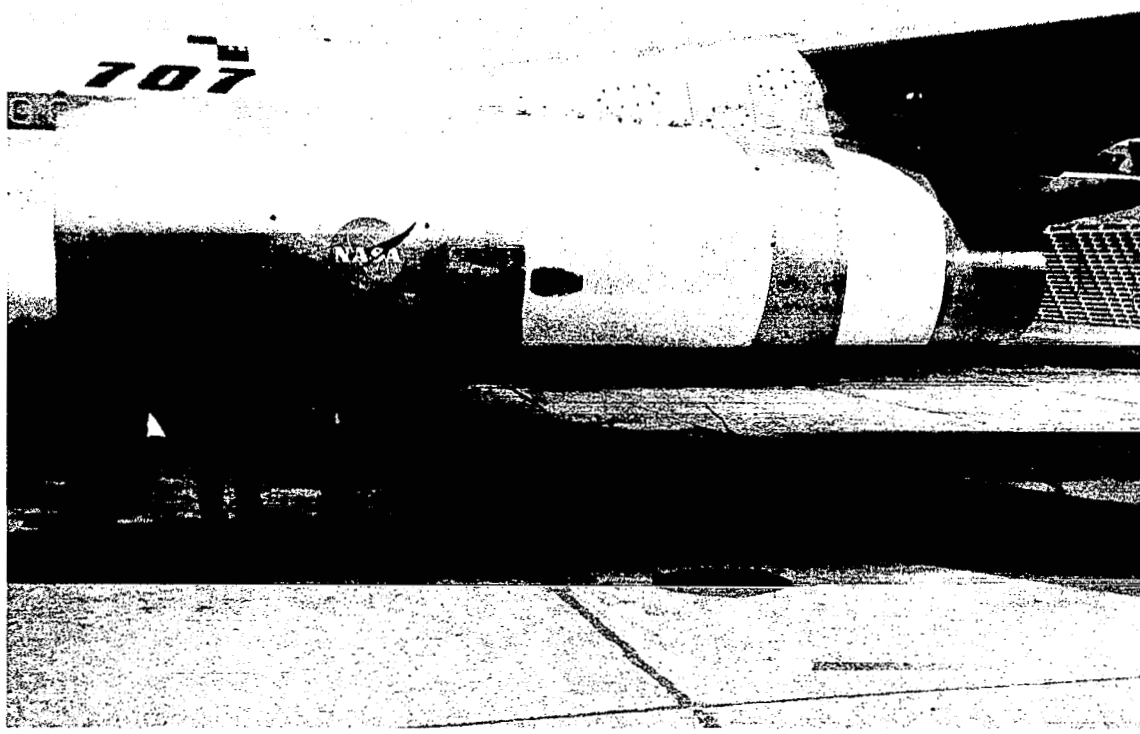

FIGURE 3.—TREATED NACELLE CONFIGURATION

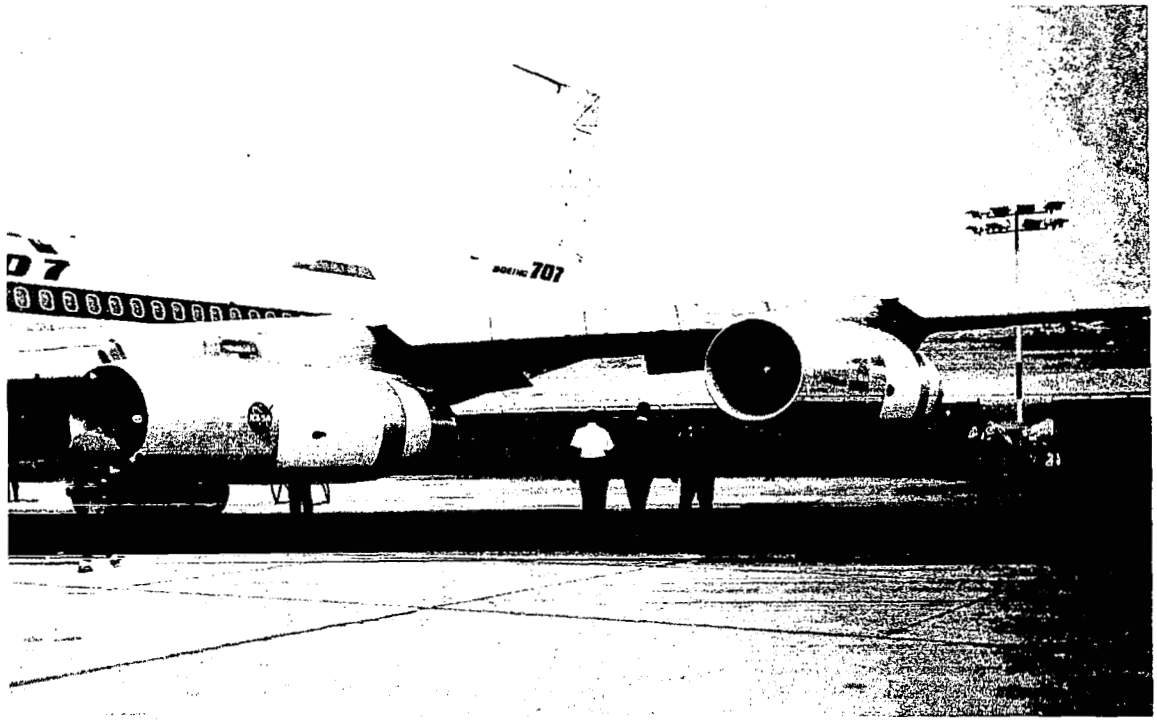

FIGURE 4.—TREATED NACELLE INSTALLATION ON THE TEST AIRPLANE

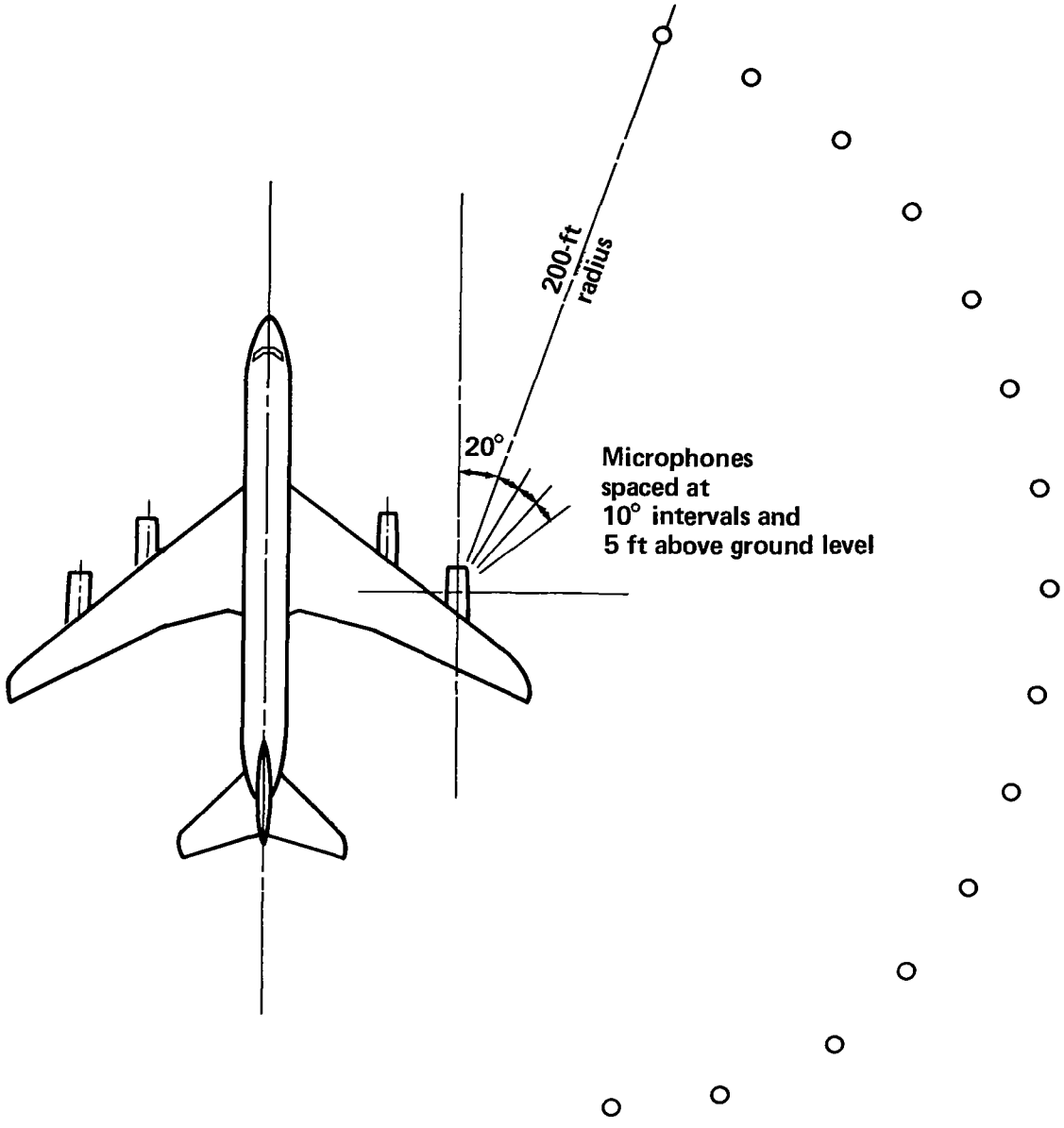

FIGURE 5.–ACOUSTIC TEST RANGE FOR GROUND TESTS AT MOSES LAKE

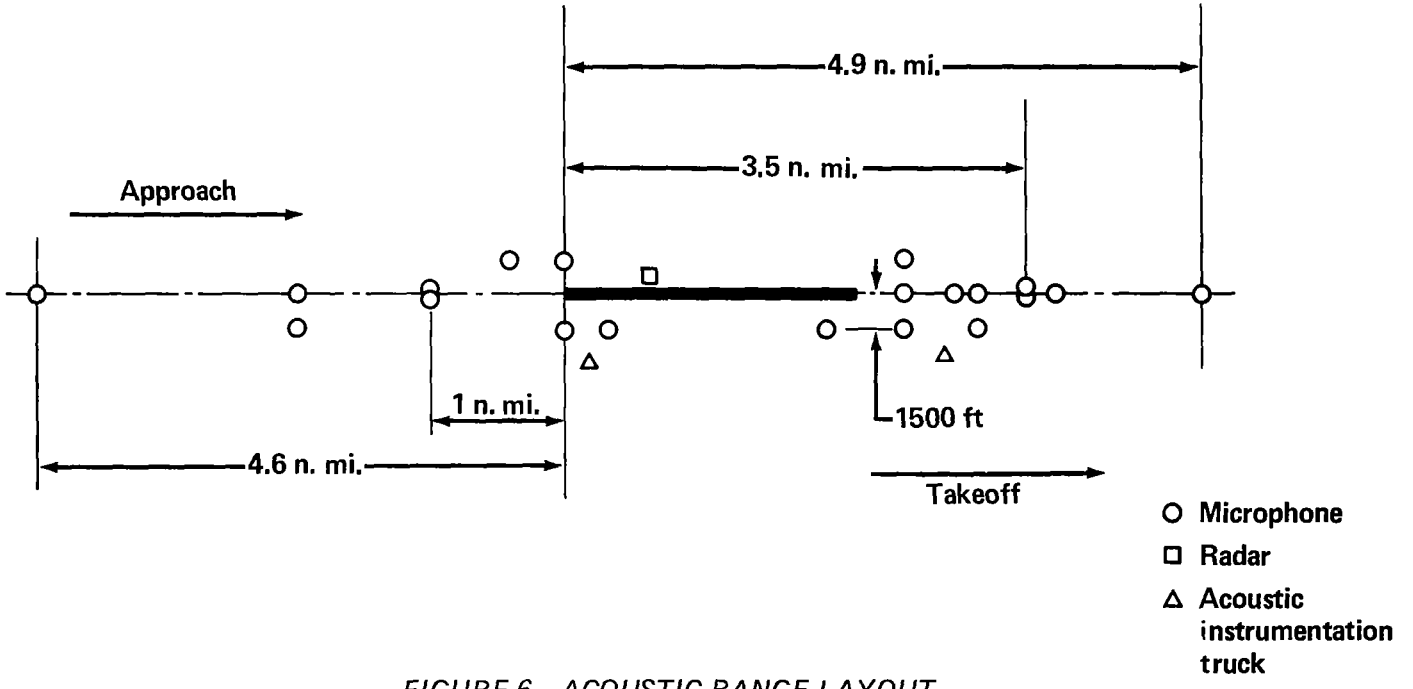

FIGURE 6.–ACOUSTIC RANGE LAYOUT

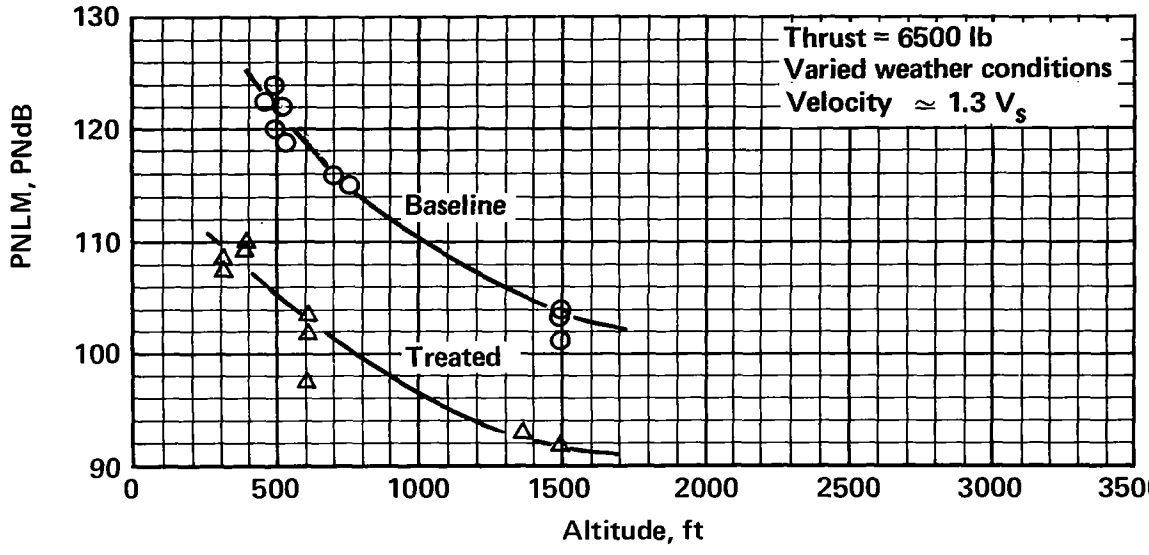

FIGURE 7.–PERCEIVED NOISE AS MEASURED UNDER FLIGHTPATH DURING LANDING APPROACH

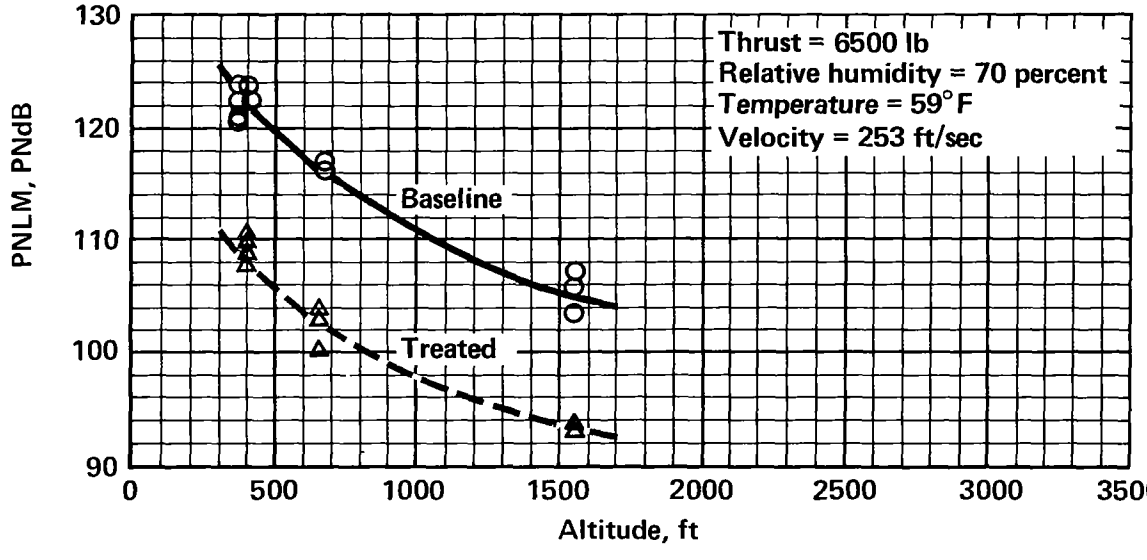

FIGURE 8.–STANDARDIZED PERCEIVED NOISE UNDER FLIGHTPATH DURING LANDING APPROACH

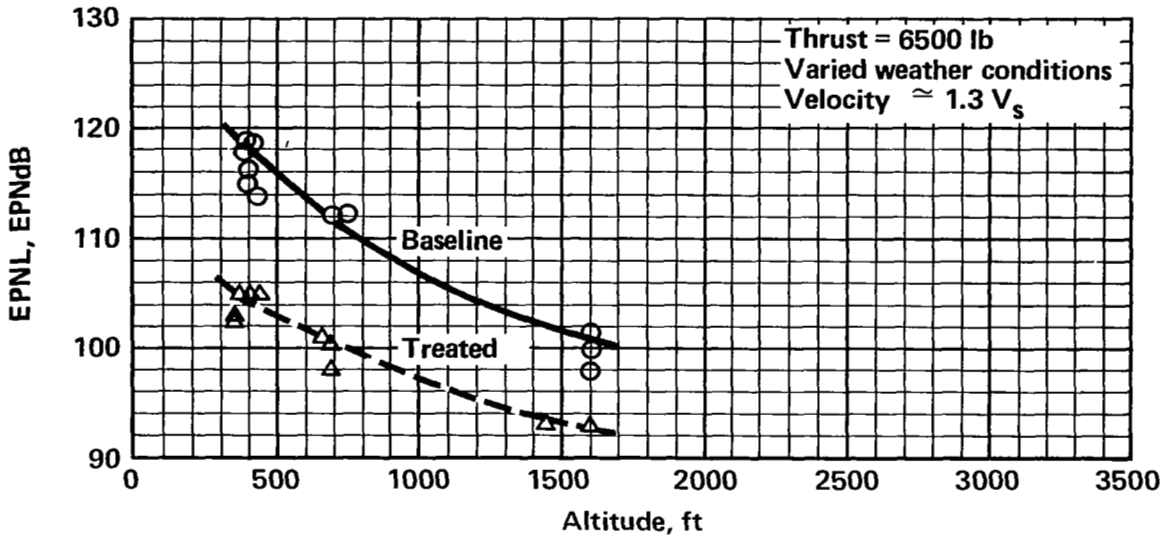

FIGURE 9.–EFFECTIVE PERCEIVED NOISE AS MEASURED UNDER FLIGHTPATH DURING LANDING APPROACH

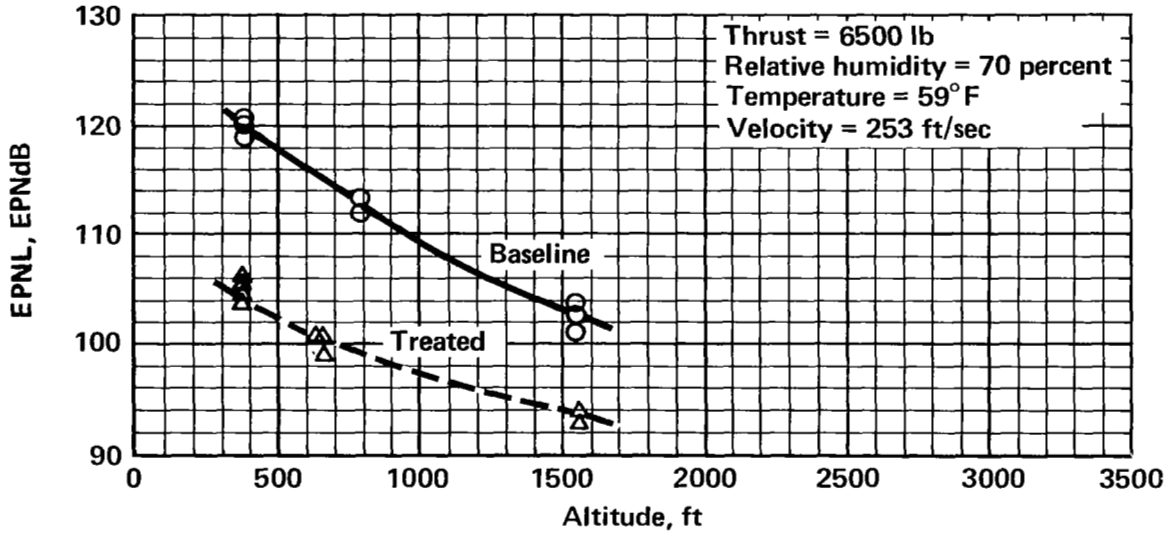

FIGURE 10.–STANDARDIZED EFFECTIVE PERCEIVED NOISE UNDER FLIGHTPATH DURING LANDING APPROACH

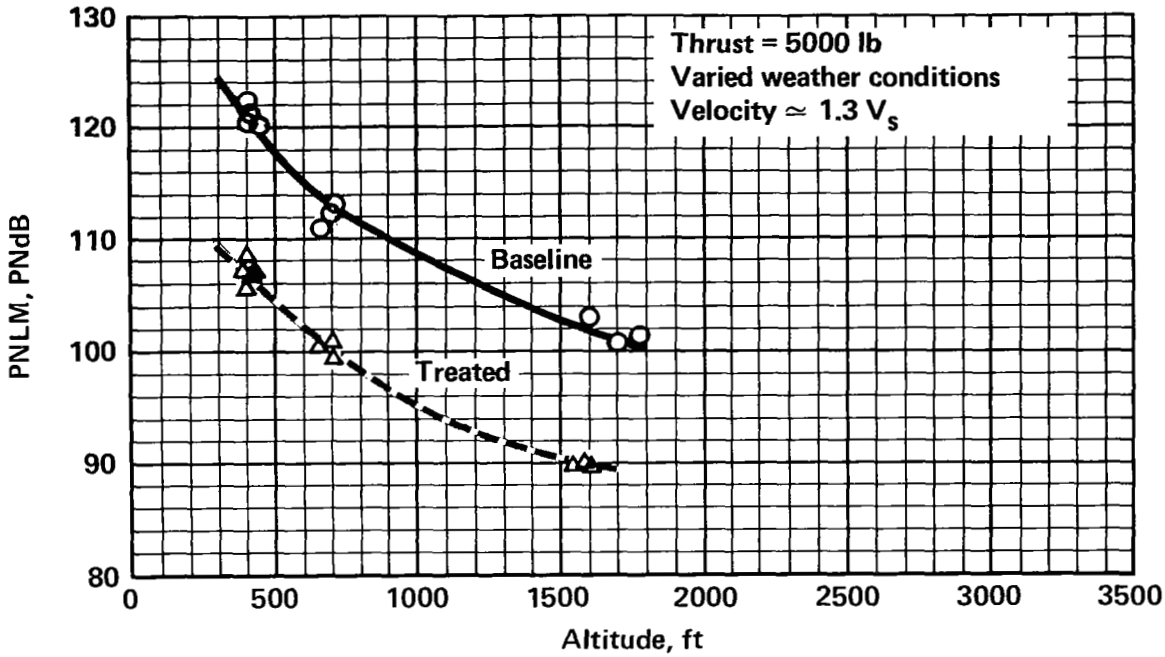

FIGURE 11.–PERCEIVED NOISE AS MEASURED UNDER FLIGHTPATH DURING LANDING APPROACH

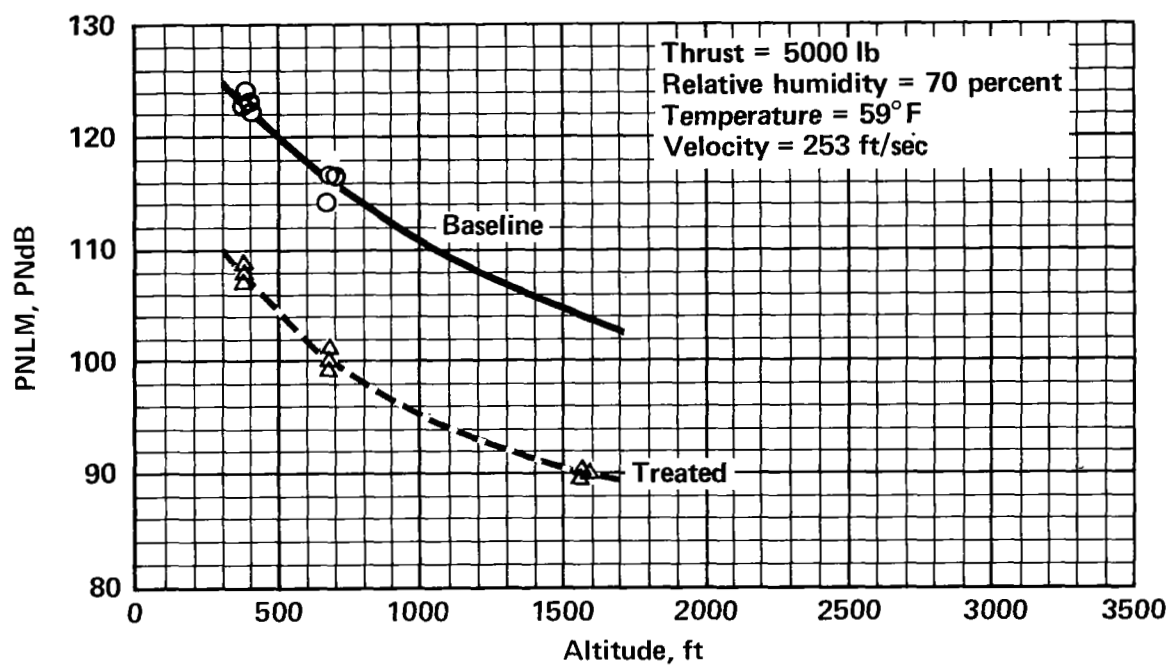

FIGURE 12.–STANDARDIZED PERCEIVED NOISE UNDER FLIGHTPATH DURING LANDING APPROACH

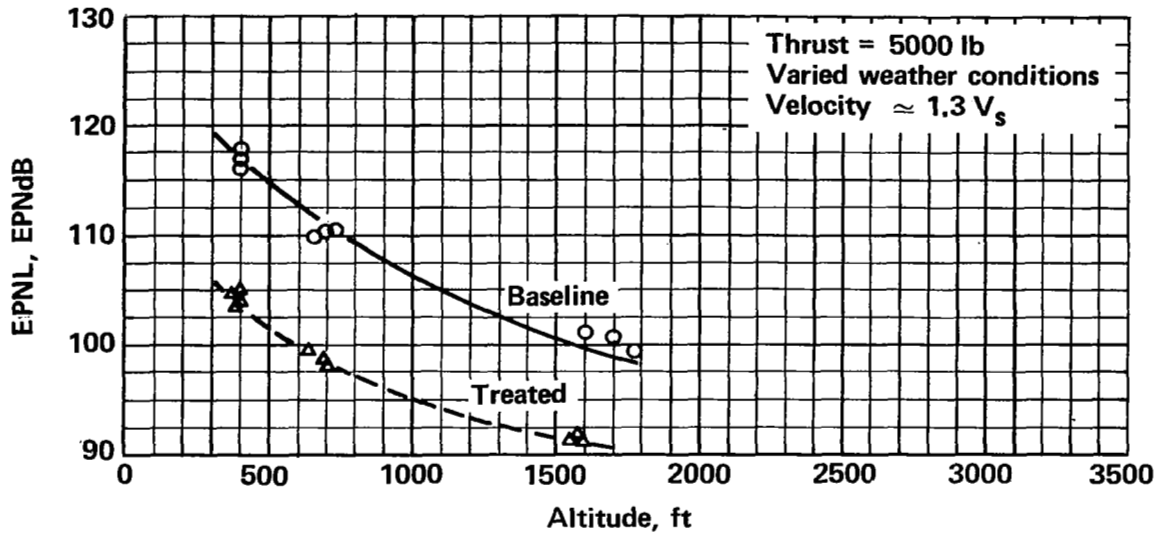

FIGURE 13.–EFFECTIVE PERCEIVED NOISE AS MEASURED UNDER FLIGHTPATH DURING LANDING APPROACH

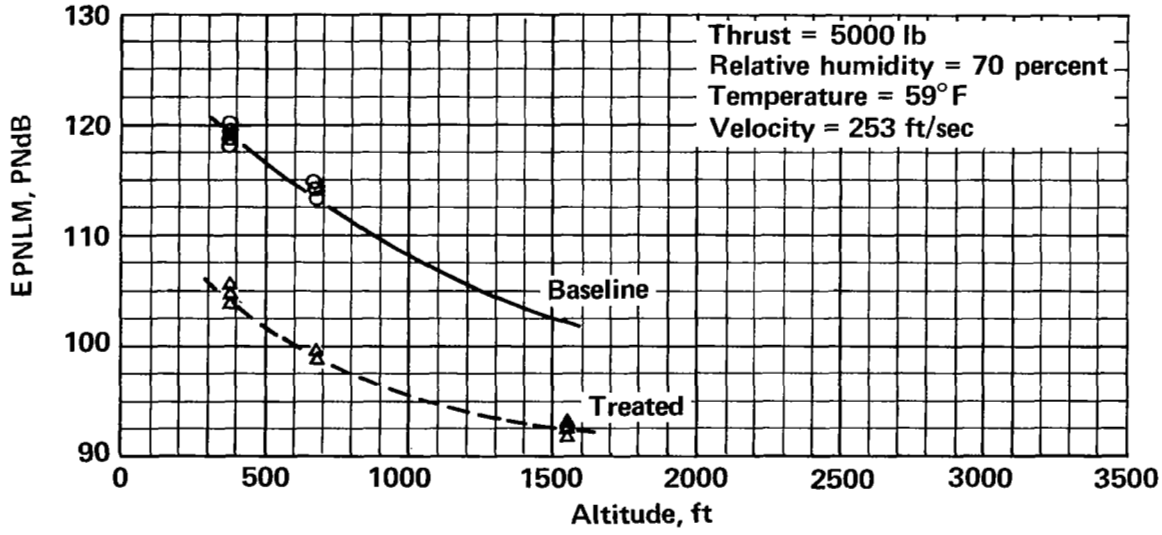

FIGURE 14.–STANDARDIZED EFFECTIVE PERCEIVED NOISE UNDER FLIGHTPATH DURING LANDING APPROACH

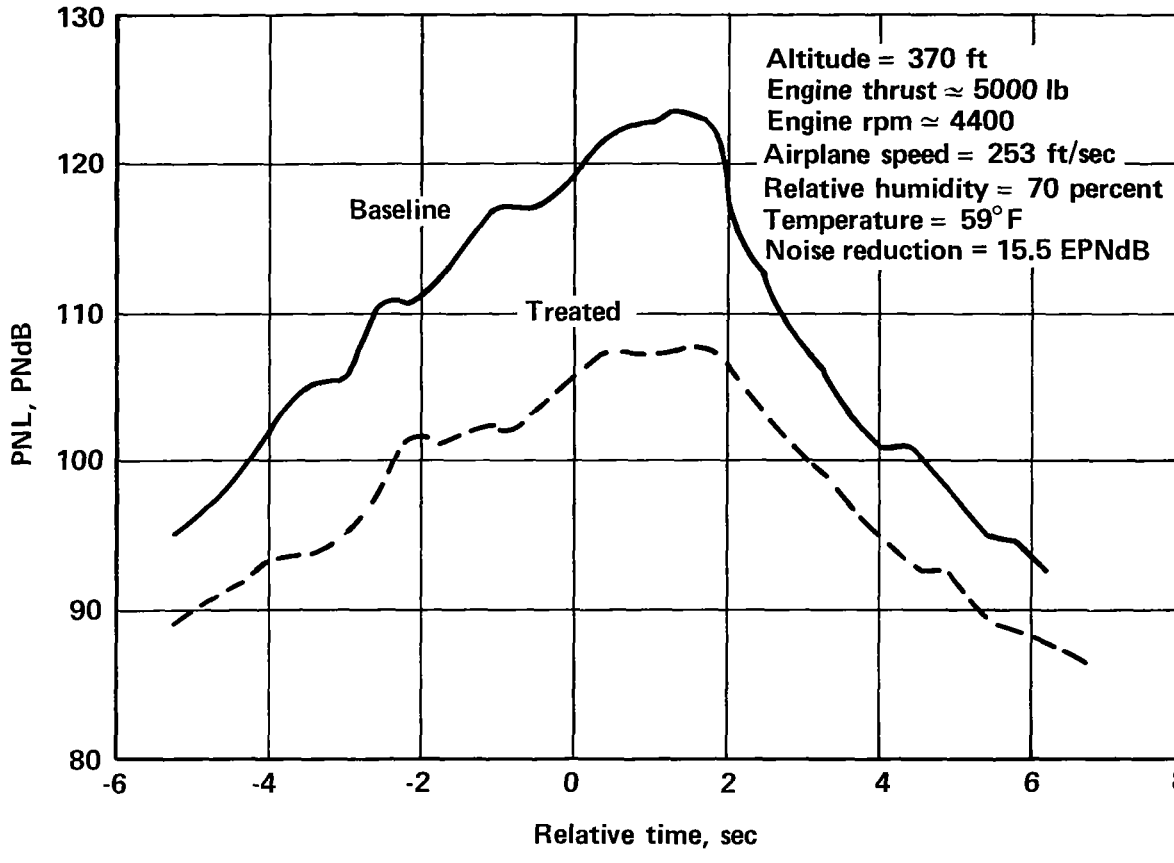

FIGURE 15.–PERCEIVED NOISE TIME HISTORY DURING LANDING APPROACH

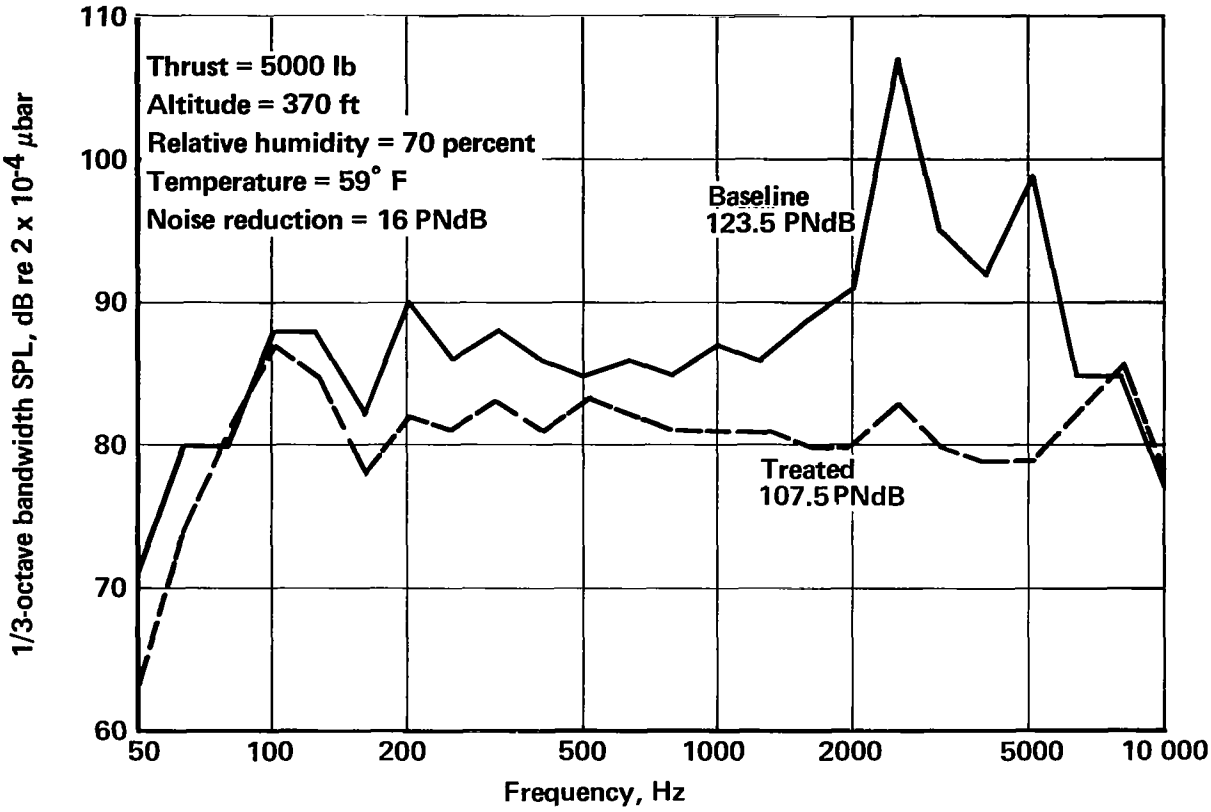

FIGURE 16.–MAXIMUM PERCEIVED NOISE SPECTRA DURING LANDING APPROACH

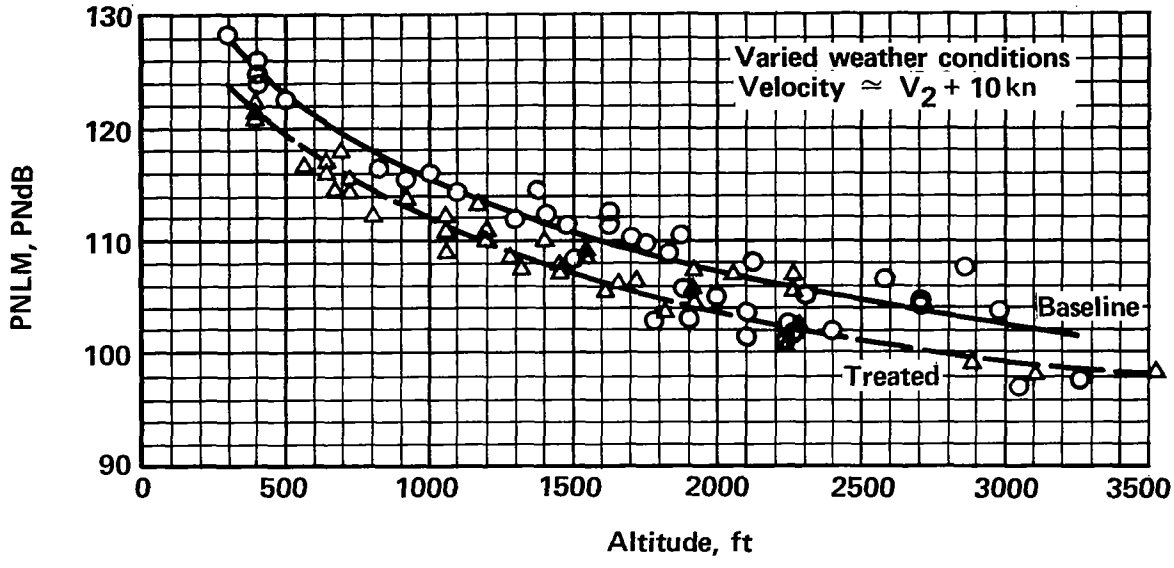

FIGURE 17.–PERCEIVED NOISE AS MEASURED UNDER FLIGHTPATH AT TAKEOFF POWER

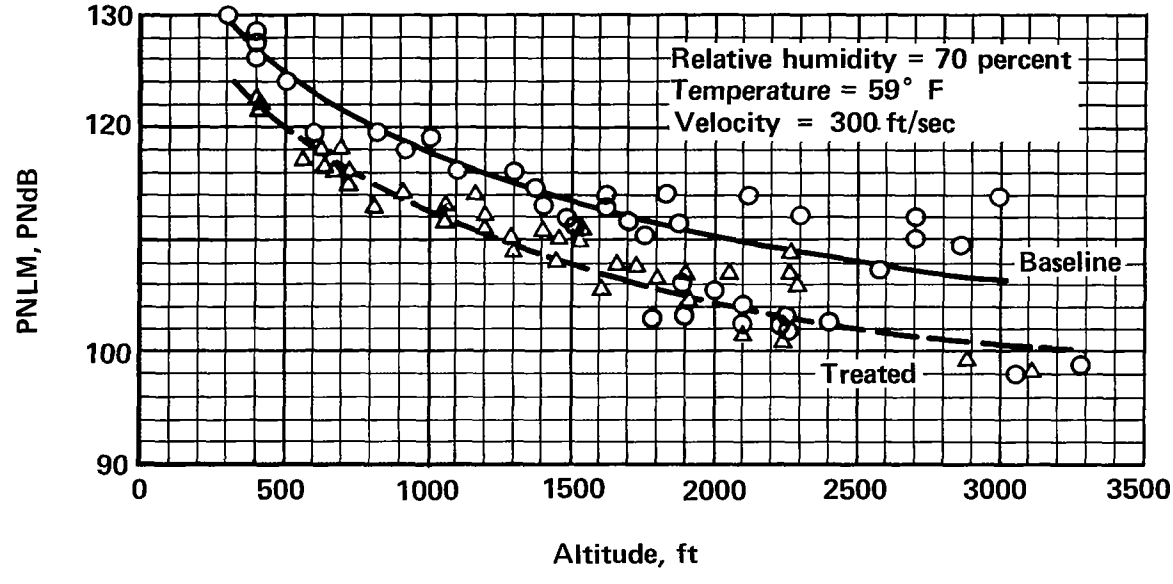

FIGURE 18.–STANDARDIZED PERCEIVED NOISE UNDER FLIGHTPATH AT TAKEOFF POWER

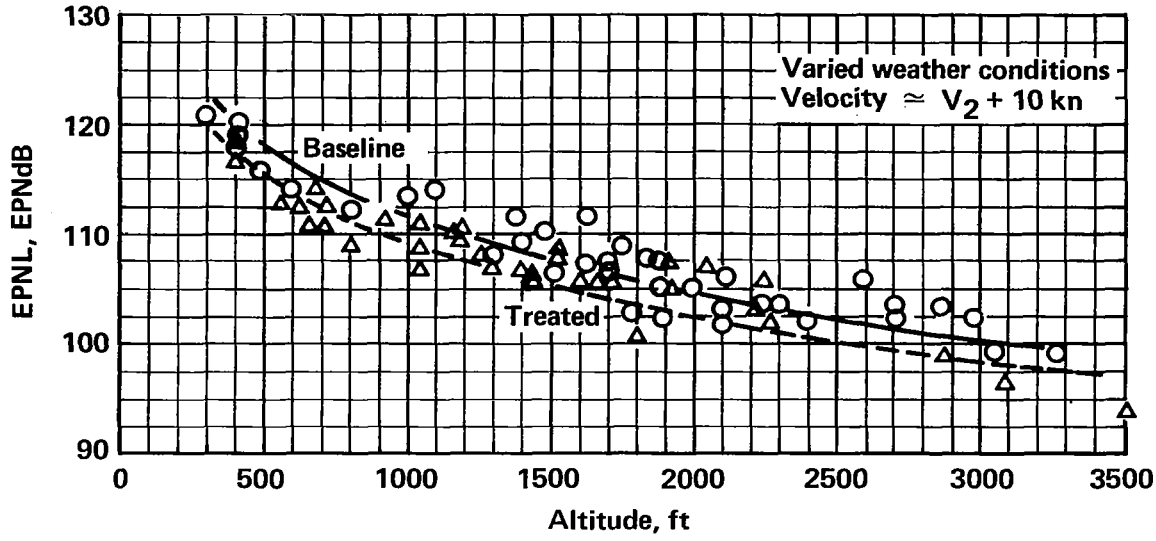

FIGURE 19.–EFFECTIVE PERCEIVED NOISE AS MEASURED UNDER FLIGHTPATH AT TAKEOFF POWER

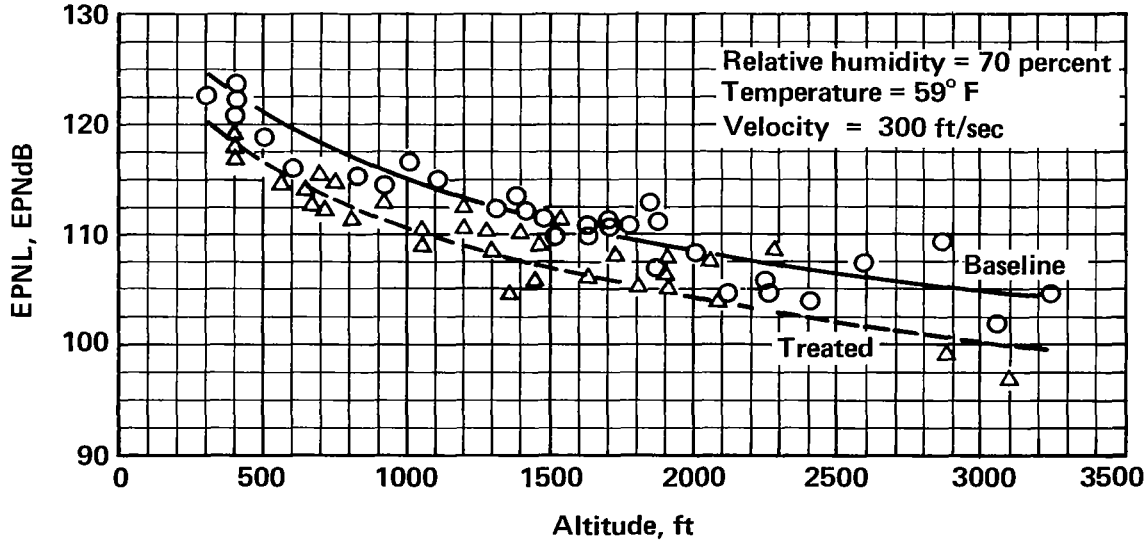

FIGURE 20.–STANDARDIZED EFFECTIVE PERCEIVED NOISE UNDER FLIGHTPATH AT TAKEOFF POWER

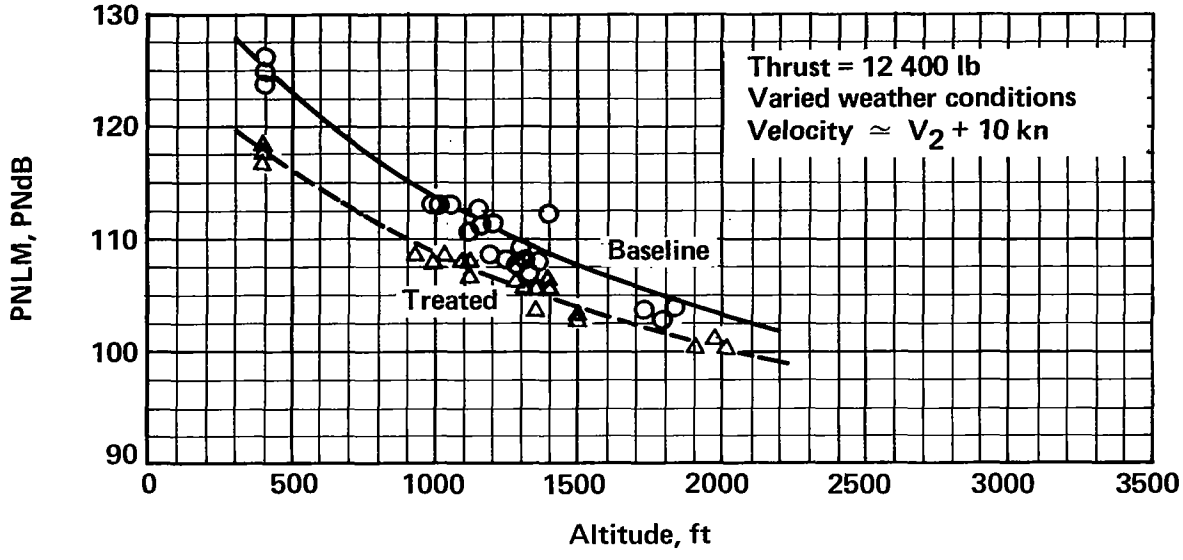

FIGURE 21.–MAXIMUM PERCEIVED NOISE AS MEASURED UNDER FLIGHTPATH AT CUTBACK POWER

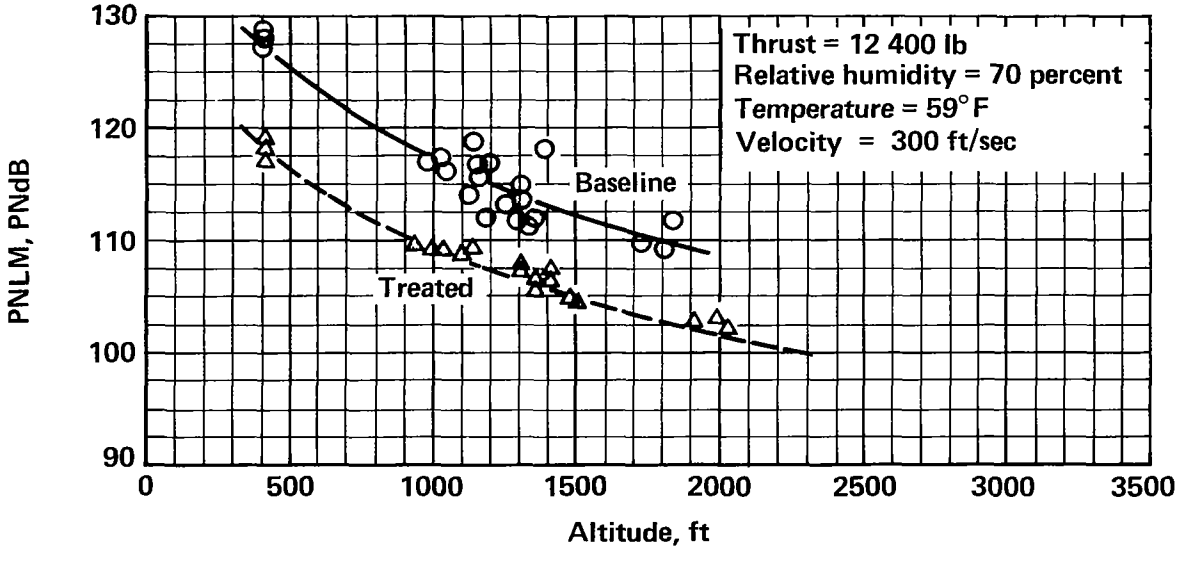

FIGURE 22.–STANDARDIZED MAXIMUM PERCEIVED NOISE UNDER FLIGHTPATH AT CUTBACK POWER

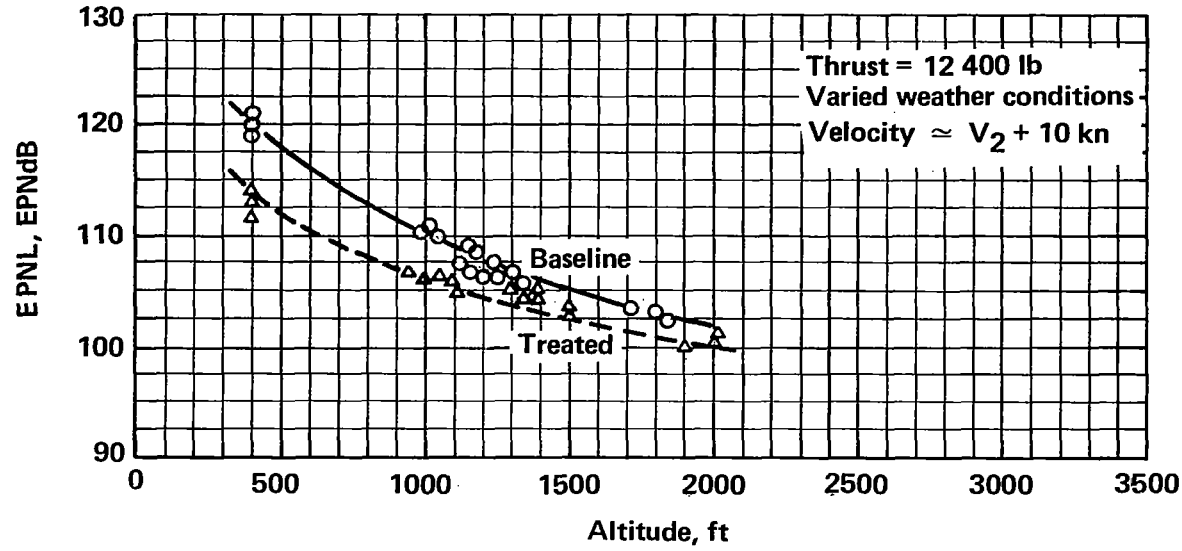

FIGURE 23.—EFFECTIVE PERCEIVED NOISE AS MEASURED UNDER FLIGHTPATH AT CUTBACK POWER

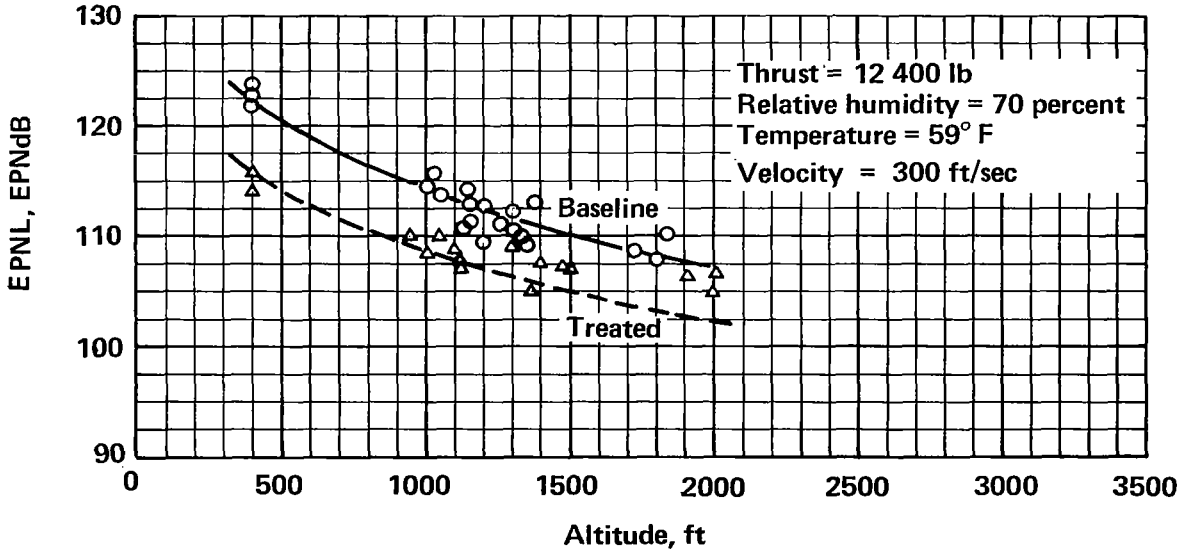

FIGURE 24.—STANDARDIZED EFFECTIVE PERCEIVED NOISE UNDER FLIGHTPATH AT CUTBACK POWER

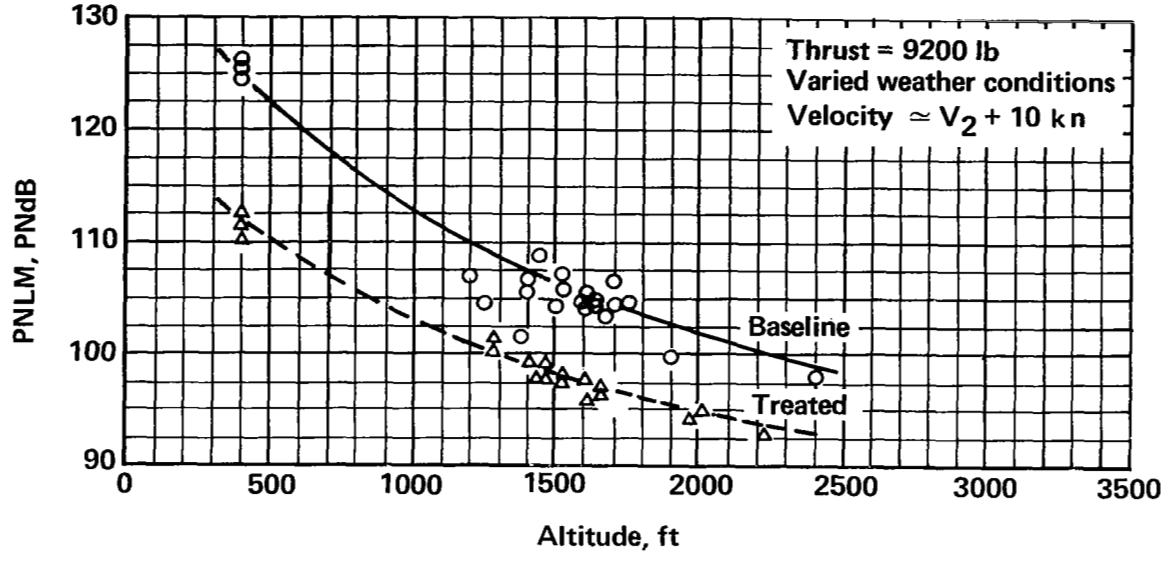

FIGURE 25.–PERCEIVED NOISE AS MEASURED UNDER FLIGHTPATH AT CUTBACK POWER

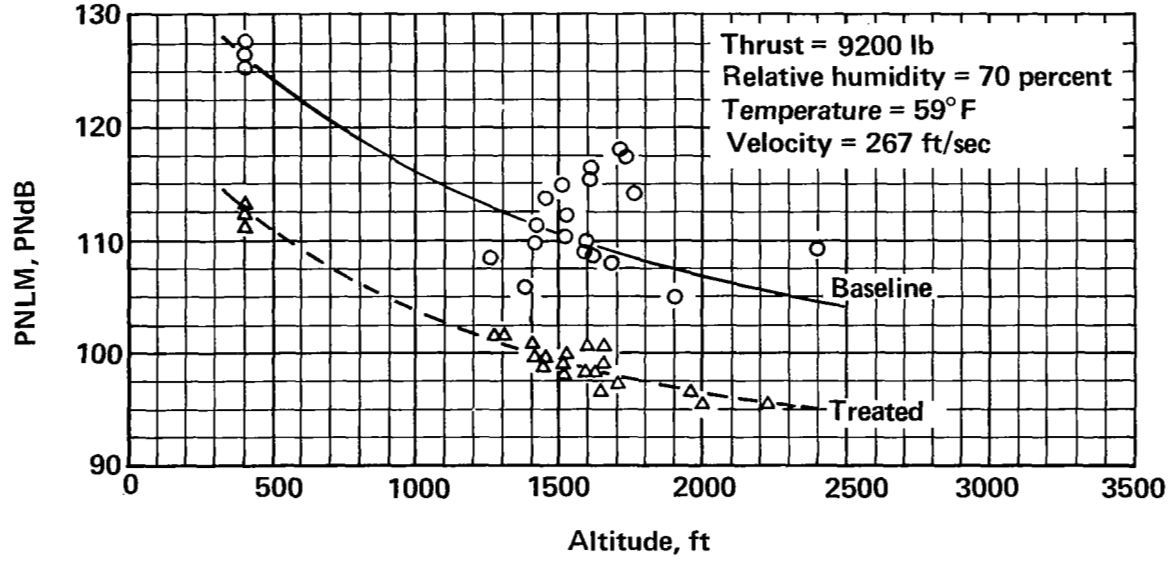

FIGURE 26.–STANDARDIZED PERCEIVED NOISE UNDER FLIGHTPATH AT CUTBACK POWER

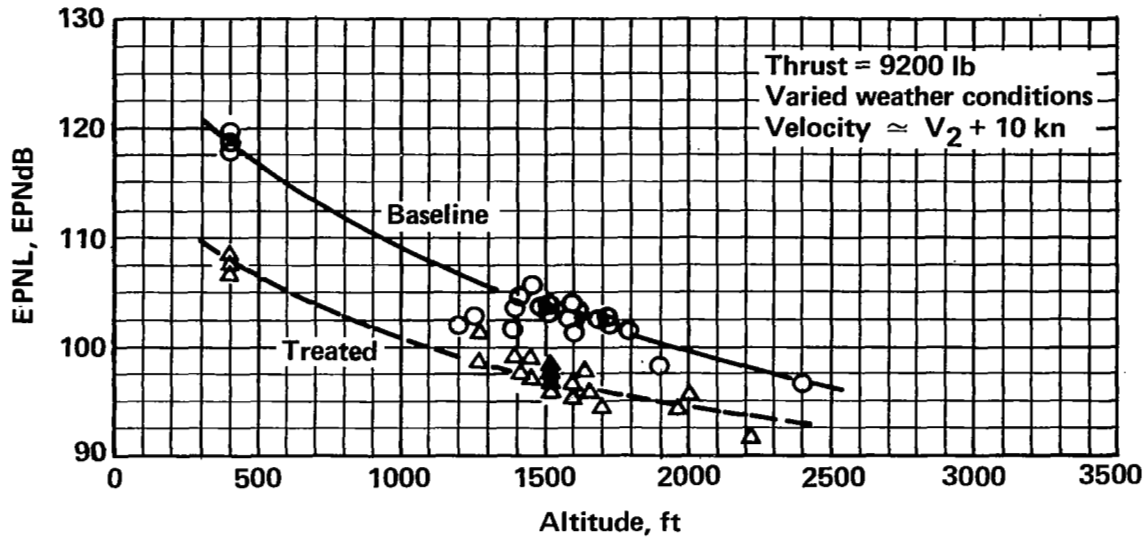

FIGURE 27.–EFFECTIVE PERCEIVED NOISE AS MEASURED UNDER FLIGHTPATH AT CUTBACK POWER

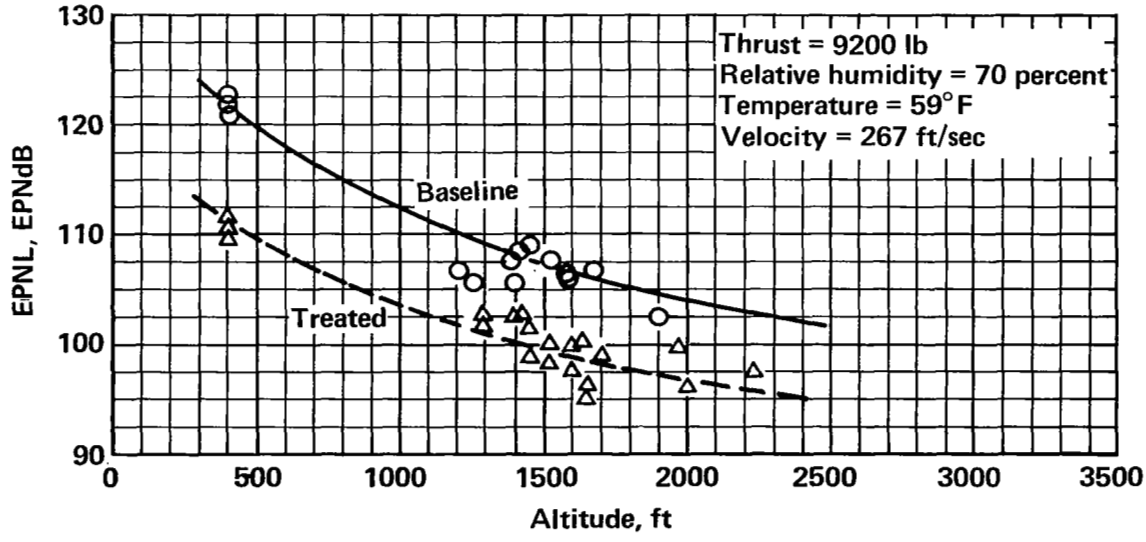

FIGURE 28.–STANDARDIZED EFFECTIVE PERCEIVED NOISE UNDER FLIGHTPATH AT CUTBACK POWER

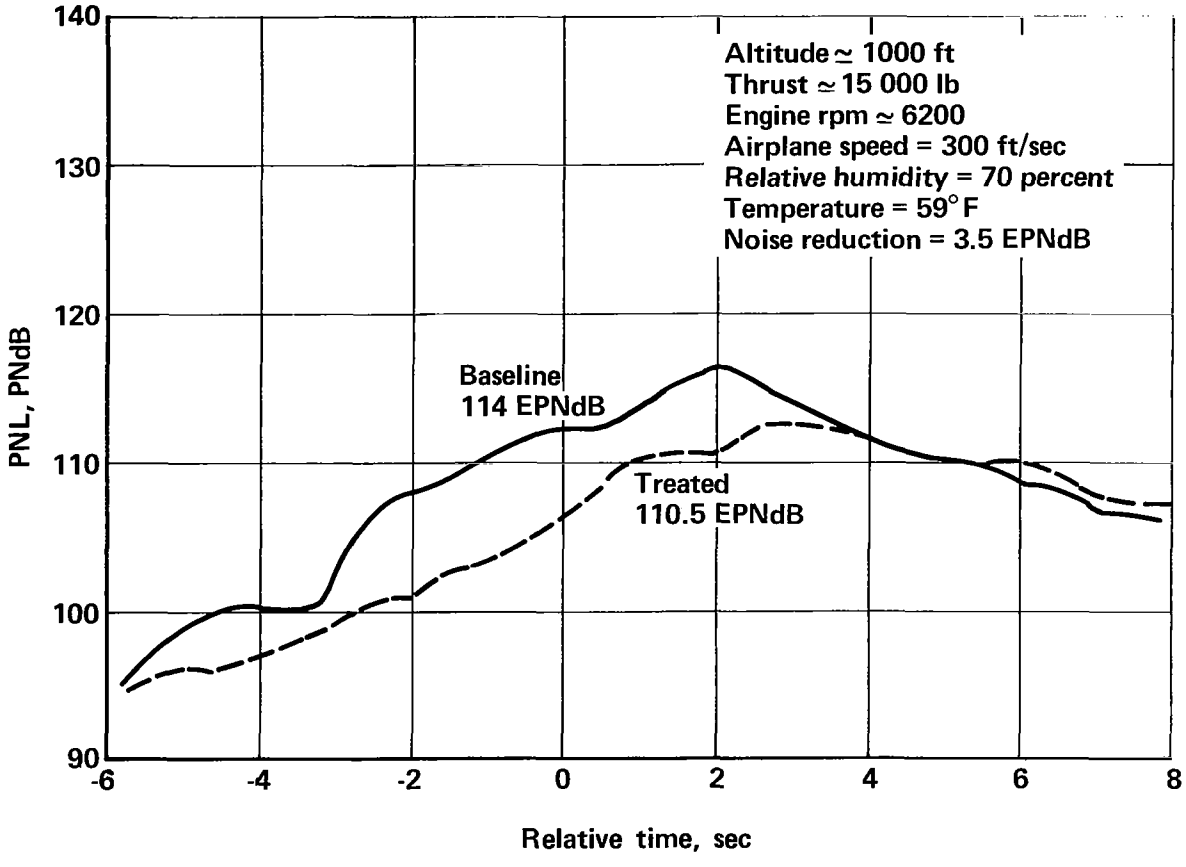

FIGURE 29.–PERCEIVED NOISE TIME HISTORY FOR MAXIMUM GROSS WEIGHT TAKEOFF, 3.5 N. MI. FROM BRAKE RELEASE

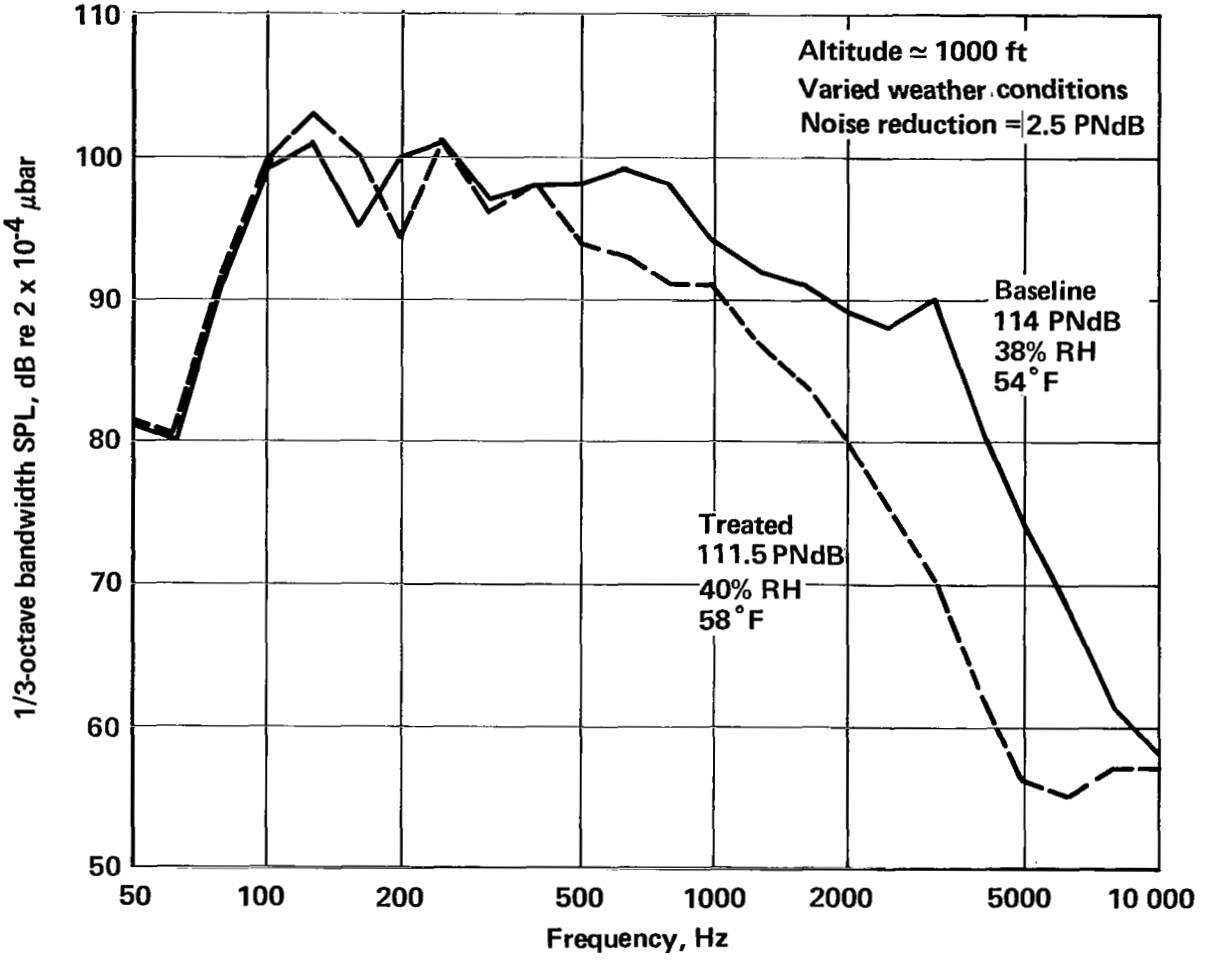

FIGURE 30.–MAXIMUM PERCEIVED NOISE SPECTRA AS MEASURED FOR TAKEOFF POWER

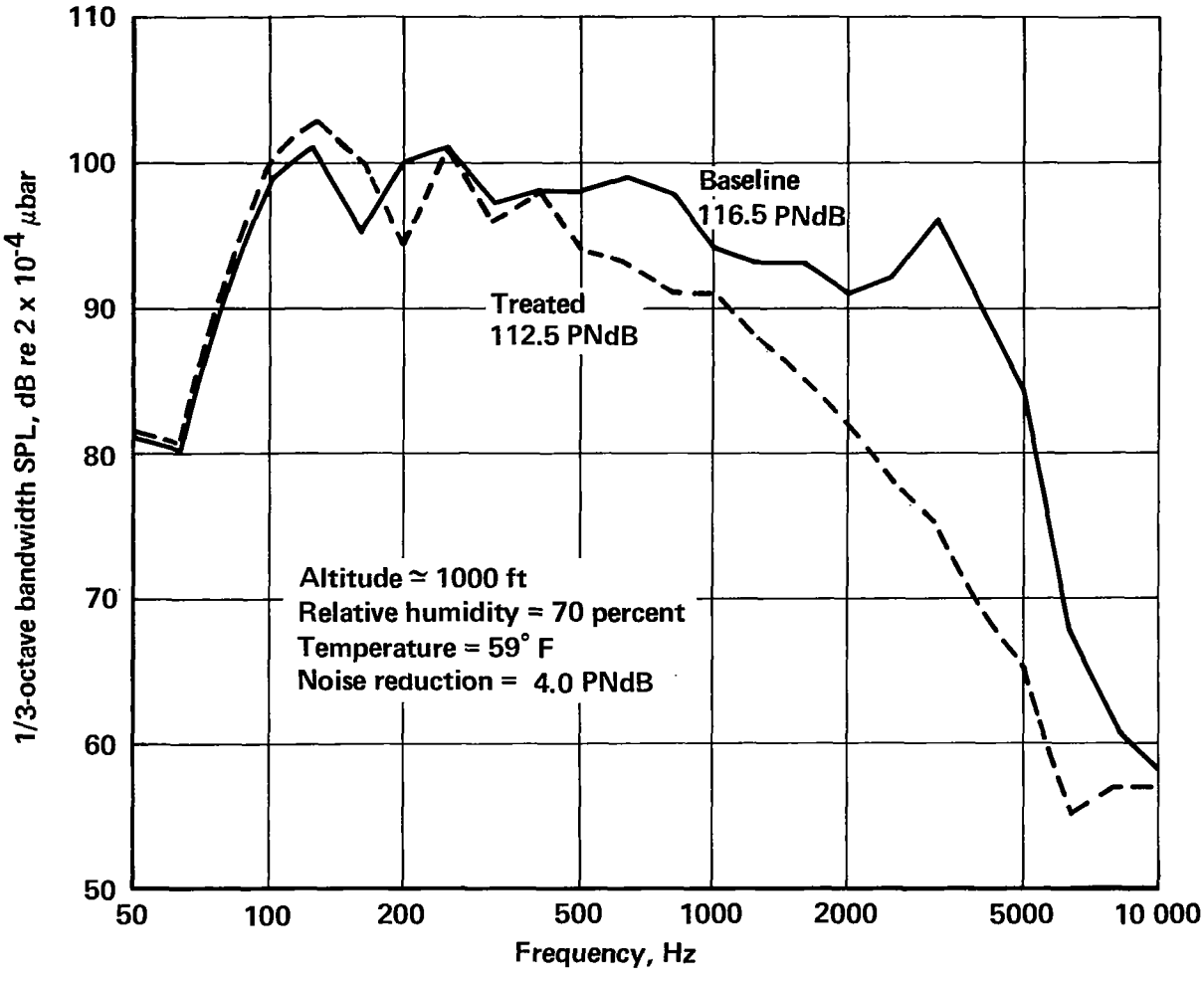

FIGURE 31.—STANDARDIZED MAXIMUM PERCEIVED NOISE SPECTRA FOR TAKEOFF POWER

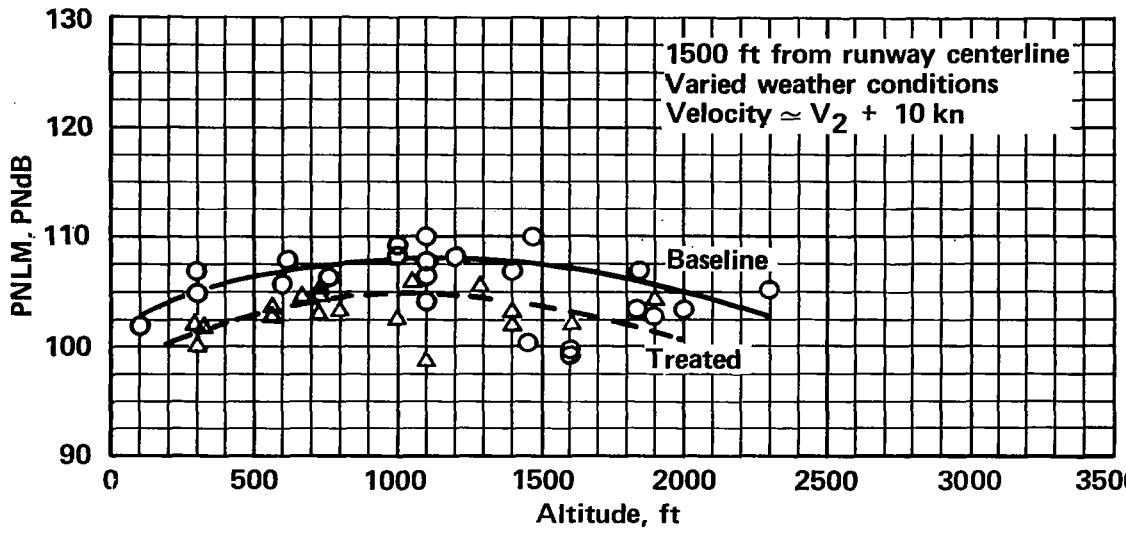

FIGURE 32.–MAXIMUM MEASURED SIDELINE PERCEIVED NOISE

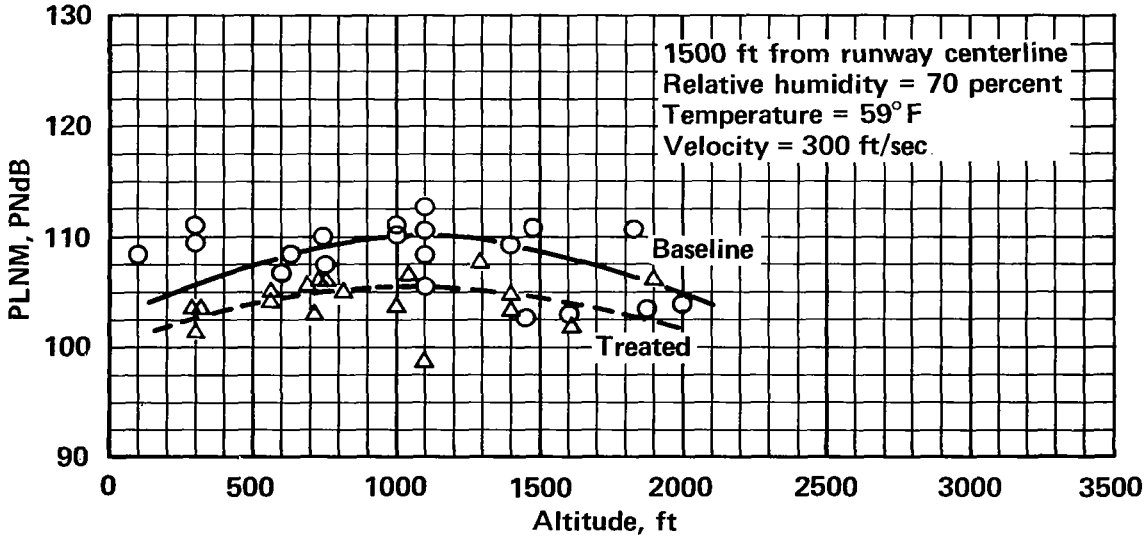

FIGURE 33.–STANDARDIZED MAXIMUM SIDELINE PERCEIVED NOISE

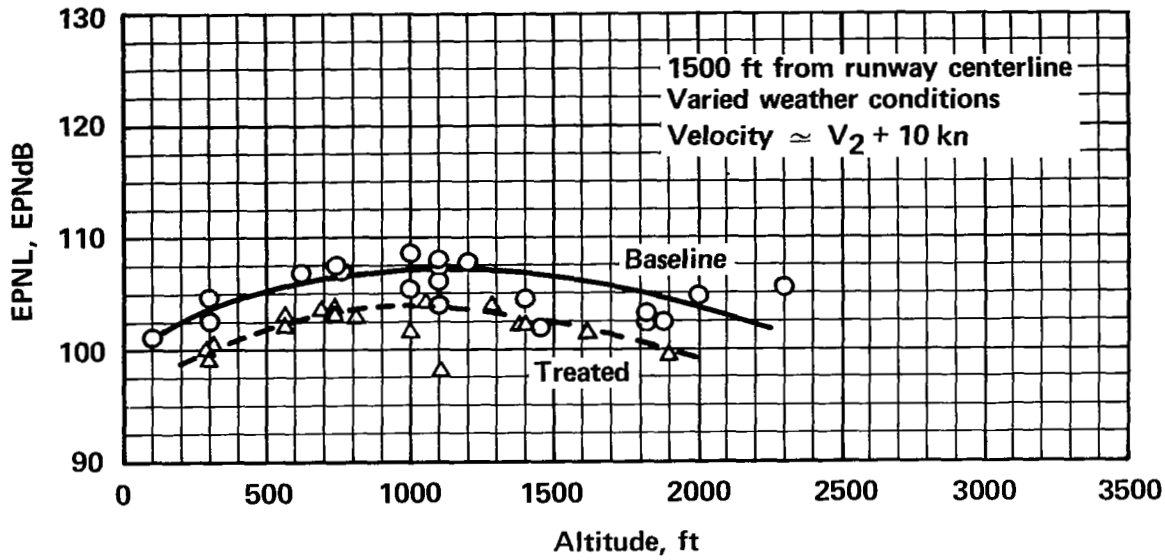

FIGURE 34.–MAXIMUM MEASURED SIDELINE EFFECTIVE PERCEIVED NOISE

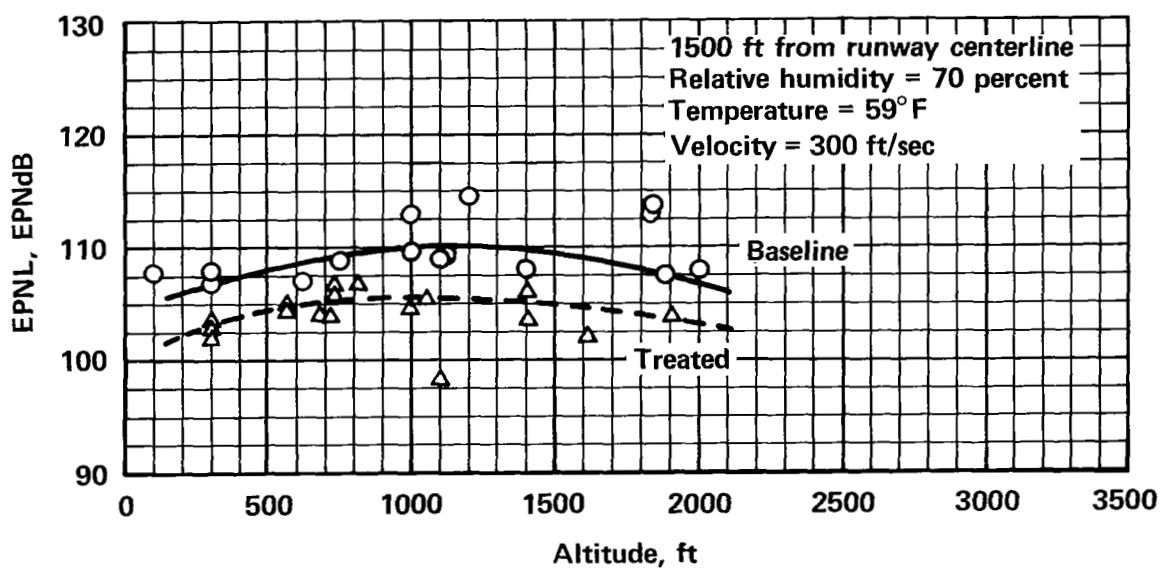

FIGURE 35.–STANDARDIZED MAXIMUM SIDELINE EFFECTIVE PERCEIVED NOISE

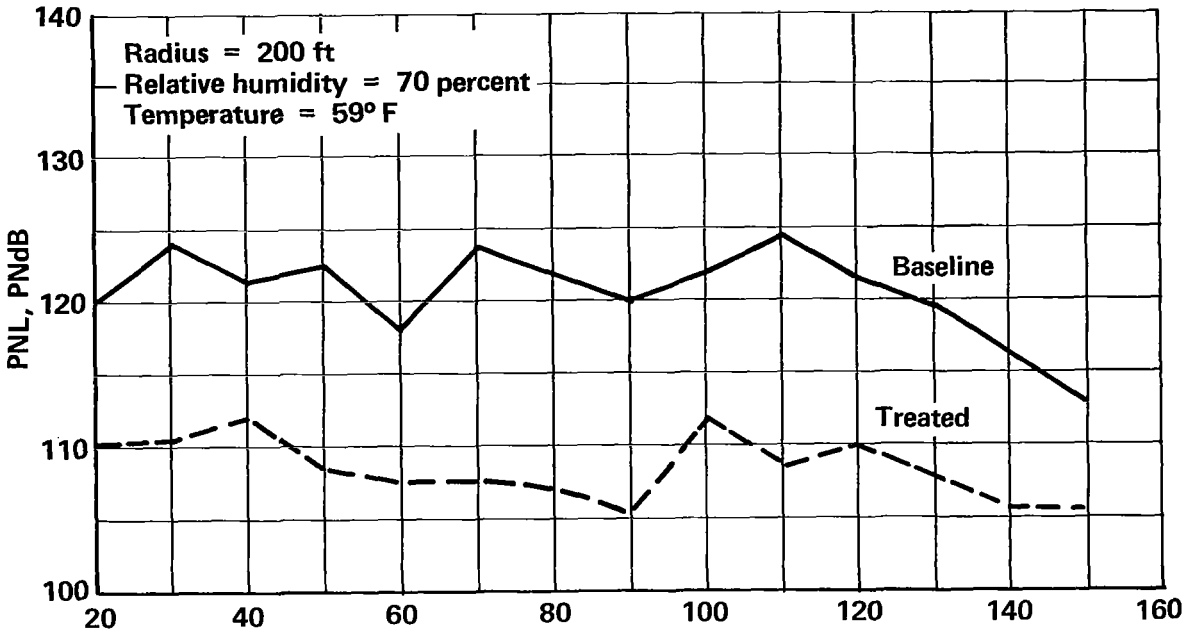

(a) N_1 = 4450 RPM

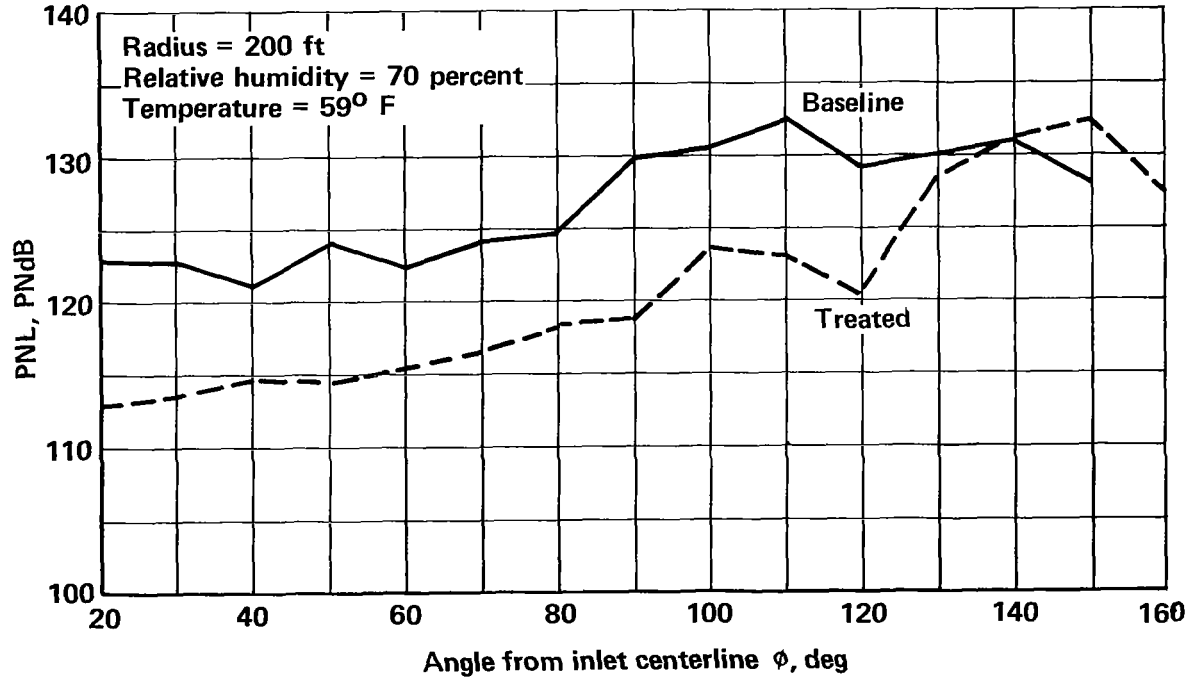

(b) N_1 = 6200 RPM

FIGURE 36.—PERCEIVED NOISE LEVELS AVERAGED FROM THREE GROUND TEST RUNS

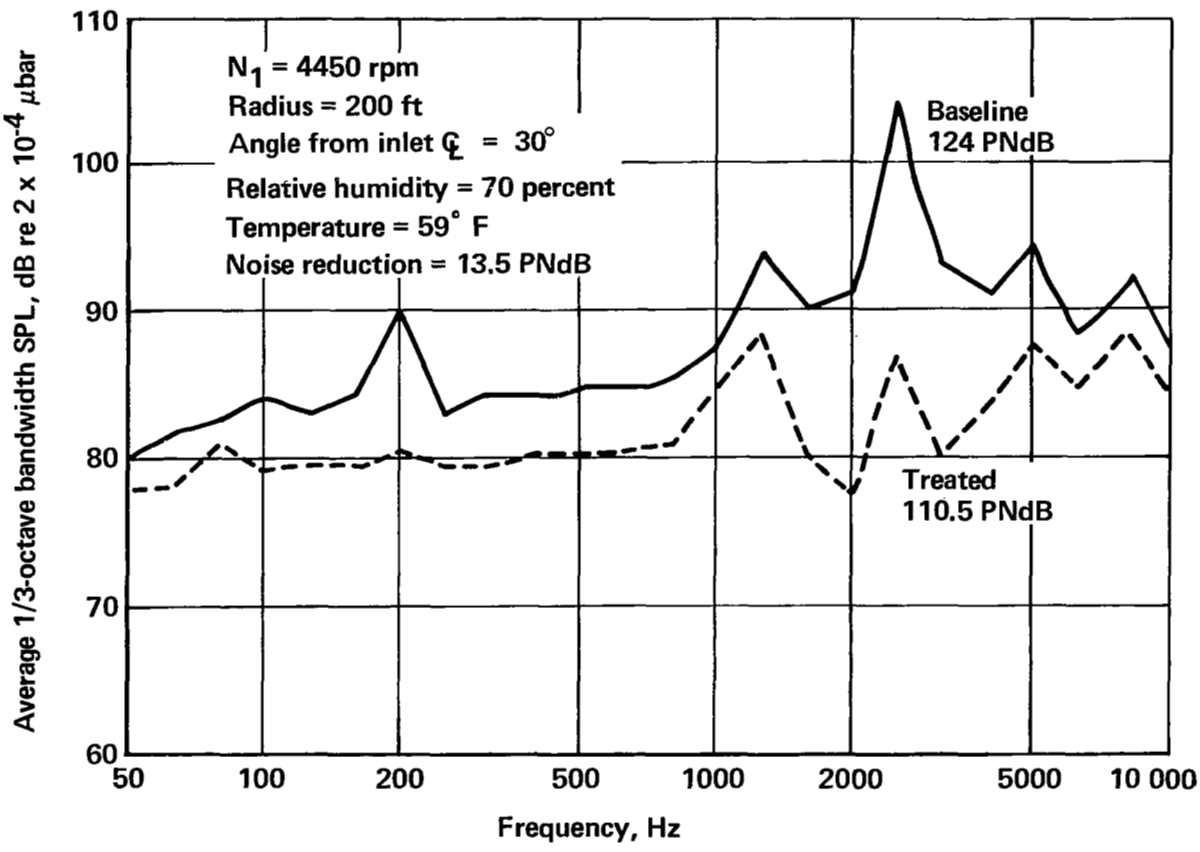

FIGURE 37.–MAXIMUM INLET NOISE AT APPROACH POWER–GROUND TEST

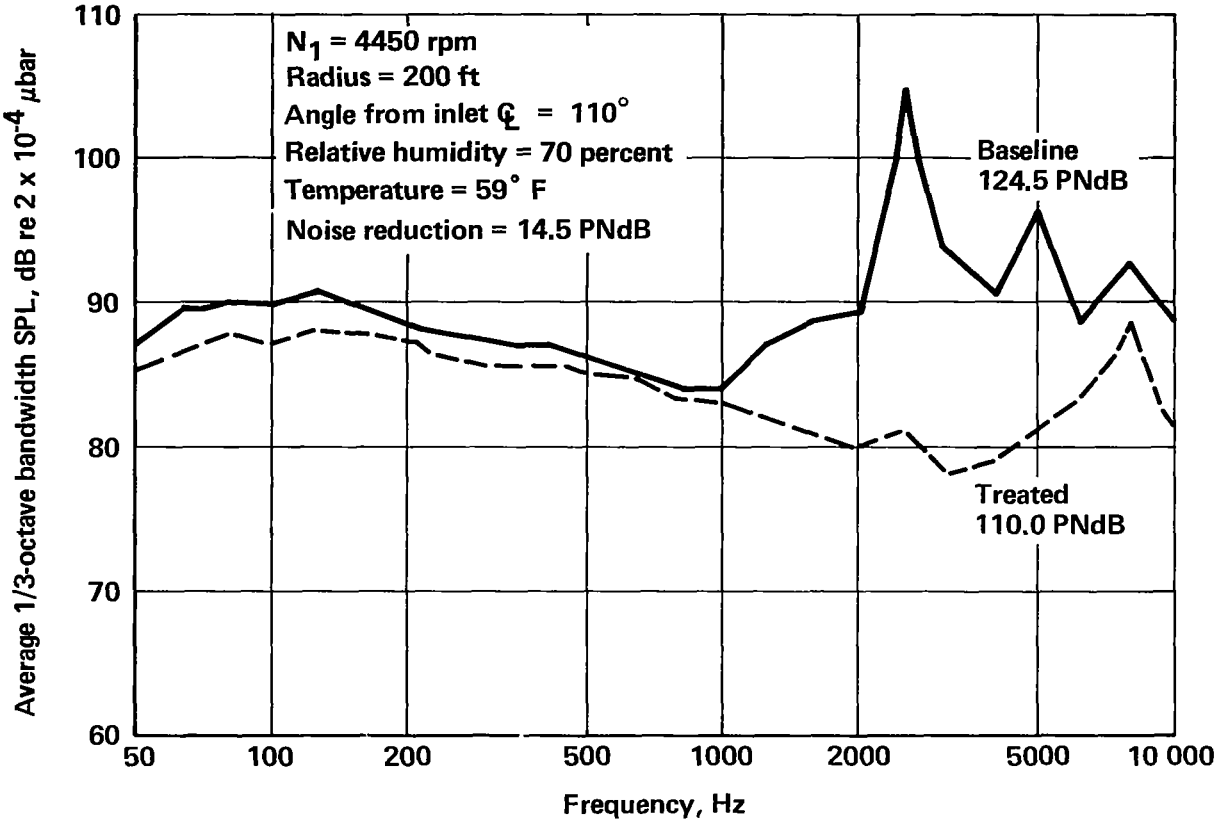

FIGURE 38.—MAXIMUM FAN EXHAUST NOISE AT APPROACH POWER—GROUND TEST

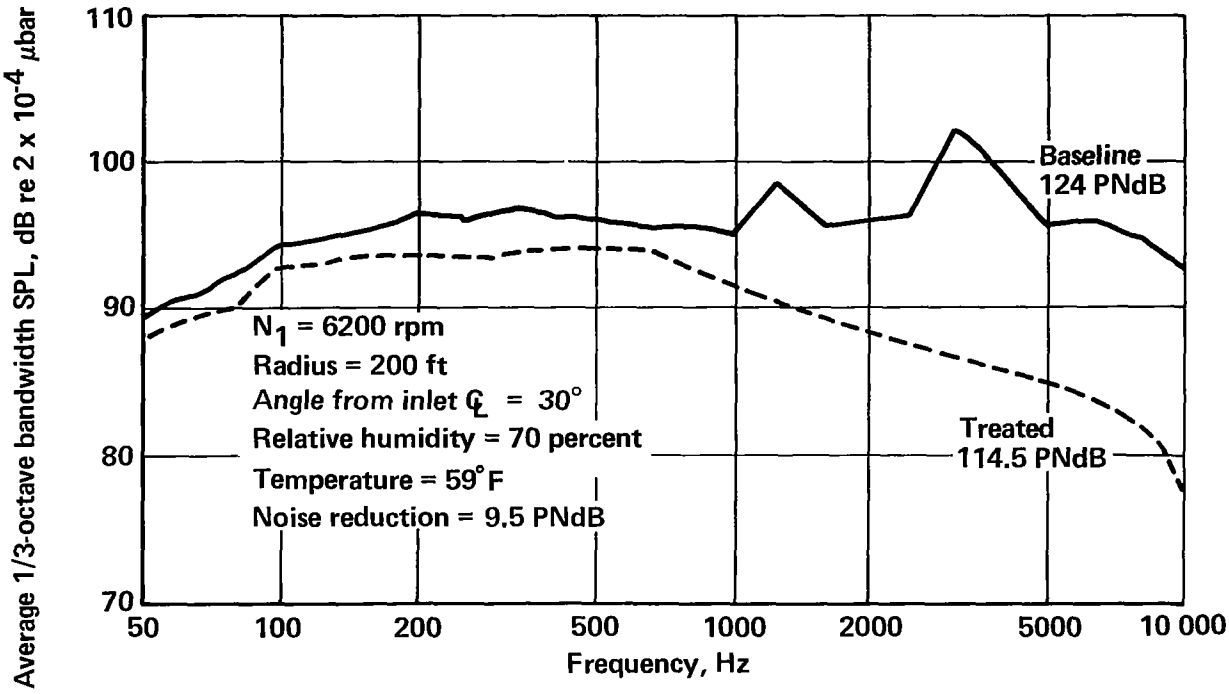

FIGURE 39.—MAXIMUM INLET NOISE AT TAKEOFF POWER—GROUND TEST

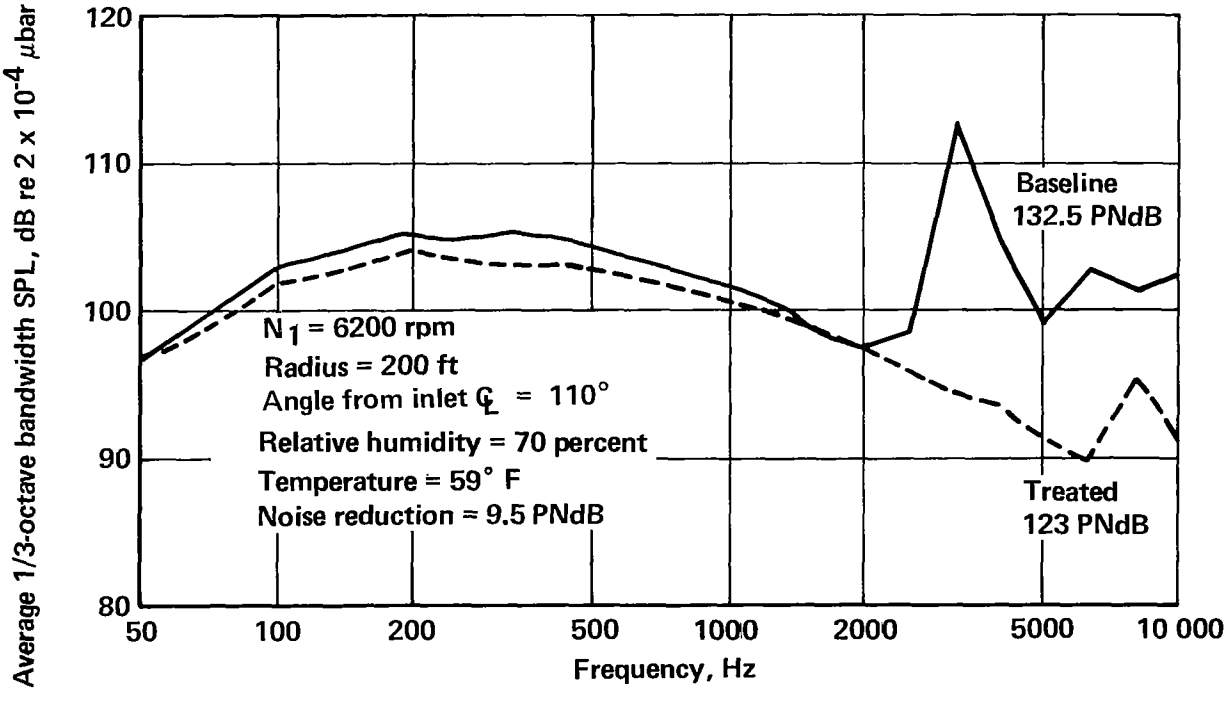

FIGURE 40.—MAXIMUM FAN EXHAUST NOISE AT TAKEOFF POWER—GROUND TEST

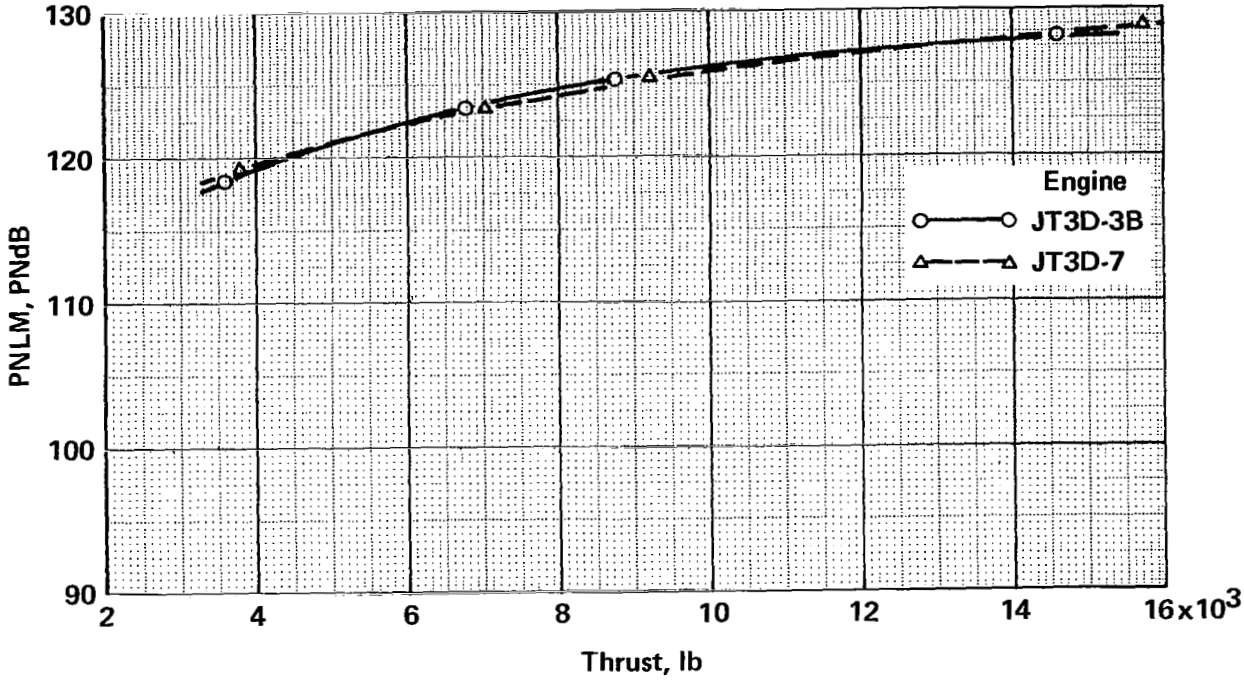

FIGURE 41.— COMPARISON OF NOISE LEVELS FOR JT3D-3B AND JT3D-7 TURBOFAN ENGINES

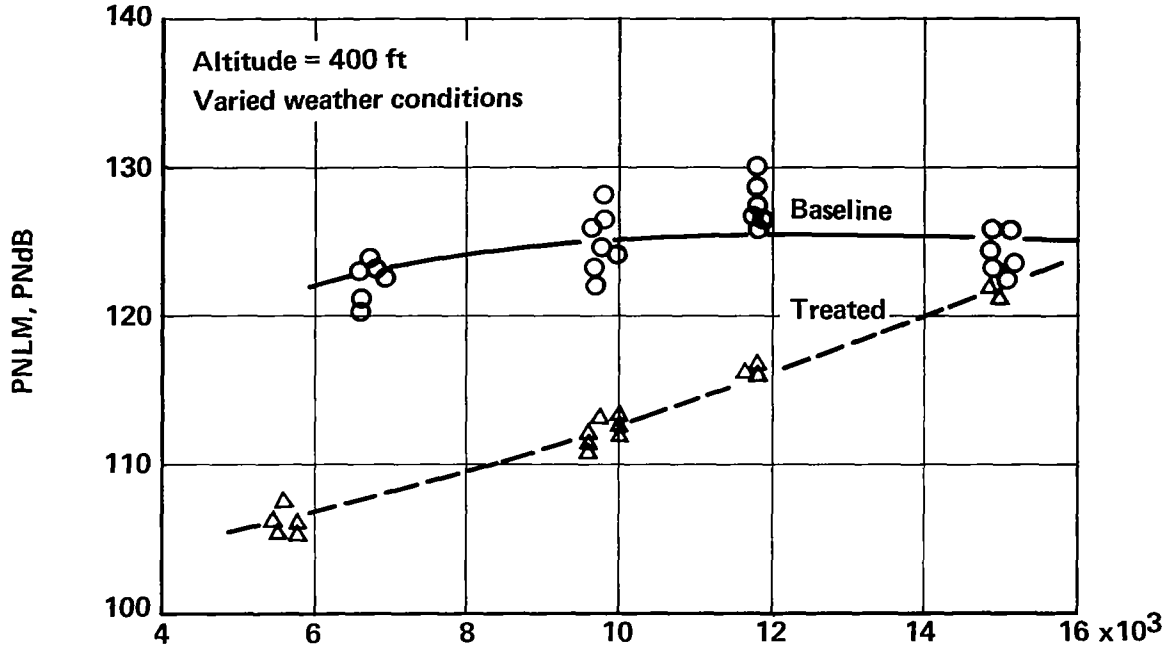

(a) PERCEIVED NOISE LEVELS

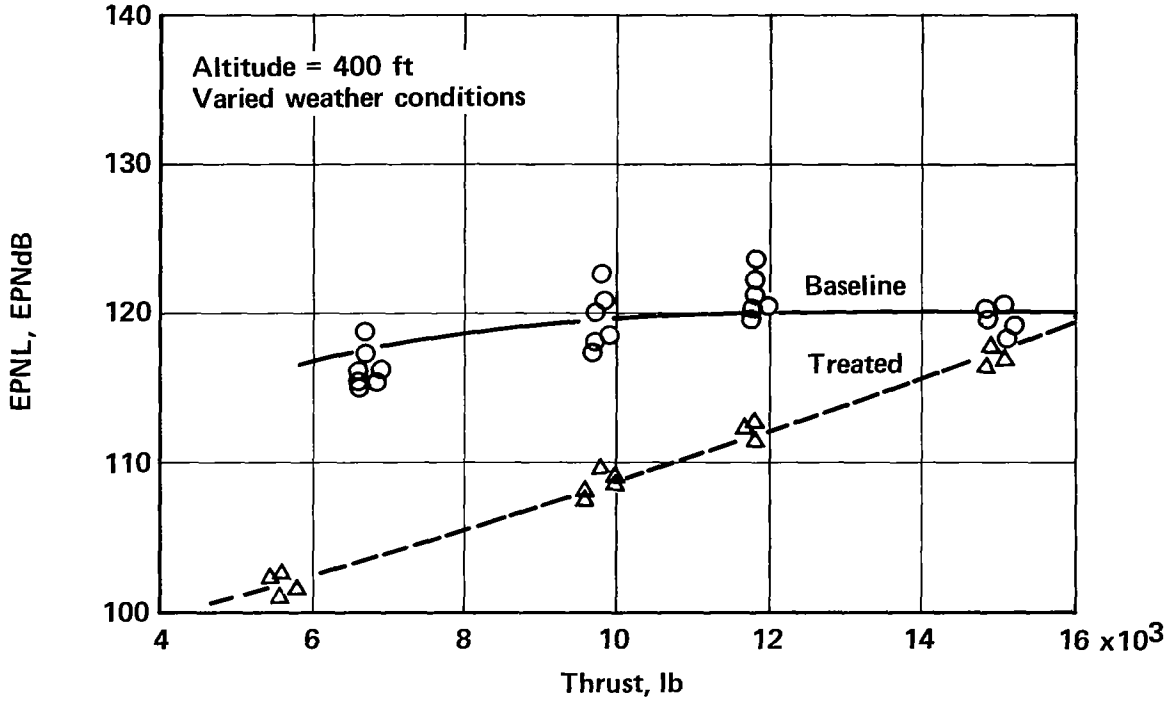

(b) EFFECTIVE PERCEIVED NOISE LEVELS

FIGURE 42.–MAXIMUM MEASURED NOISE LEVEL FOR LEVEL FLIGHT CONDITIONS

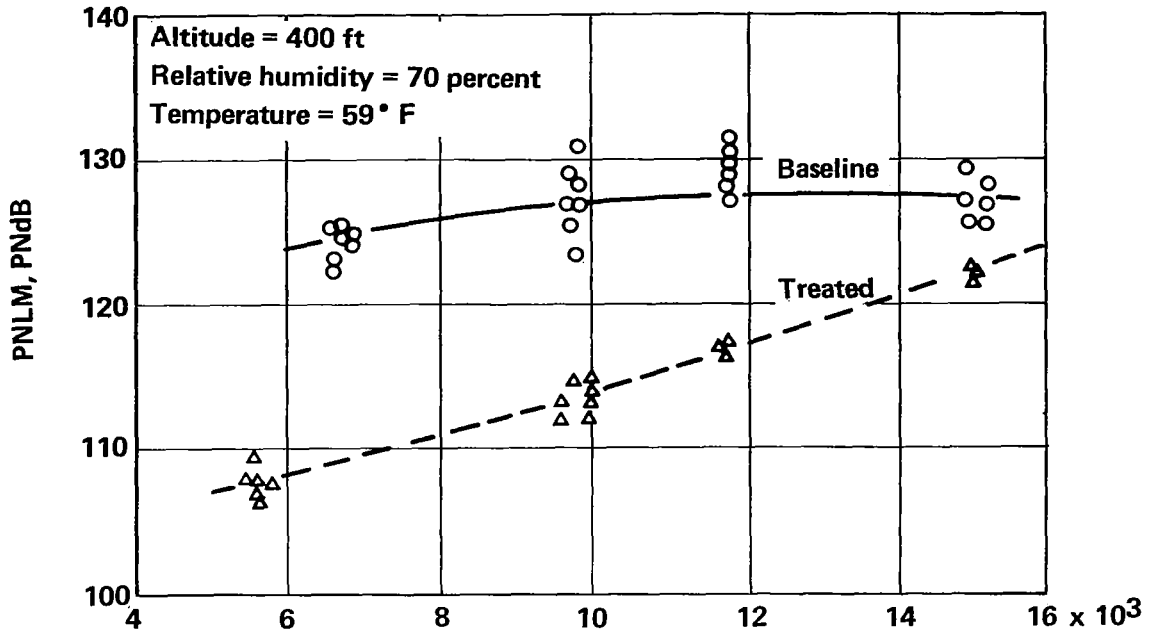

(a) PERCEIVED NOISE LEVELS

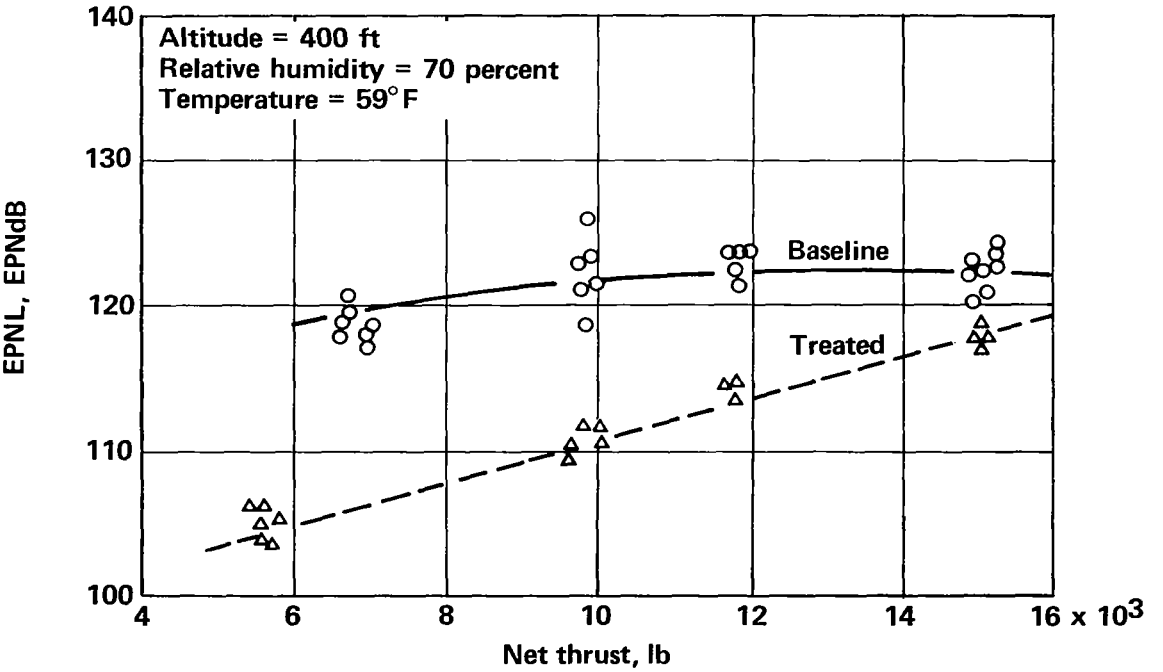

(b) EFFECTIVE PERCEIVED NOISE LEVELS

FIGURE 43.–STANDARDIZED MAXIMUM NOISE LEVEL FOR LEVEL FLIGHT CONDITIONS

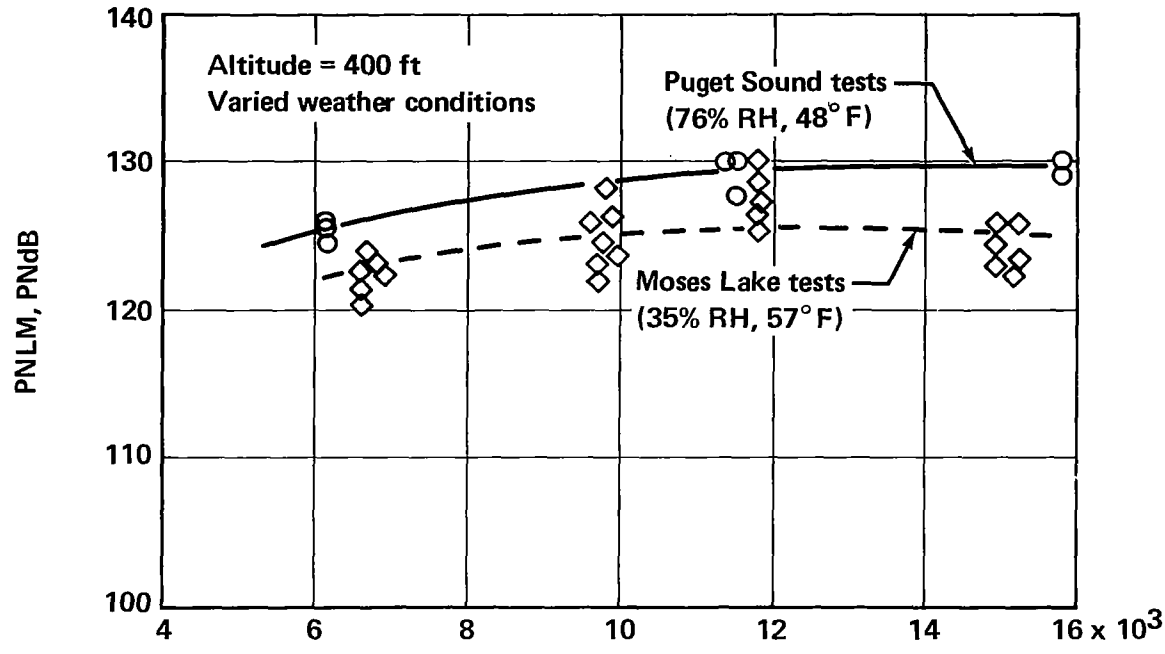

(a) PERCEIVED NOISE LEVELS

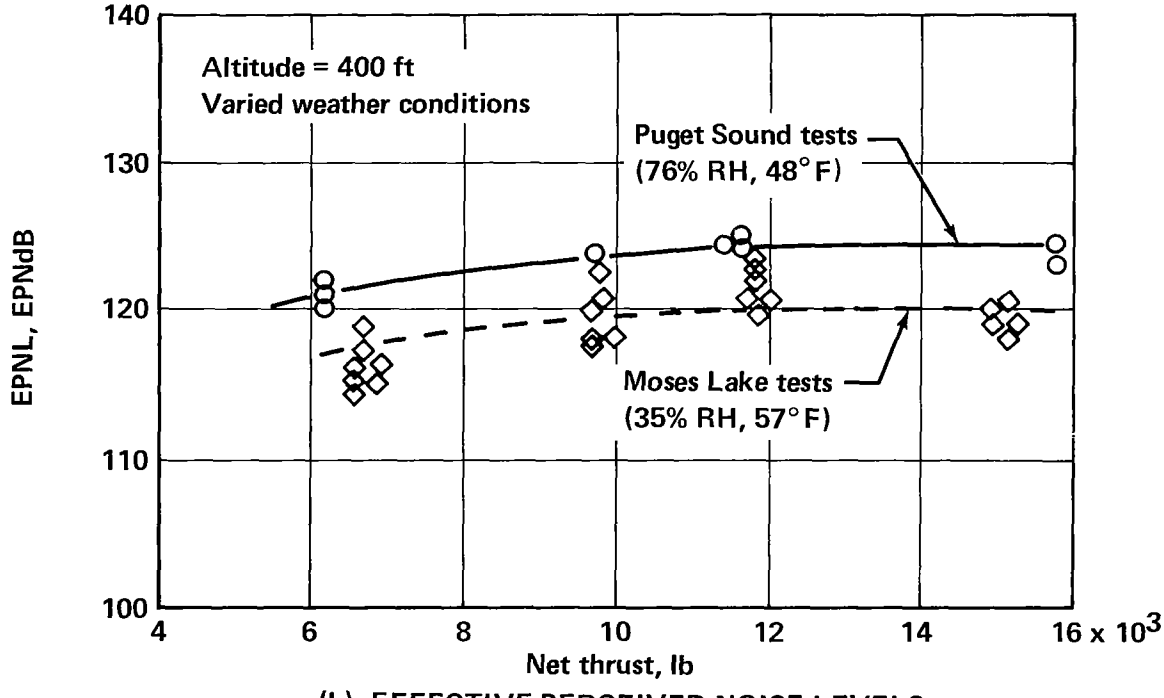

(b) EFFECTIVE PERCEIVED NOISE LEVELS

FIGURE 44.–MAXIMUM LEVEL FLYBY NOISE–PUGET SOUND AND MOSES LAKE TEST RANGES

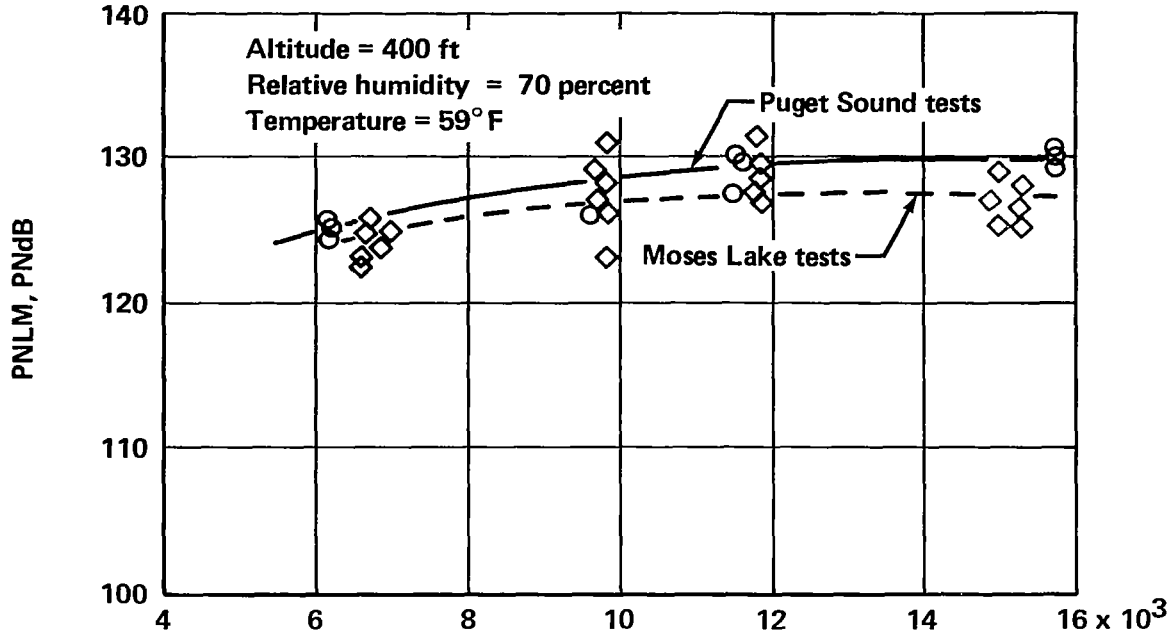

(a) PERCEIVED NOISE LEVELS

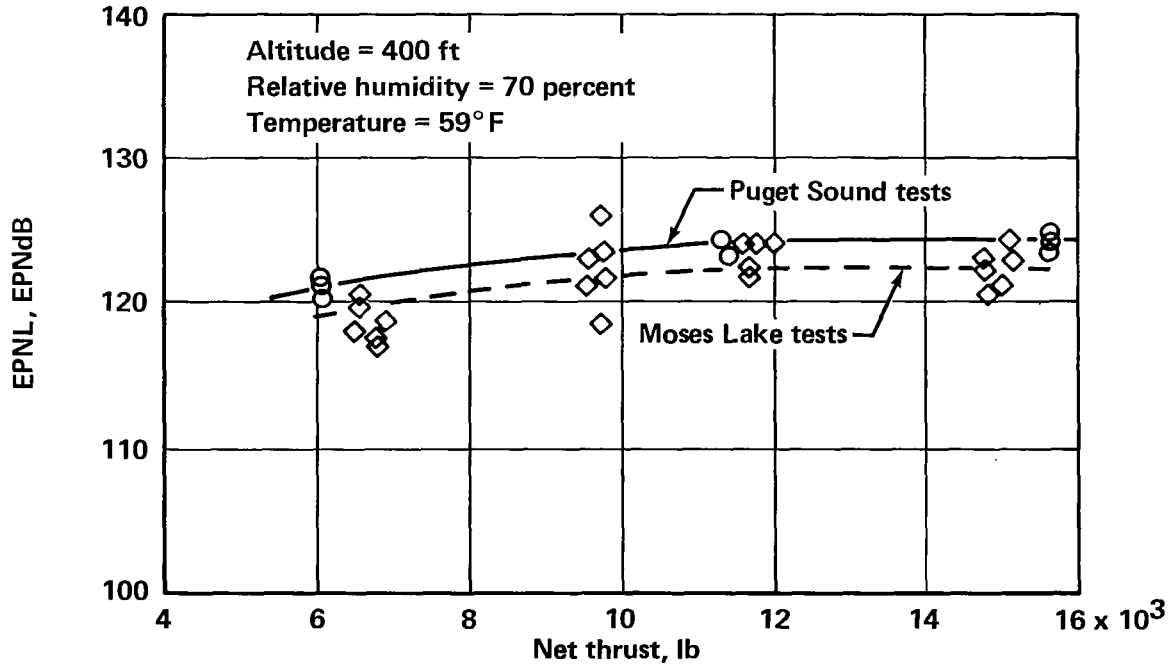

(b) EFFECTIVE PERCEIVED NOISE LEVELS

FIGURE 45.–STANDARDIZED MAXIMUM LEVEL FLYBY NOISE–PUGET SOUND AND MOSES LAKE TEST RANGES

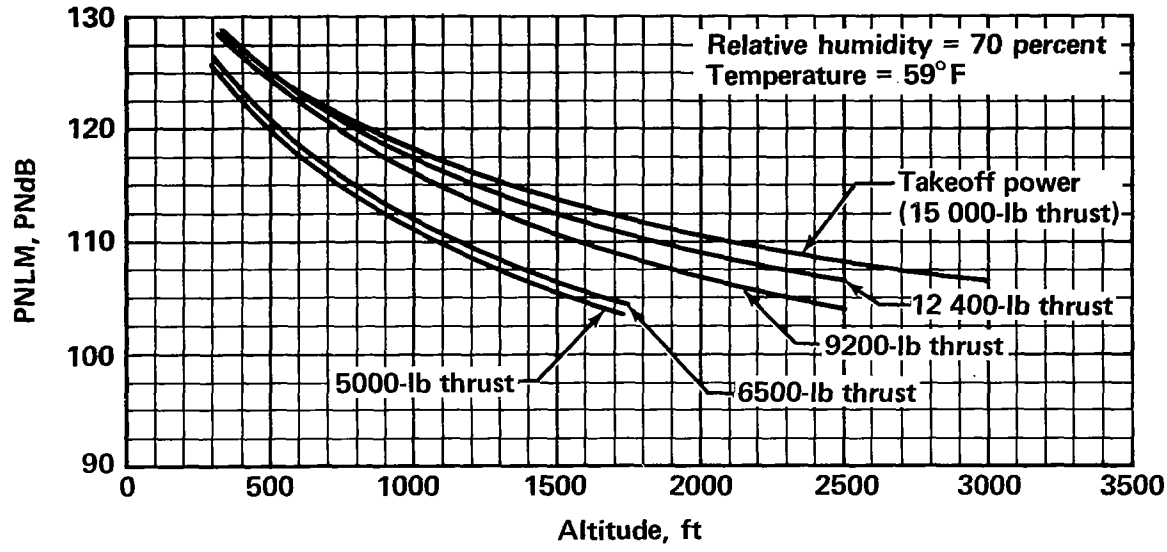

FIGURE 46.–STANDARDIZED MAXIMUM PERCEIVED NOISE LEVEL UNDER FLIGHTPATH AT VARIOUS POWER SETTINGS–BASELINE AIRPLANE

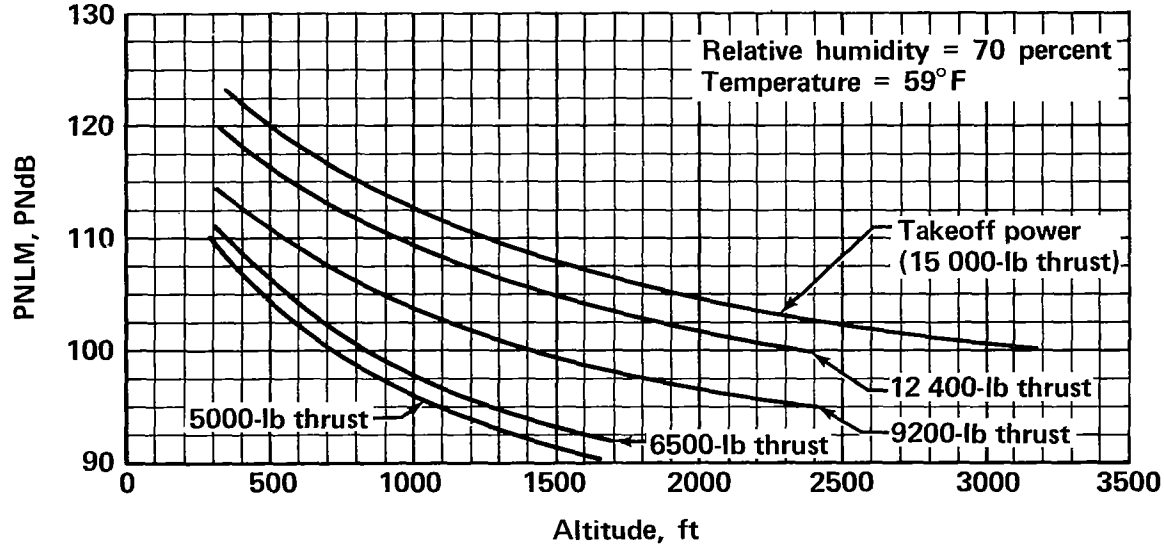

FIGURE 47.–STANDARDIZED MAXIMUM PERCEIVED NOISE LEVEL UNDER FLIGHTPATH AT VARIOUS POWER SETTINGS–TREATED AIRPLANE

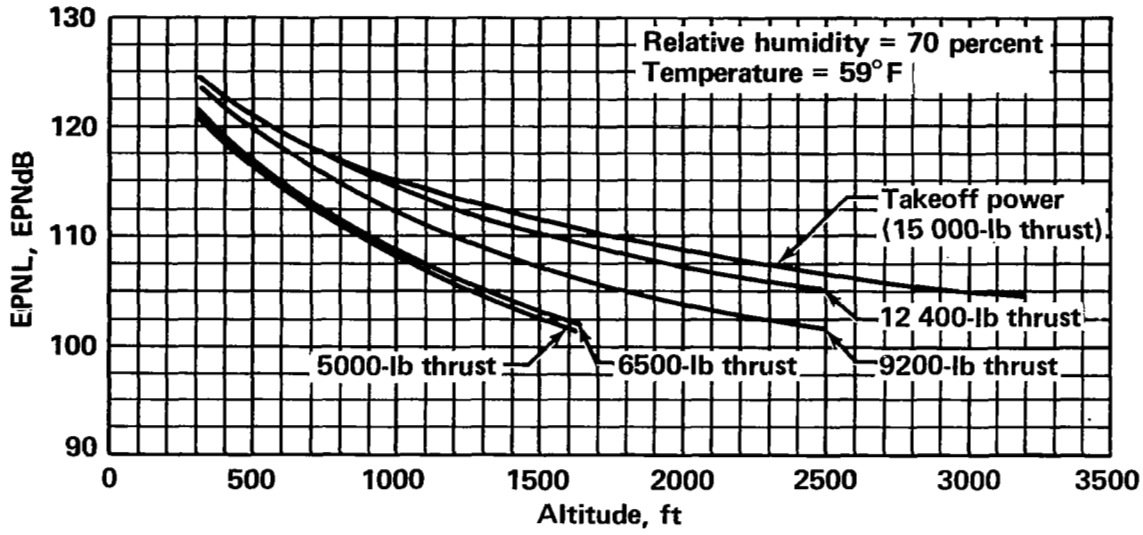

FIGURE 48.–STANDARDIZED EFFECTIVE PERCEIVED NOISE LEVEL UNDER FLIGHTPATH AT VARIOUS POWER SETTINGS–BASELINE AIRPLANE

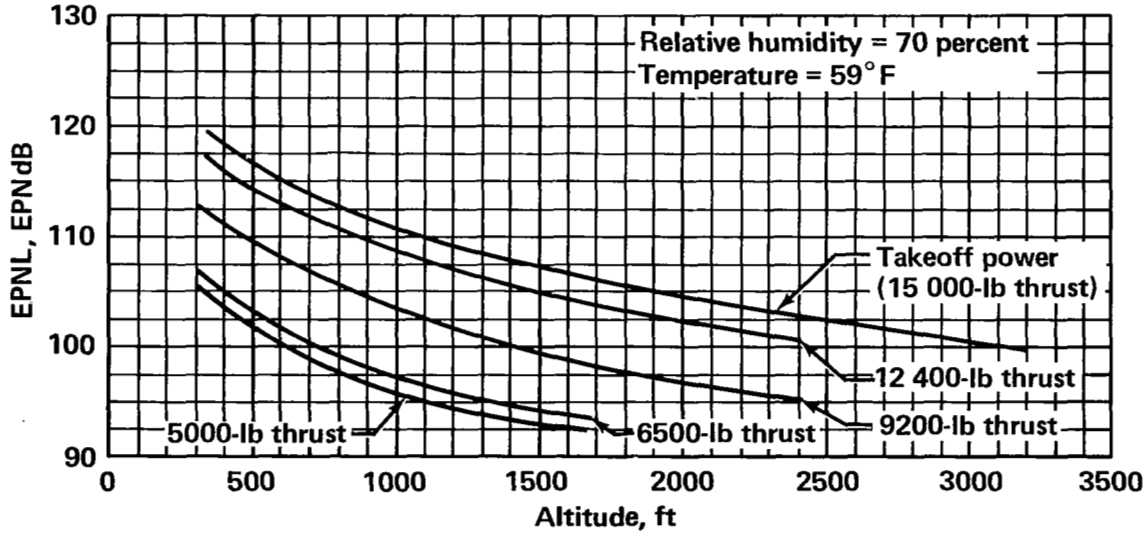

FIGURE 49.–STANDARDIZED EFFECTIVE PERCEIVED NOISE LEVEL UNDER FLIGHTPATH AT VARIOUS POWER SETTINGS–TREATED AIRPLANE

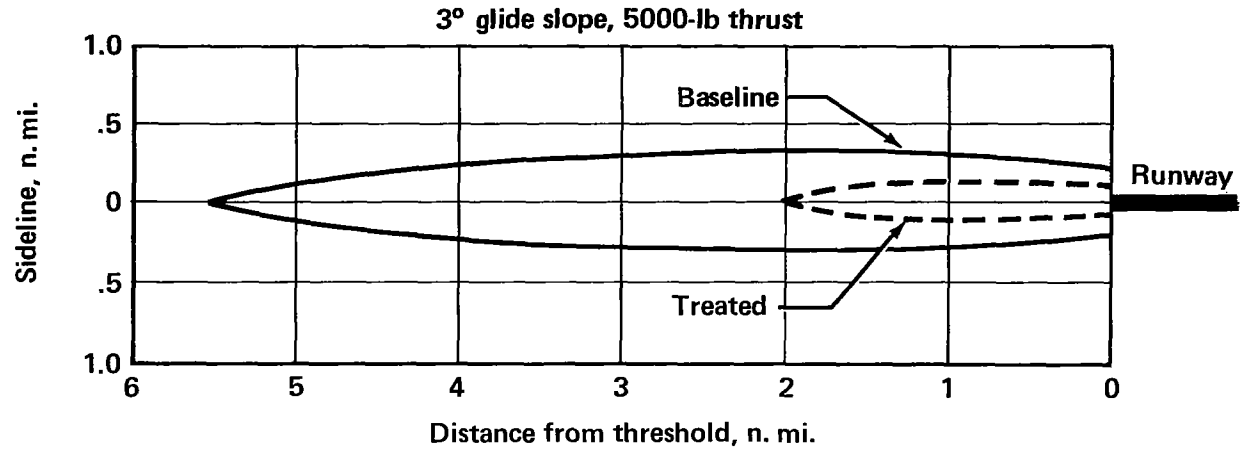

FIGURE 50.—LANDING APPROACH 100-EPNdB NOISE CONTOURS

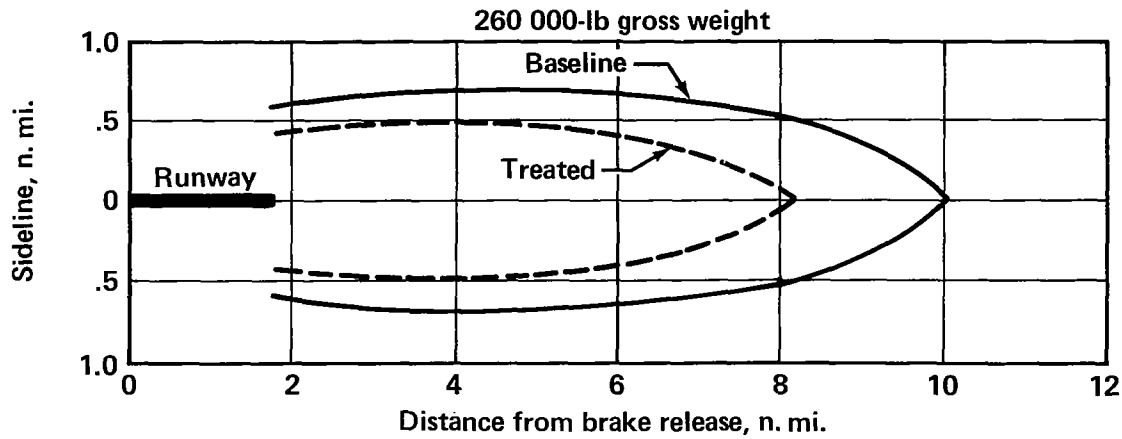

FIGURE 51.—TAKEOFF 100-EPNdB NOISE CONTOURS

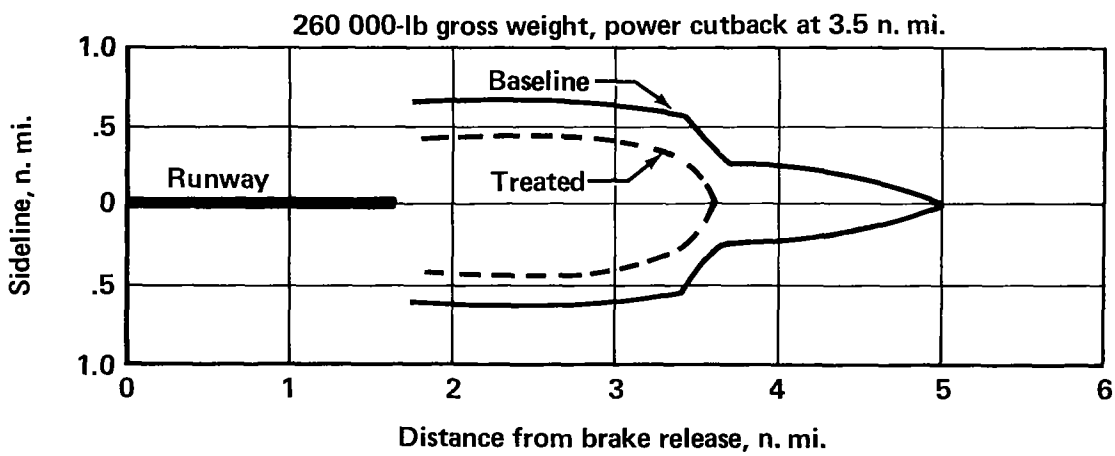

FIGURE 52.—TAKEOFF WITH POWER CUTBACK 100-EPNdB NOISE CONTOURS

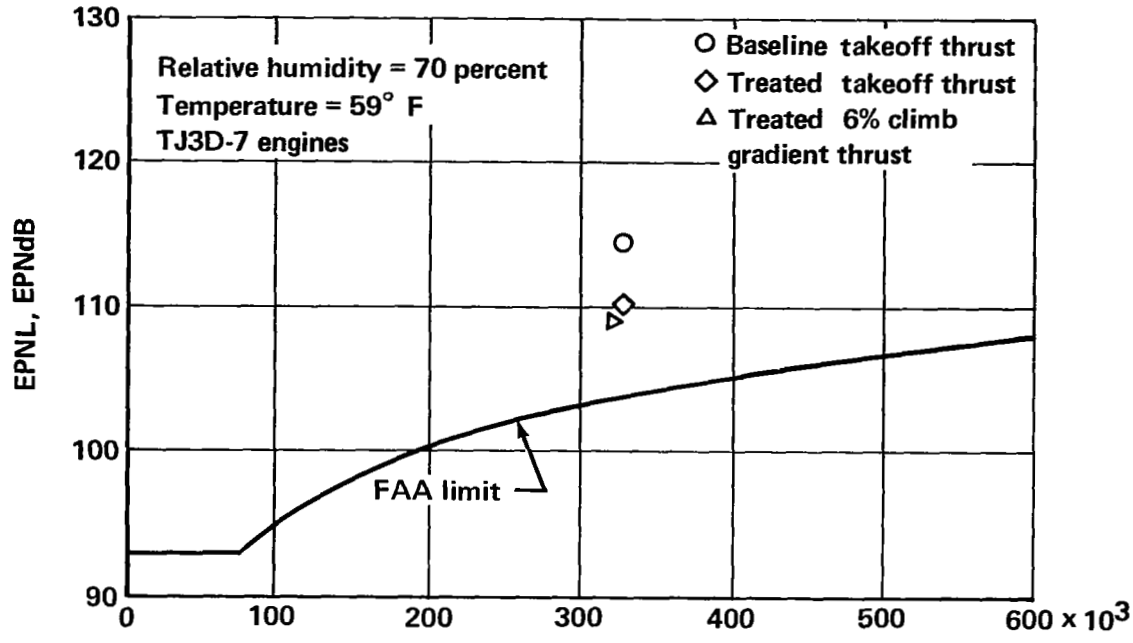

(a) TAKEOFF

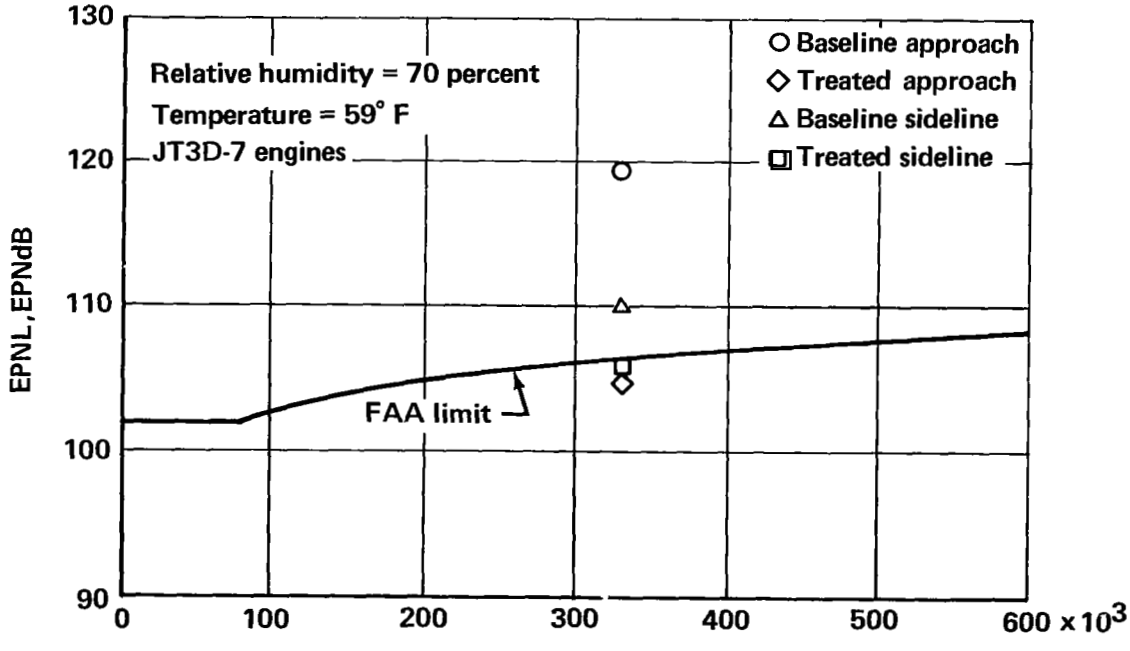

(b) APPROACH AND SIDELINE

FIGURE 53.—COMPARISON OF MEASURED NOISE WITH PROPOSED FAA CERTIFICATION LEVELS FOR NEW AIRPLANES

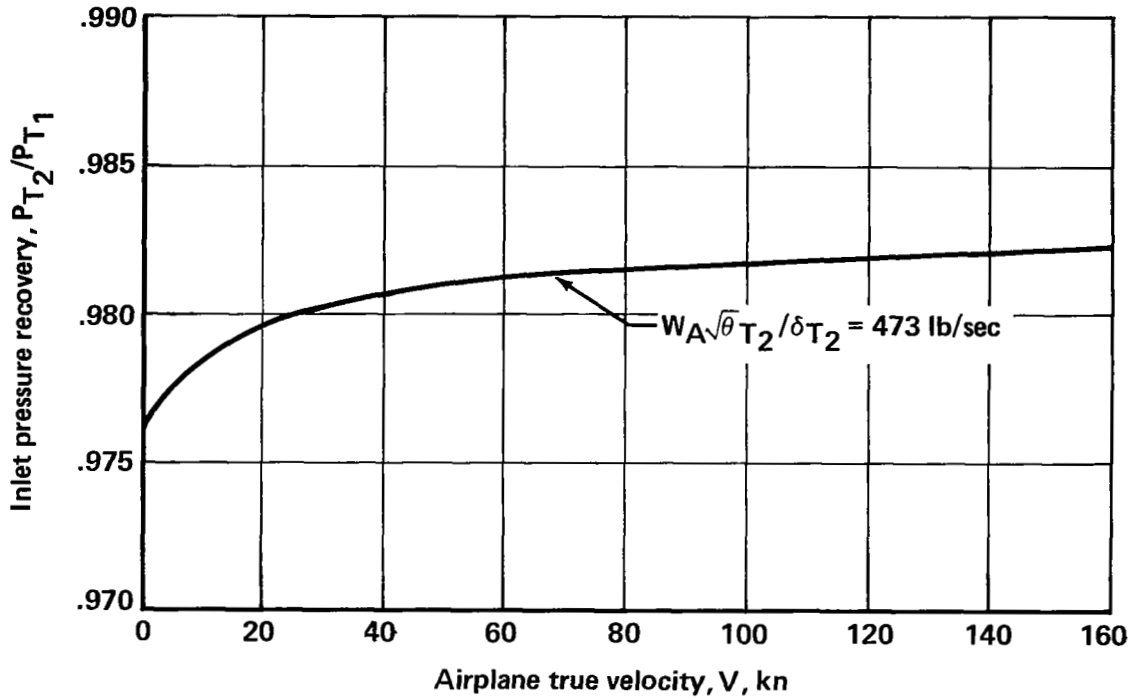

FIGURE 54.– INLET PRESSURE RECOVERY, TAKEOFF

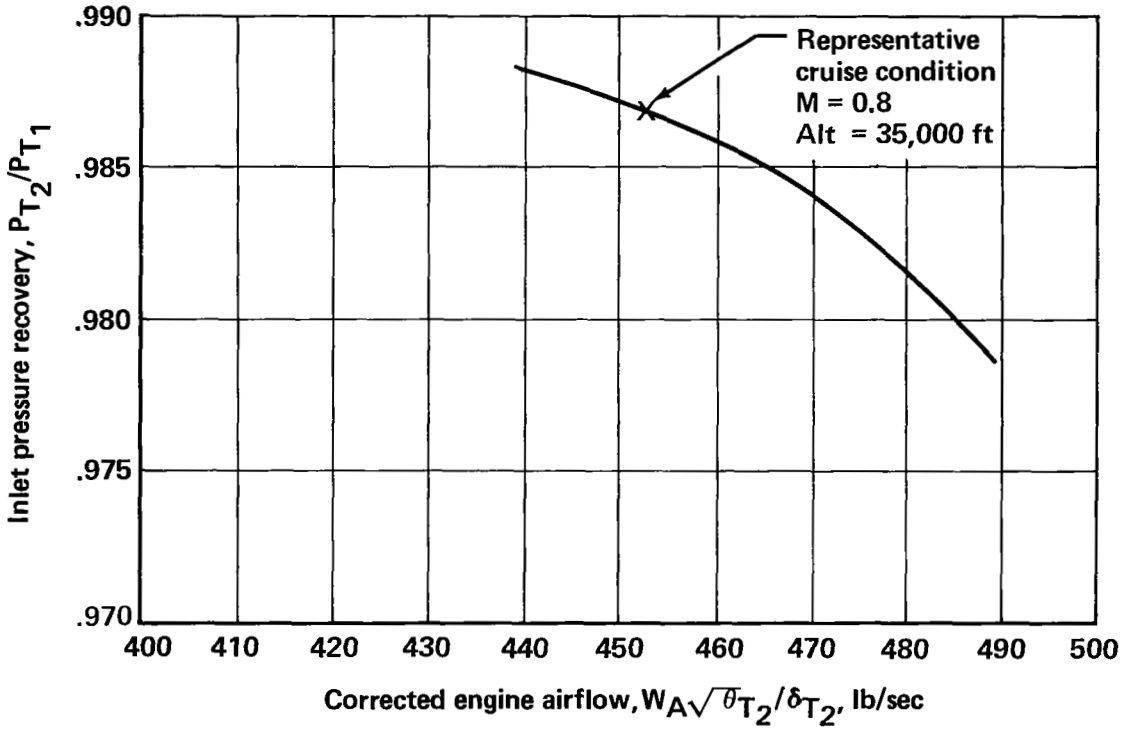

FIGURE 55.– INLET PRESSURE RECOVERY, CRUISE

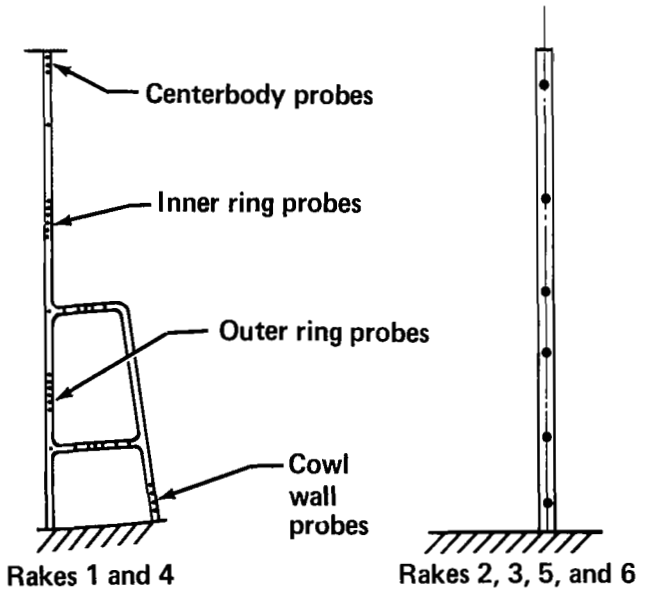

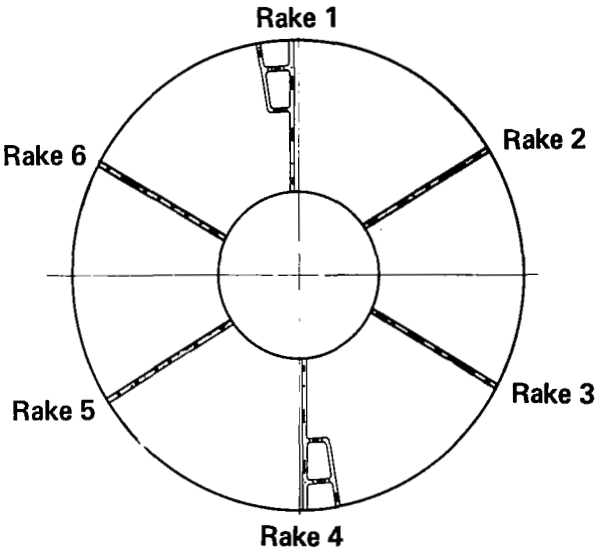

FRONT VIEW OF ENGINE FACE

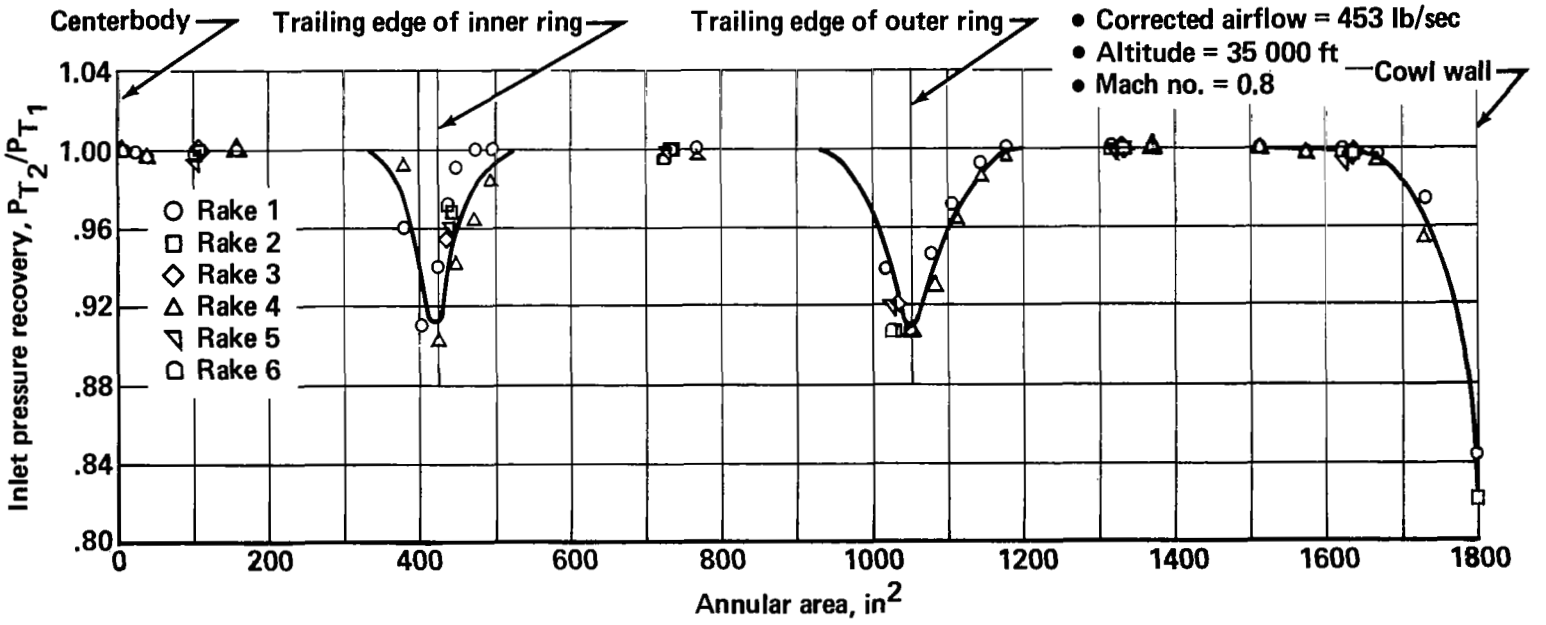

FIGURE 56.–TOTAL PRESSURE DISTRIBUTION NEAR FAN FACE

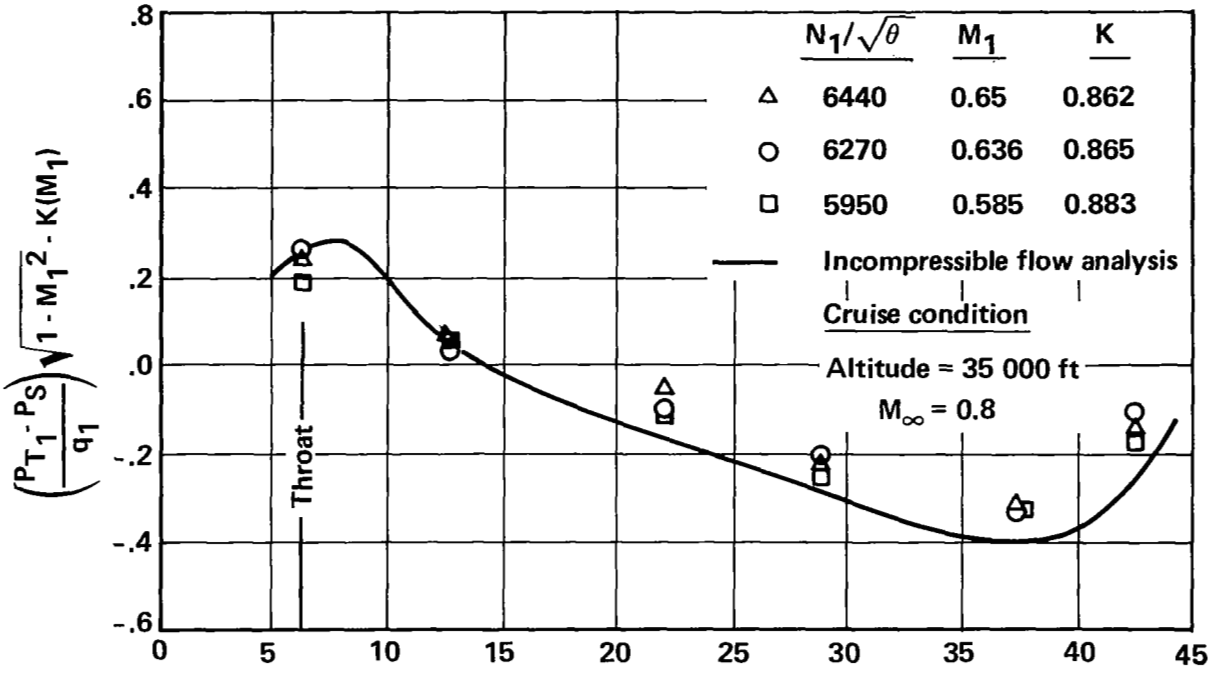

(a) COWL WALL

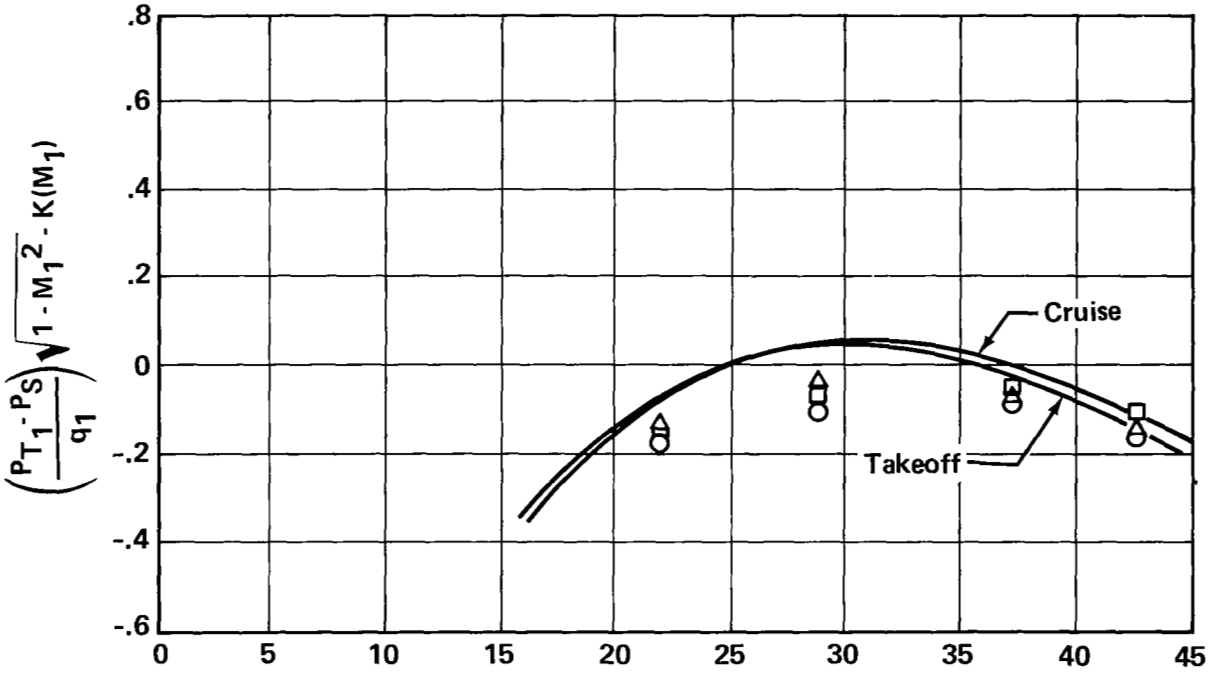

Axial distance from inlet highlight, L, in.

(b) CENTERBODY

FIGURE 59.—INLET PRESSURE CORRELATION

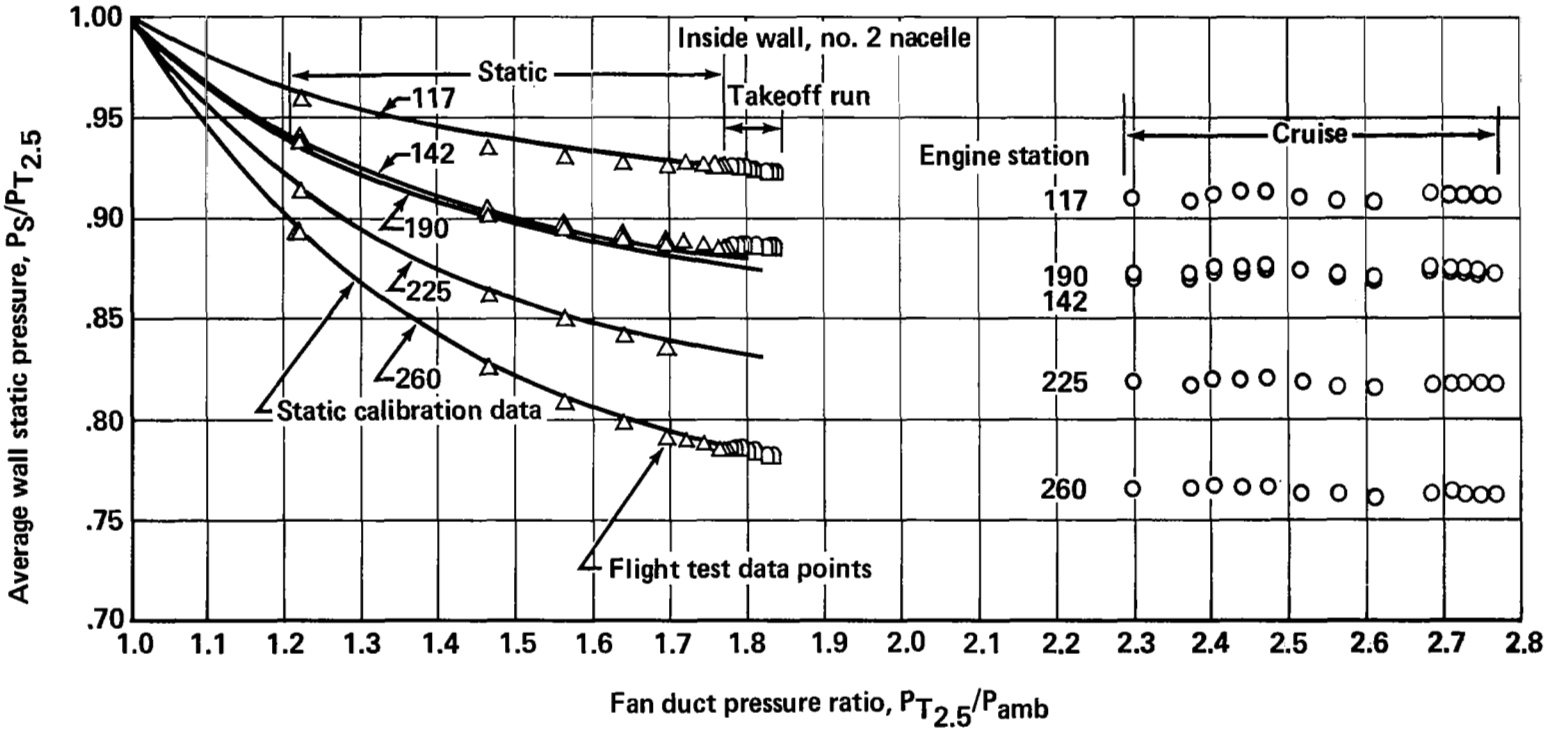

FIGURE 60.– FLIGHT TEST DUCT STATIC PRESSURE DATA

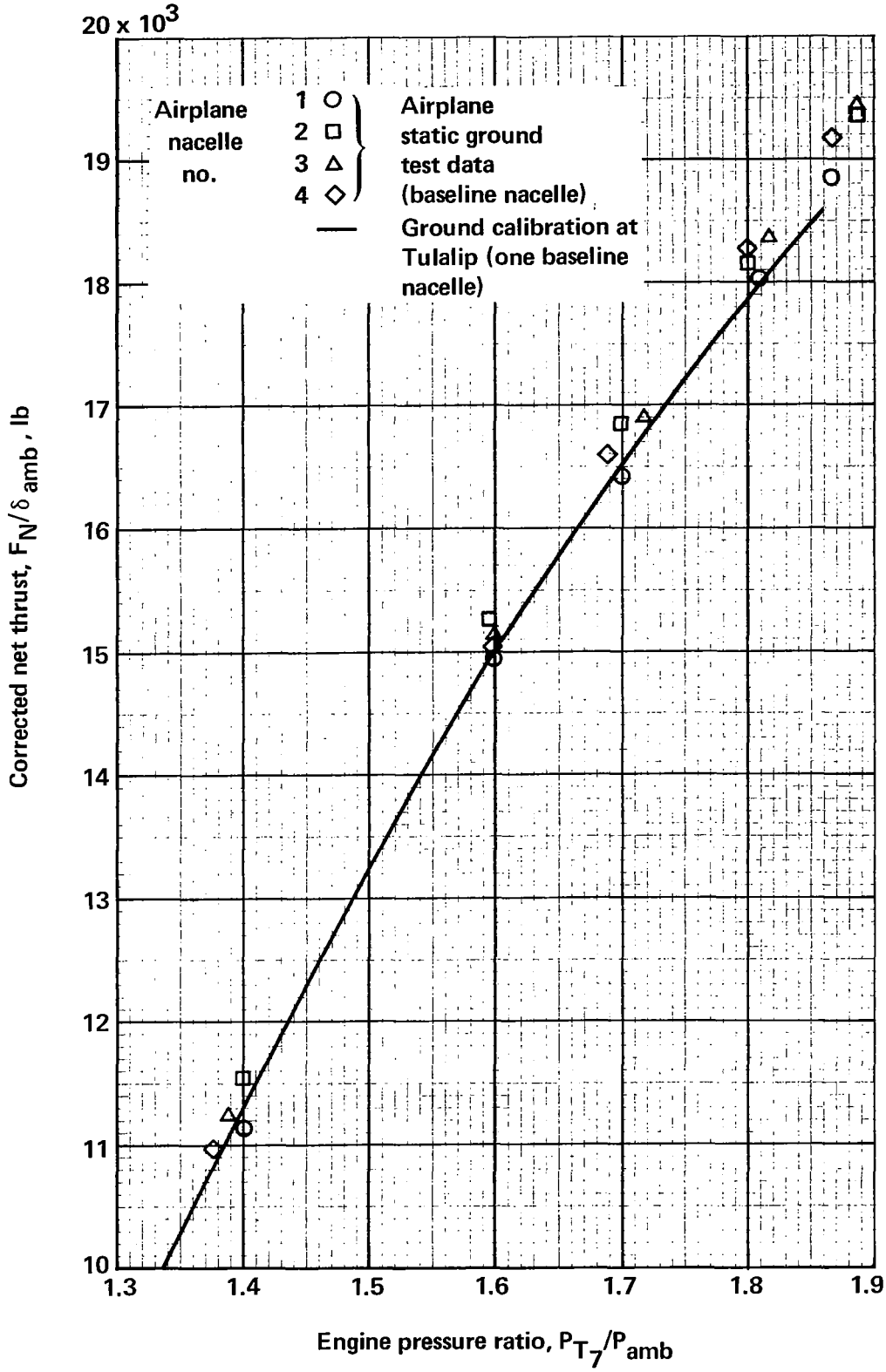

FIGURE 61.—THRUST, BASELINE NACELLES—FLIGHT TEST STATIC DATA

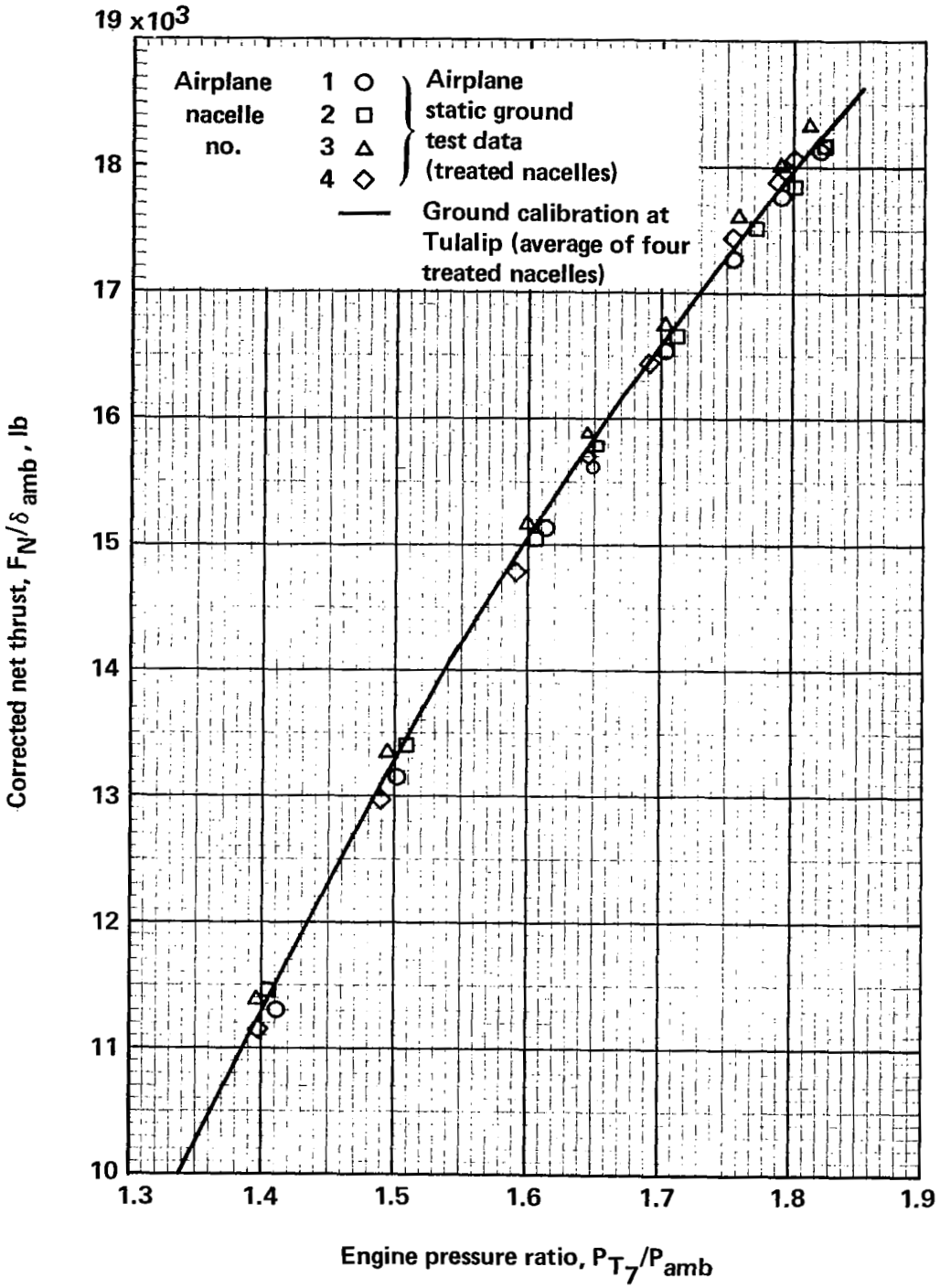

FIGURE 62.– THRUST, TREATED NACELLES – FLIGHT TEST STATIC DATA

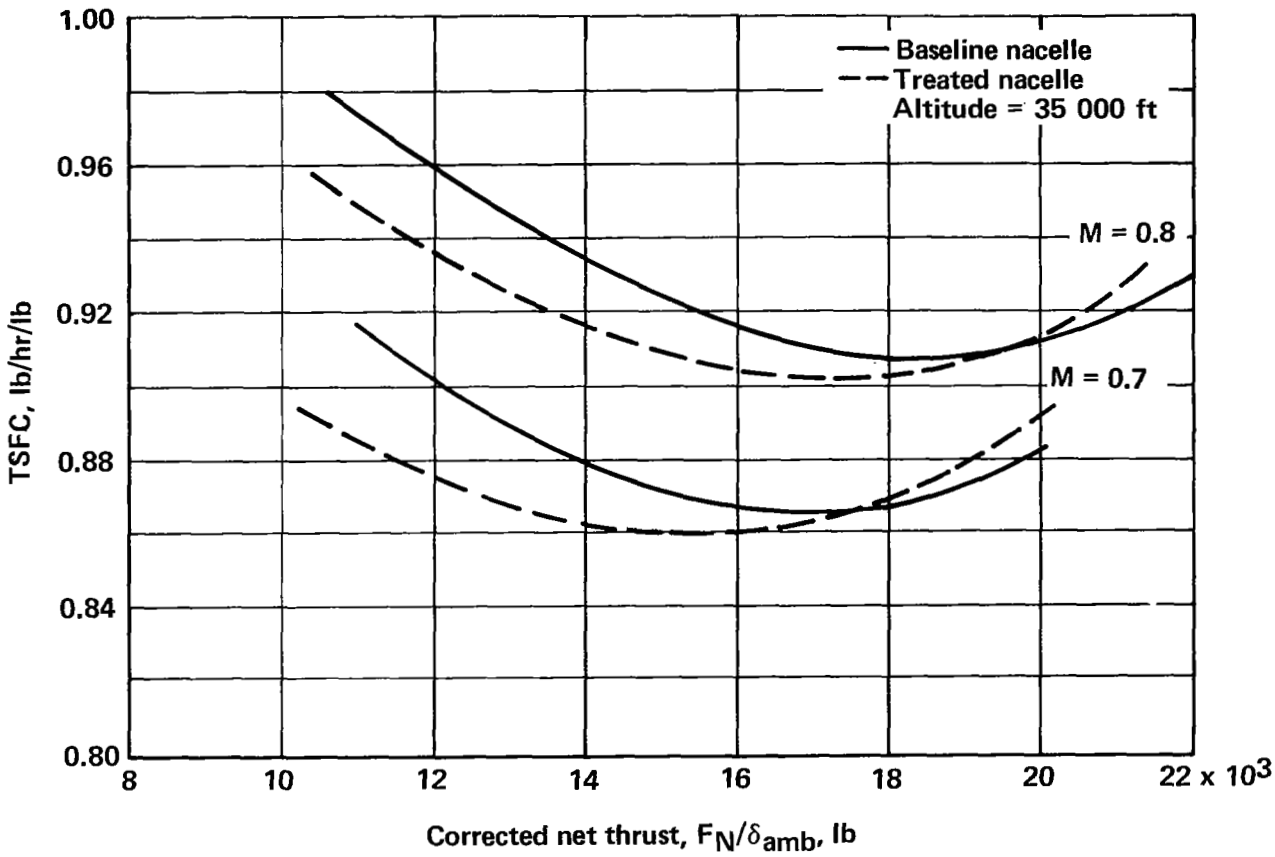

FIGURE 63.– SPECIFIC FUEL CONSUMPTION COMPARISON

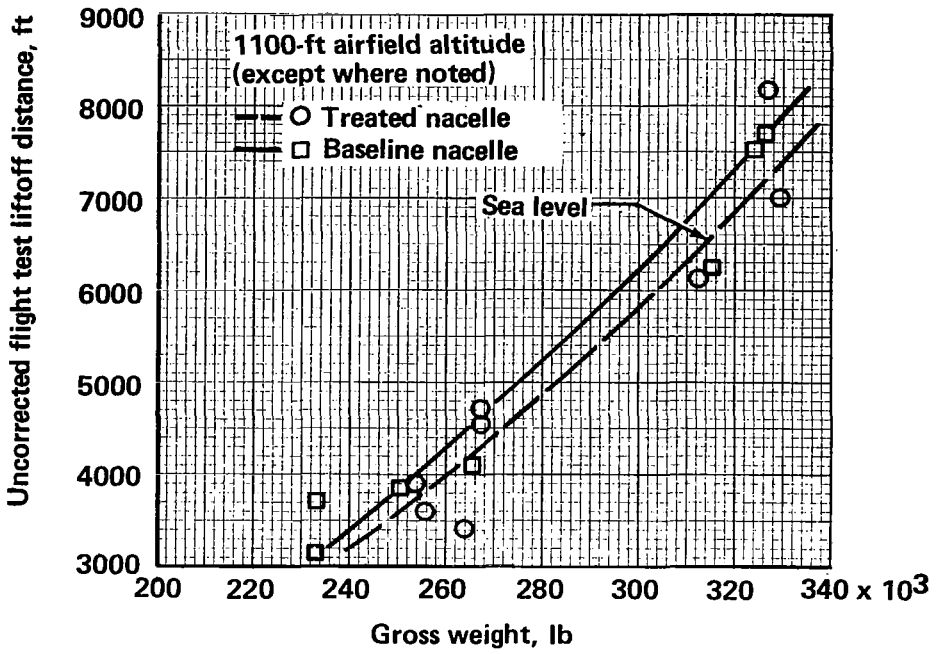

FIGURE 64.– UNCORRECTED FLIGHT TEST LIFTOFF DISTANCES VERSUS GROSS WEIGHT

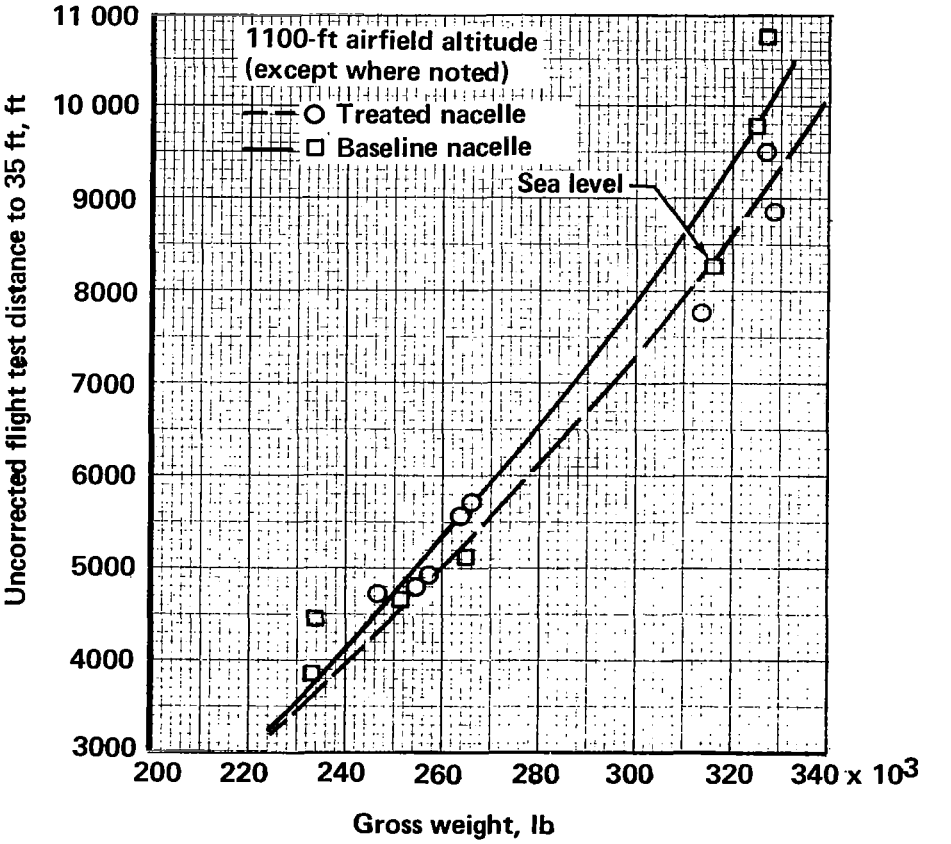

FIGURE 65.– UNCORRECTED FLIGHT TEST DISTANCE TO 35 FT VERSUS GROSS WEIGHT

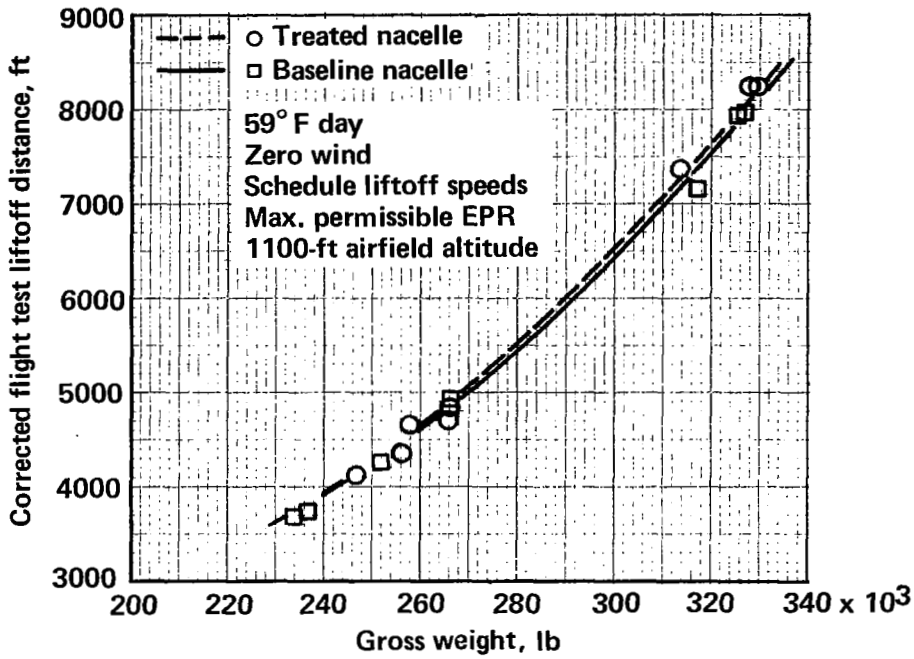

FIGURE 66.—CORRECTED FLIGHT TEST LIFTOFF DISTANCES VERSUS GROSS WEIGHT

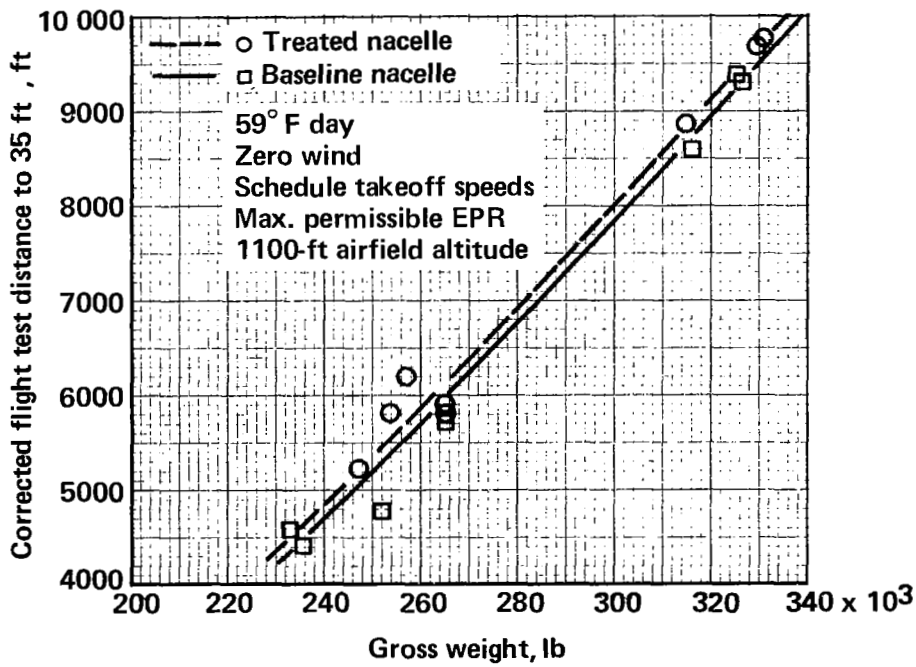

FIGURE 67.—CORRECTED FLIGHT TEST DISTANCE TO 35 FT VERSUS GROSS WEIGHT

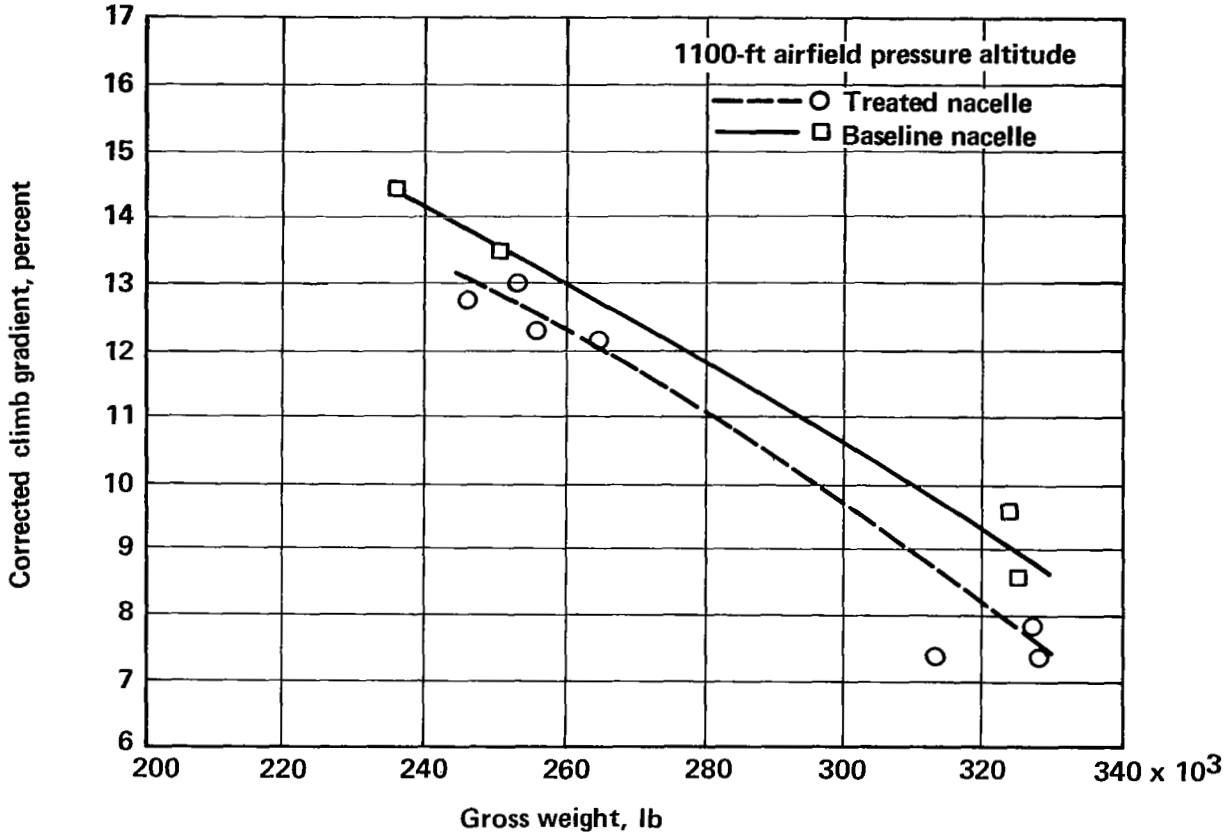

FIGURE 68.– CORRECTED CLIMB GRADIENT VERSUS GROSS WEIGHT

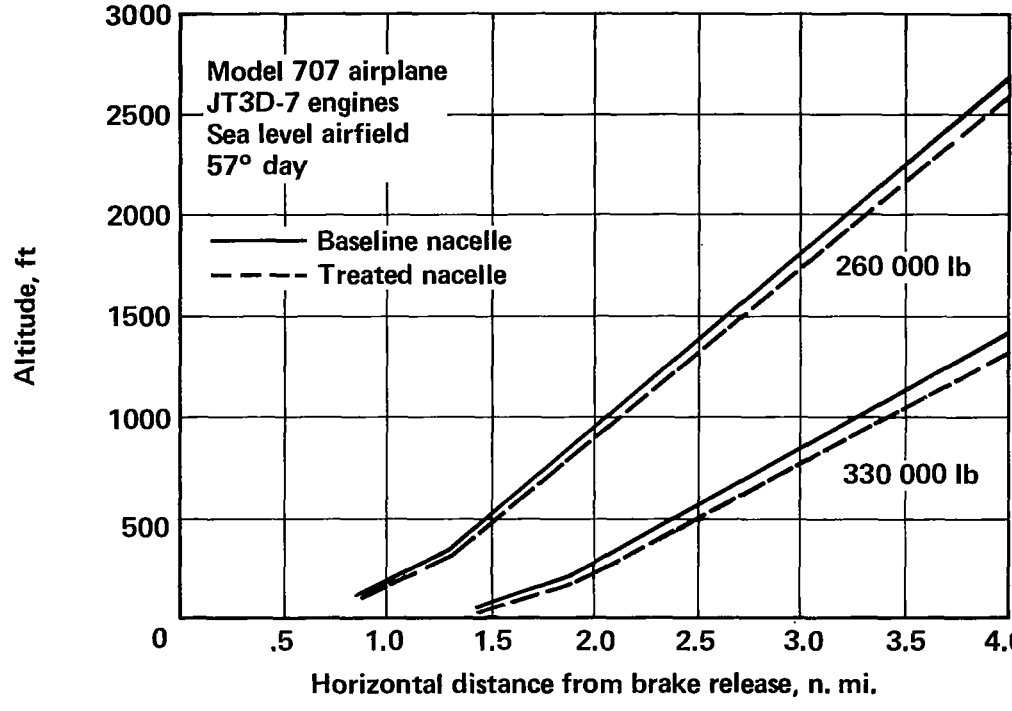

FIGURE 69.– STANDARDIZED TAKEOFF PROFILES

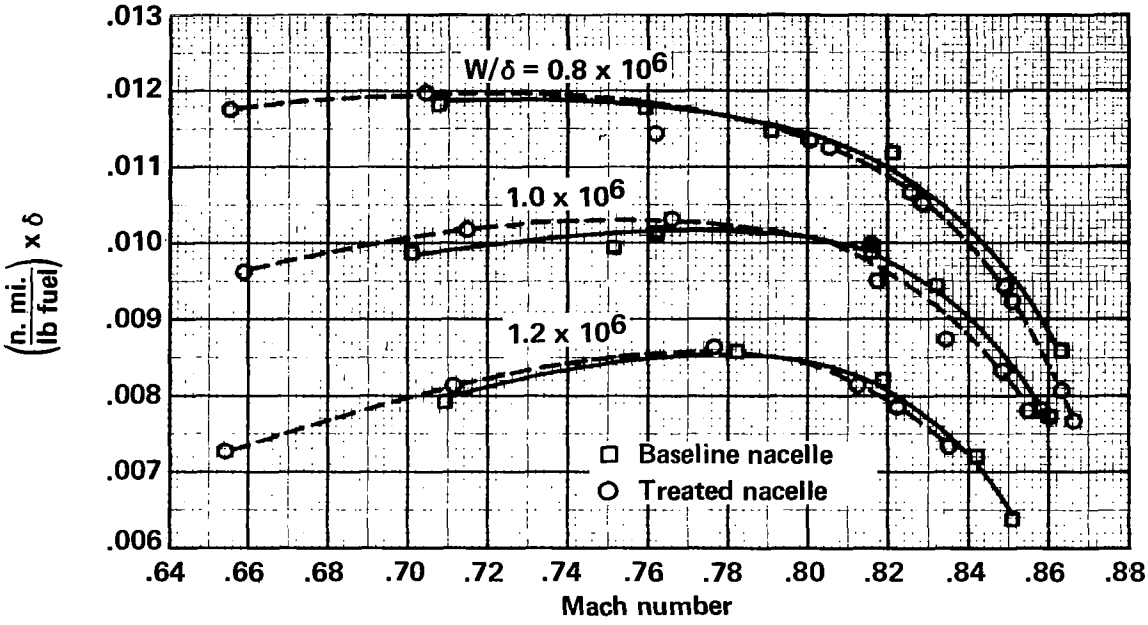

FIGURE 70.– FUEL MILEAGE COMPARISON

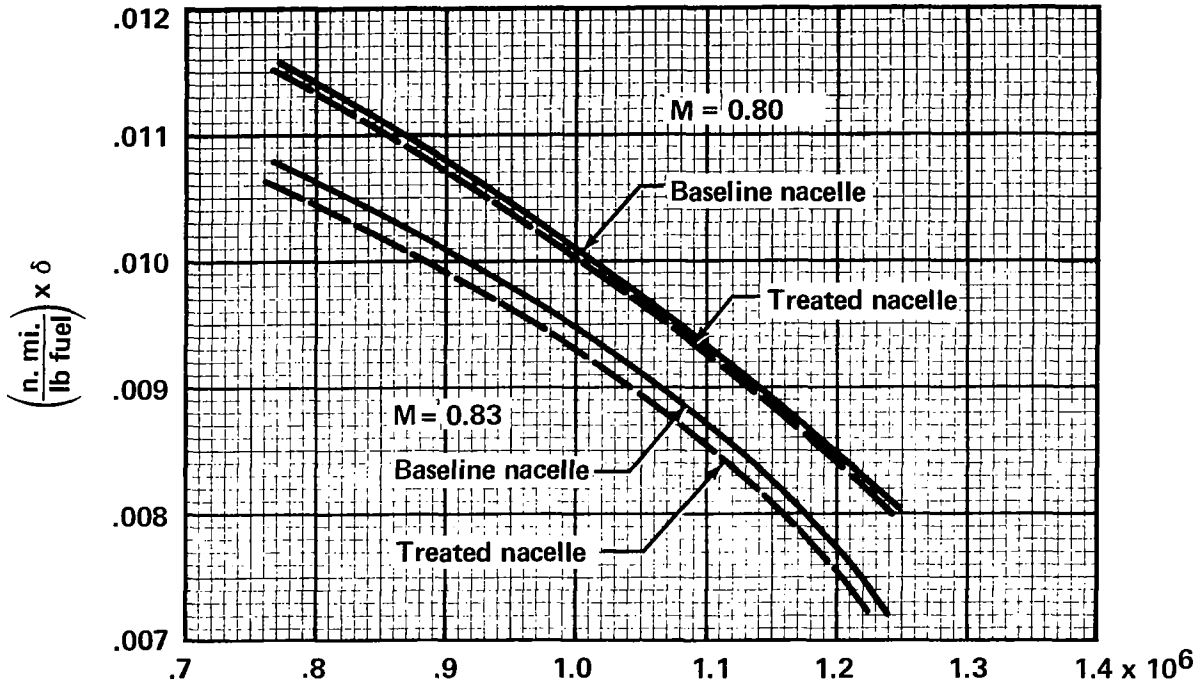

(a) VARIATION OF FUEL MILEAGE WITH WEIGHT

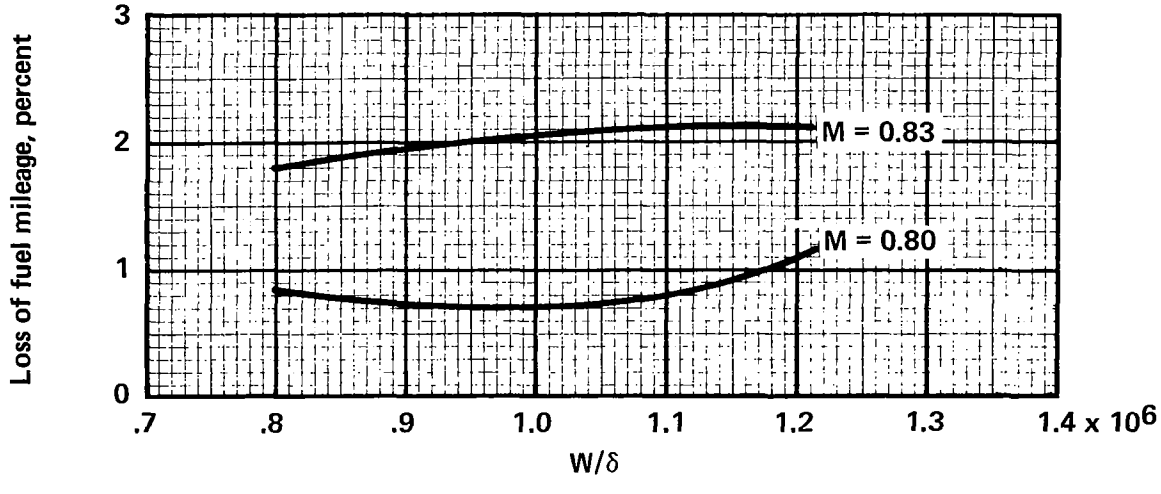

(b) PERCENTAGE LOSS IN FUEL MILEAGE DUE TO TREATED NACELLES

FIGURE 71.—FUEL MILEAGE COMPARISON—BASELINE AND TREATED NACELLE CONFIGURATIONS

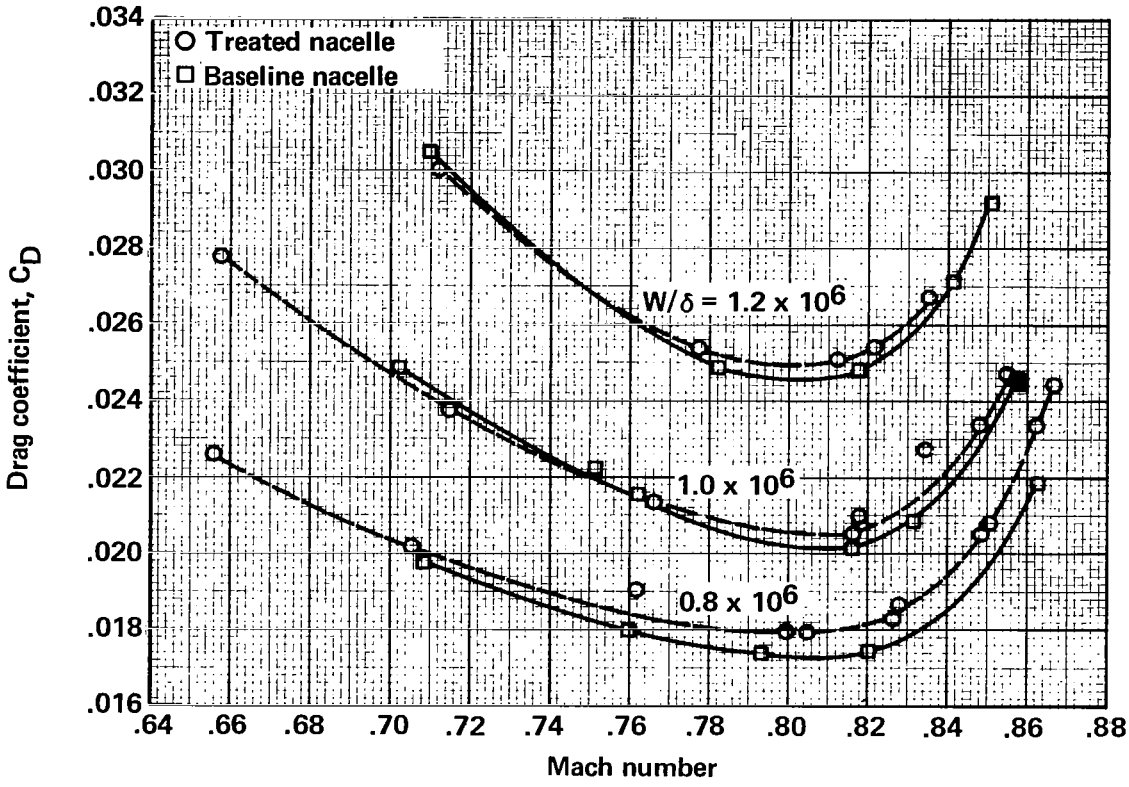

FIGURE 72.– CRUISE DRAG COMPARISON

- 707-320B/C
- Zero wind, standard day

Weight	Baseline nacelle, lb	Treated nacelle, lb
Max. gross takeoff	327 000	327 000
Operating empty	140 238	143 378
Max. zero fuel	190 000	193 140

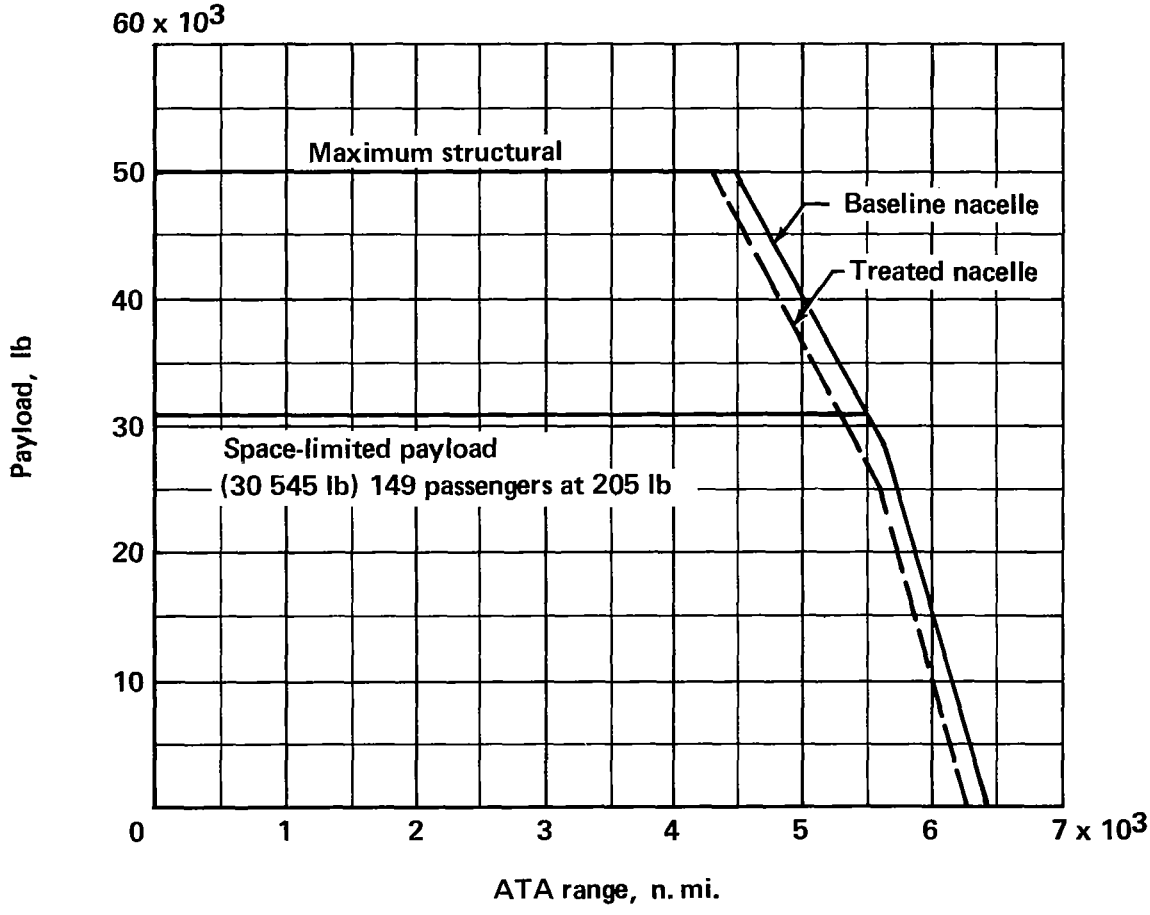

FIGURE 73.—RANGE PERFORMANCE—ATA DOMESTIC RESERVES, LONG-RANGE CRUISE TECHNIQUE

- 707-320B/C
- Zero wind, standard day

Weight	Baseline nacelle, lb	Treated nacelle, lb
Max. gross takeoff	327 000	327 000
Operating empty	140 238	143 378
Max. zero fuel	190 000	193 140

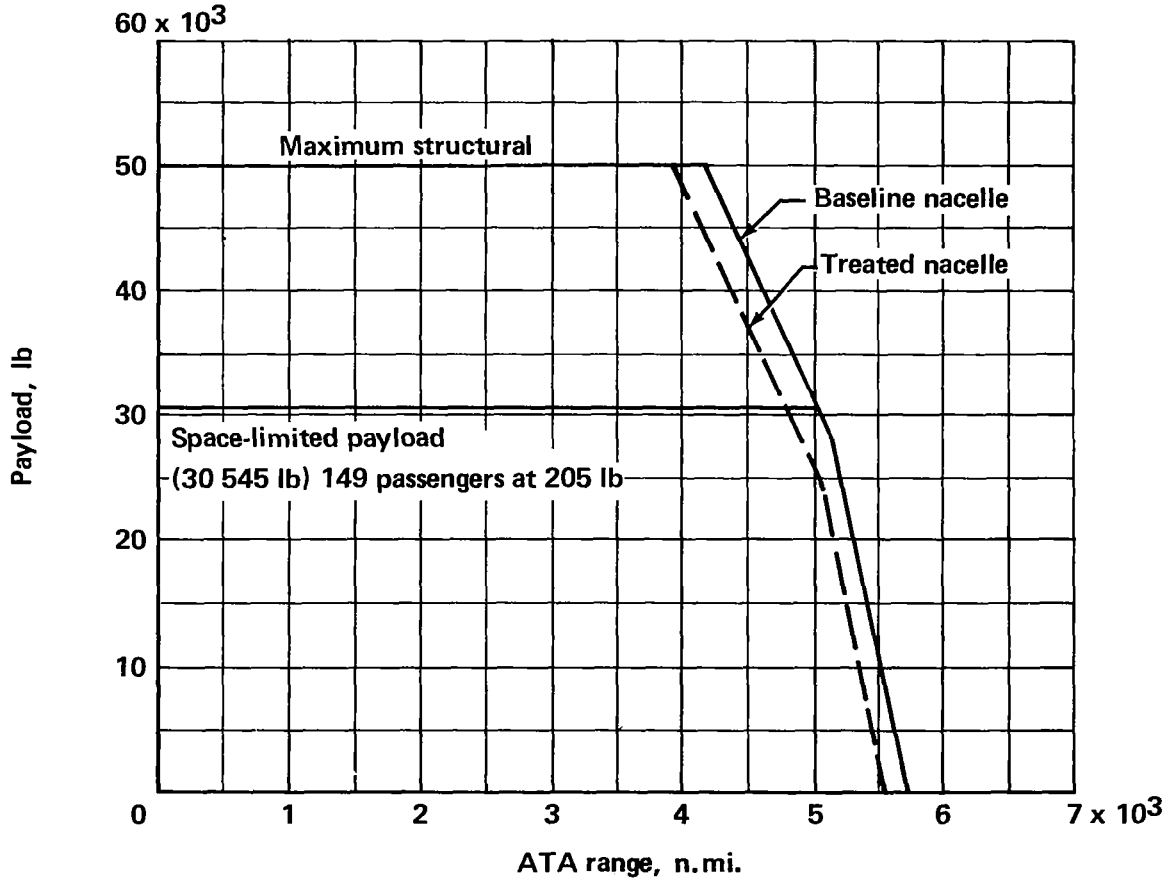

FIGURE 74.– RANGE PERFORMANCE–ATA DOMESTIC RESERVES, MINIMUM DIRECT OPERATING COST TECHNIQUE

- 707-320B/C
- Zero wind, standard day

Weight	Baseline nacelle, lb	Treated nacelle, lb
Max. gross takeoff	327 000	327 000
Operating empty	140 238	143 378
Max. zero fuel	190 000	193 140

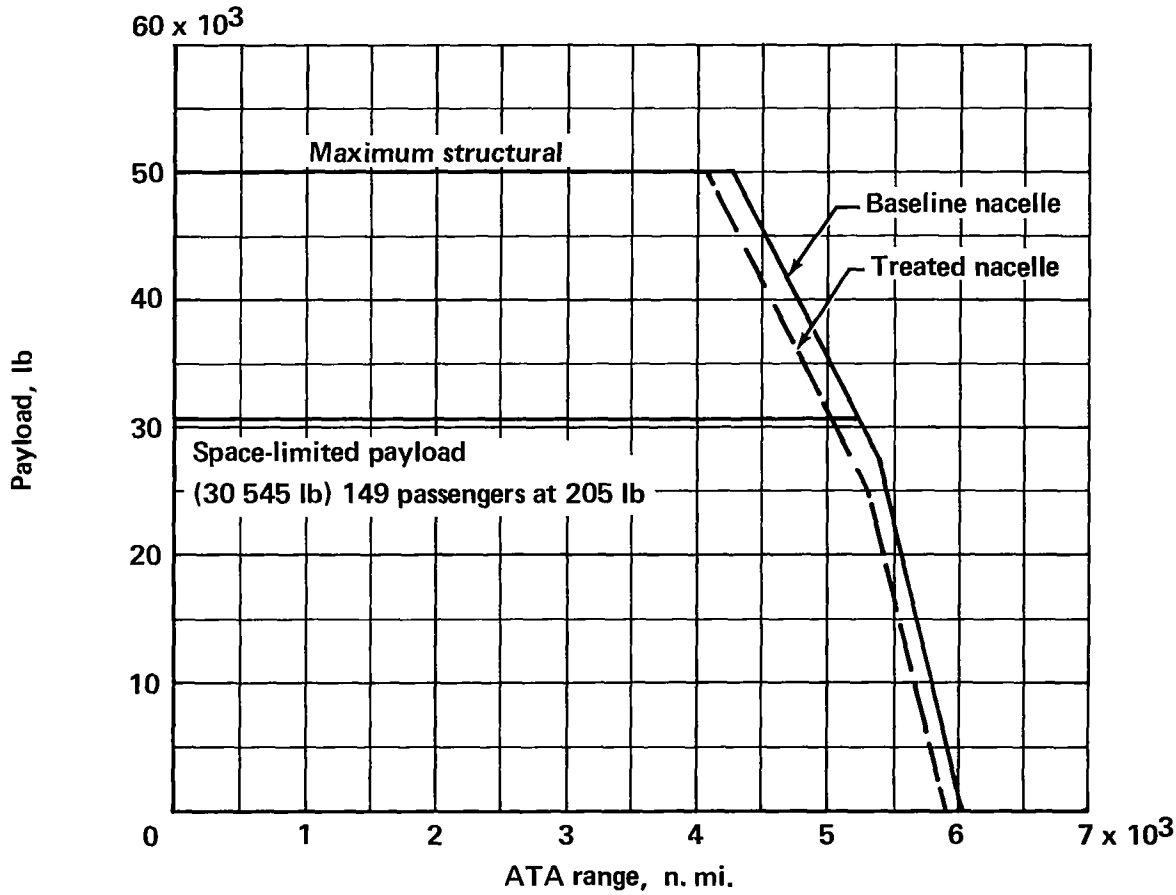

FIGURE 75.– RANGE PERFORMANCE–ATA INTERNATIONAL RESERVES, LONG-RANGE CRUISE TECHNIQUE

- 707-320B/C
- Zero wind, standard day

Weight	Baseline nacelle, lb	Treated nacelle, lb
Max. gross takeoff	327 000	327 000
Operating empty	140 238	143 378
Max. zero fuel	190 000	193 140

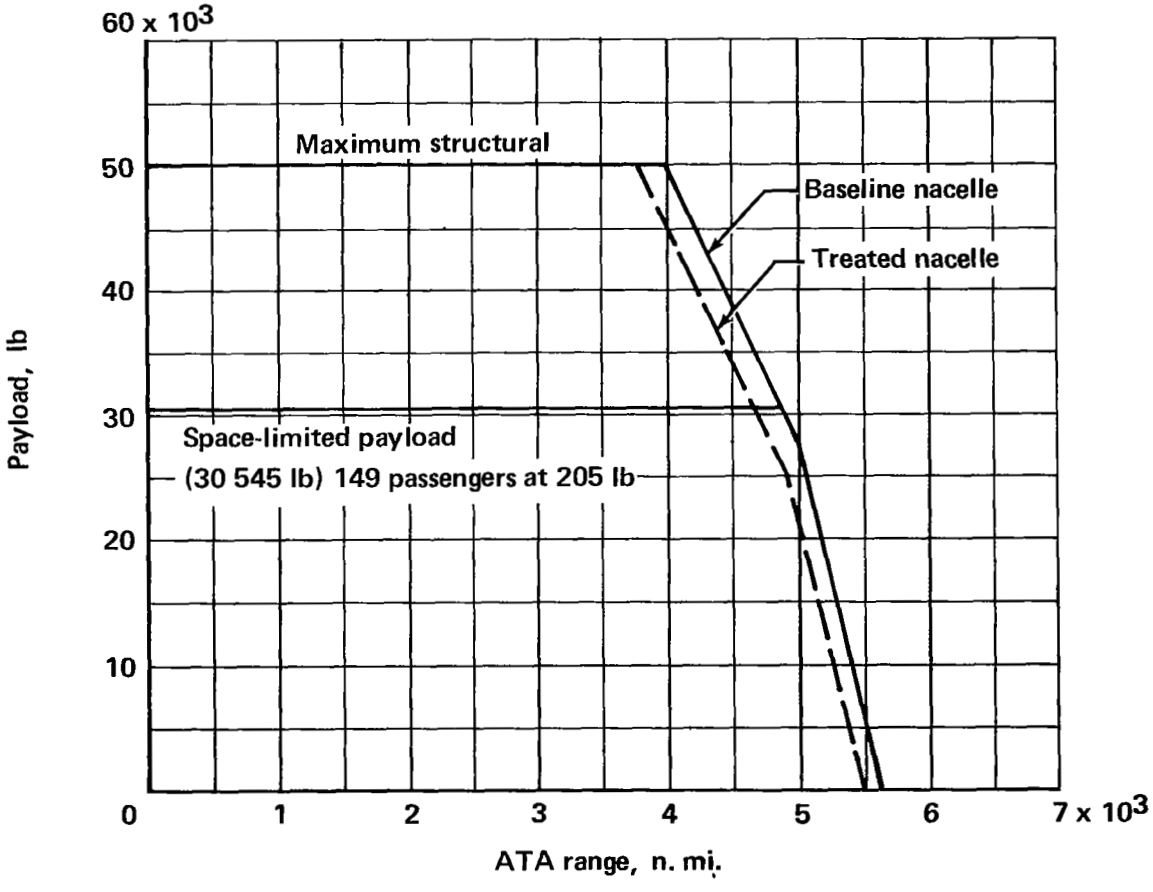

FIGURE 76.–RANGE PERFORMANCE–ATA INTERNATIONAL RESERVES, MINIMUM DIRECT OPERATING COST TECHNIQUE

NACELLE COMPONENT

- Constant speed drive
- Turbocompressor
- Ignition box connector
- Ignition exciter box
- Igniter lead
- Igniter plug
- Engine thermal anti-icing valve actuator
- Inlet rings thermal anti-icing valve actuator
- Fuel deicing valve actuator
- Fuel control body
- Fuel pump body
- Fuel pressure and dump valve
- Engine gas temperature harness
- Bleed actuator control body
- Water regulator
- Starter valve actuator
- N_2 tach generator mount flange
- Engine oil pressure transmitter

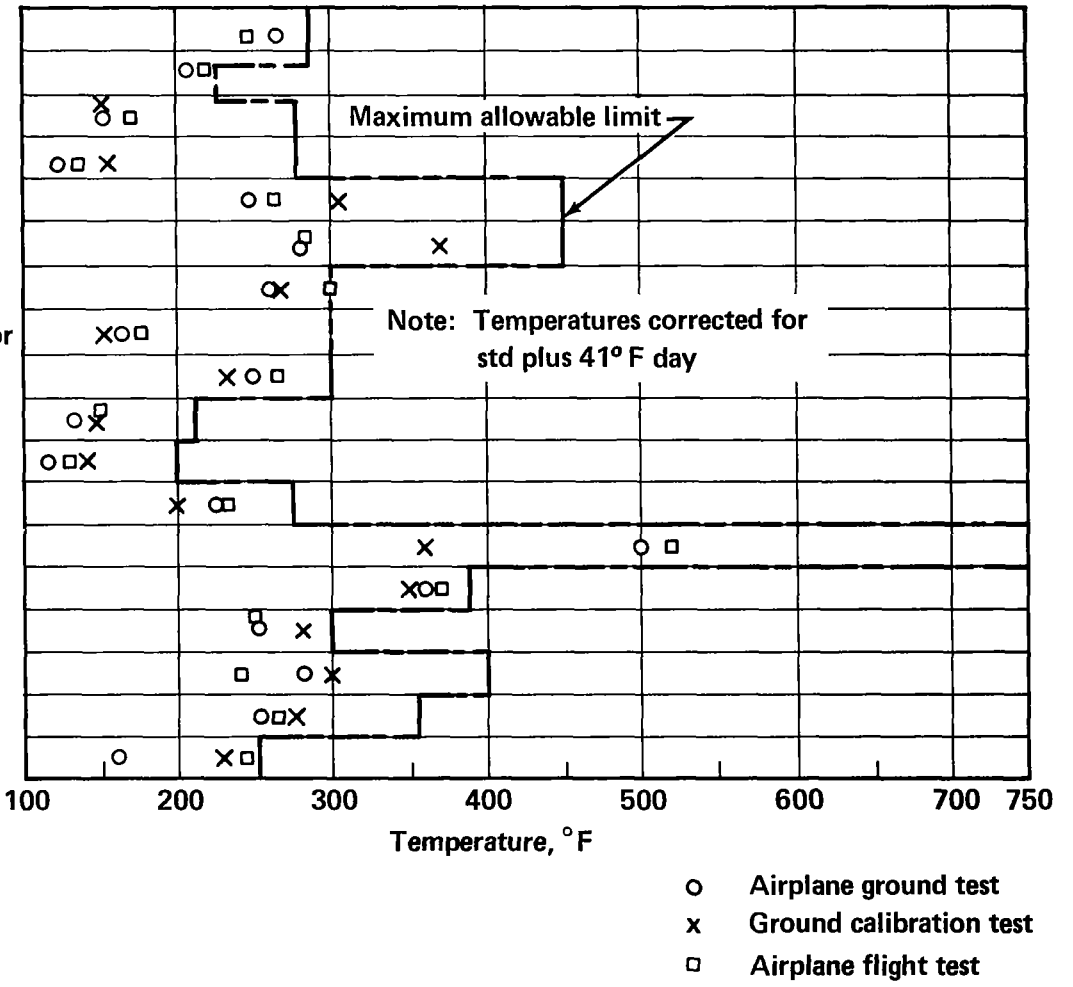

FIGURE 77.–FLIGHTWORTHY TREATED NACELLE MAXIMUM COMPONENT TEMPERATURES

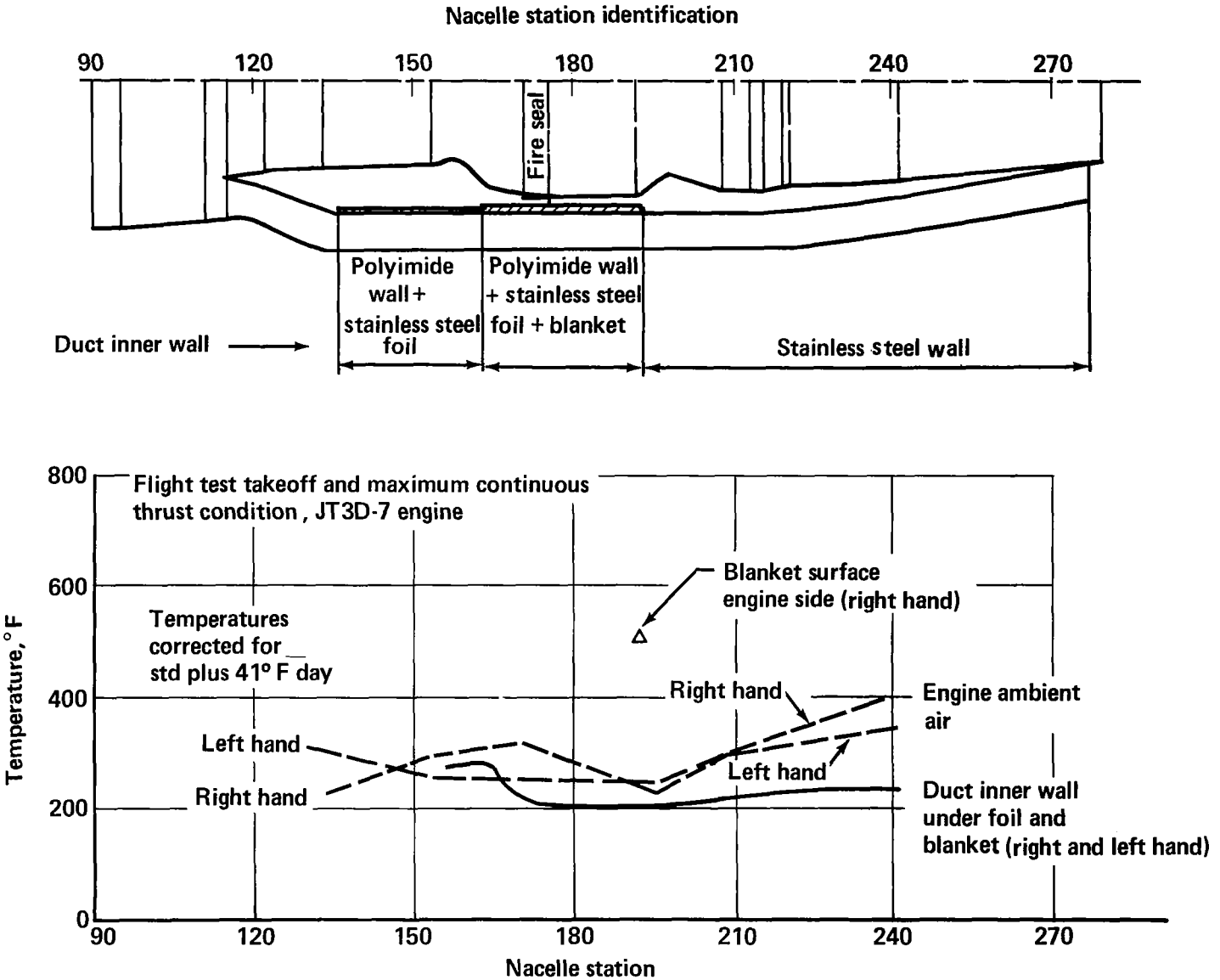

FIGURE 78.– FLIGHTWORTHY TREATED NACELLE MAXIMUM TEMPERATURES DURING FLIGHT TEST

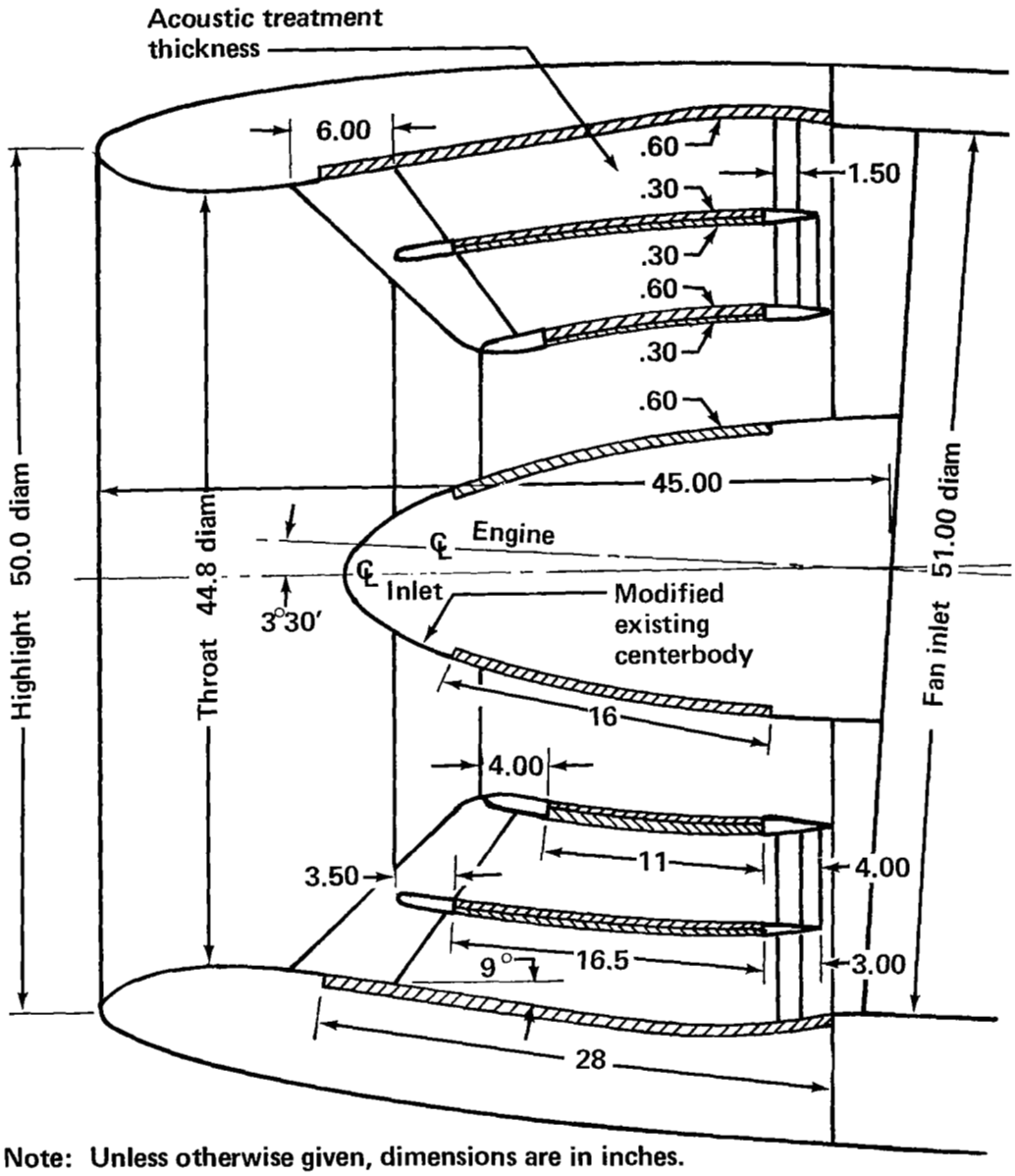

Note: Unless otherwise given, dimensions are in inches.

INLET CROSS SECTION

FIGURE 79.–FLIGHTWORTHY TREATED INLET CONFIGURATION (TWO TREATED RINGS, EIGHT VANES)

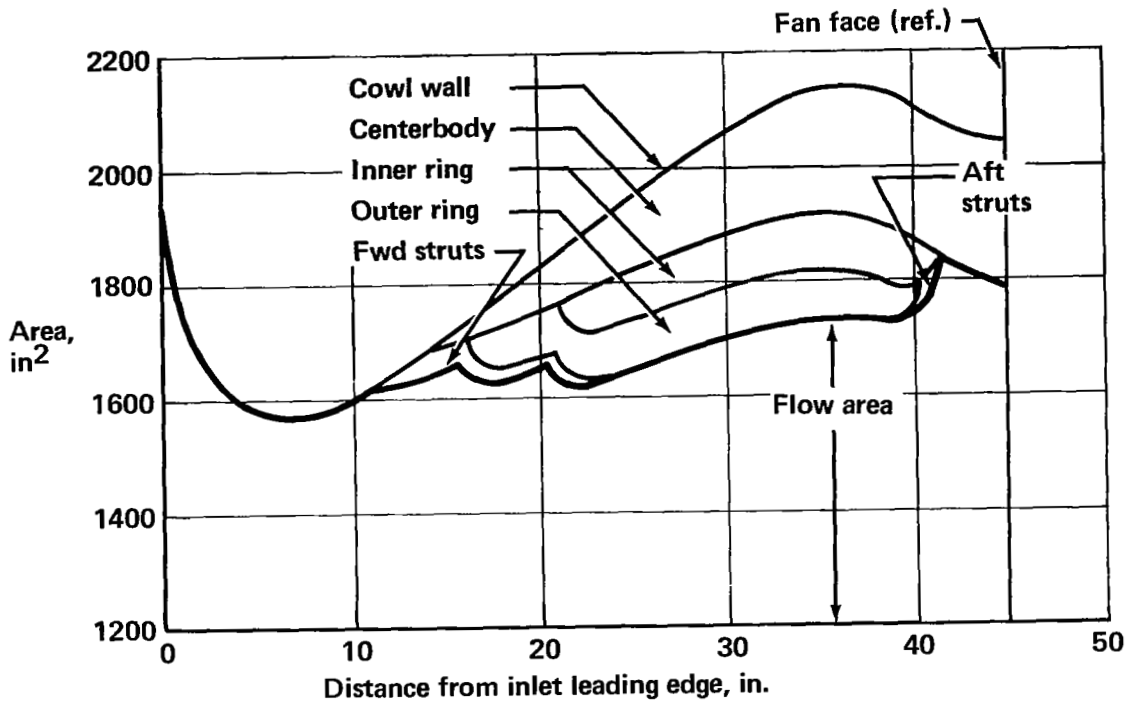

FIGURE 80.– INLET AREA DISTRIBUTION

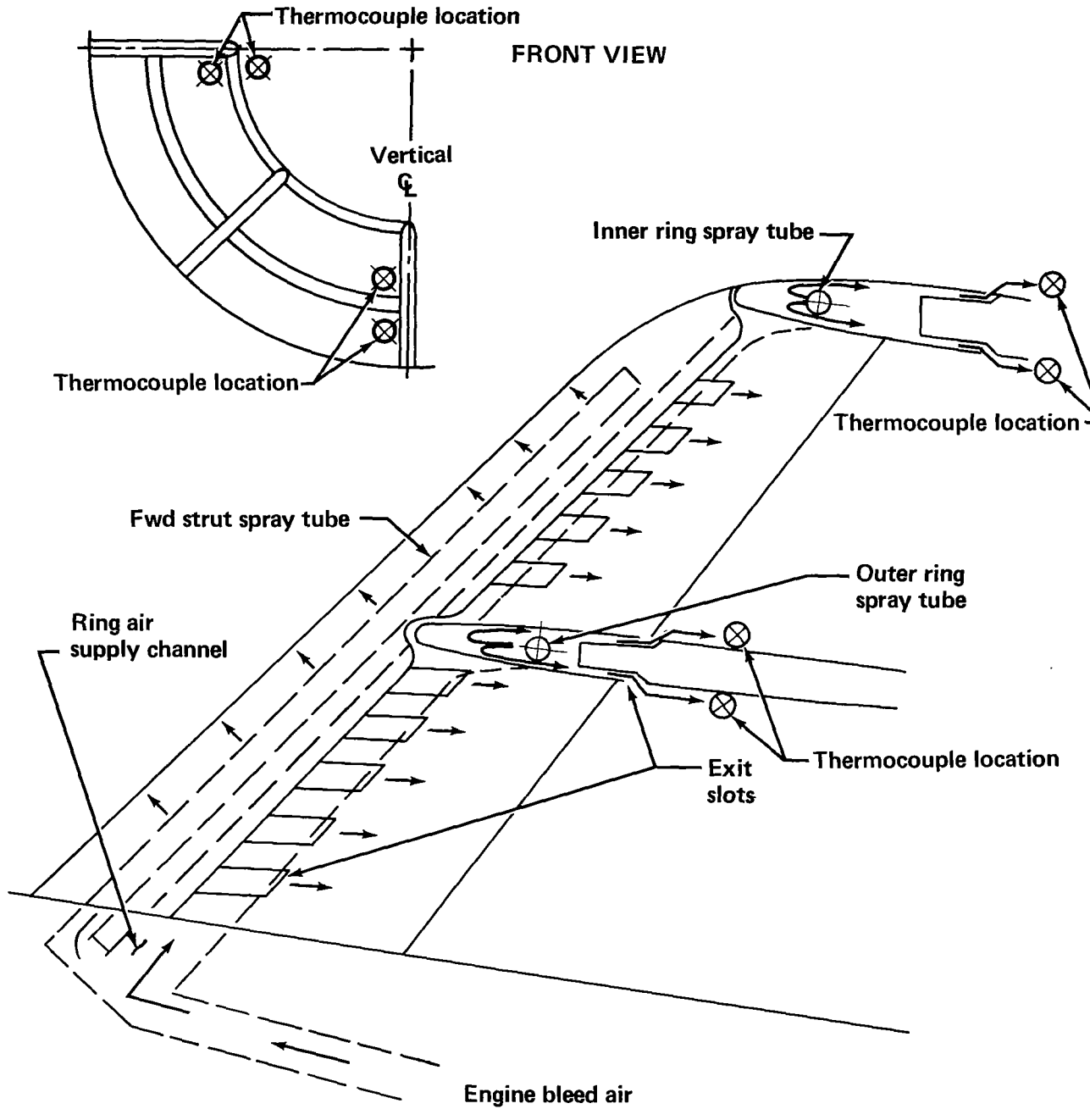

FIGURE 81.—TREATED INLET RINGS AND STRUTS, THERMAL ANTI-ICING

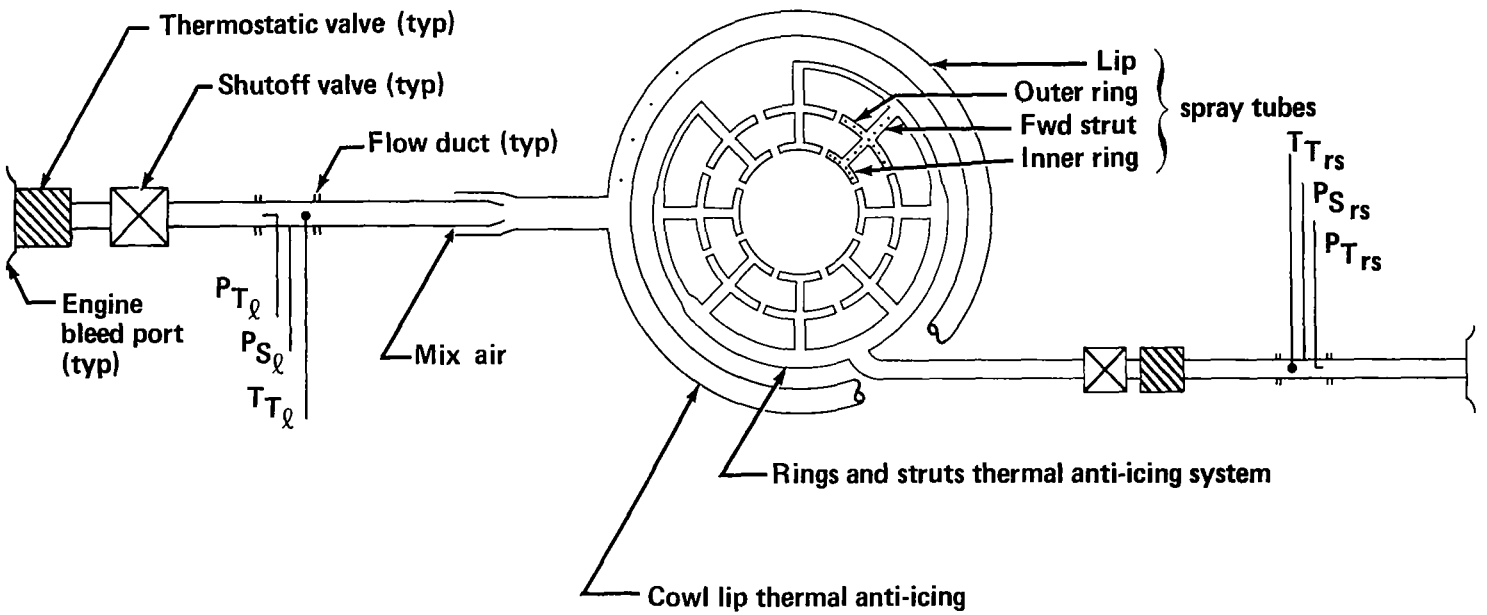

FIGURE 82.—THERMAL ANTI-ICING TEST, JT3D TREATED NACELLE

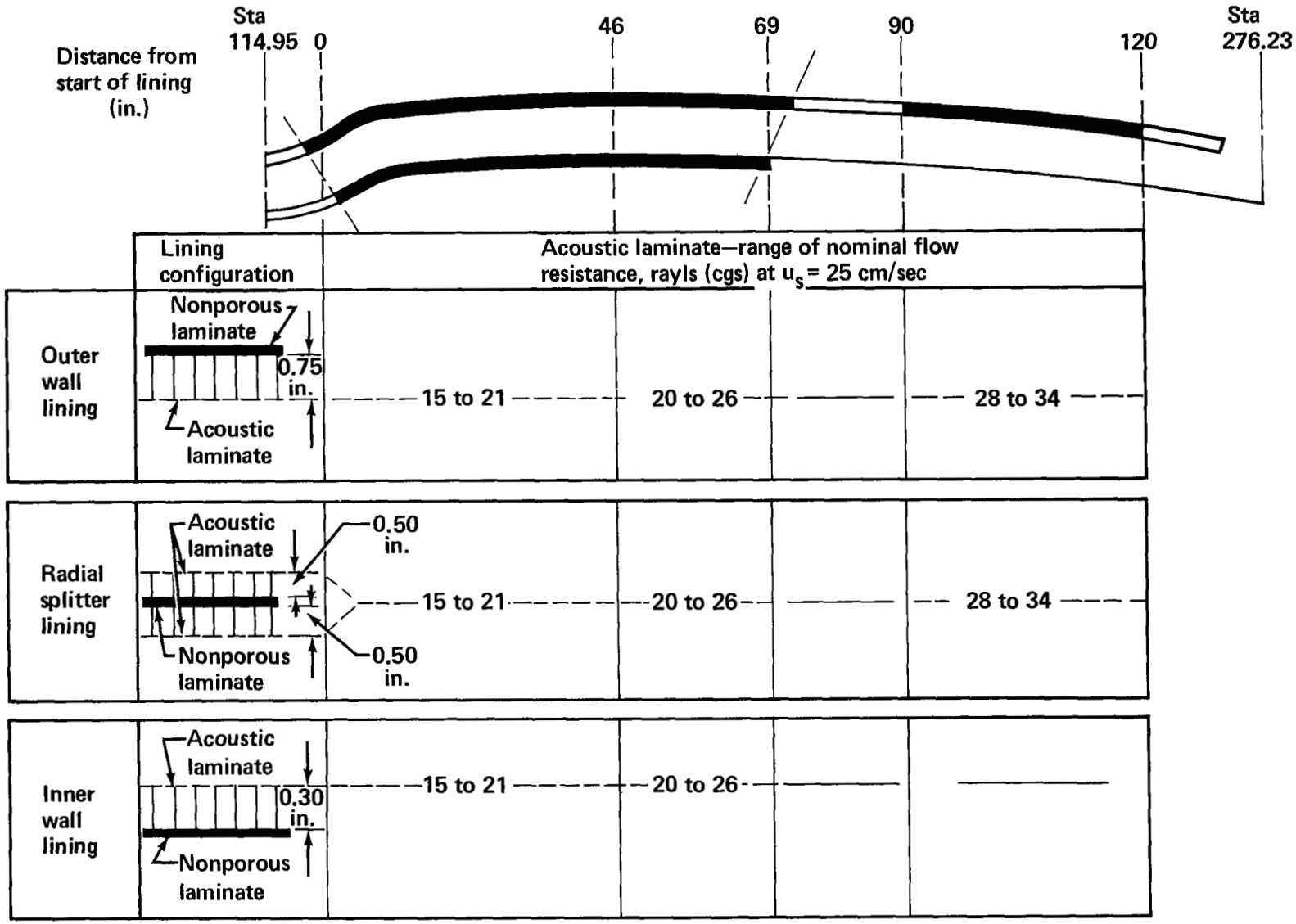

FIGURE 83.—FLIGHTWORTHY FAN DUCT ACOUSTIC LINING CONFIGURATION

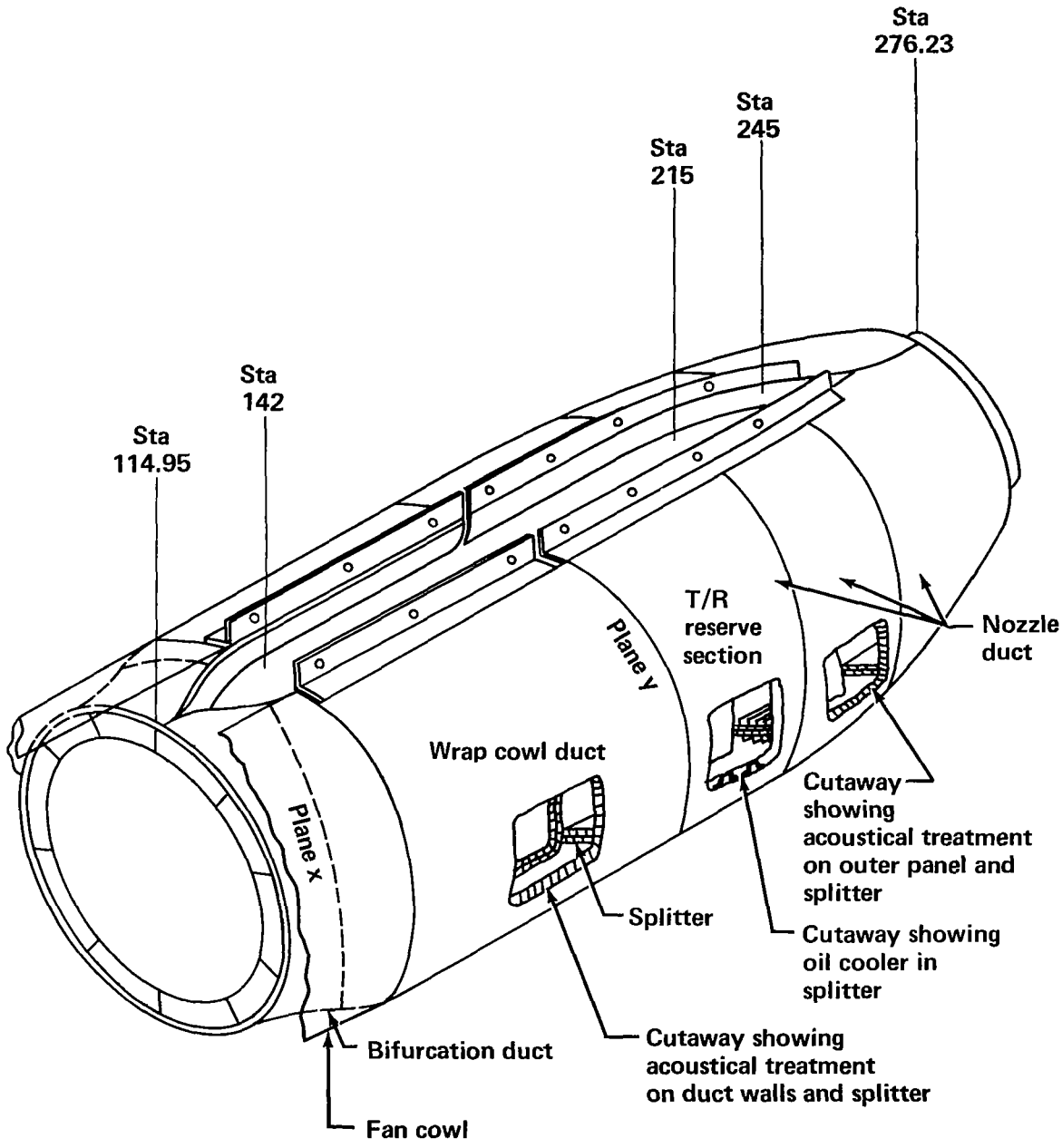

FIGURE 84.– FLIGHTWORTHY FAN DUCT INSTALLATION

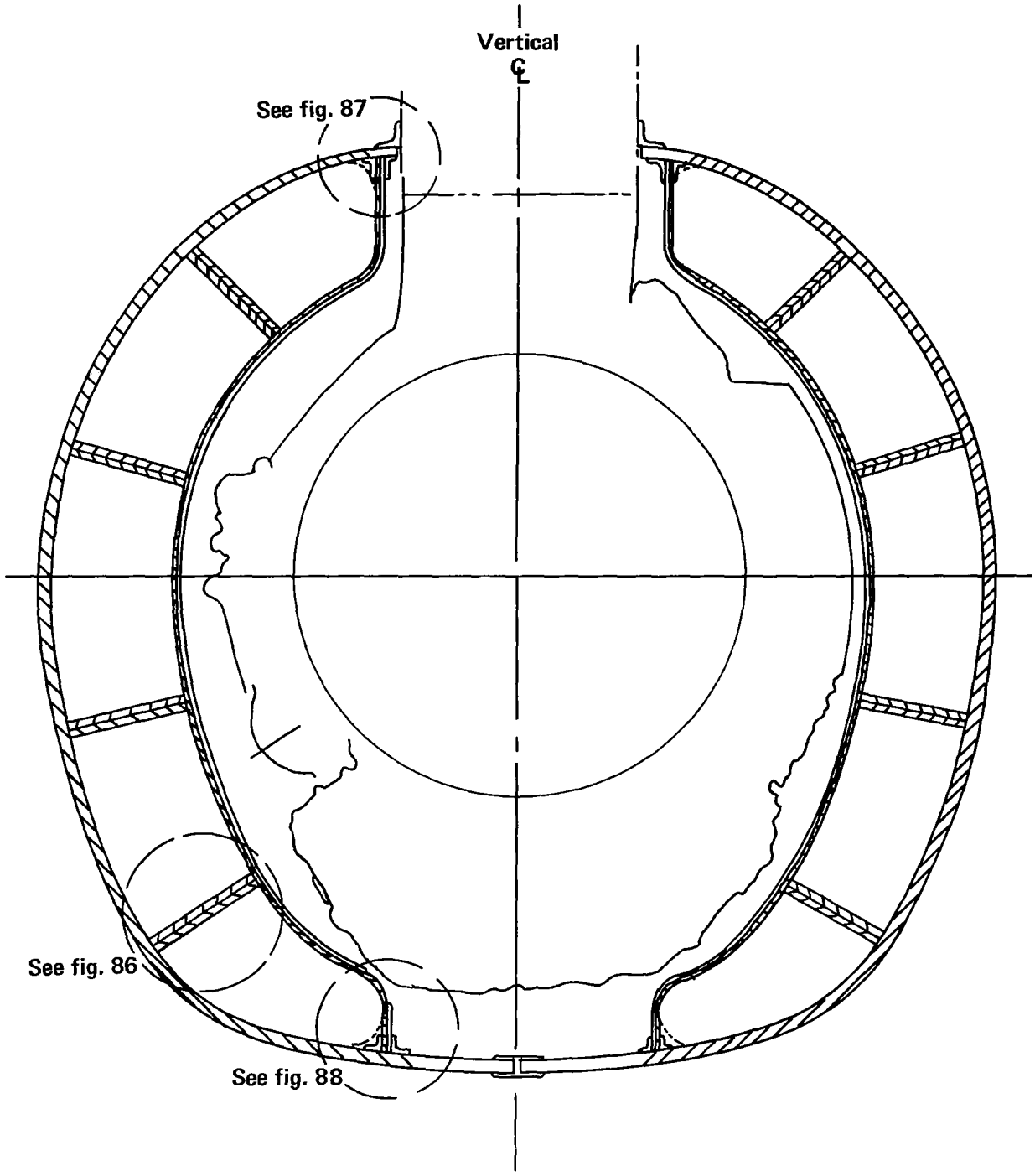

FIGURE 85.– WRAP COWL DUCT–SECTION AT CONSTANT AREA

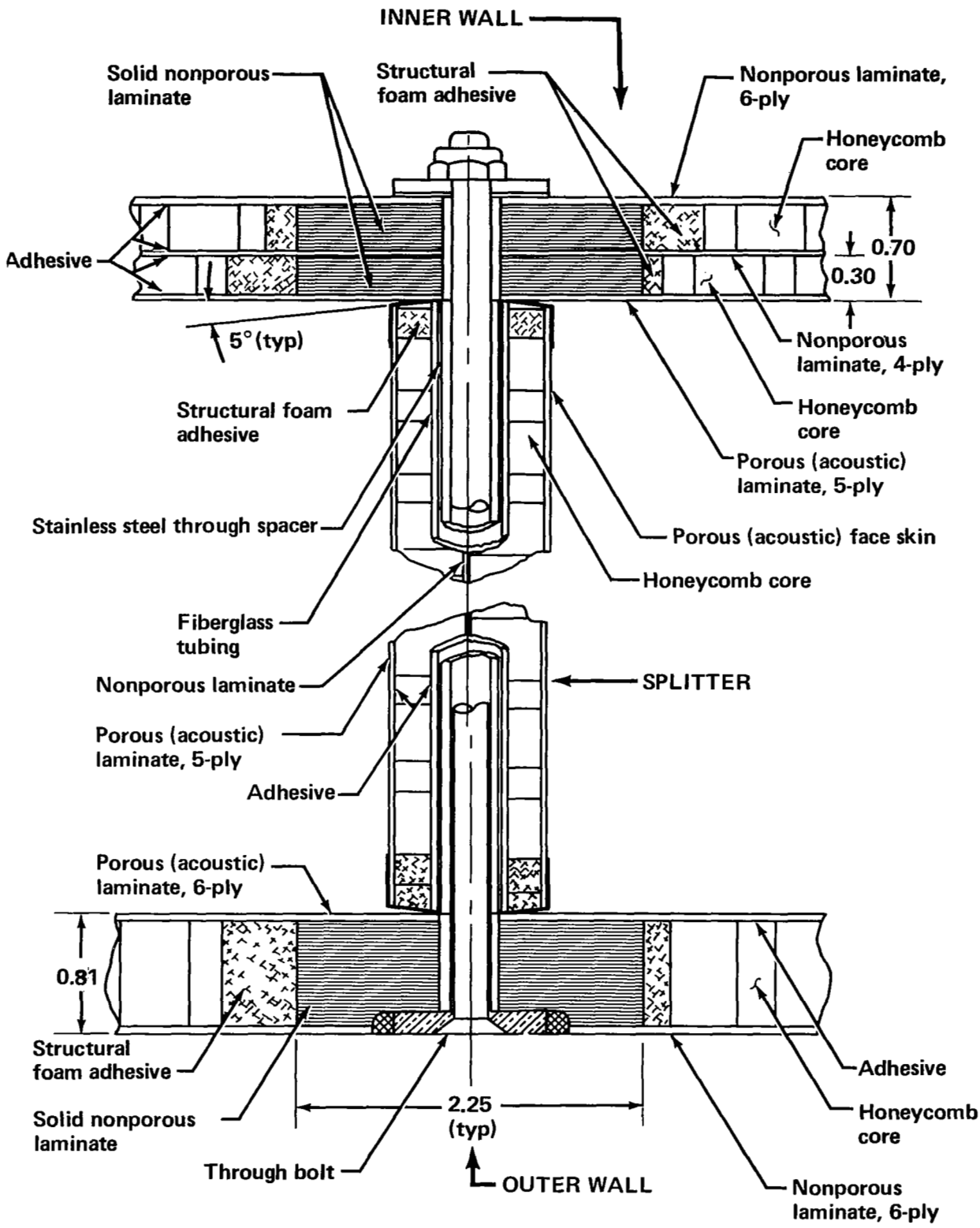

FIGURE 86.—WRAP COWL DUCT SPLITTER ATTACHMENT

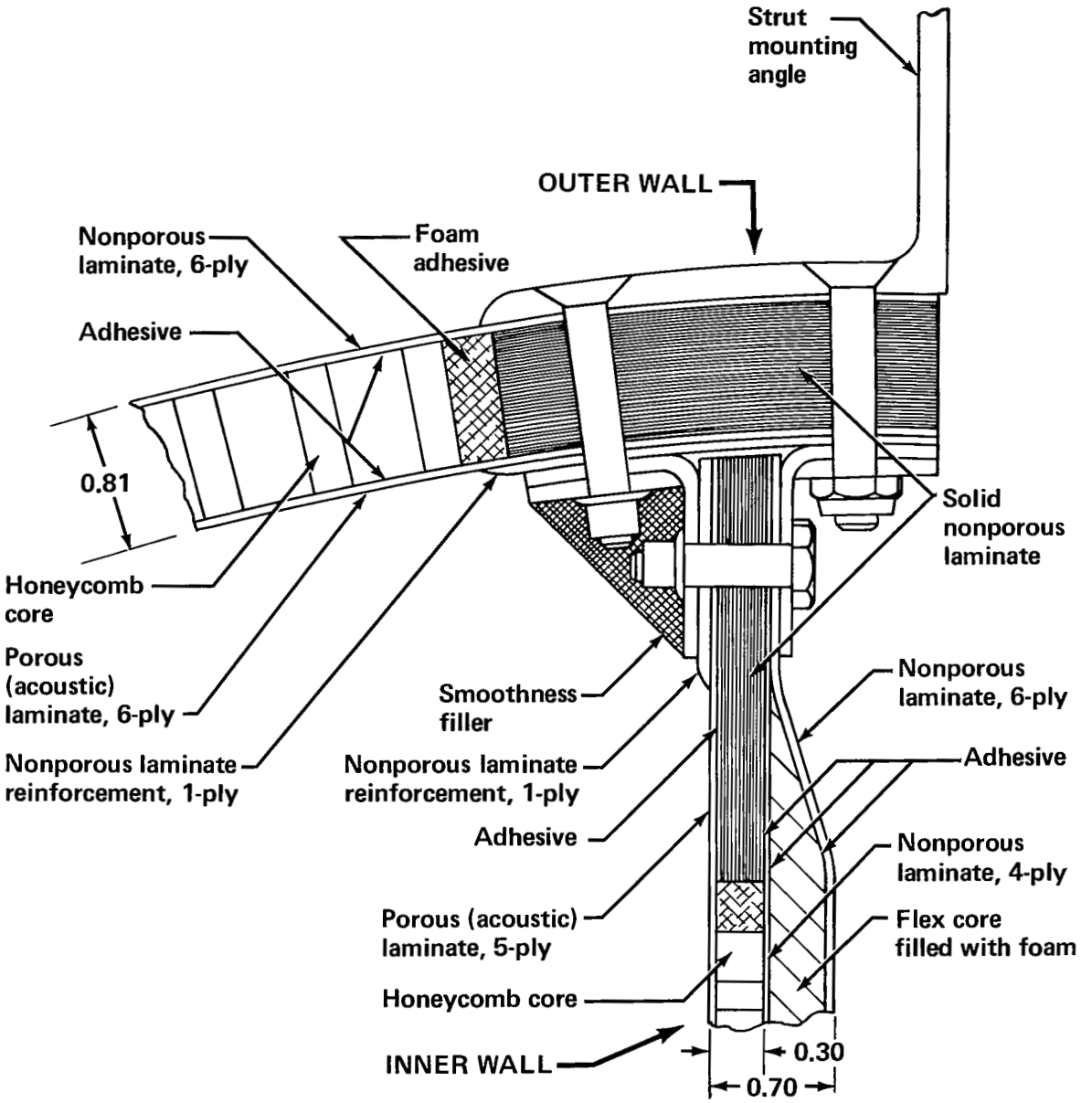

FIGURE 87.– WRAP COWL DUCT UPPER JOINT, INNER AND OUTER WALL PANELS

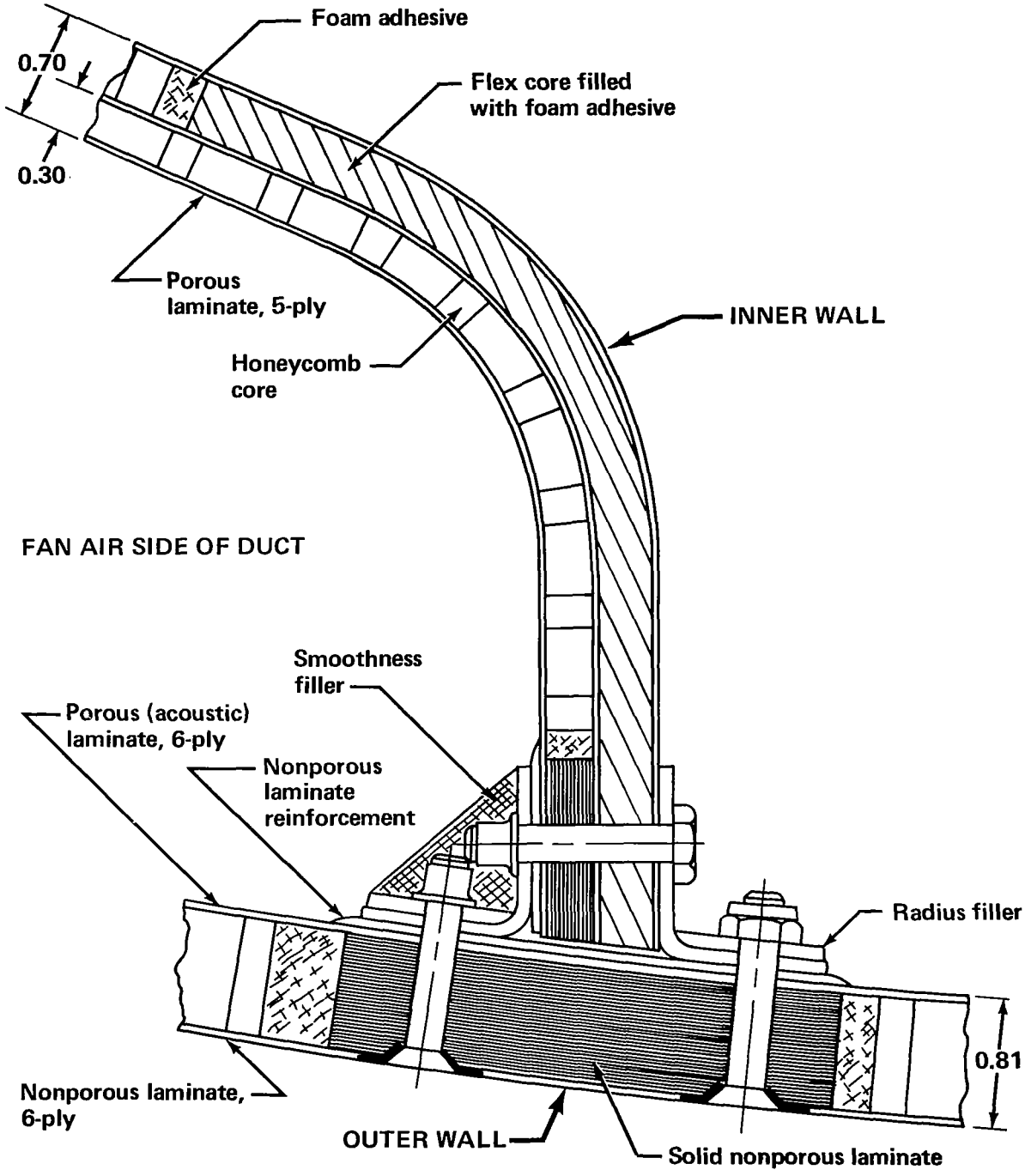

FIGURE 88.—WRAP COWL DUCT LOWER JOINT, INNER AND OUTER WALL PANELS

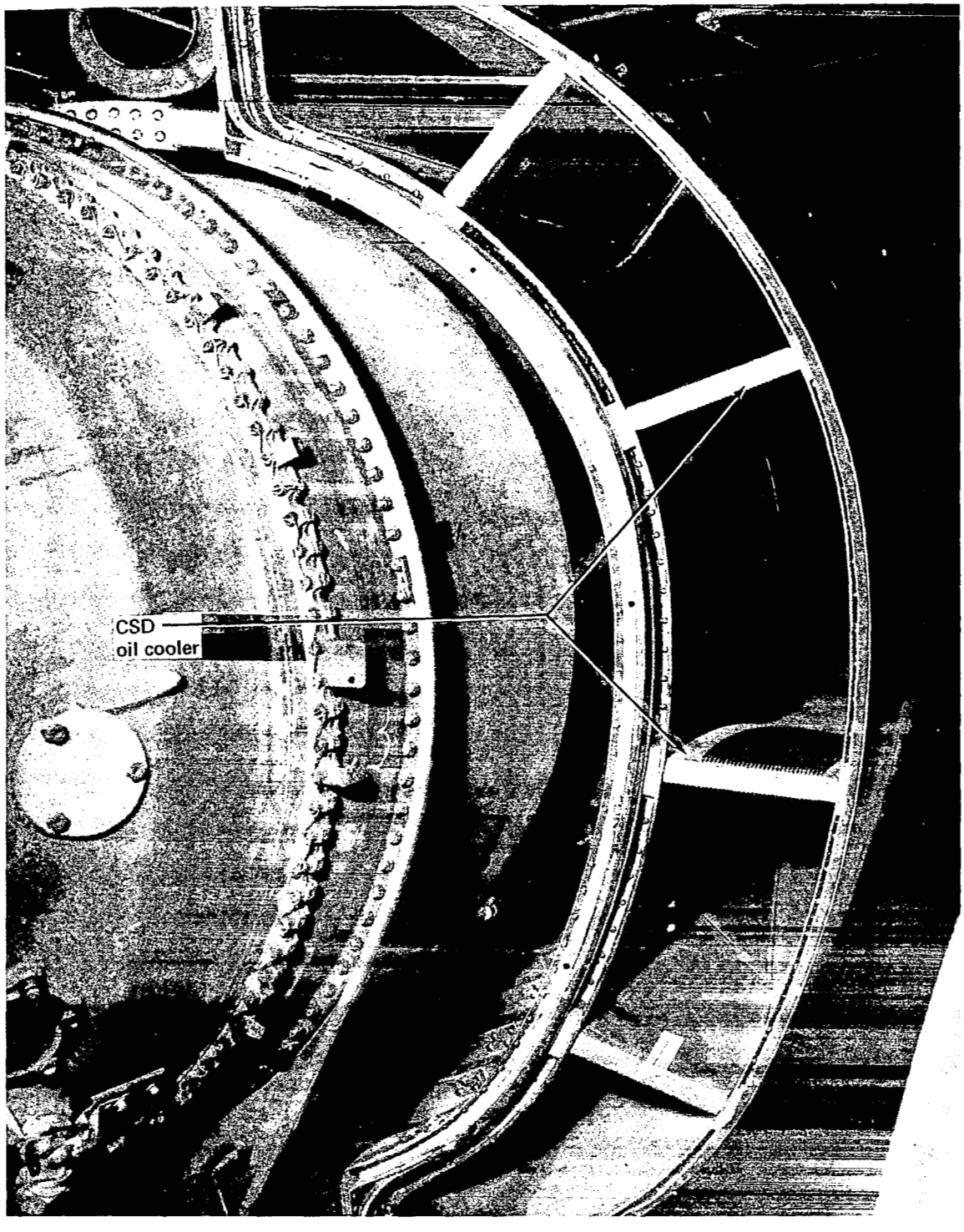

FIGURE 89.—FLIGHTWORTHY FAN DUCT—NOZZLE DUCT, LEFT-HAND SIDE

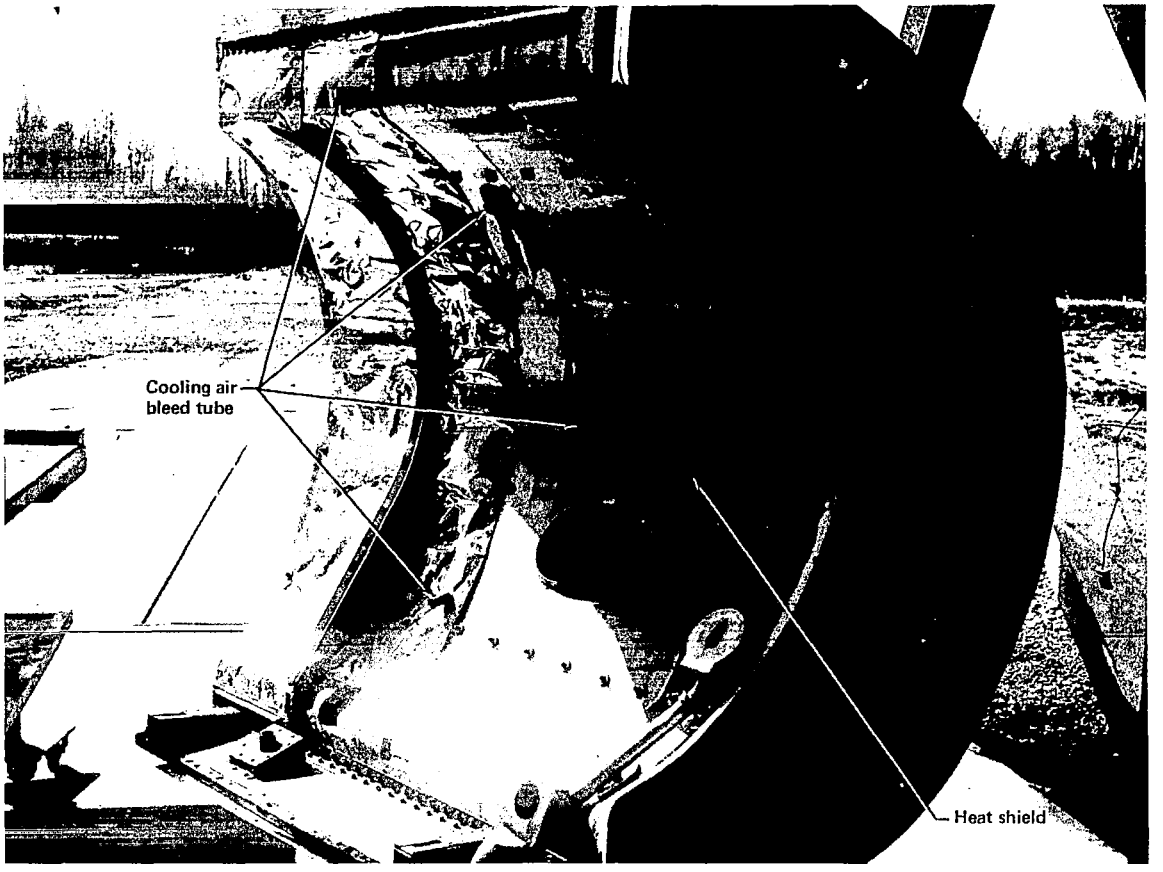

FIGURE 90.– FLIGHTWORTHY FAN DUCT–LEFT-HAND WRAP COWL

FIGURE 91.– TREATED INLET–FINAL ASSEMBLY OF EXTERNAL COWL

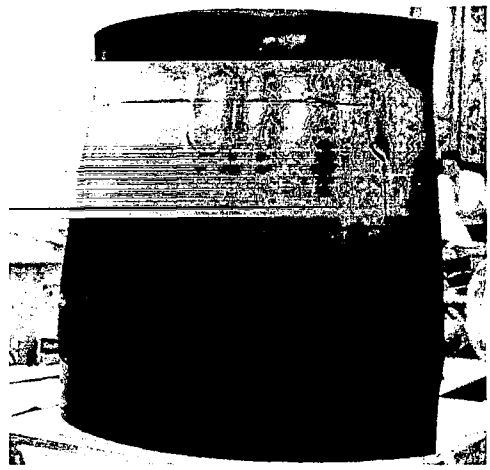

FIGURE 92.– TREATED INLET–TYPICAL SANDWICH PANEL TOOLING SURFACE

FIGURE 93.– TREATED INLET–TYPICAL PLASTER MANDREL TOOL

FIGURE 94.– TREATED INLET–ACOUSTIC TREATMENT ASSEMBLIES

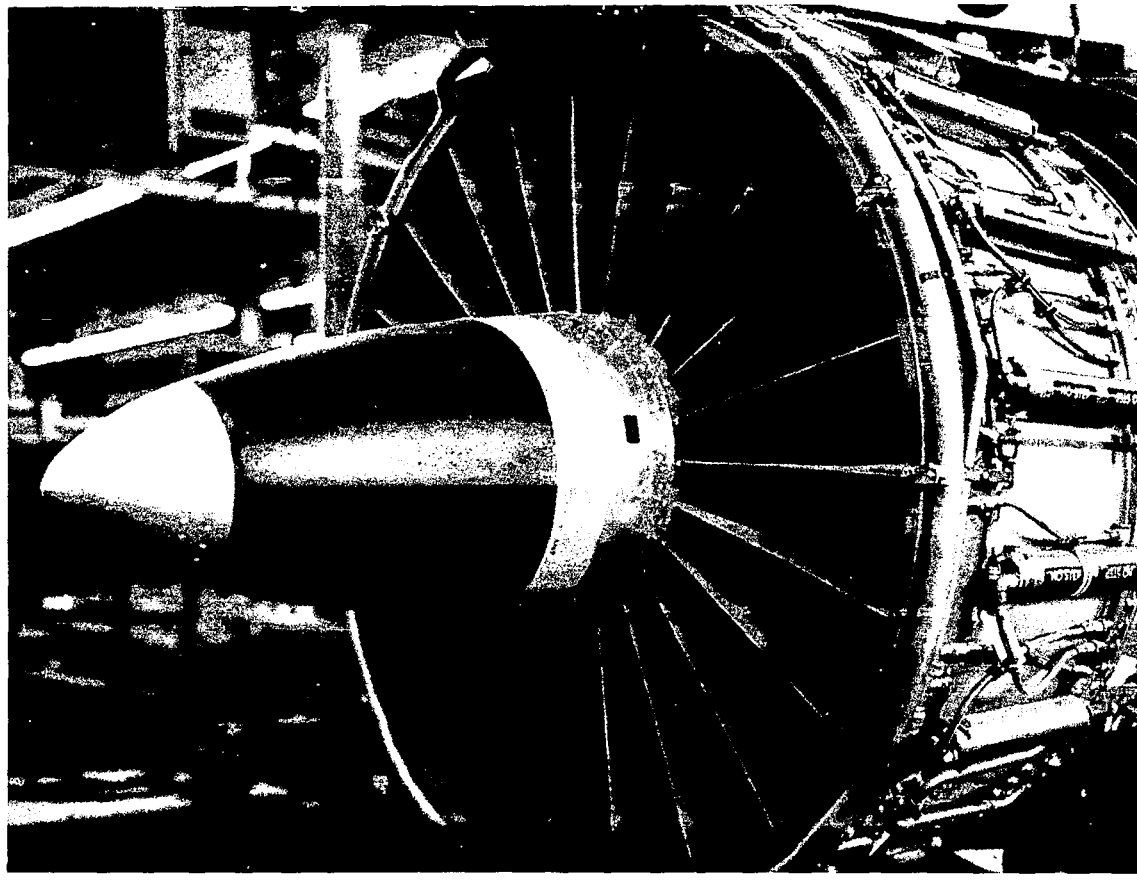

FIGURE 95.-- TREATED INLET--ACOUSTICALLY TREATED CENTERBODY

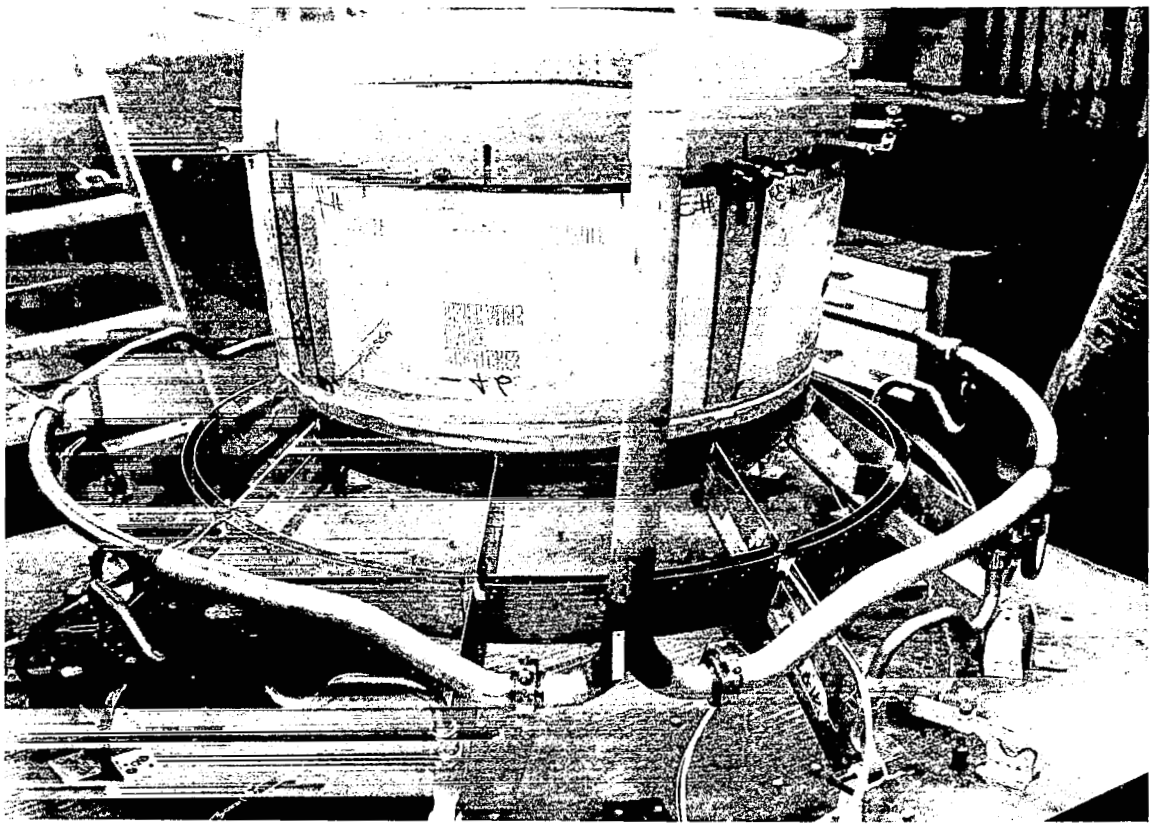

FIGURE 96.– TREATED INLET–ACOUSTIC TREATMENT SUBASSEMBLY

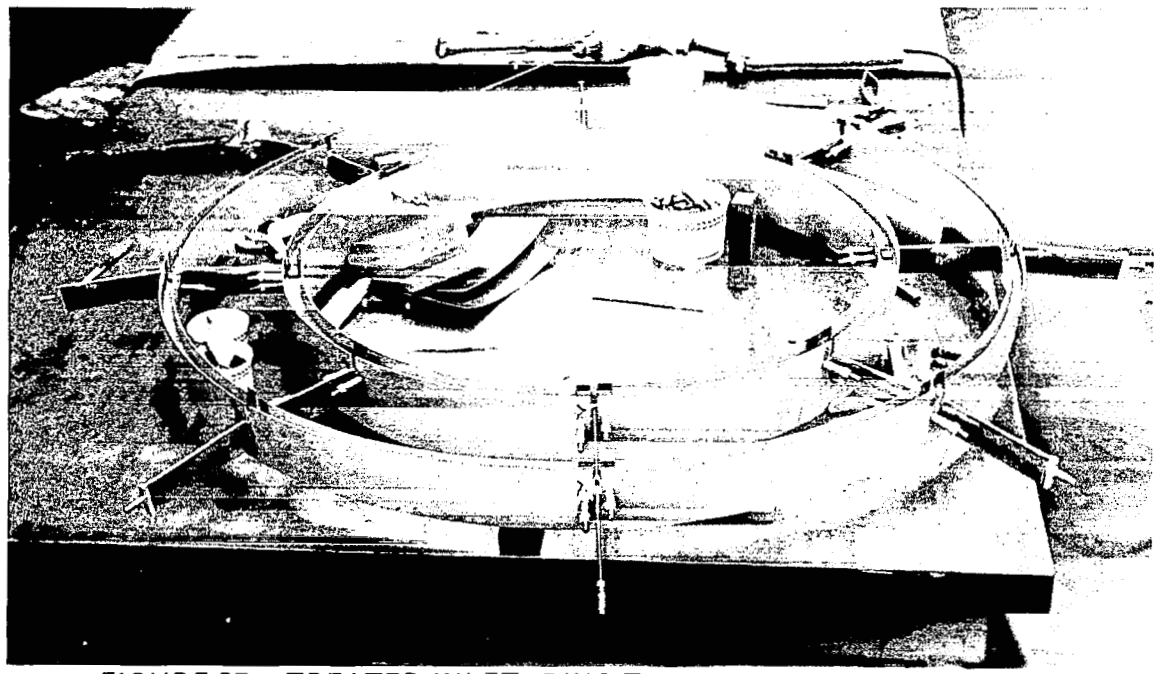

FIGURE 97.– TREATED INLET–RING TRAILING-EDGE SUBASSEMBLY

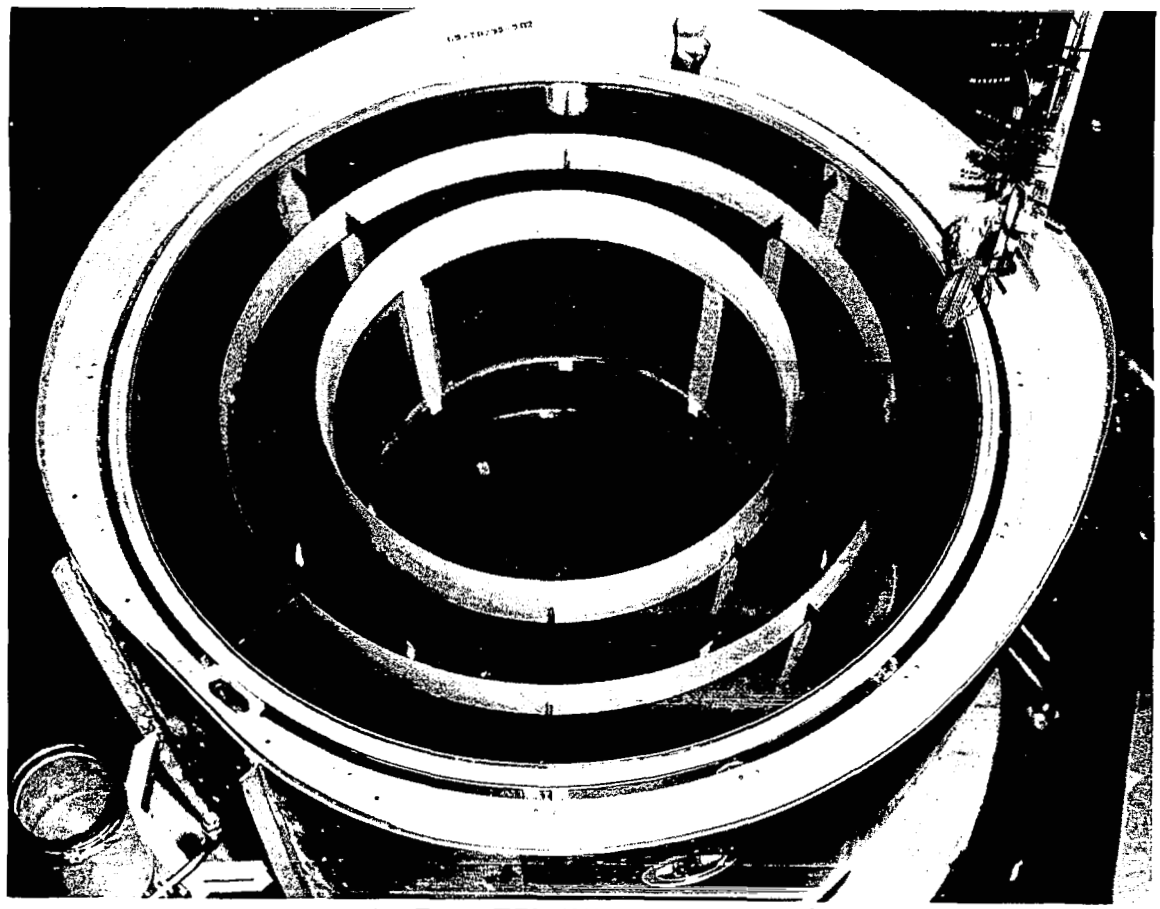

FIGURE 98.–TREATED INLET–FINAL ASSEMBLY

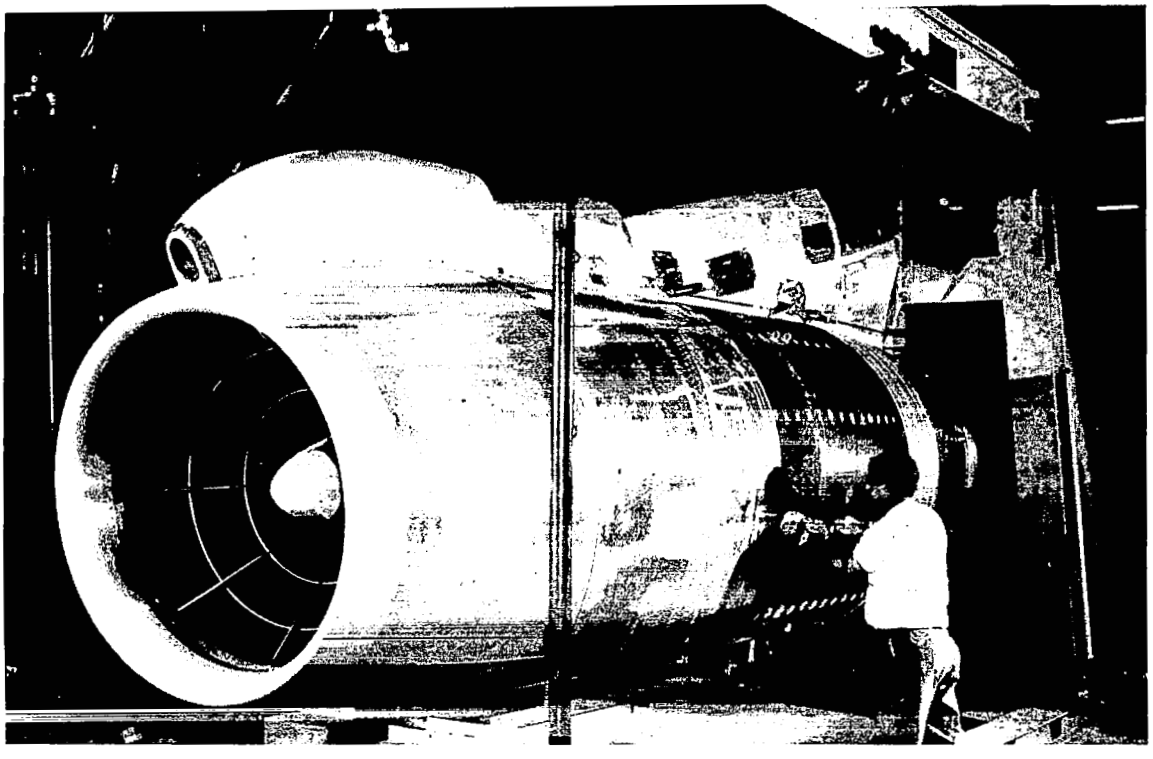

FIGURE 99.—TREATED NACELLE—MOCKUP FIT CHECK

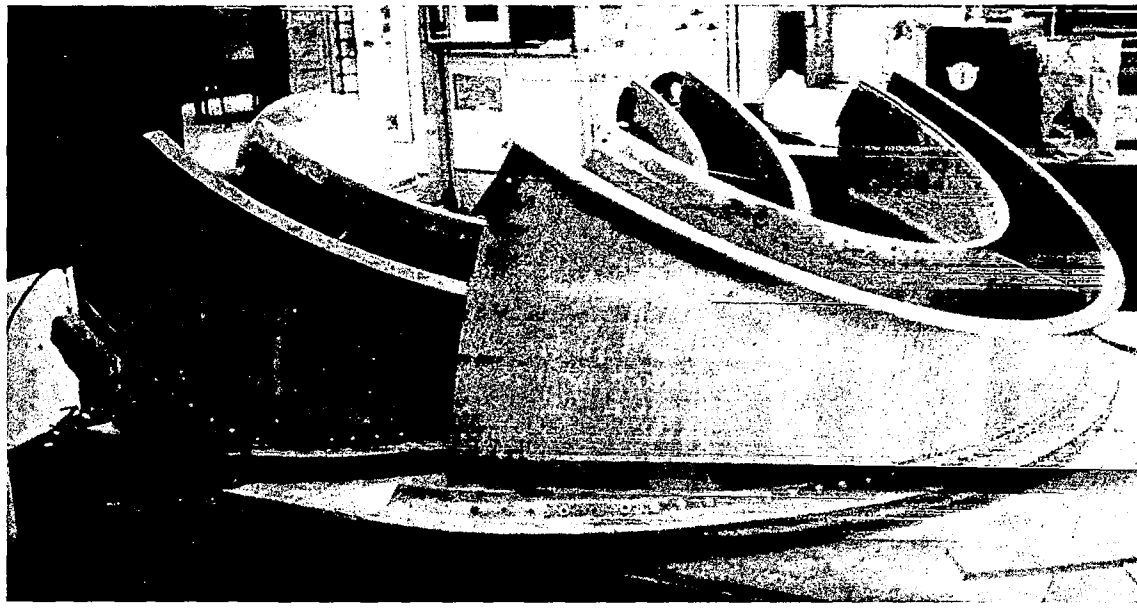

FIGURE 100.– FLIGHTWORTHY NACELLE BIFURCATION DUCT

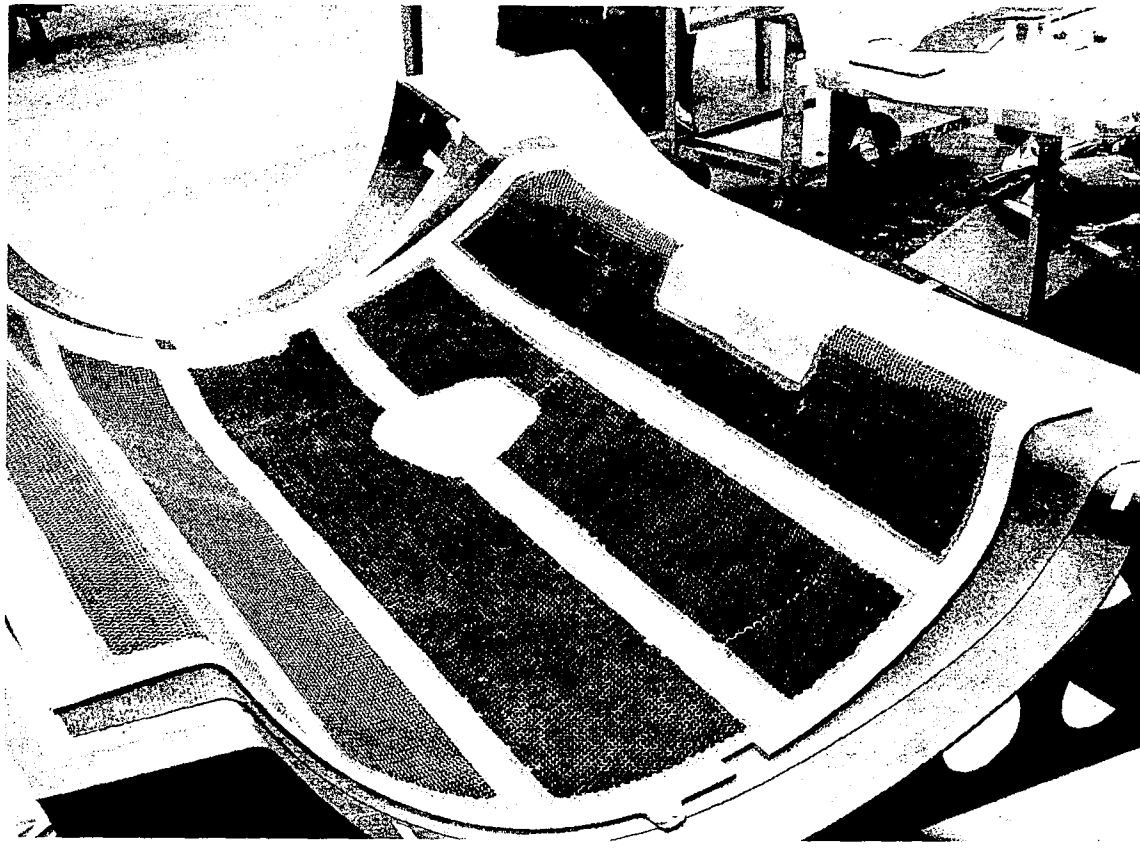

FIGURE 101.–FLIGHTWORTHY NACELLE WRAP COWL DUCT INNER WALL

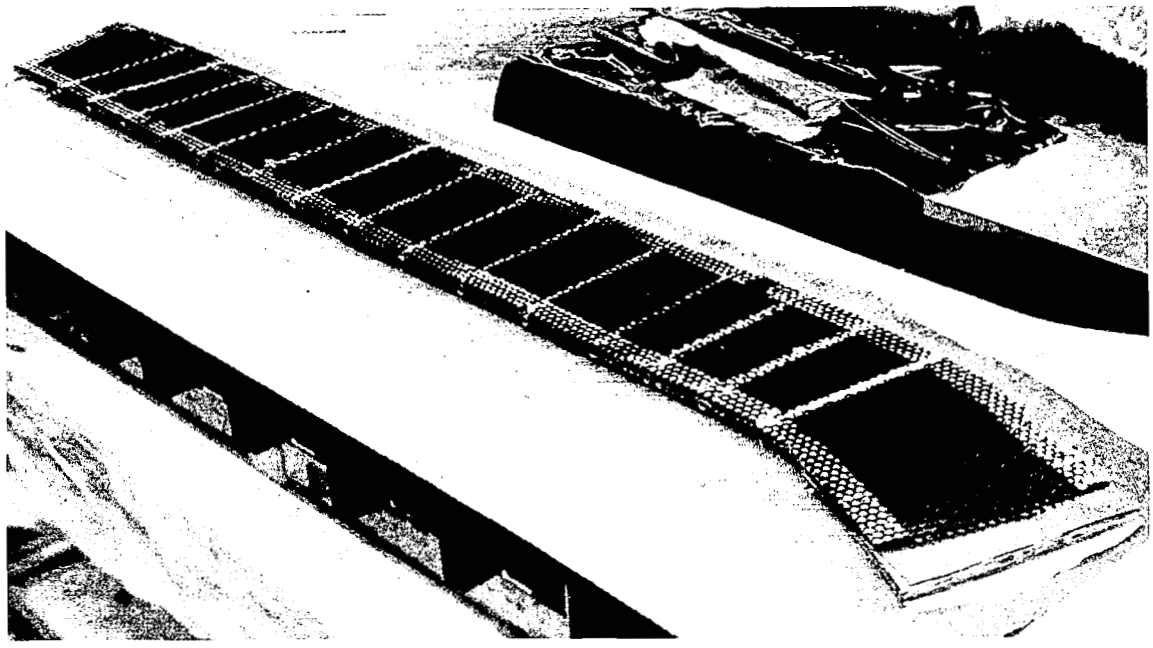

FIGURE 102.—FLIGHTWORTHY NACELLE WRAP COWL DUCT SPLITTER

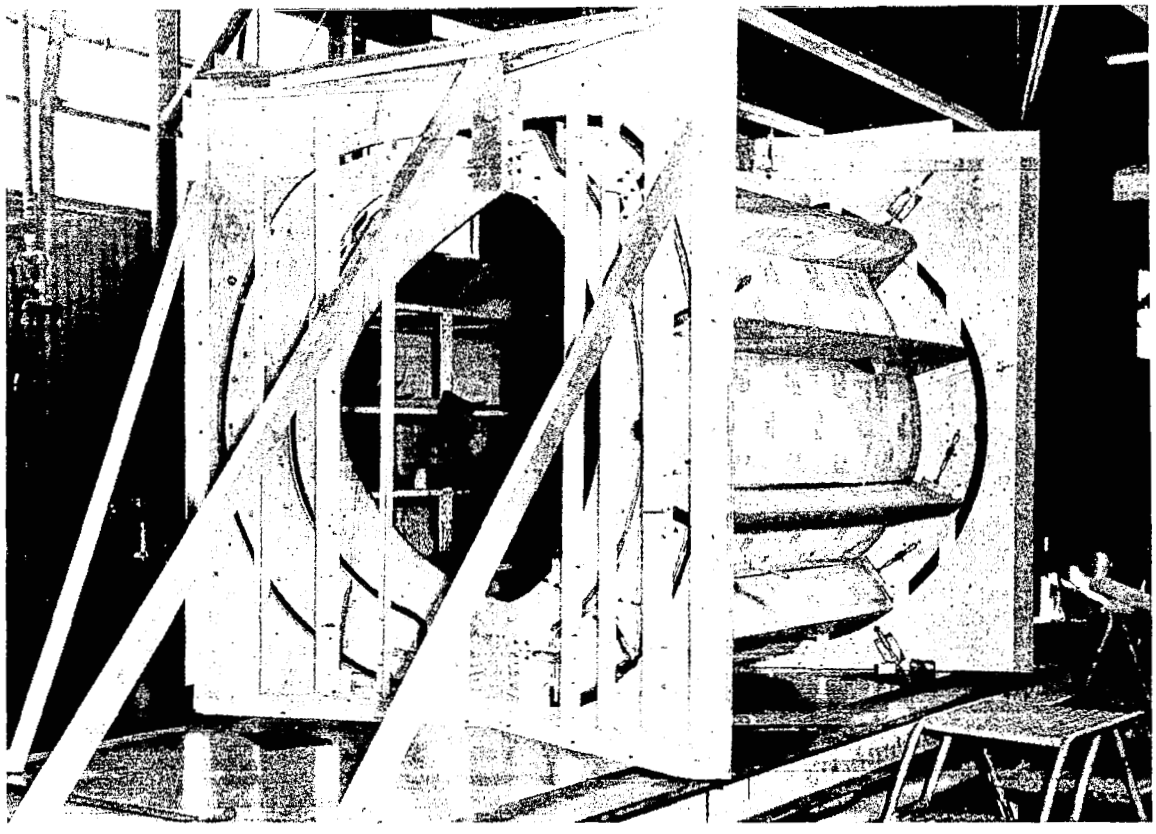

FIGURE 103.—FLIGHTWORTHY NACELLE DRILL AND ASSEMBLY FIXTURE WRAP COWL DUCT

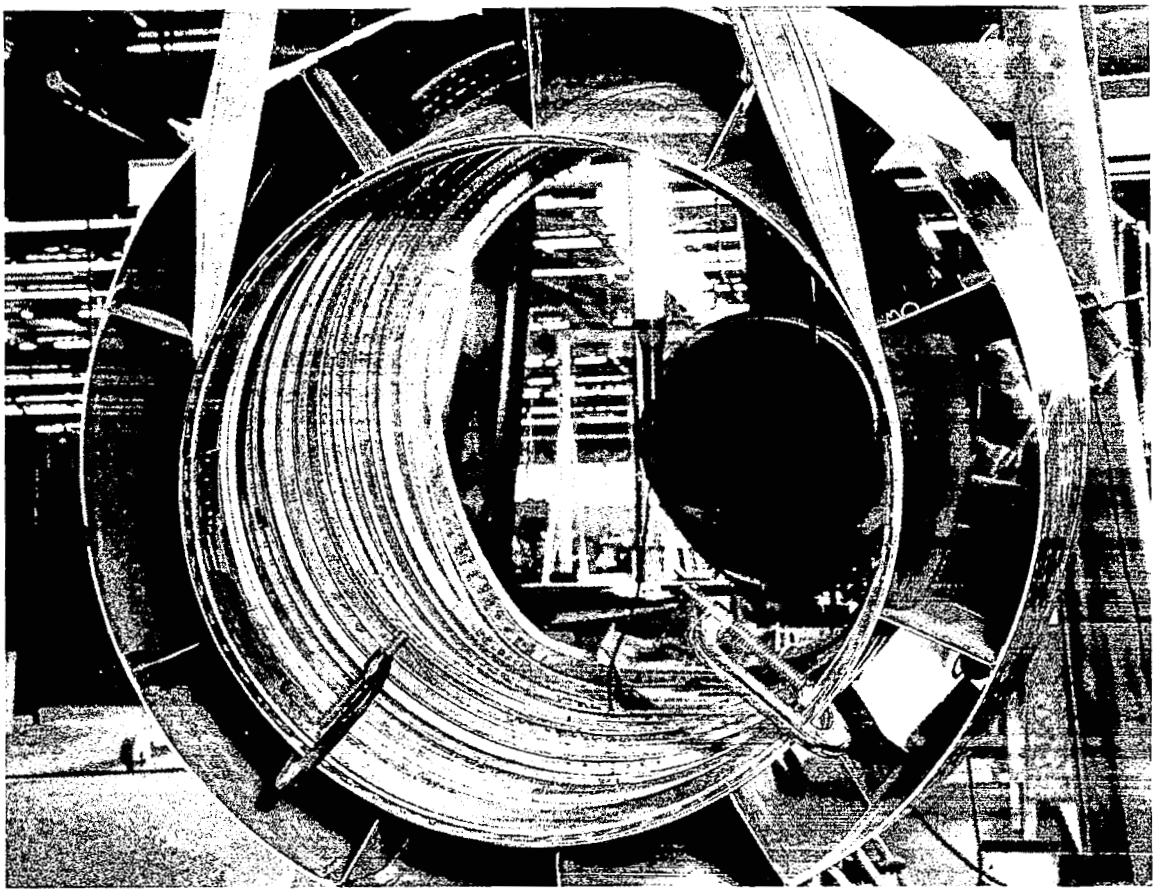

FIGURE 104.—FLIGHTWORTHY NACELLE NOZZLE DUCT, REAR VIEW

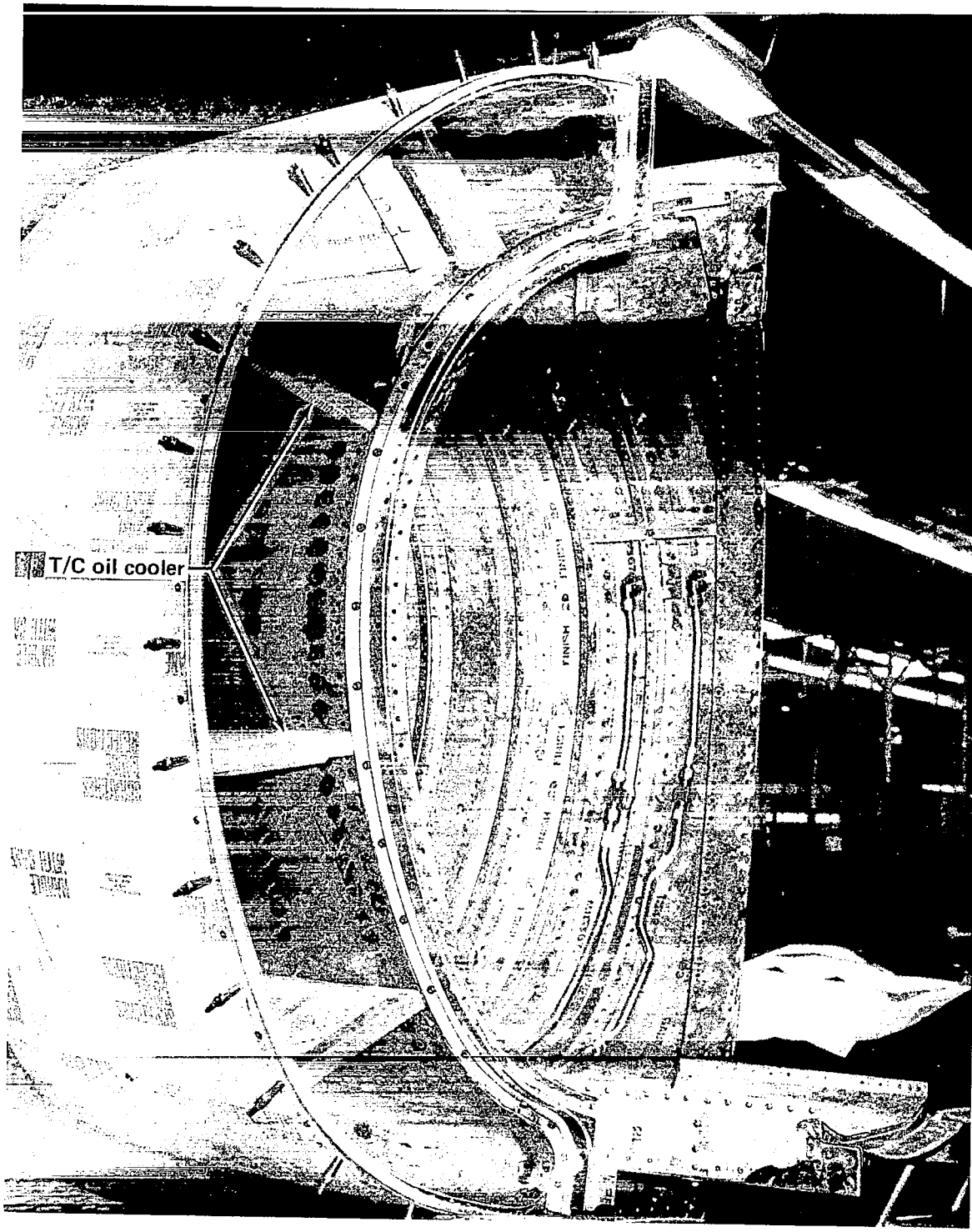

FIGURE 105.– FLIGHTWORTHY NACELLE THRUST REVERSER SECTION OF NOZZLE

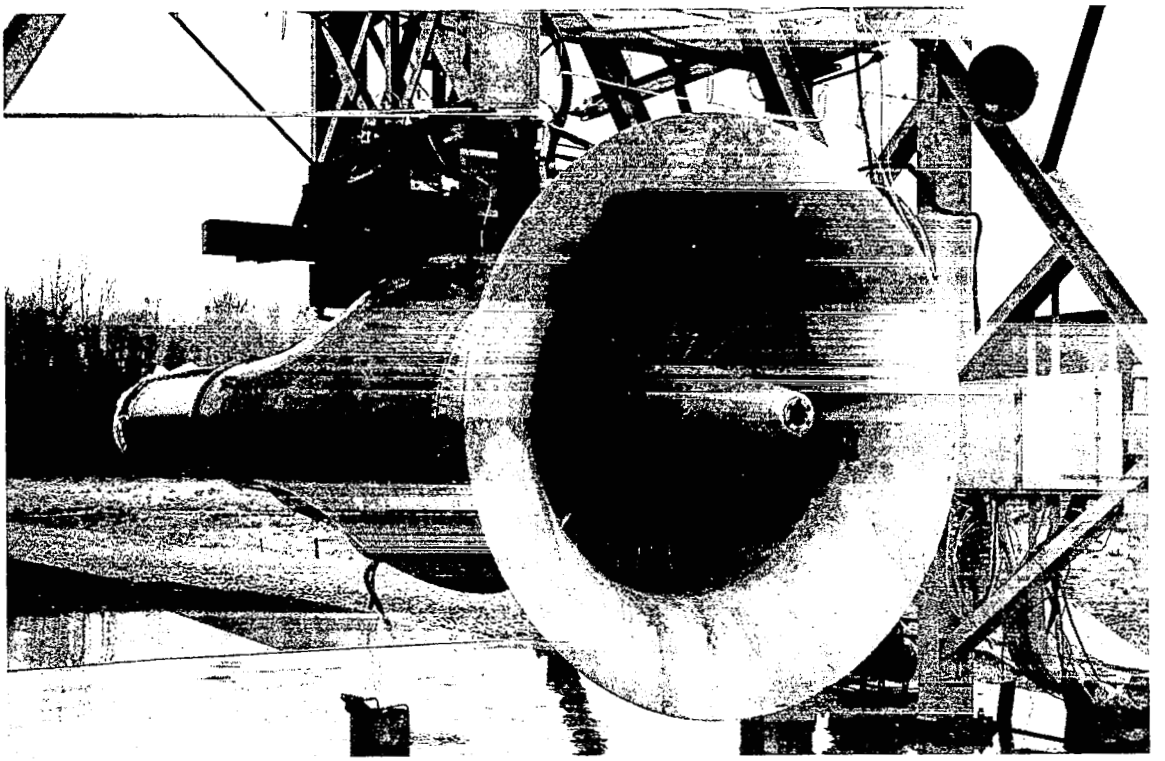

FIGURE 106.– PRATT & WHITNEY REFERENCE INLET AND FAN DUCT INSTALLED ON TEST RIG

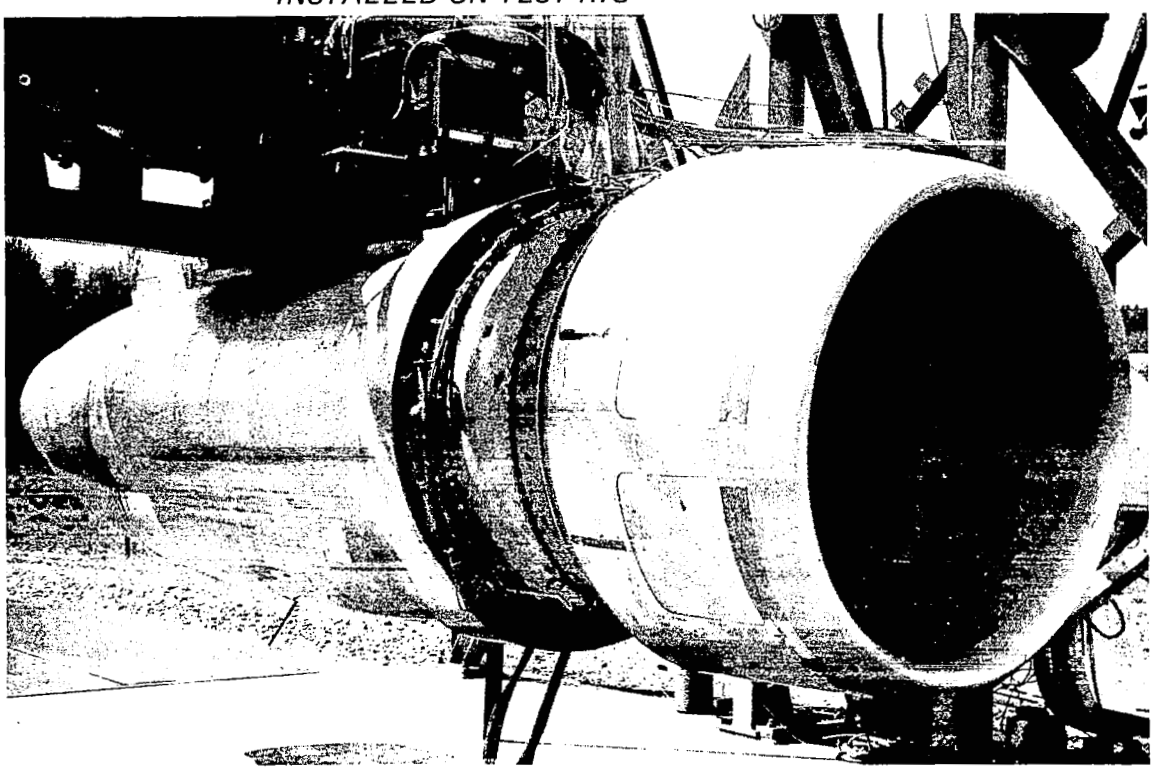

FIGURE 107.– BASELINE NACELLE

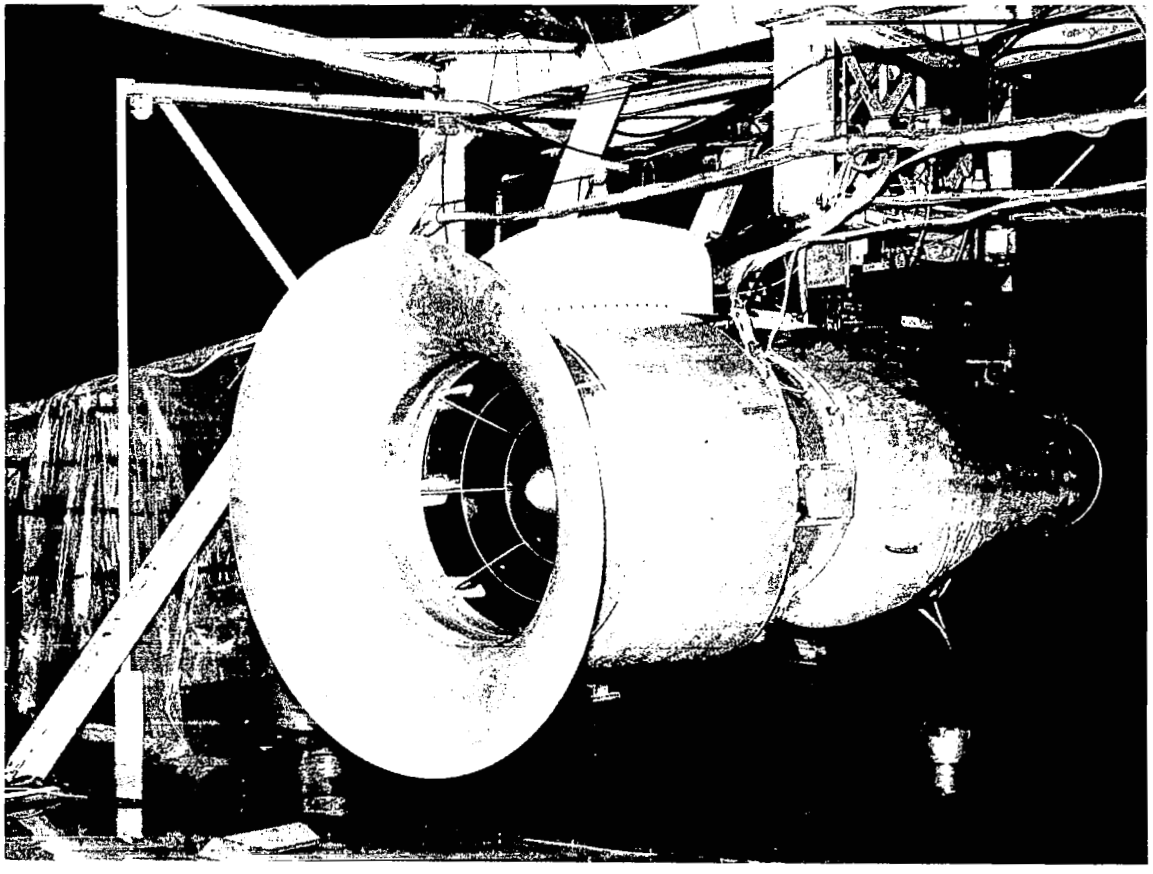

FIGURE 108.– SIMULATED CRUISE BELLMOUTH LIP INSTALLED ON TREATED INLET

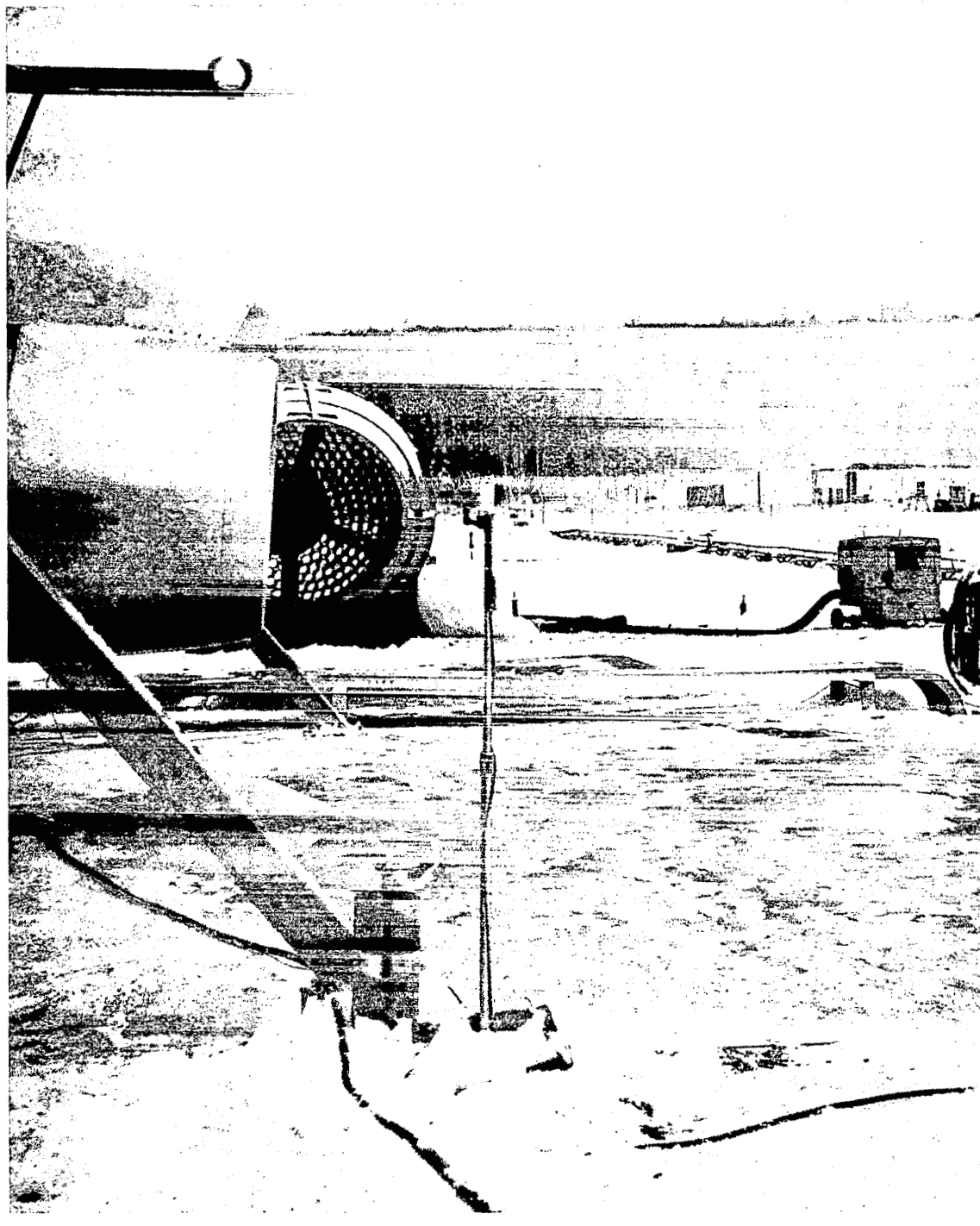

FIGURE 109.—RELATIVE LOCATION OF WIND MACHINE TO TREATED INLET

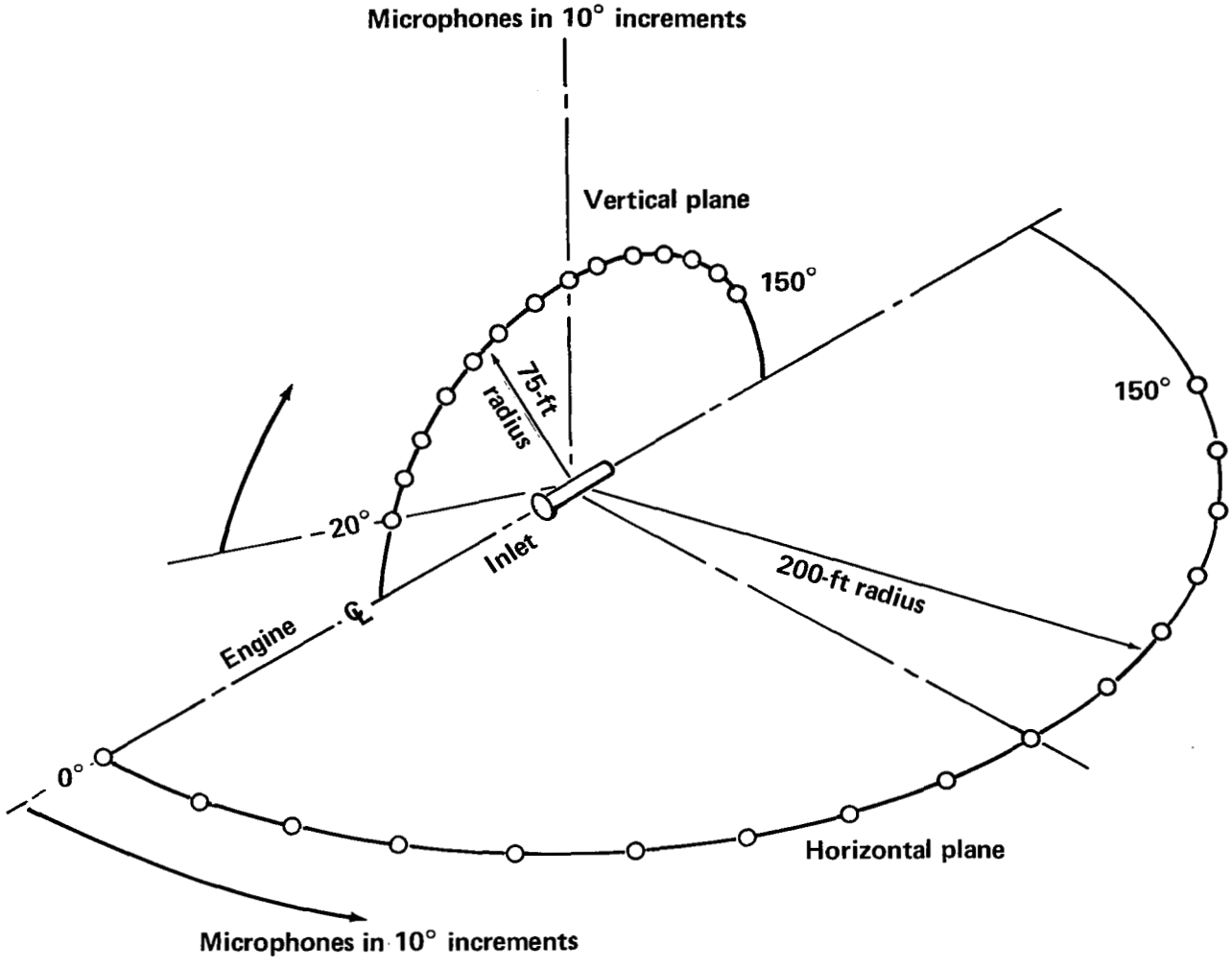

FIGURE 110.—MICROPHONE LOCATIONS

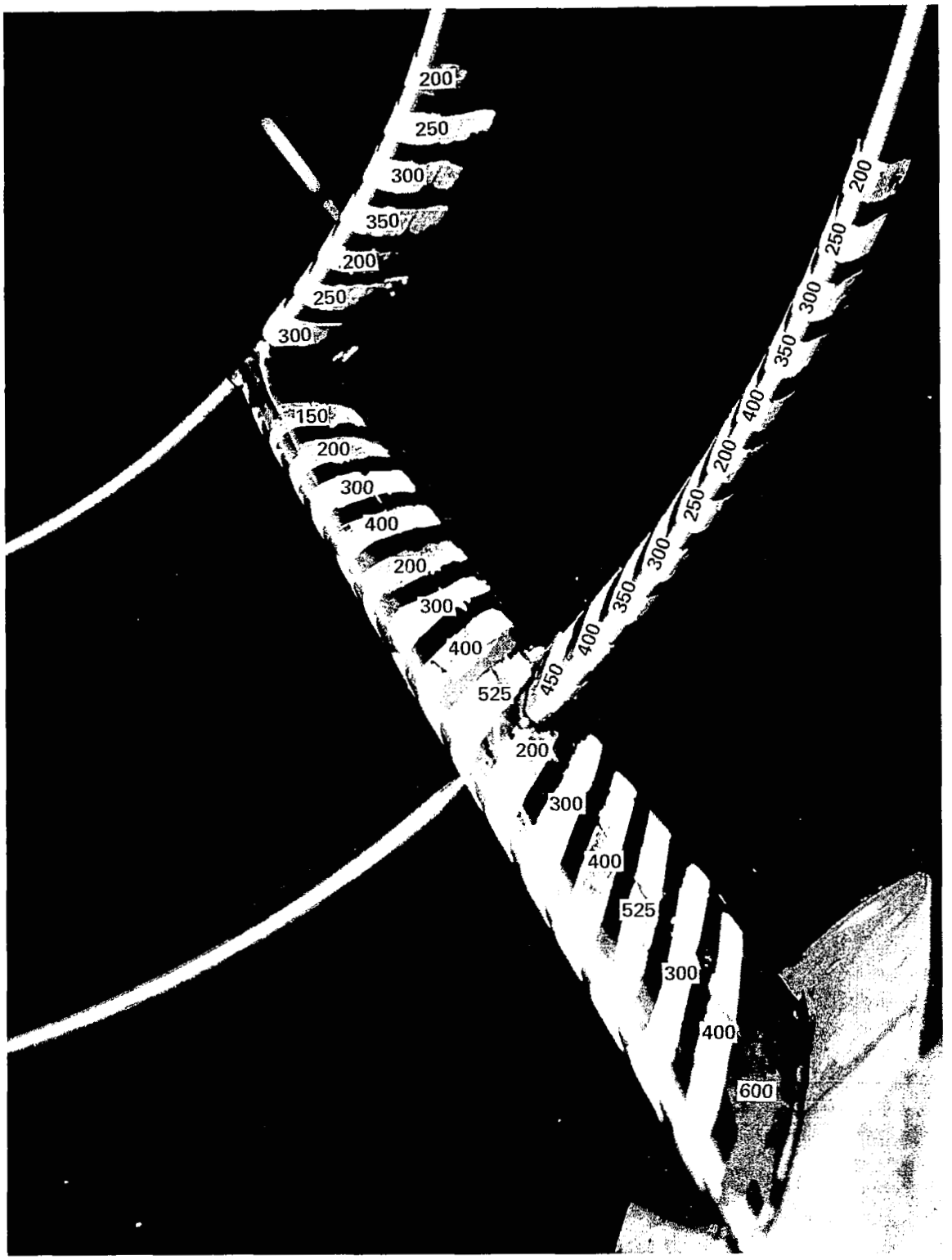

FIGURE 111.–TREATED INLET–RING AND STRUT TEMPILAQ MELTING TEMPERATURES, °F

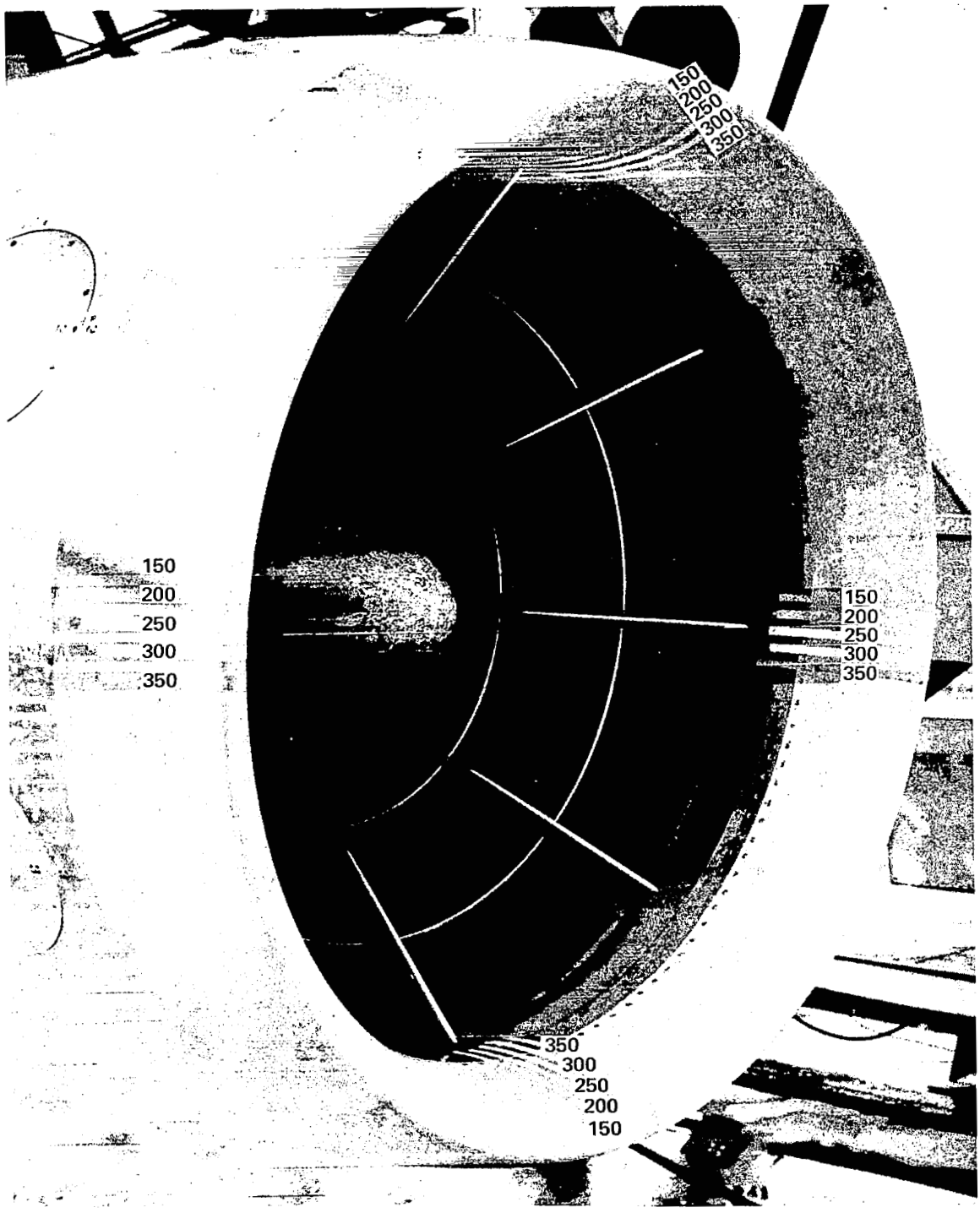

FIGURE 112.—TREATED INLET—COWL LIP TEMPILAQ MELTING TEMPERATURES, °F

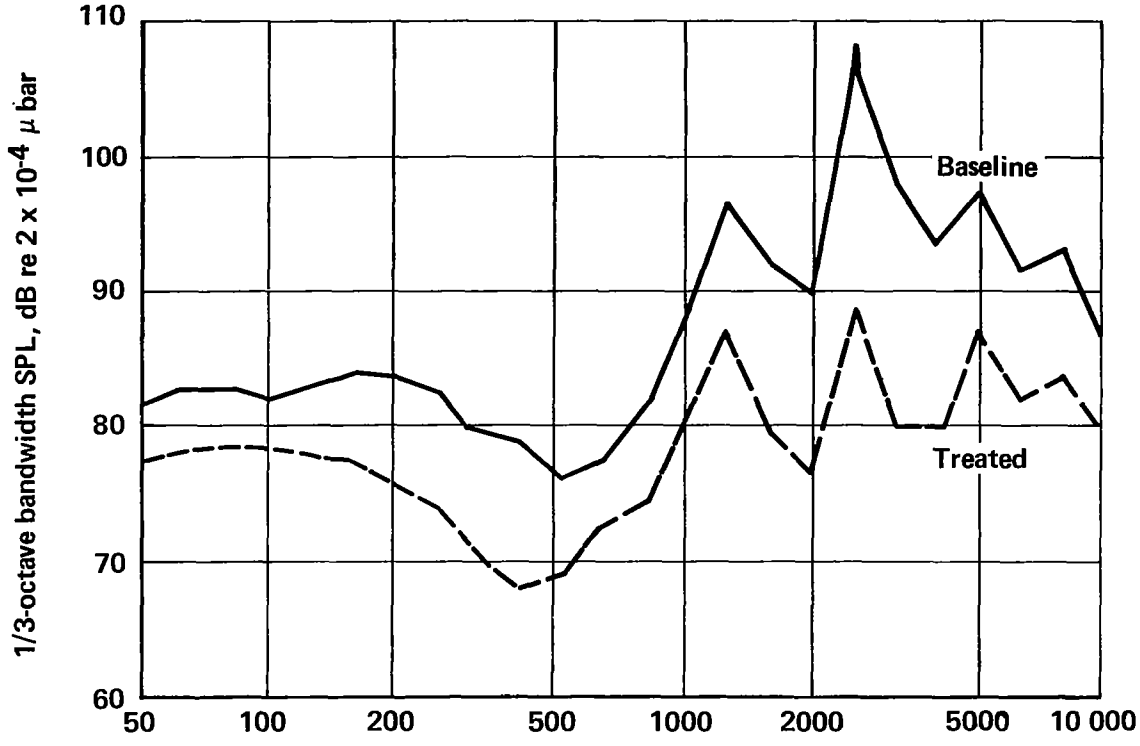

(a) MEASURED ON 200-FT RADIUS, HORIZONTAL PLANE, 20° FROM INLET CENTERLINE

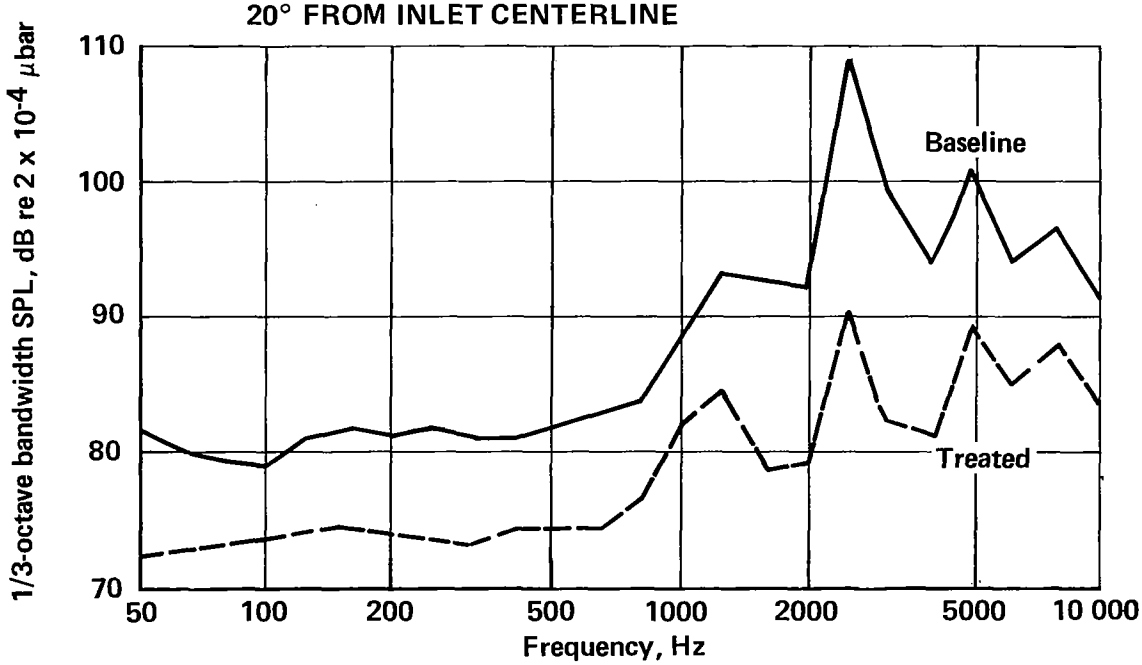

(b) MEASURED ON 75-FT RADIUS, VERTICAL PLANE, CORRECTED TO 200-FT RADIUS, 30° FROM INLET CENTERLINE

FIGURE 113.—COMPARATIVE INLET NOISE SPECTRA—APPROACH THRUST

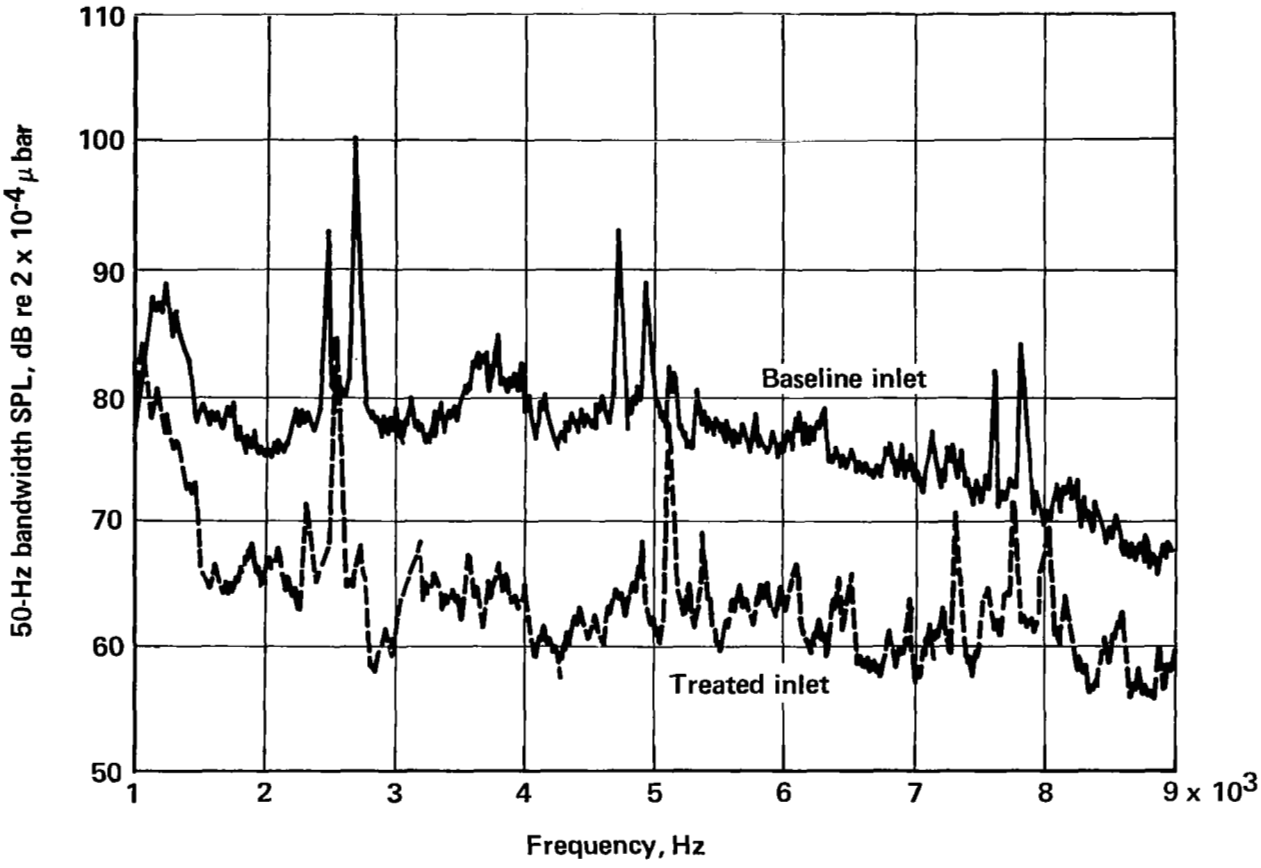

FIGURE 114.—TYPICAL NARROWBAND INLET NOISE SPECTRA—APPROACH THRUST

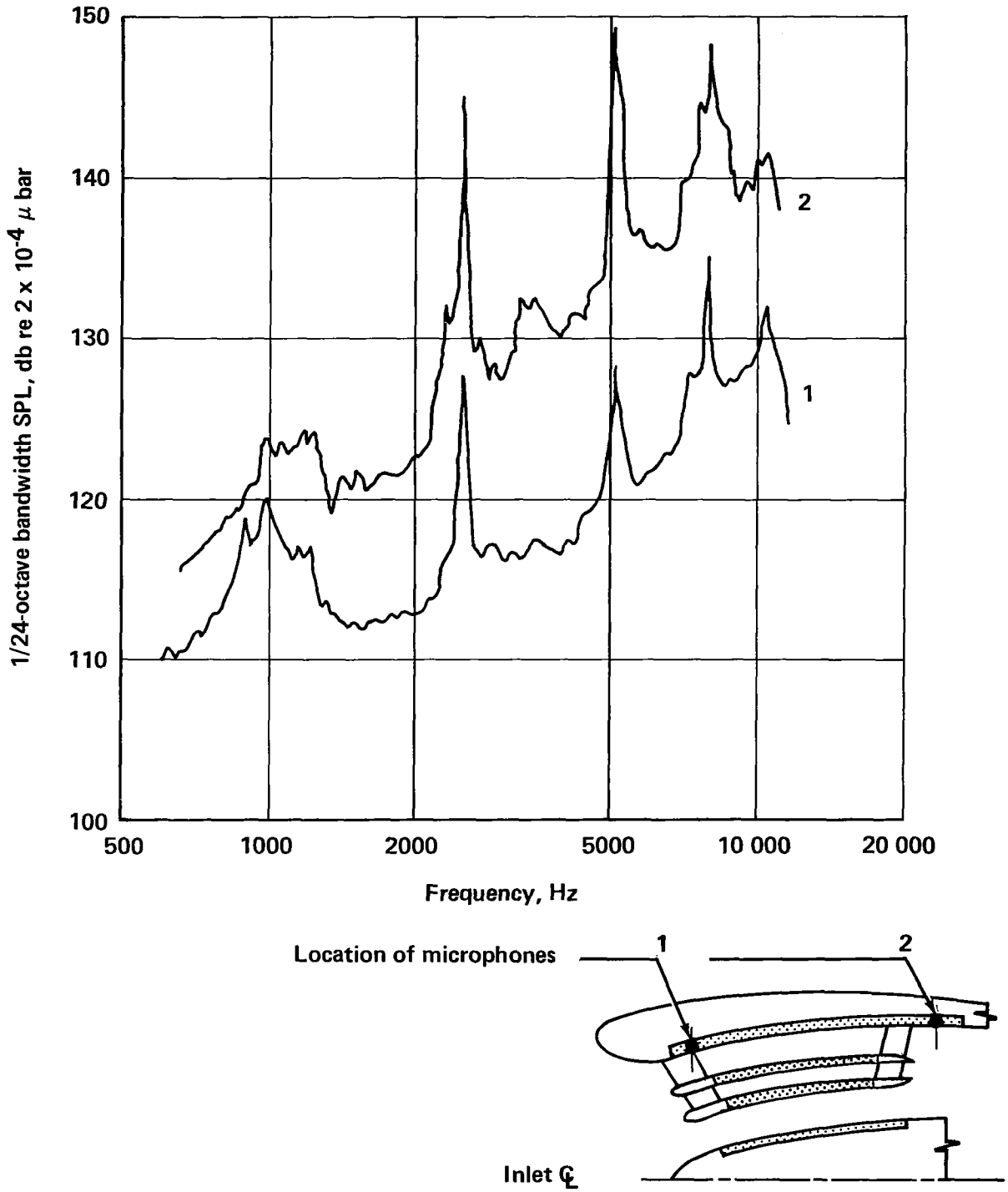

FIGURE 115.–SPECTRA MEASURED INSIDE TREATED INLET–APPROACH THRUST

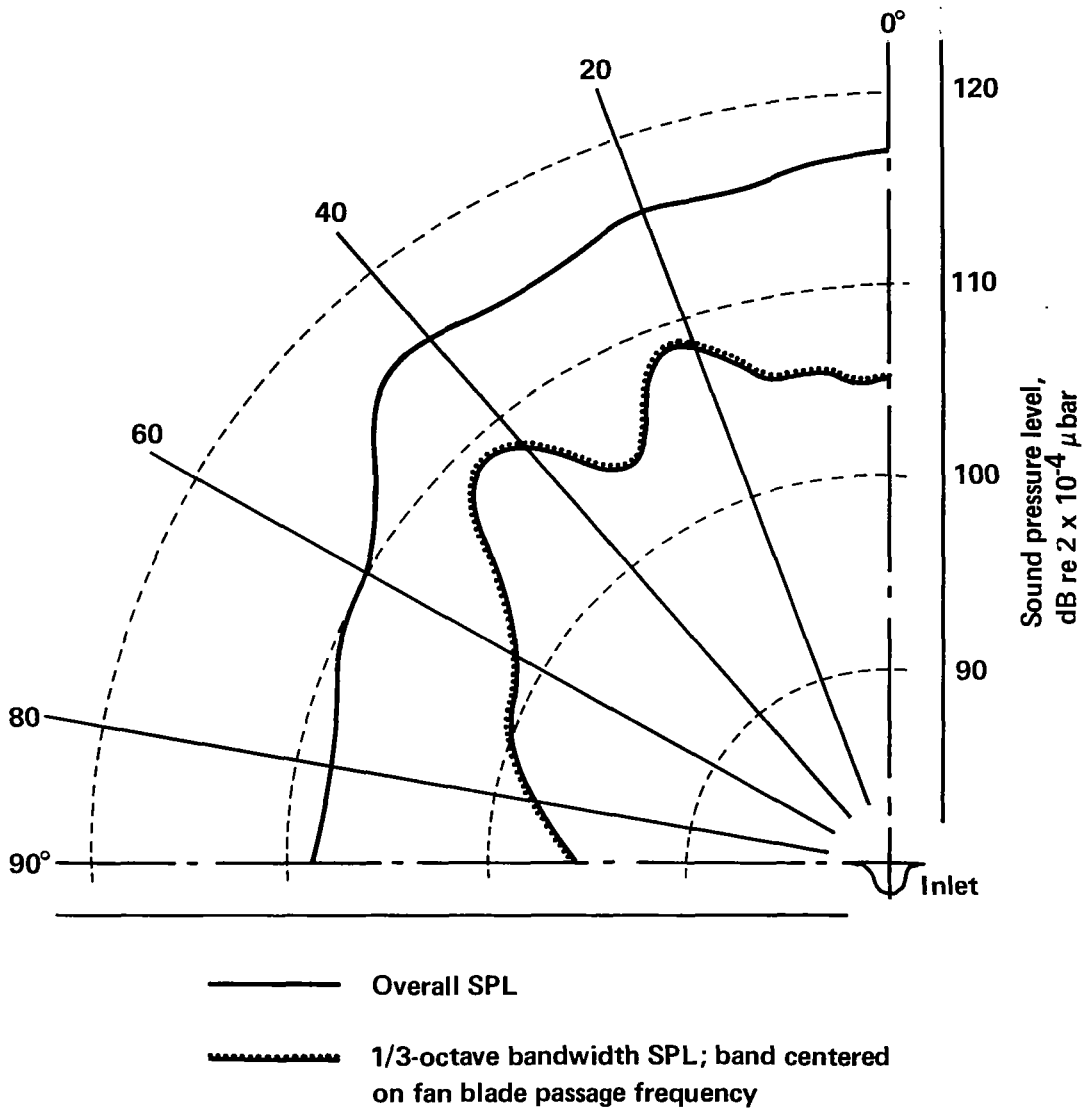

FIGURE 116.– TREATED INLET NOISE RADIATION PATTERNS– APPROACH THRUST

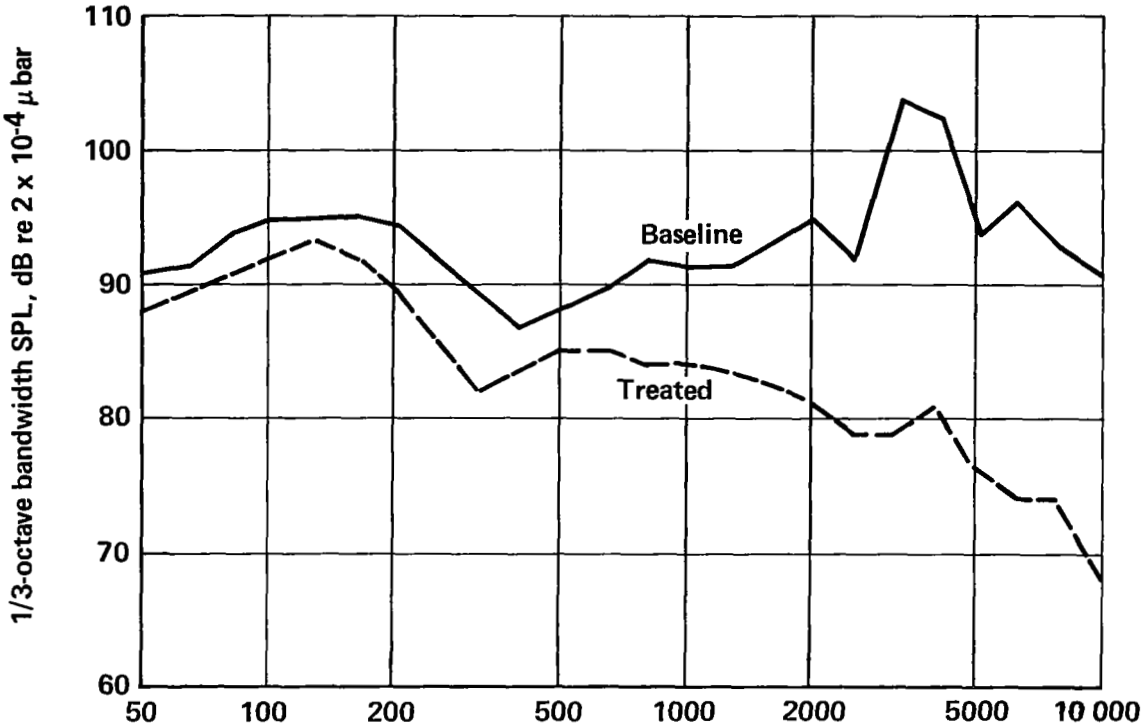

(a) MEASURED ON 200-FT RADIUS, HORIZONTAL PLANE, 40° FROM INLET CENTERLINE

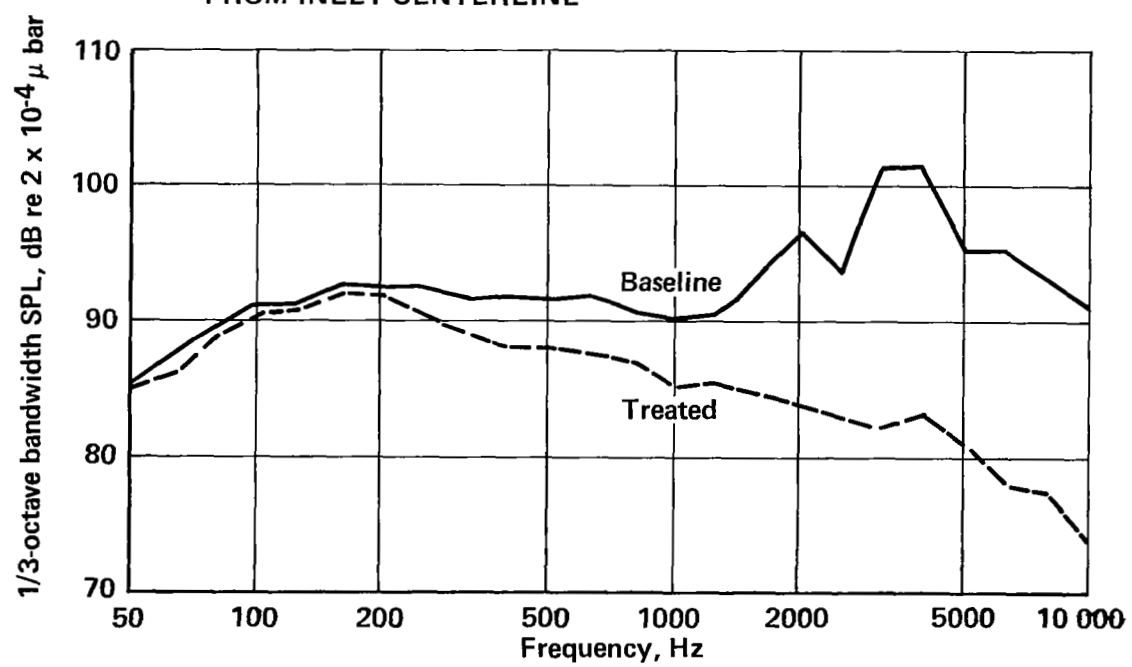

(b) MEASURED ON 75-FT RADIUS, VERTICAL PLANE, CORRECTED TO 200-FT RADIUS, 50° FROM INLET CENTERLINE

FIGURE 117.—COMPARATIVE INLET NOISE SPECTRA—TAKEOFF THRUST

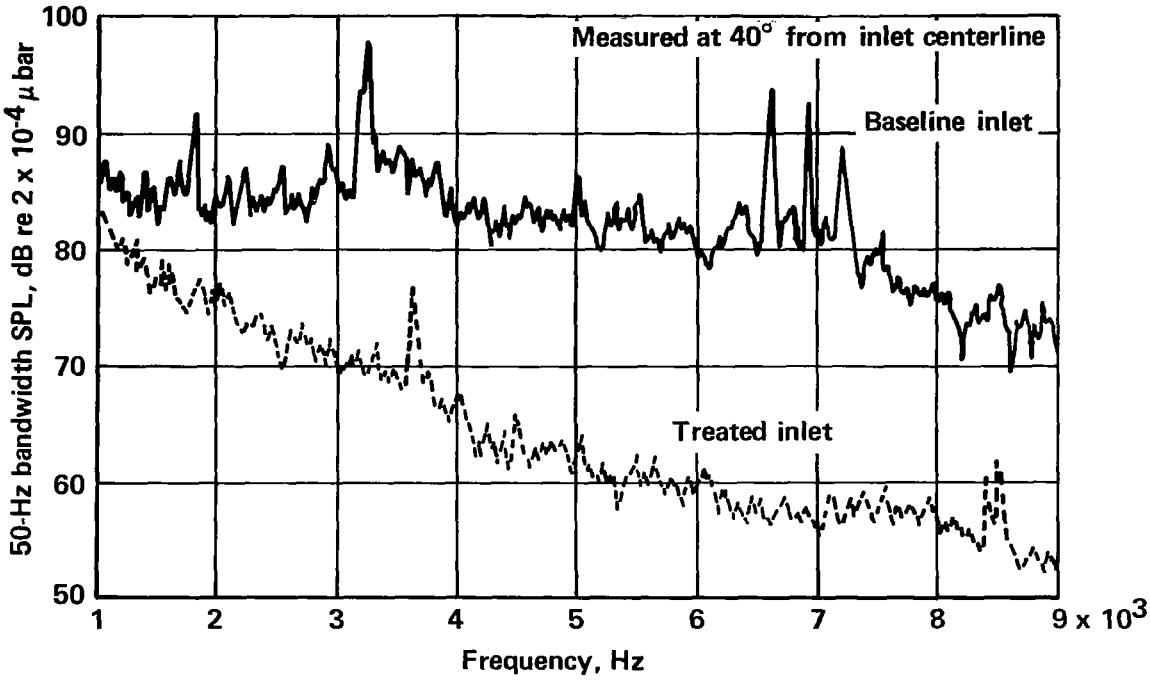

FIGURE 118.—TYPICAL NARROWBAND INLET NOISE SPECTRA—TAKEOFF THRUST

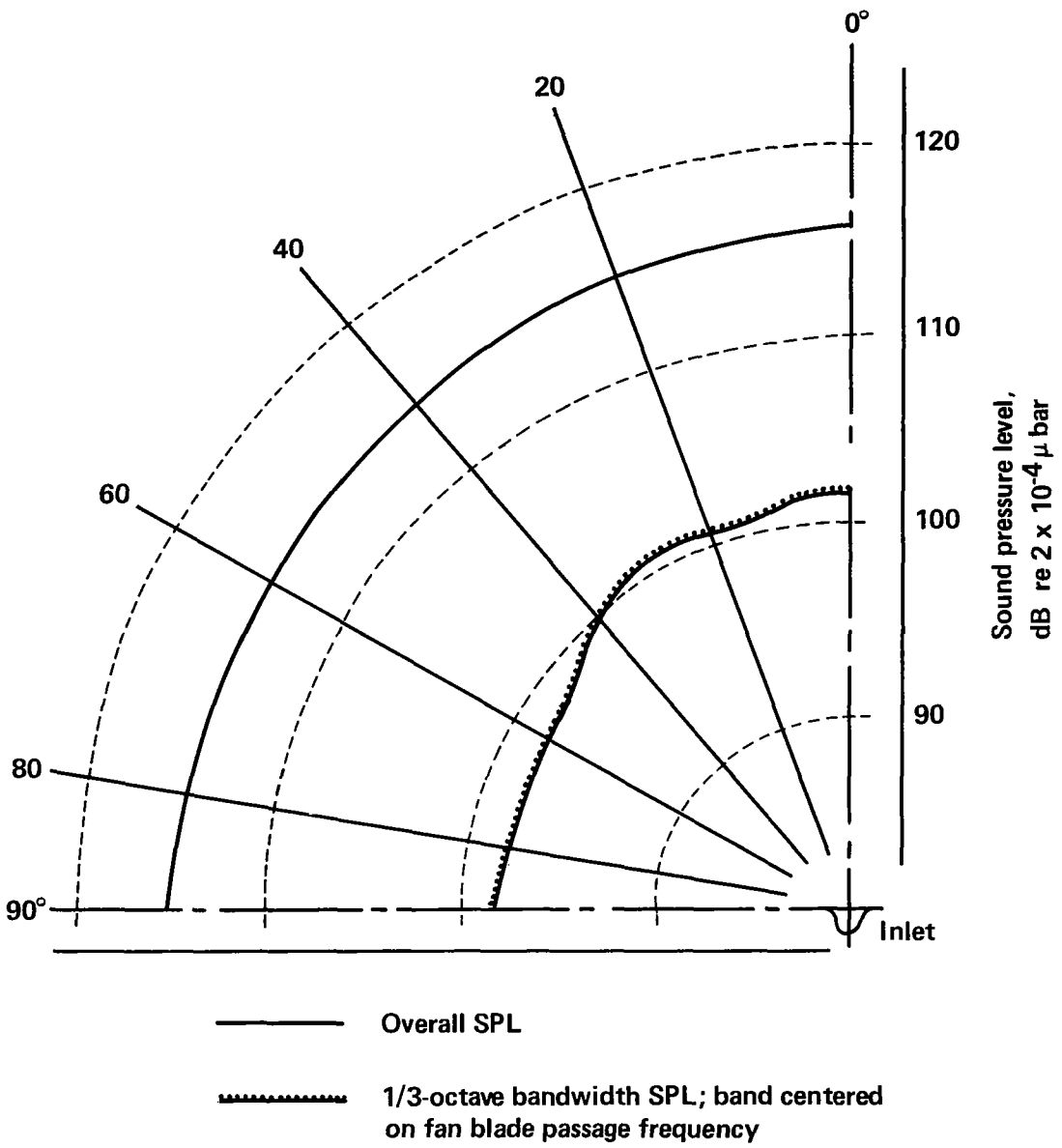

FIGURE 119.– TREATED INLET NOISE RADIATION PATTERNS– TAKEOFF THRUST

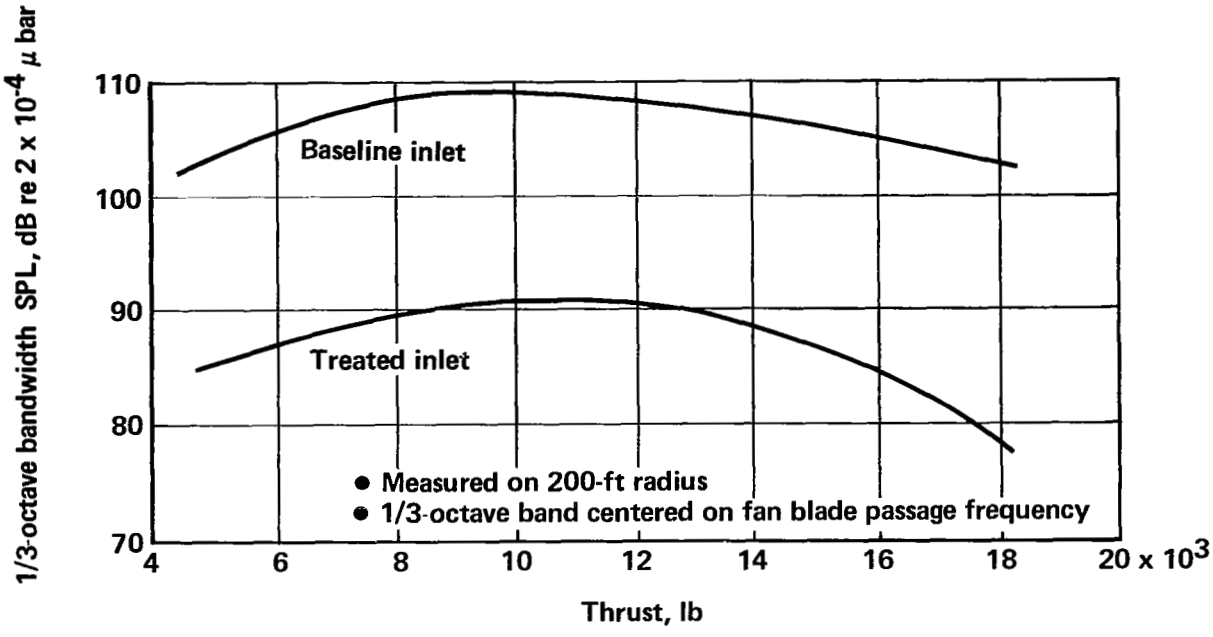

FIGURE 120.– MAXIMUM INLET-RADIATED FAN NOISE LEVELS

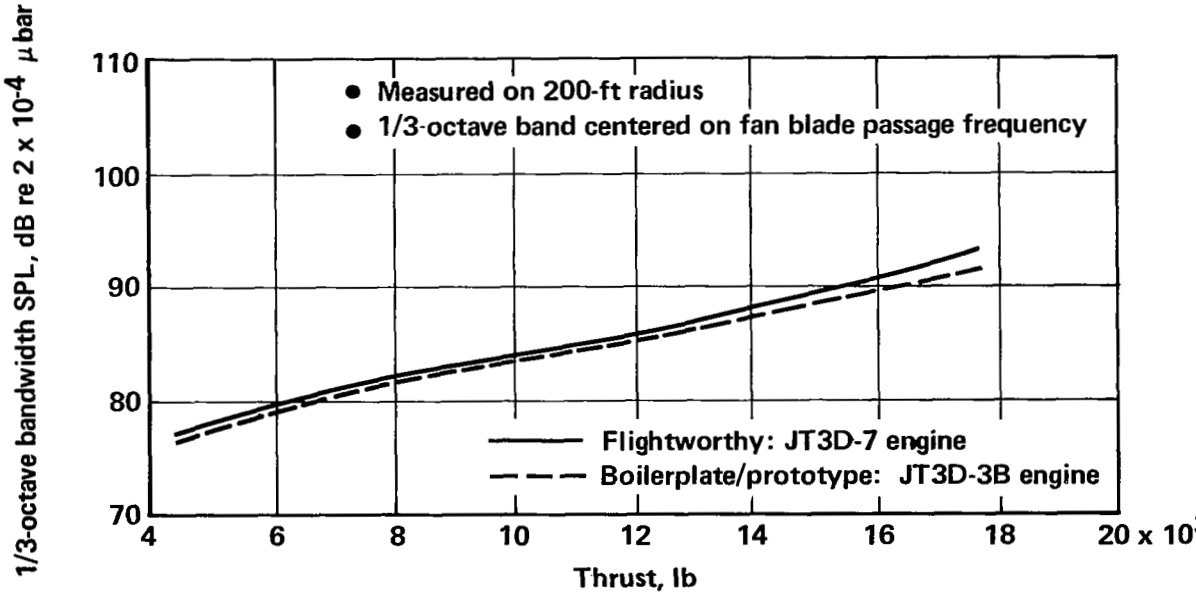

FIGURE 121.– COMPARISON OF TREATED FAN DUCT MAXIMUM NOISE LEVELS

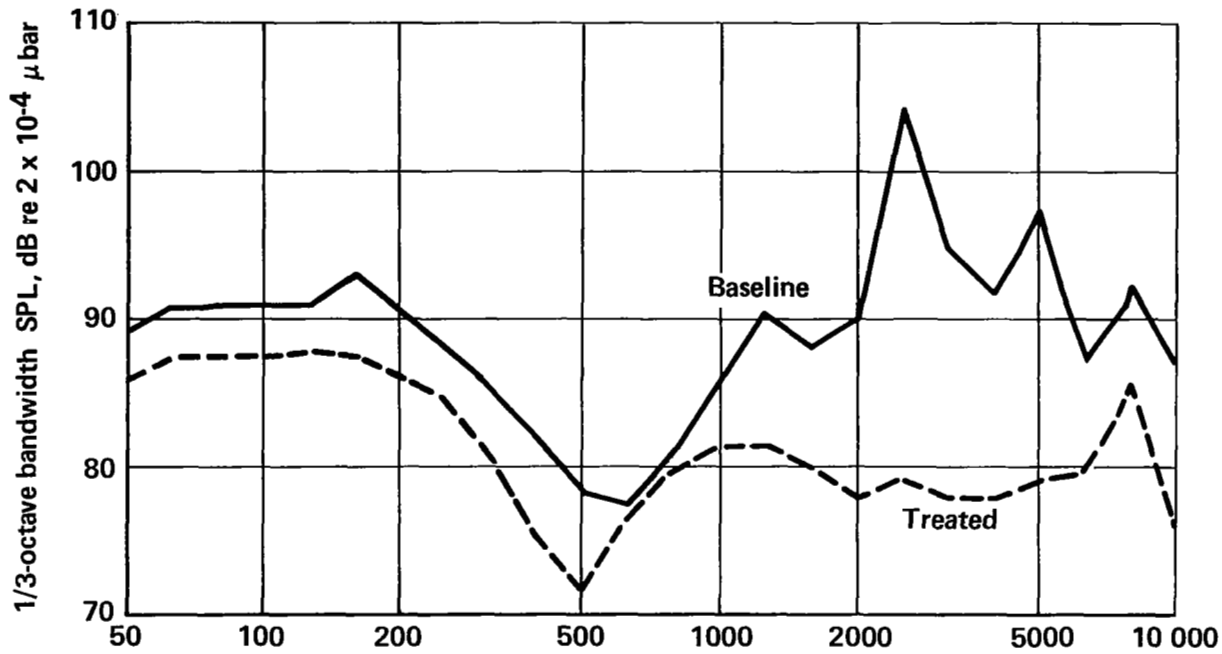

(a) MEASURED ON 200-FT RADIUS, HORIZONTAL PLANE, 110° FROM INLET CENTERLINE

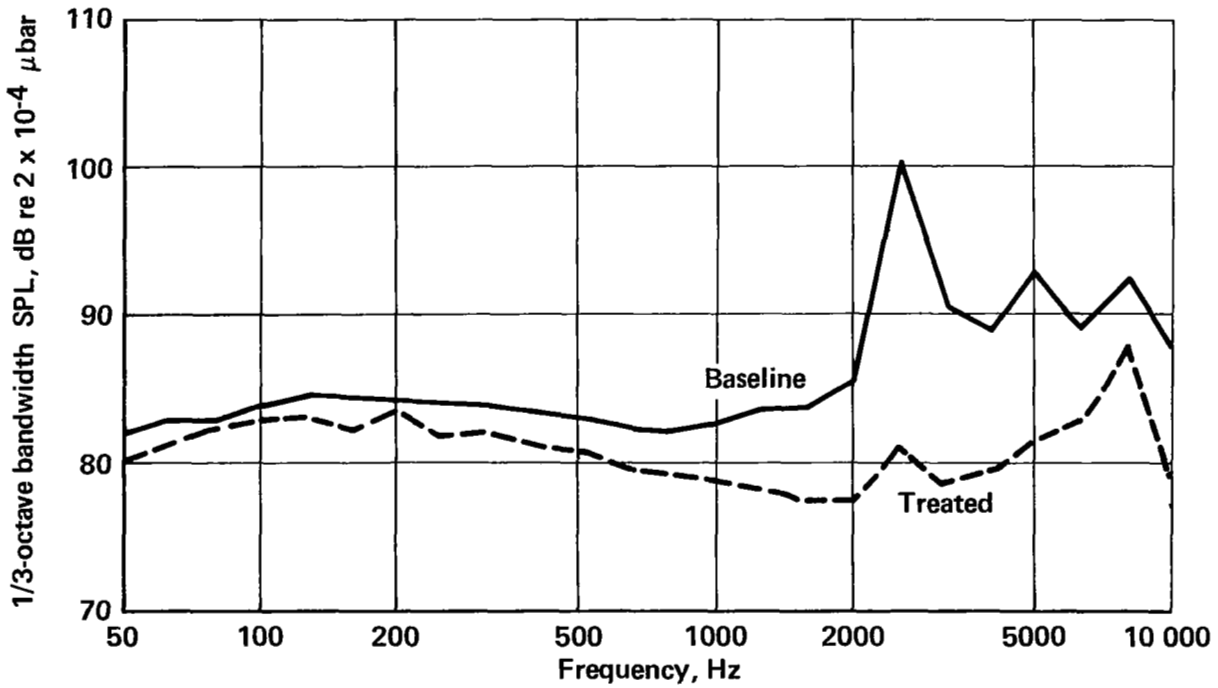

(b) MEASURED ON 75-FT RADIUS, VERTICAL PLANE, CORRECTED TO 200-FT RADIUS, 110° FROM INLET CENTERLINE

FIGURE 122.—COMPARATIVE FAN DUCT NOISE SPECTRA, APPROACH THRUST

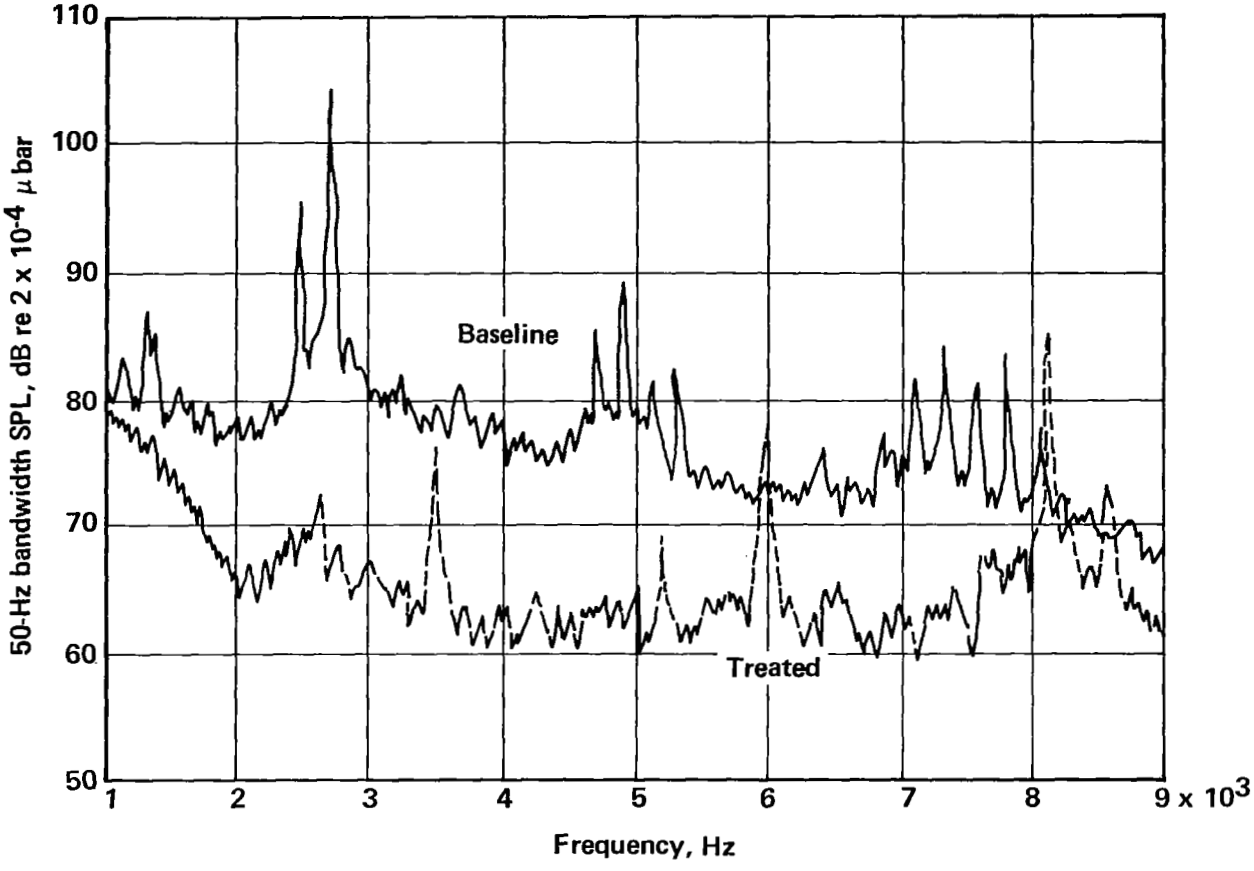

FIGURE 123.– TYPICAL NARROWBAND FAN DUCT NOISE SPECTRA, APPROACH THRUST

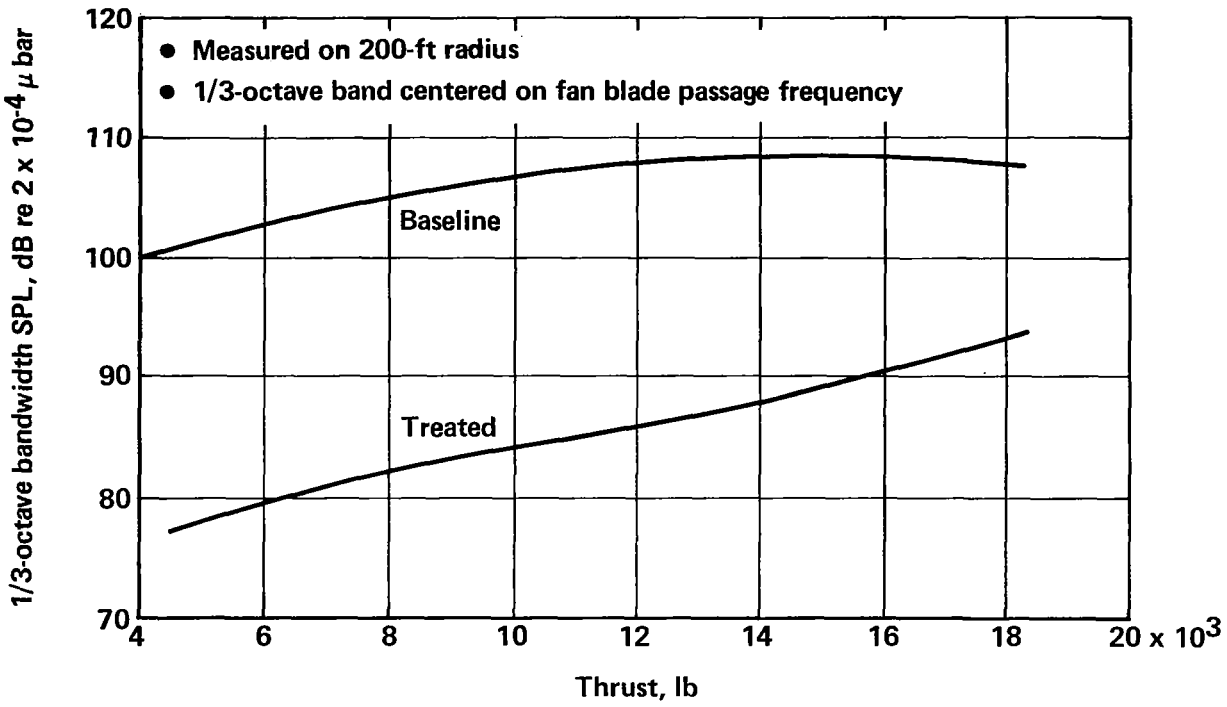

FIGURE 126.—COMPARISON OF MAXIMUM FAN NOISE LEVELS—BASELINE AND FLIGHTWORTHY TREATED FAN DUCTS

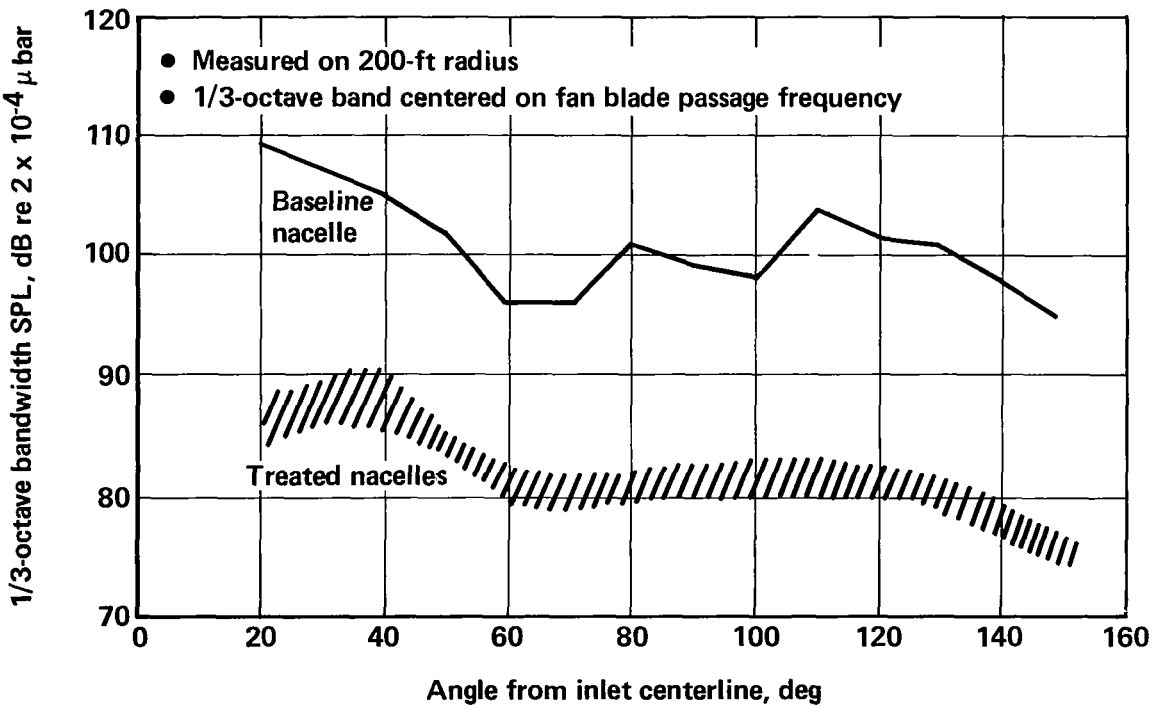

FIGURE 127.—COMPARISON OF RADIATED NOISE—APPROACH THRUST

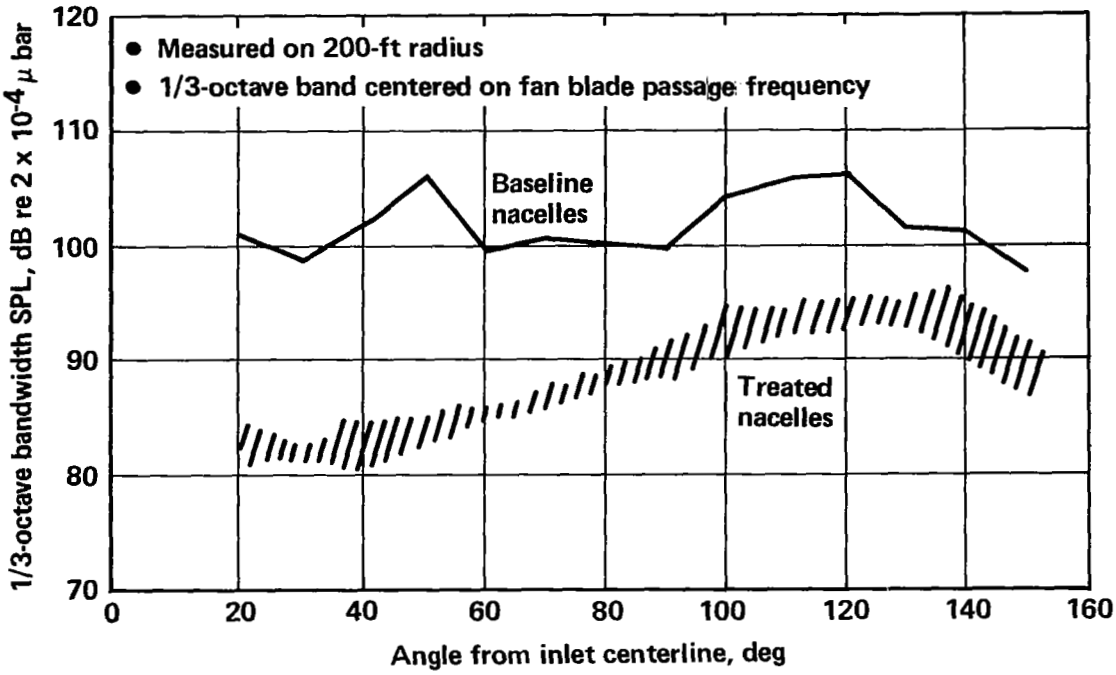

FIGURE 128.—COMPARISON OF RADIATED NOISE—TAKEOFF THRUST

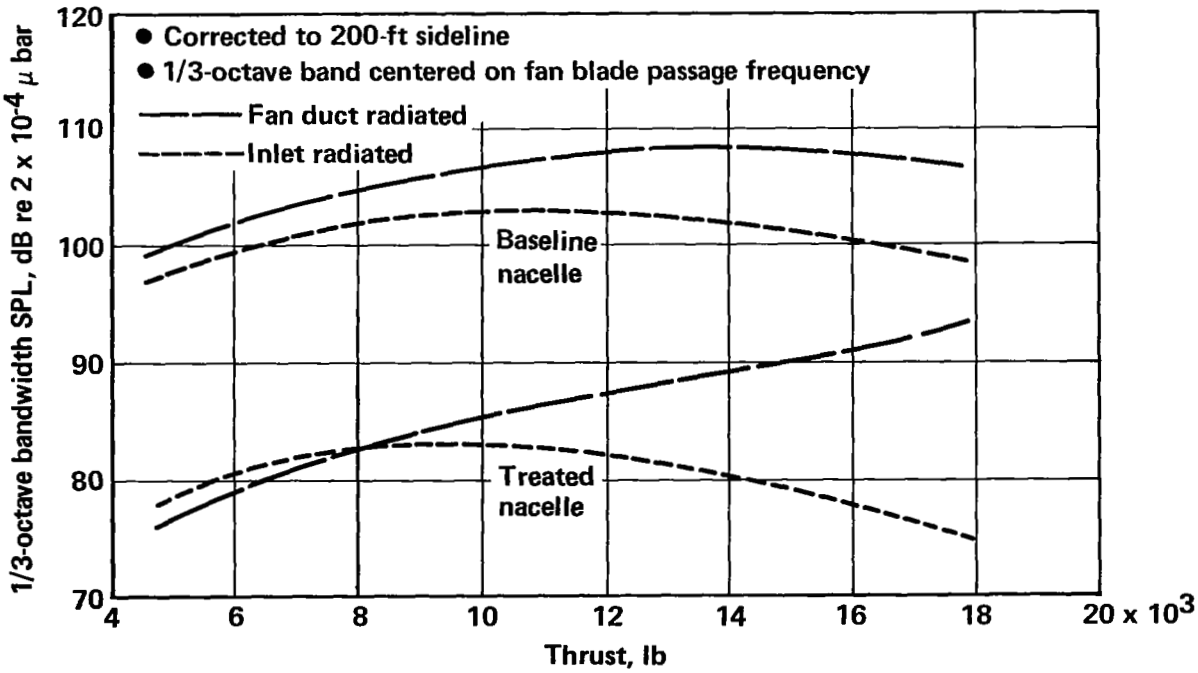

FIGURE 129.—MAXIMUM SIDELINE FAN NOISE LEVELS

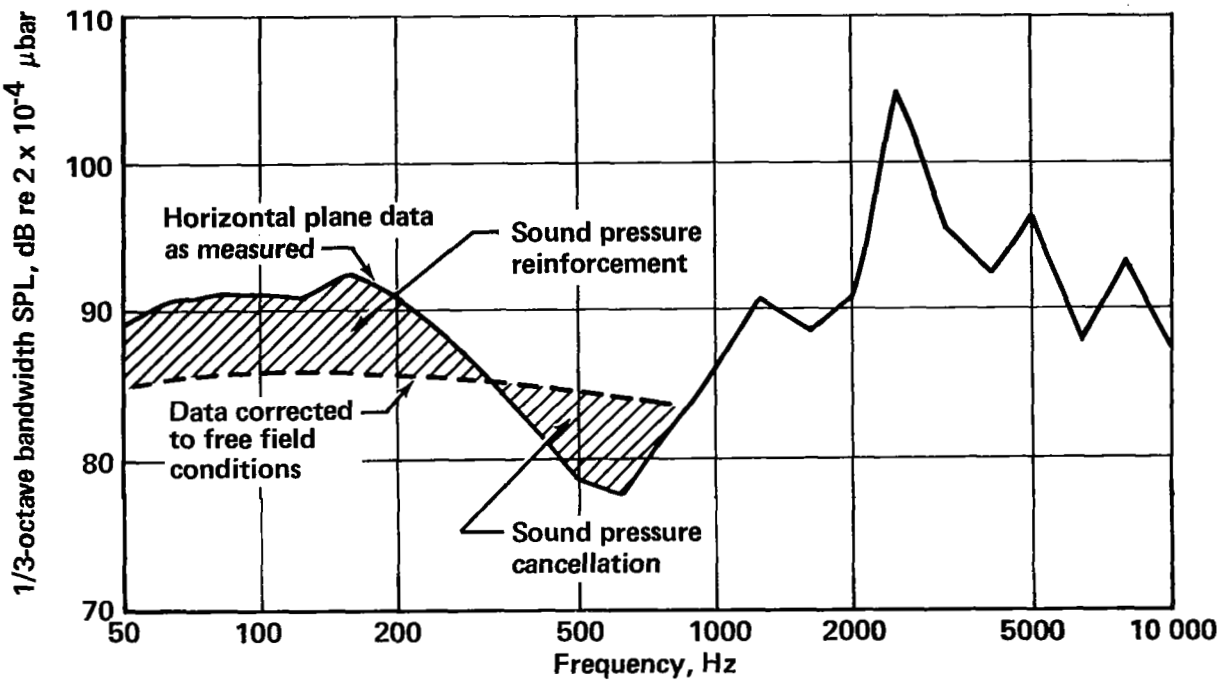

FIGURE 130.– CORRECTION OF MEASURED DATA TO FREE FIELD CONDITIONS

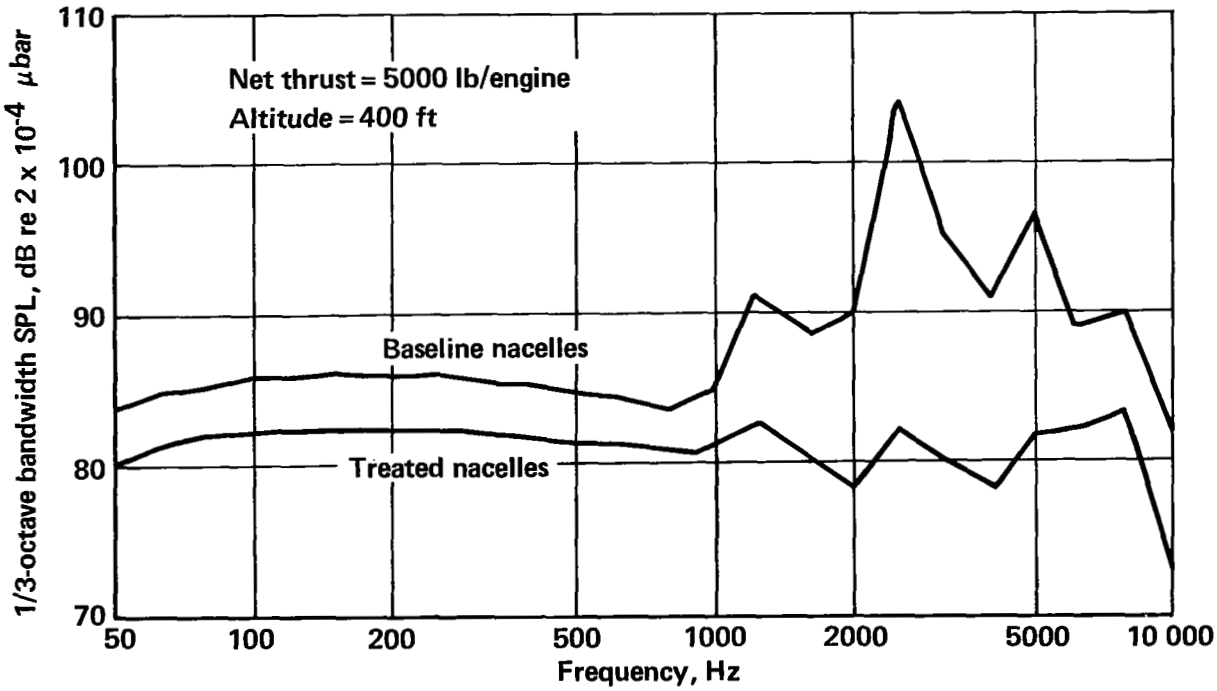

FIGURE 131.– TYPICAL PREDICTED SPECTRA AT TIME OF MAXIMUM PNL DURING LANDING APPROACH

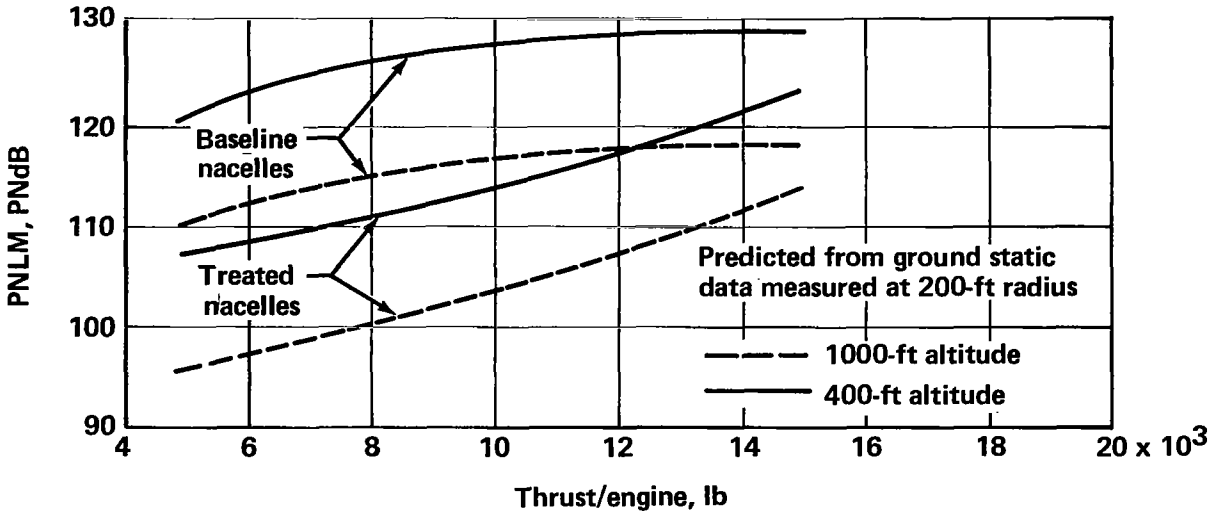

FIGURE 132.– PREDICTED PERCEIVED NOISE LEVELS

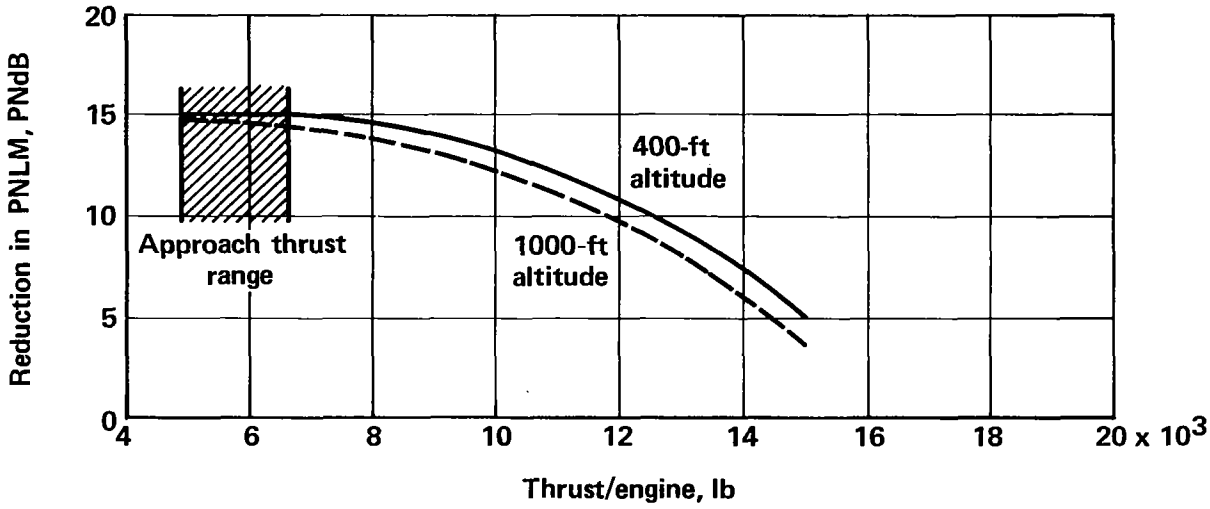

FIGURE 133.– PREDICTED REDUCTION IN PERCEIVED NOISE LEVELS

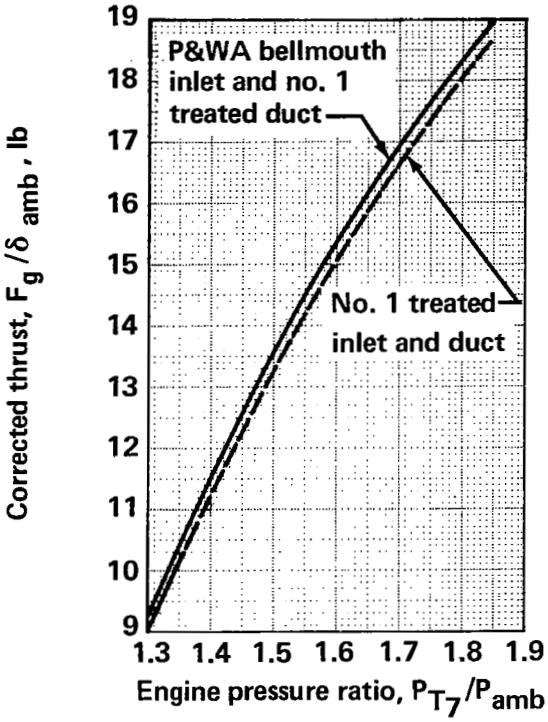

FIGURE 134.– THRUST COMPARISON, NUMBER 1 INLET

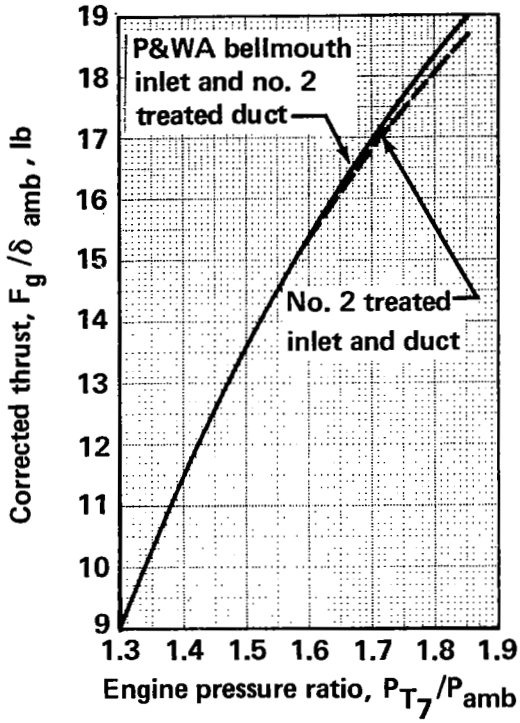

FIGURE 135.– THRUST COMPARISON, NUMBER 2 INLET

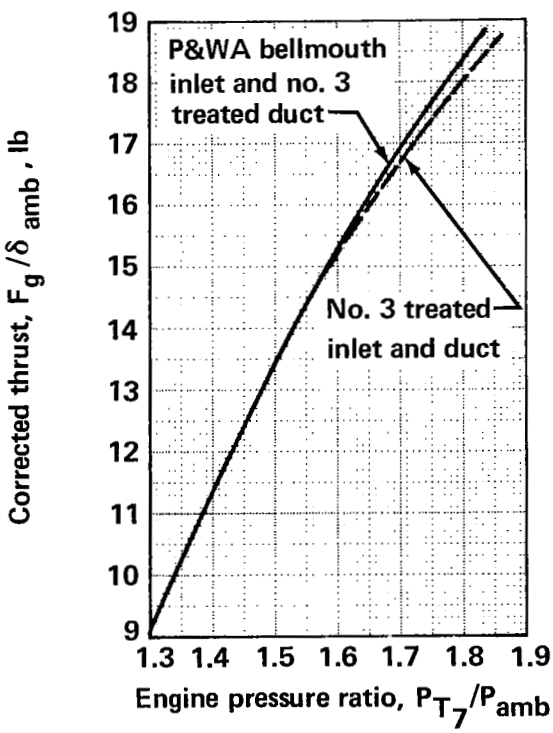

FIGURE 136.– THRUST COMPARISON, NUMBER 3 INLET

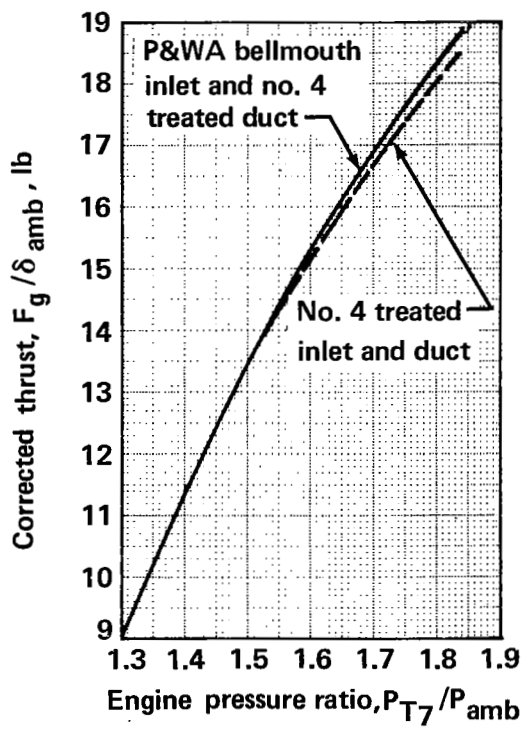

FIGURE 137.– THRUST COMPARISON, NUMBER 4 INLET

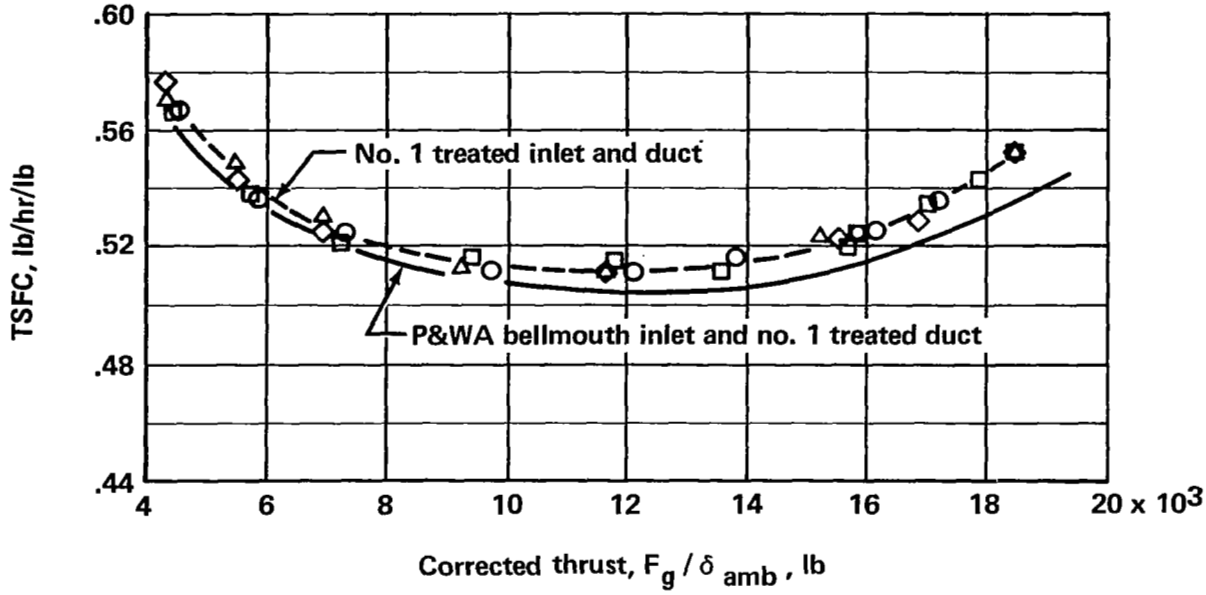

FIGURE 138.– THRUST SPECIFIC FUEL CONSUMPTION COMPARISON, NUMBER 1 INLET

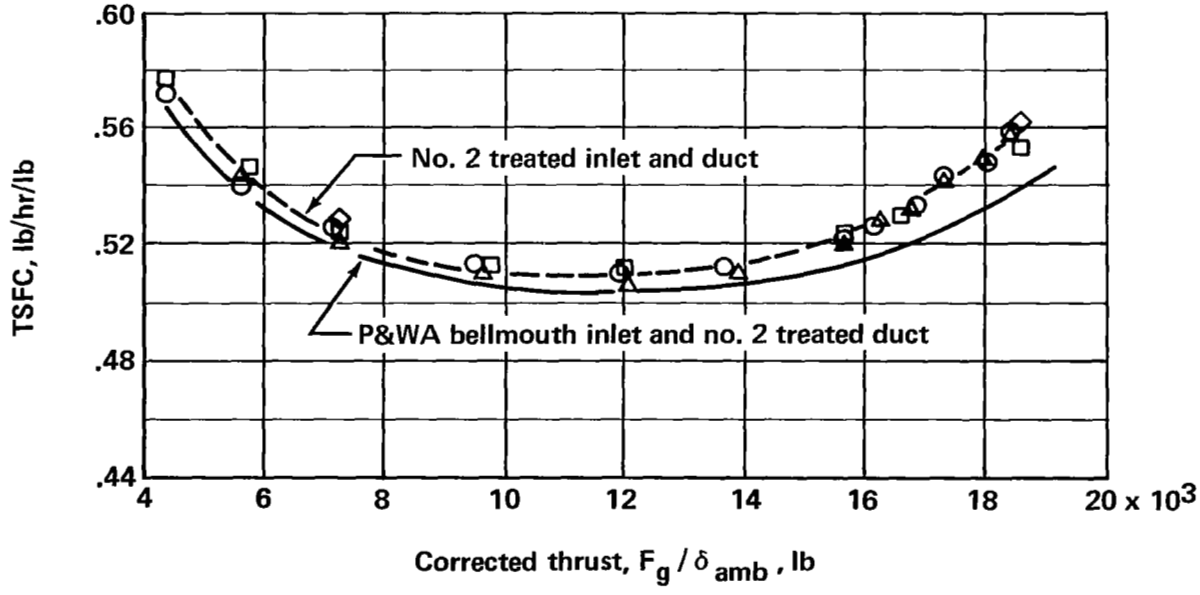

FIGURE 139.– THRUST SPECIFIC FUEL CONSUMPTION COMPARISON, NUMBER 2 INLET

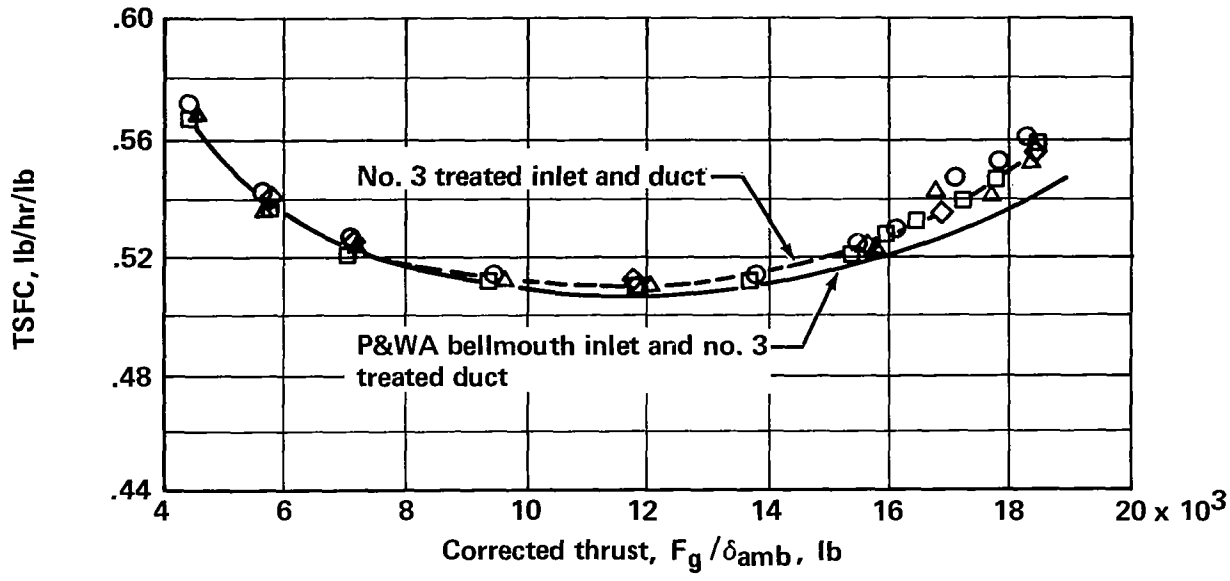

FIGURE 140.—THRUST SPECIFIC FUEL CONSUMPTION COMPARISON, NUMBER 3 INLET

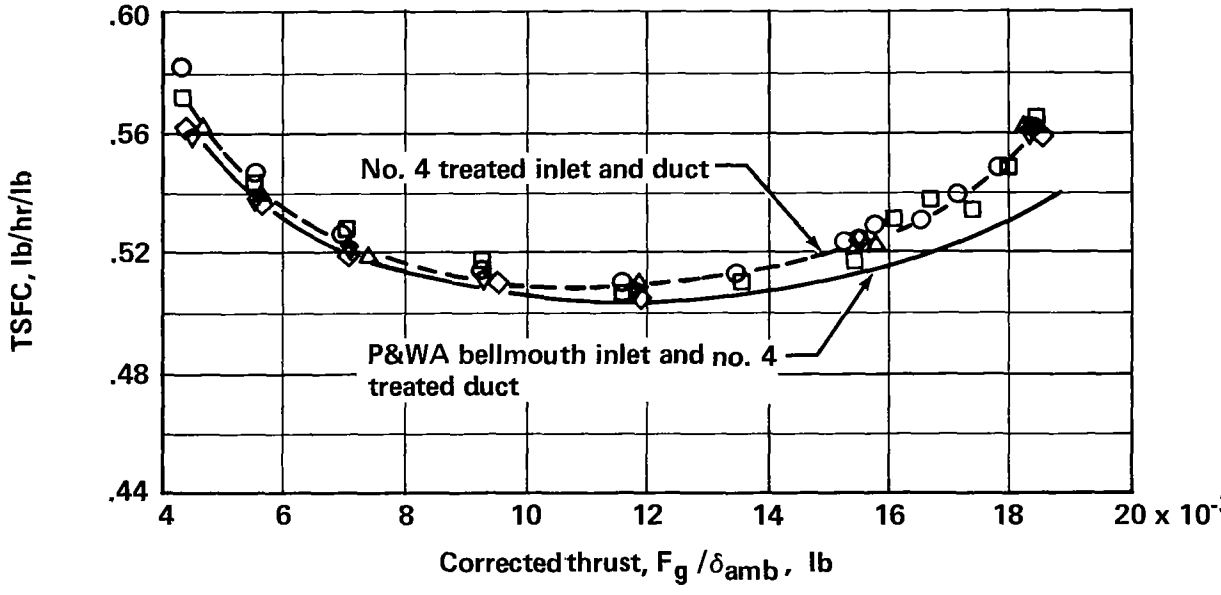

FIGURE 141.—THRUST SPECIFIC FUEL CONSUMPTION COMPARISON, NUMBER 4 INLET

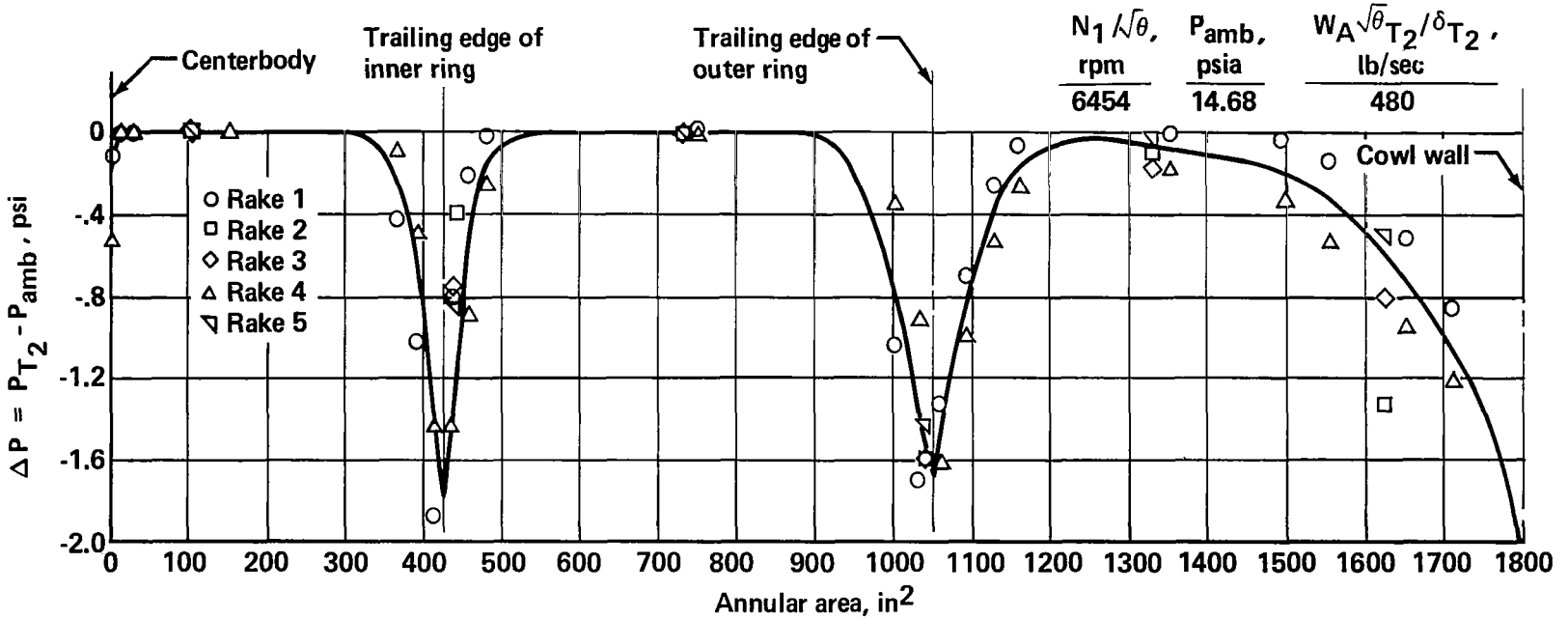

FIGURE 142.–TOTAL PRESSURE DISTRIBUTION NEAR FAN FACE

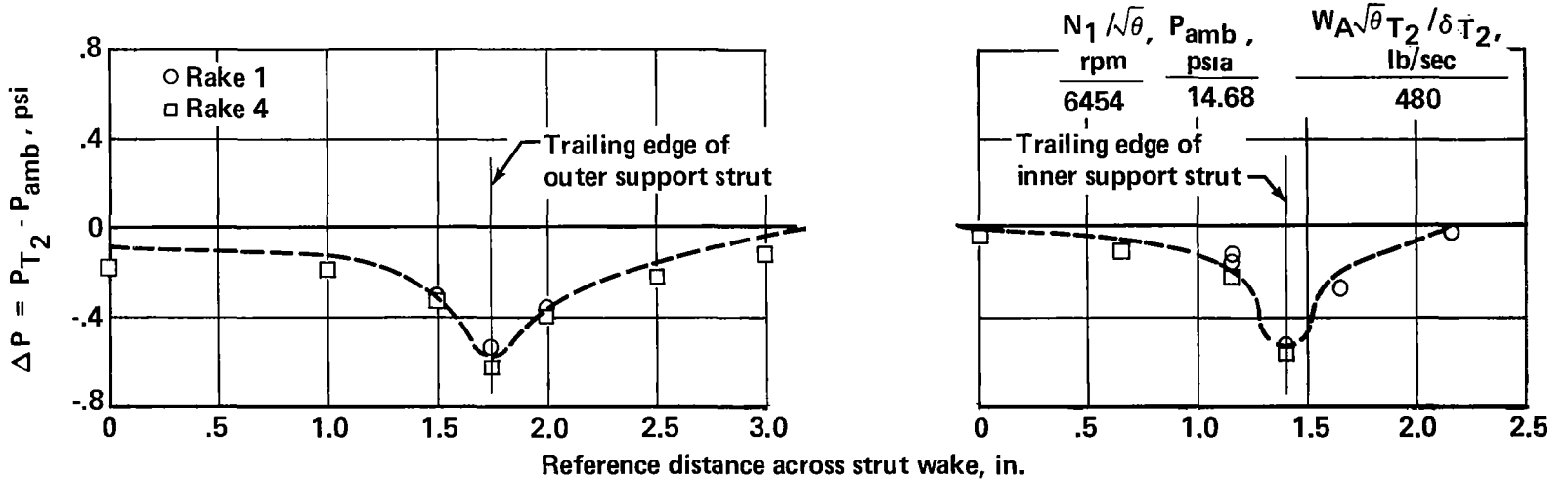

FIGURE 143.—STRUT WAKE TOTAL PRESSURE DISTRIBUTION

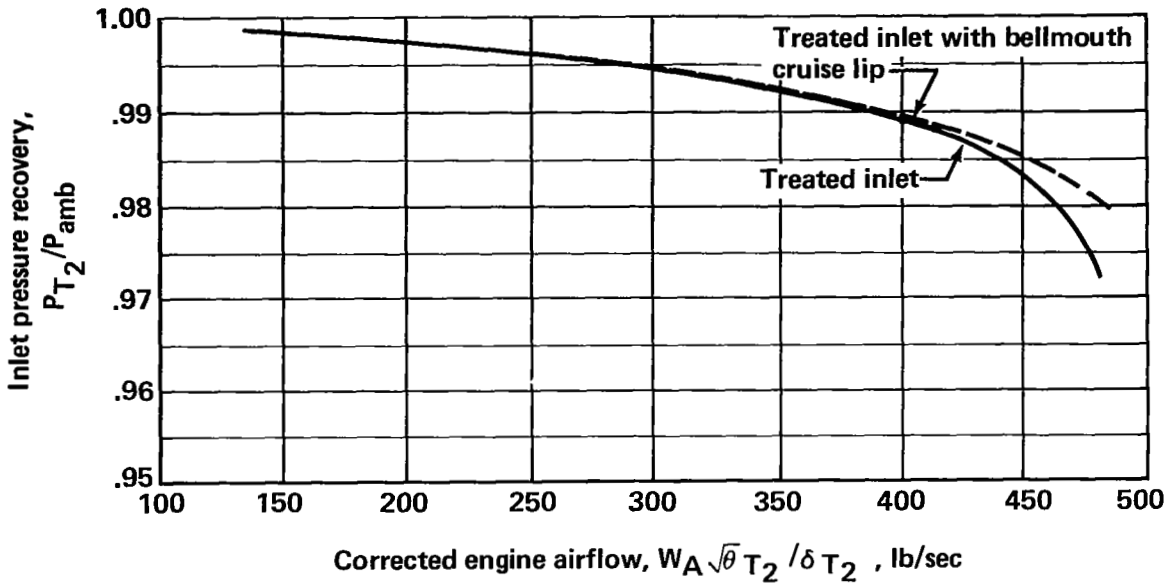

FIGURE 144.– INLET TOTAL PRESSURE RECOVERY

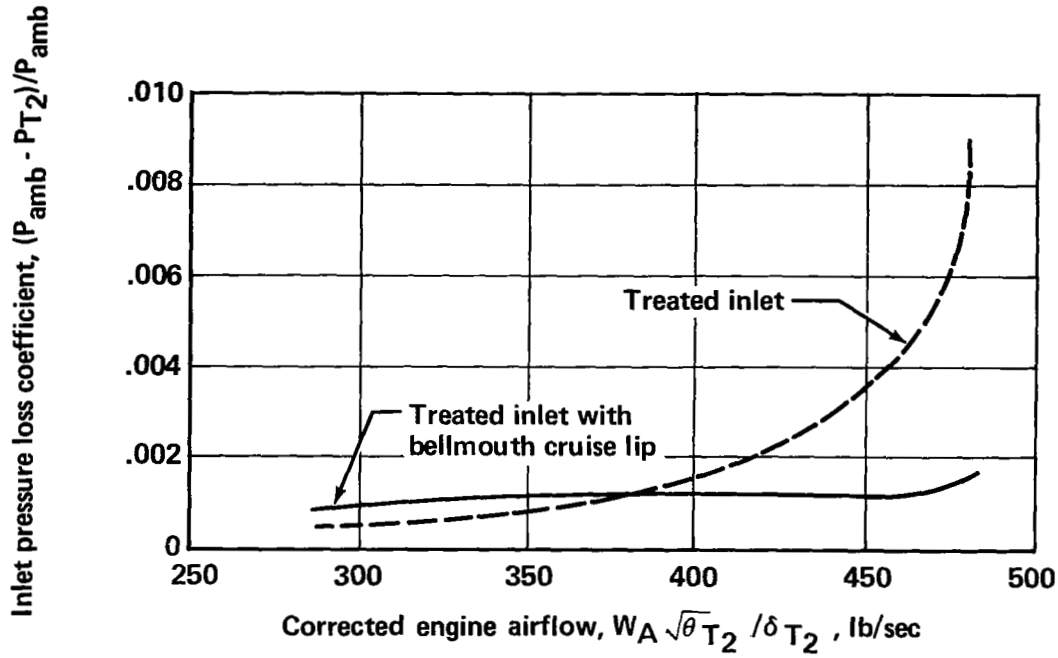

FIGURE 145.– INLET LIP LOSS

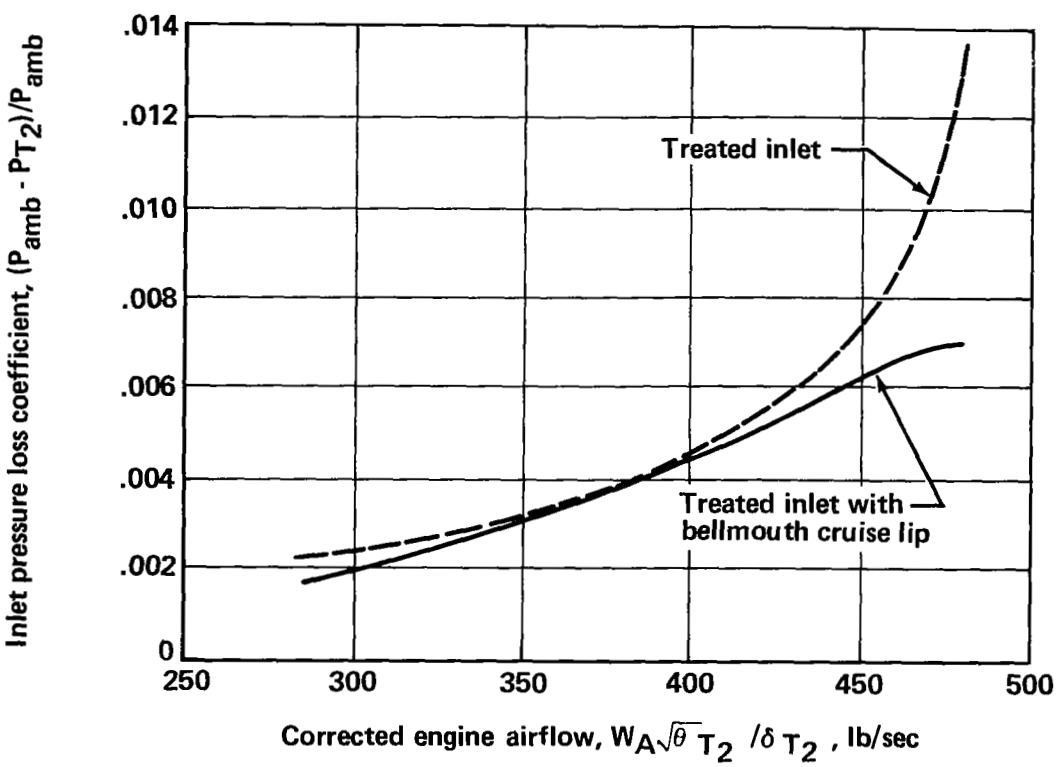

FIGURE 146.– COWL WALL LOSS

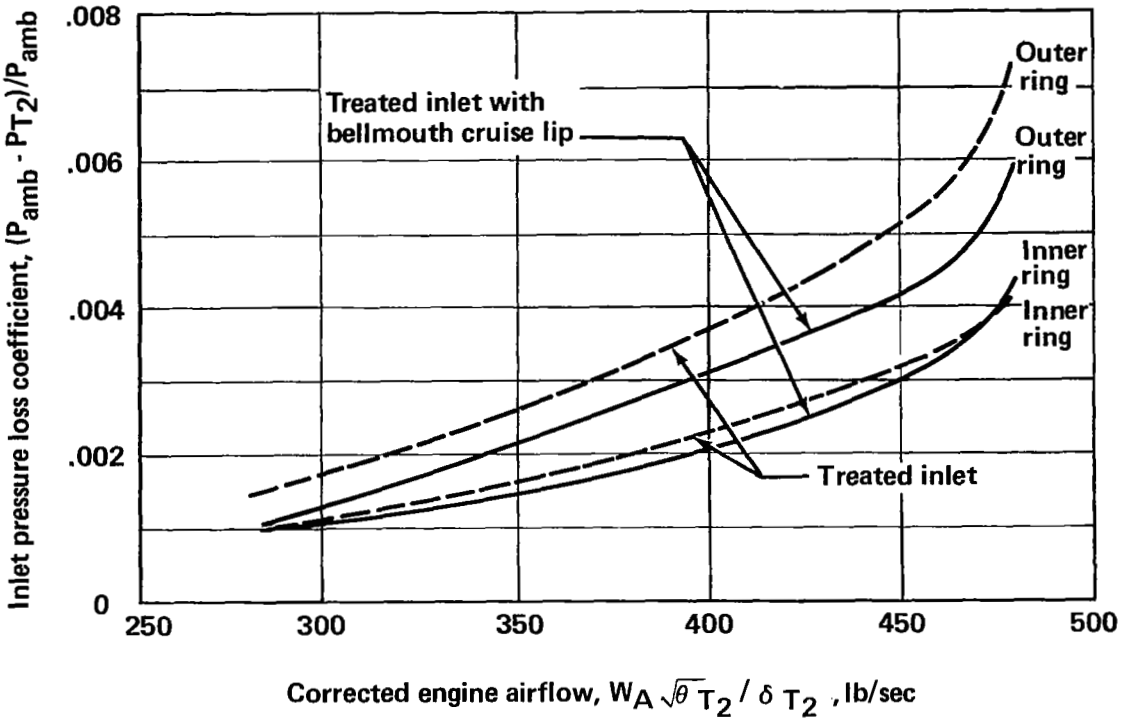

FIGURE 147.– RING LOSSES

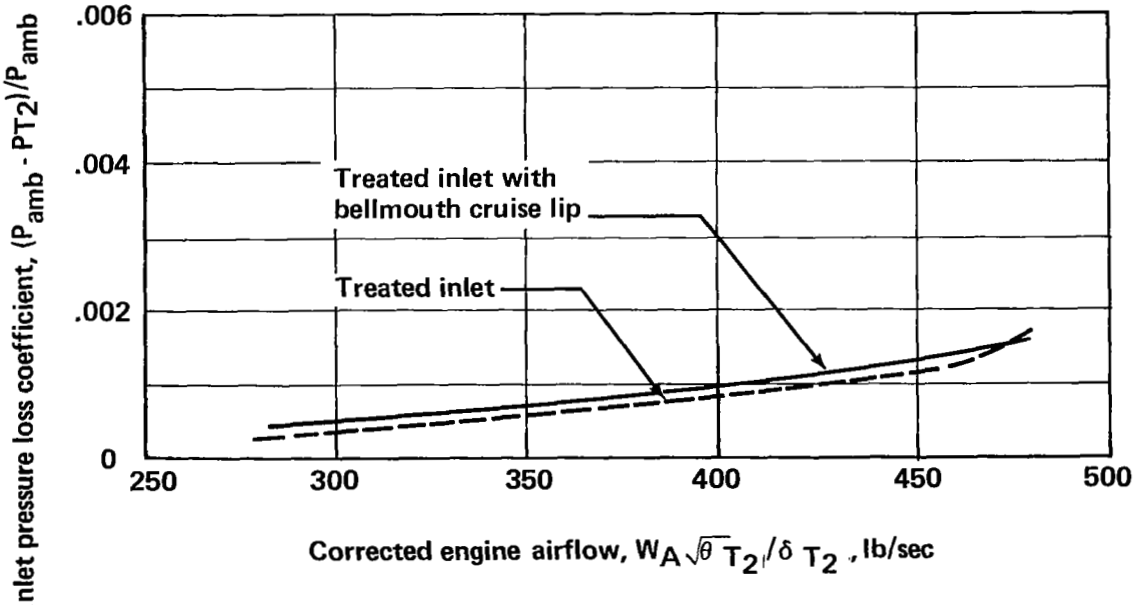

FIGURE 148.– STRUT LOSS

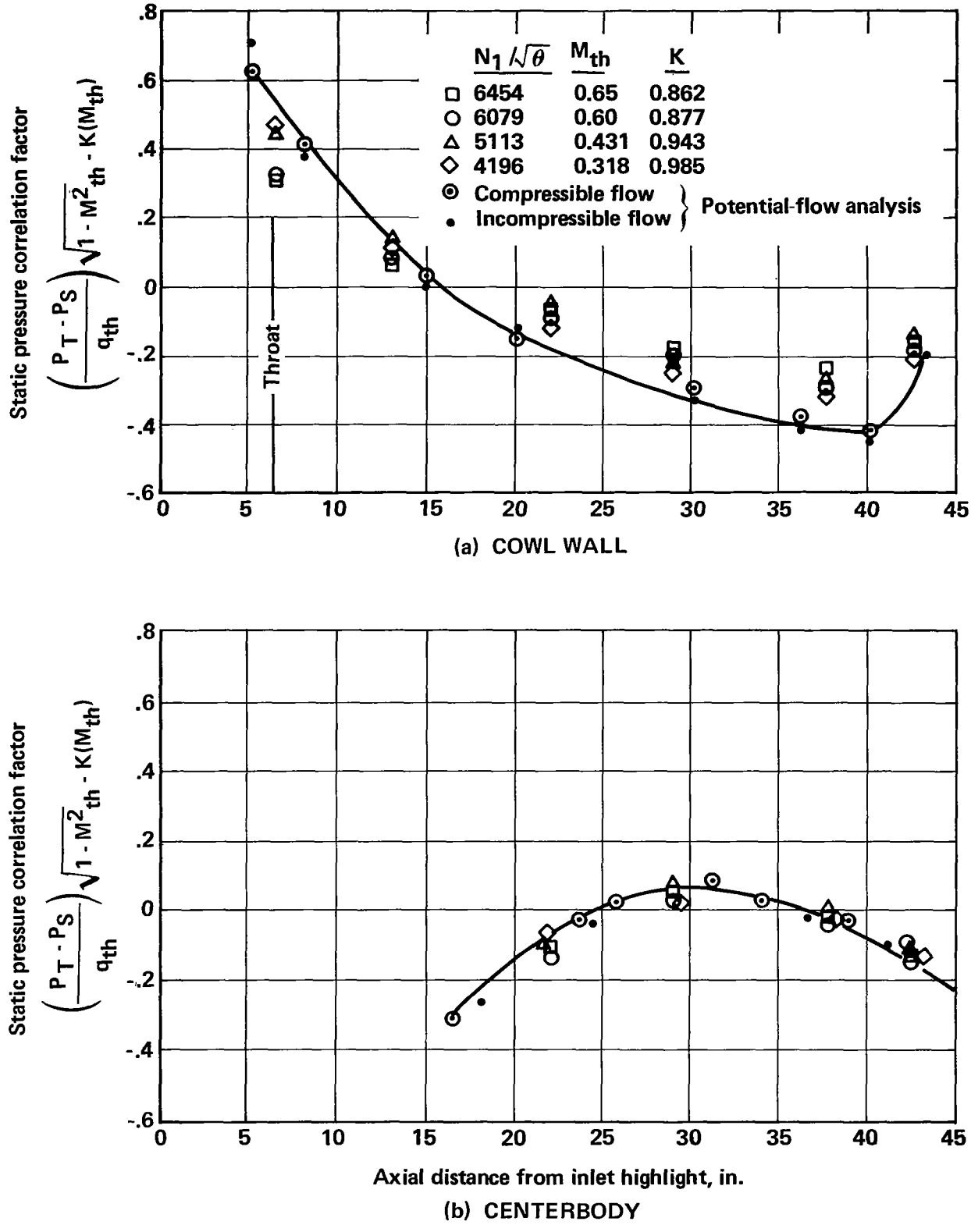

FIGURE 149.– INLET PRESSURE CORRELATION–GROUND TEST

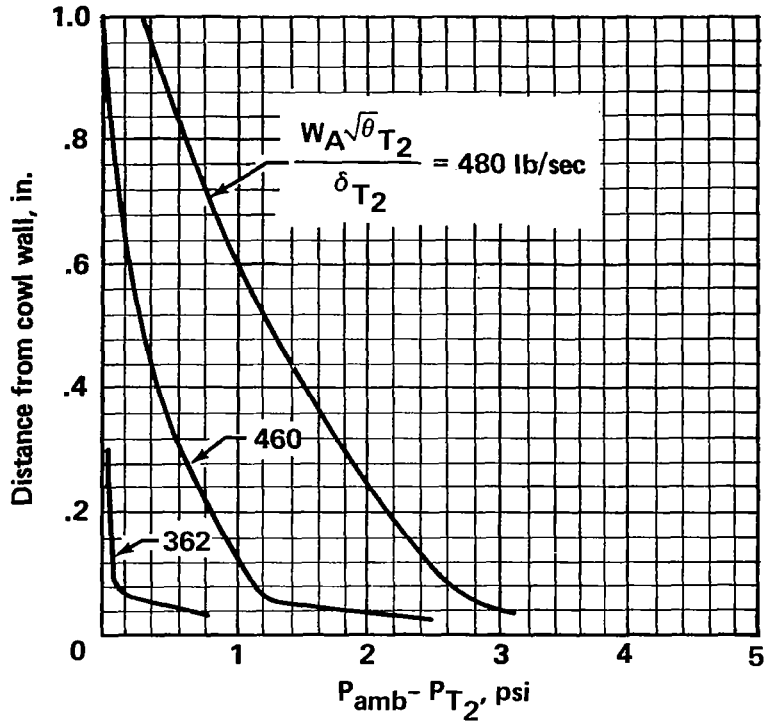

(a) PRESSURE LOSS

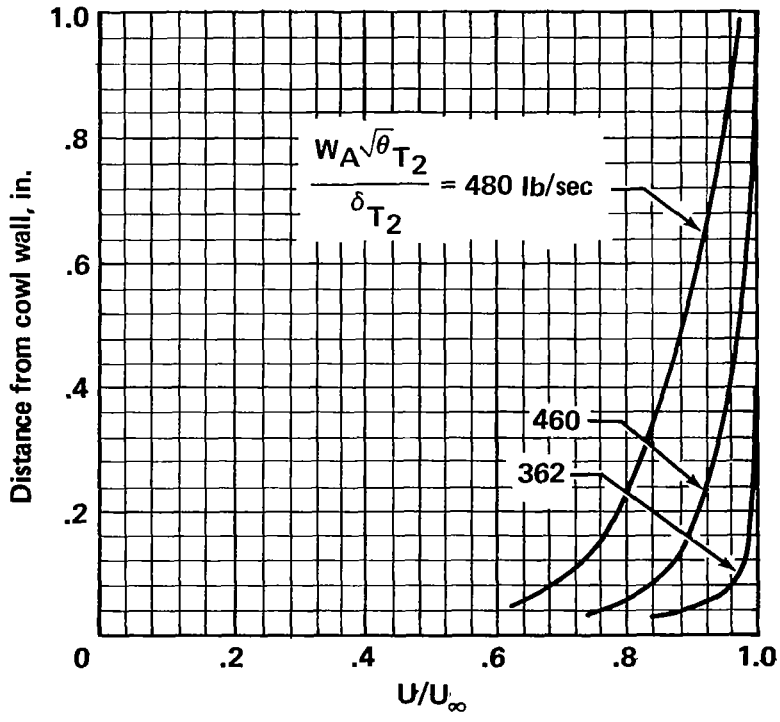

(b) VELOCITY RATIO

FIGURE 150.—BOUNDARY LAYER CHARACTERISTICS, INLET THROAT

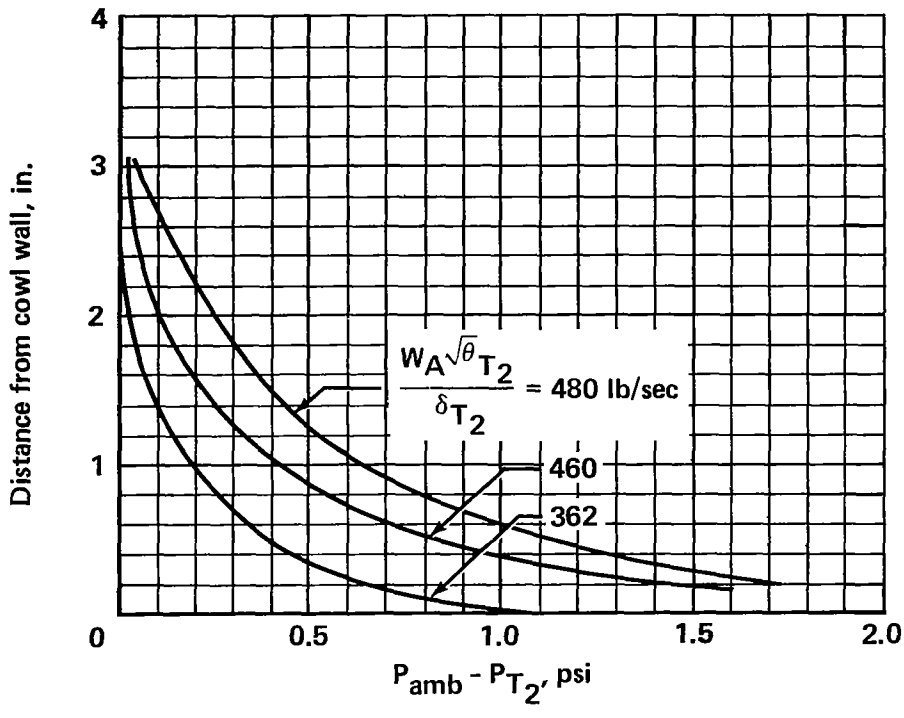

(a) PRESSURE LOSS

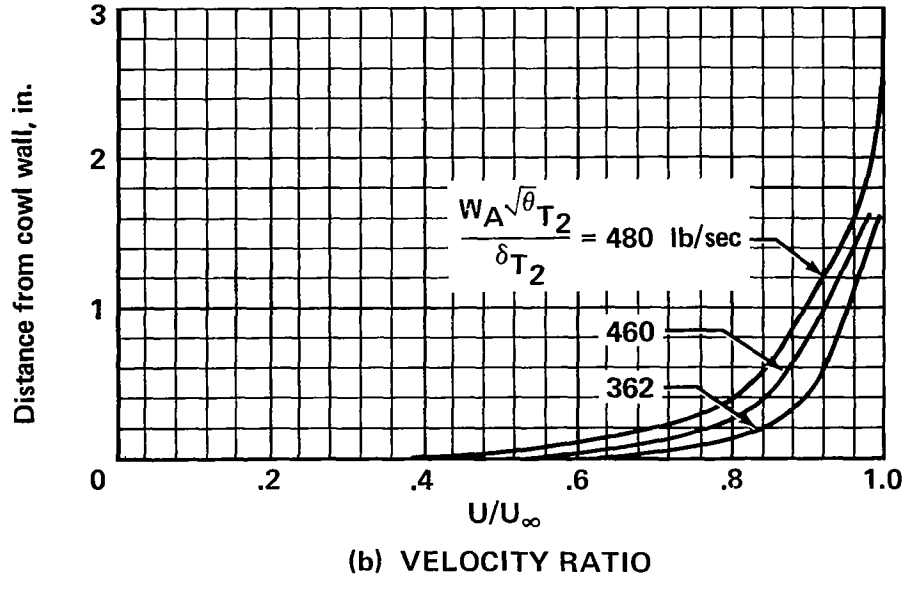

(b) VELOCITY RATIO

FIGURE 151.—BOUNDARY LAYER CHARACTERISTICS, FAN FACE

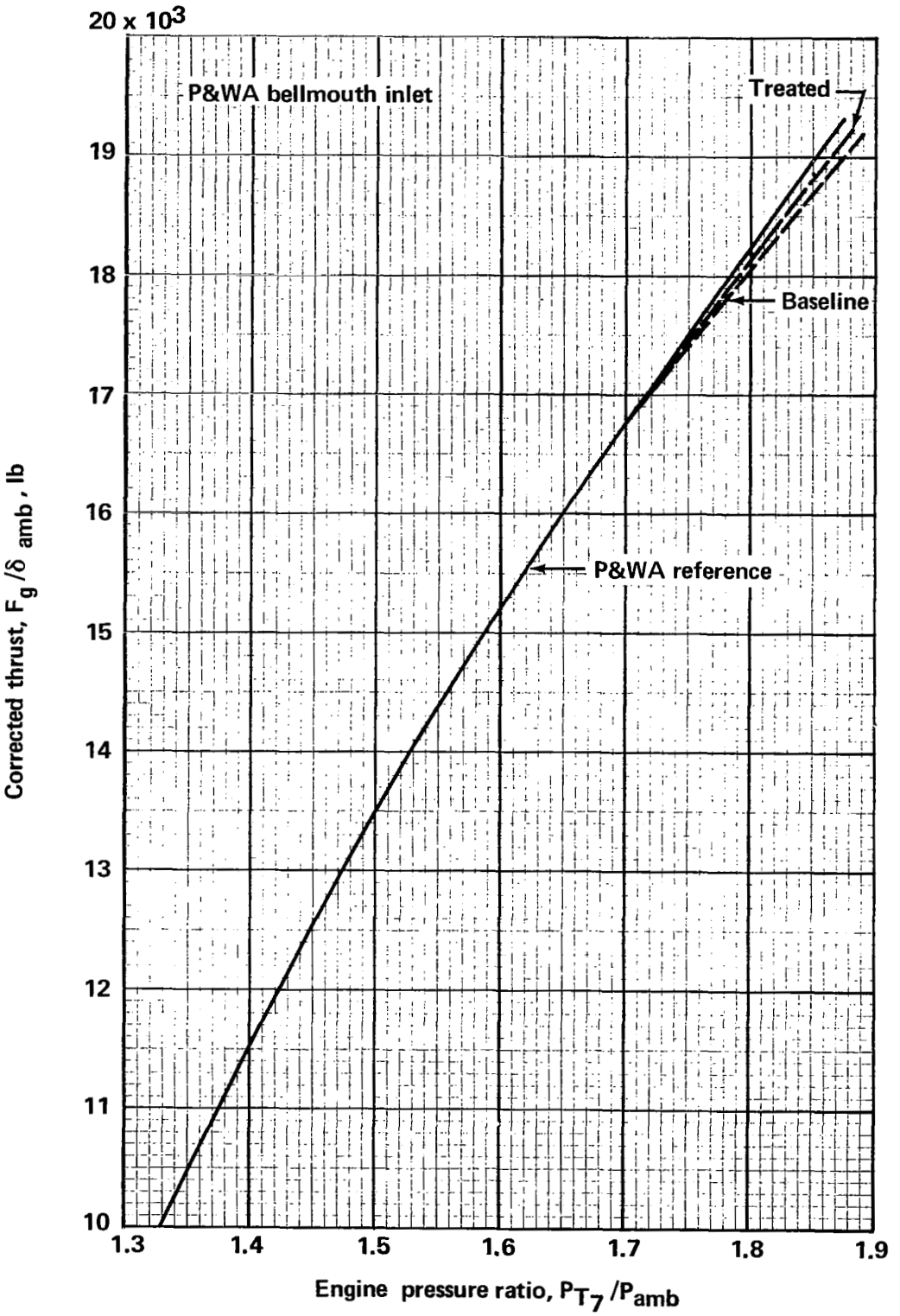

FIGURE 152.– THRUST COMPARISON–TREATED, BASELINE, AND P&WA FAN DUCTS

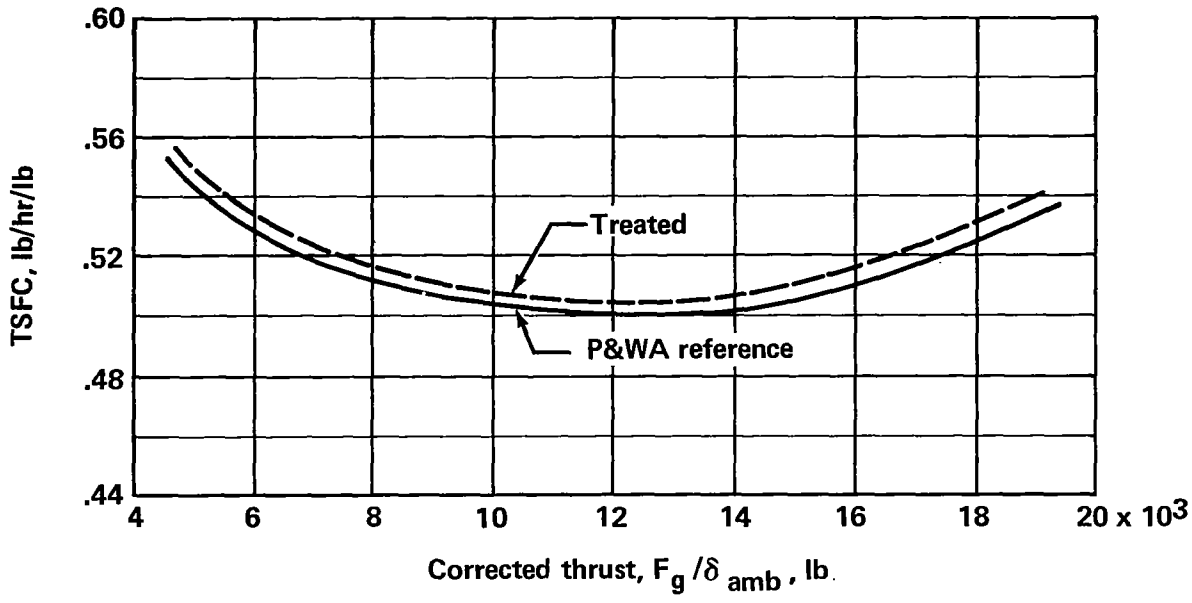

FIGURE 153.–THRUST SPECIFIC FUEL CONSUMPTION COMPARISON, TREATED AND P&WA FAN DUCTS

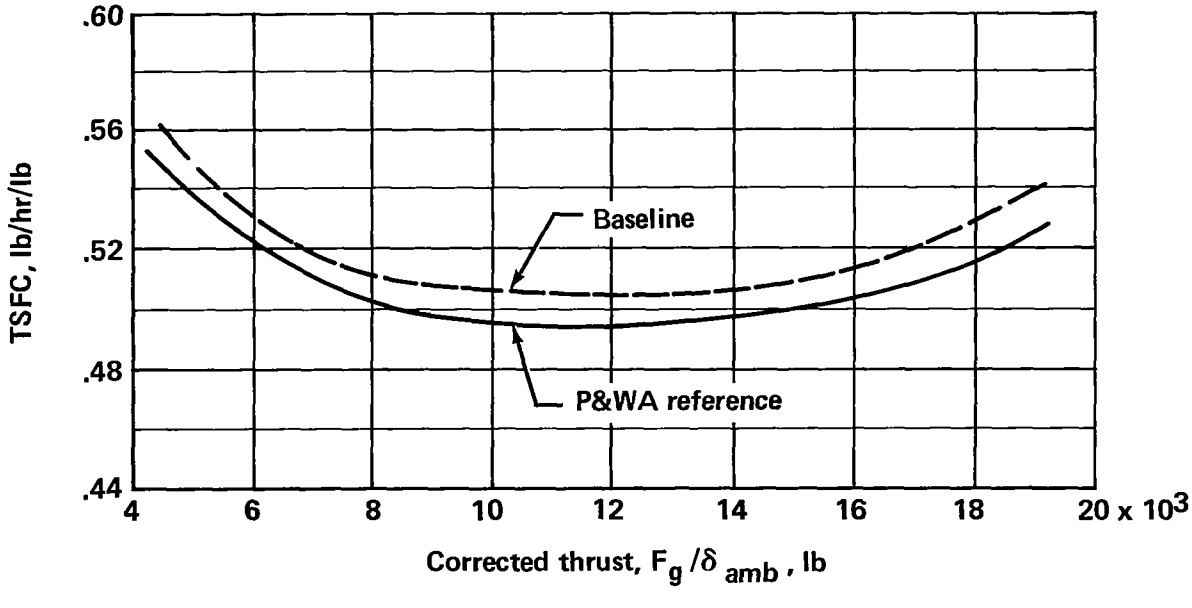

FIGURE 154.–THRUST SPECIFIC FUEL CONSUMPTION COMPARISON, BASELINE AND P&WA FAN DUCTS

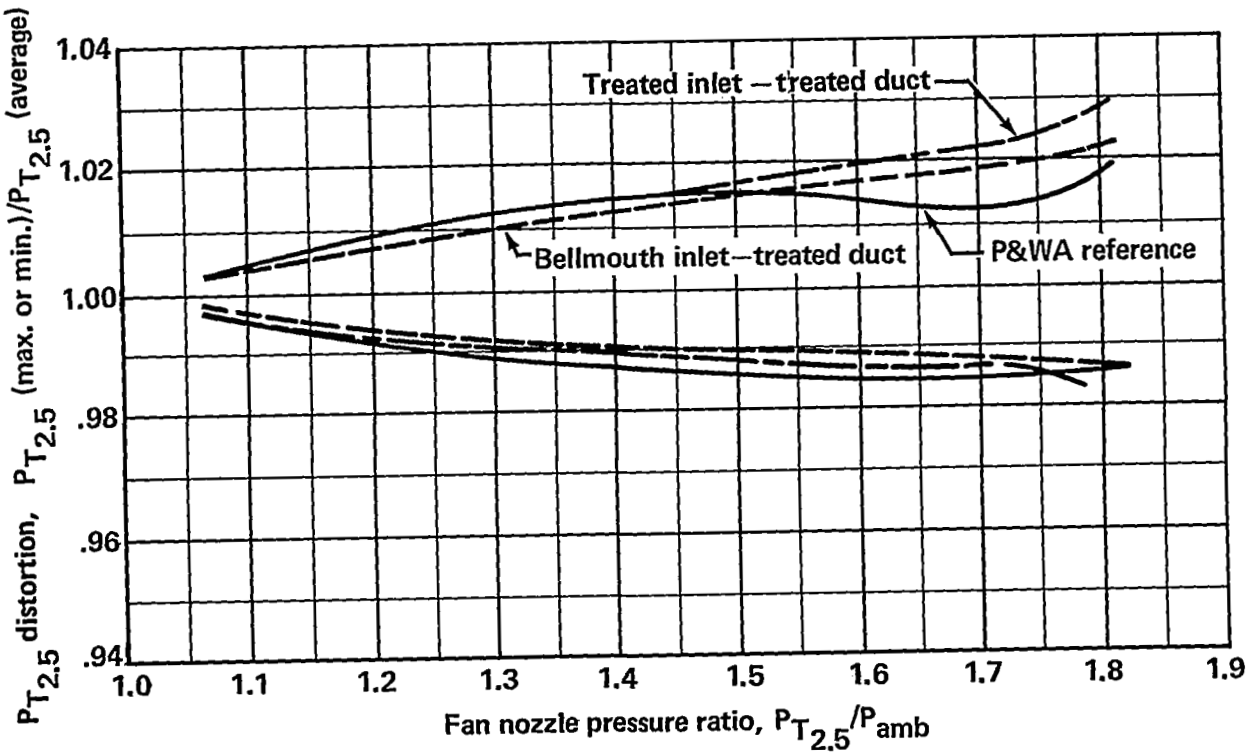

FIGURE 155.–TOTAL PRESSURE DISTORTION AT FAN EXIT

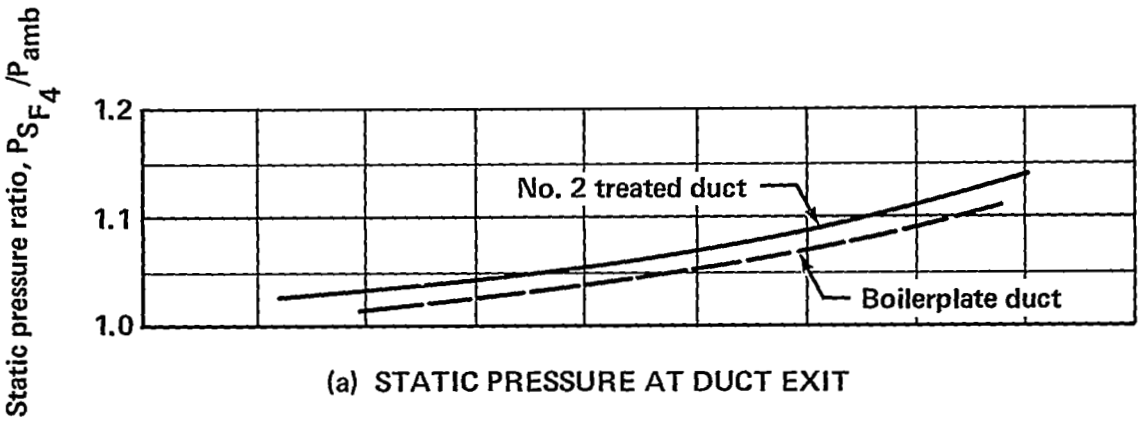

(a) STATIC PRESSURE AT DUCT EXIT

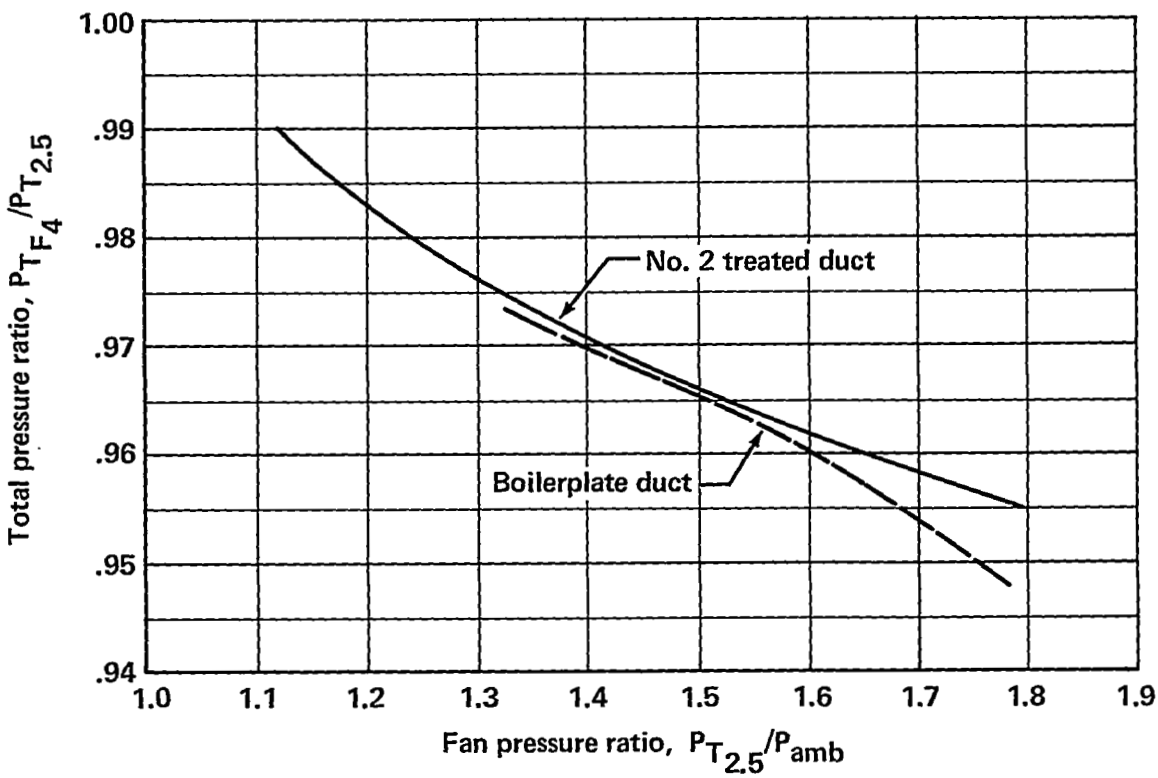

(b) TOTAL PRESSURE AT DUCT EXIT

FIGURE 156.—EXIT PRESSURE DATA, TREATED DUCTS

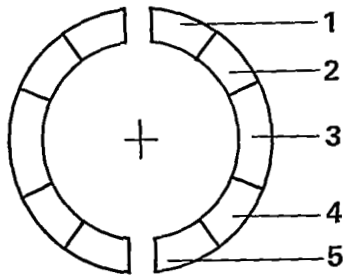

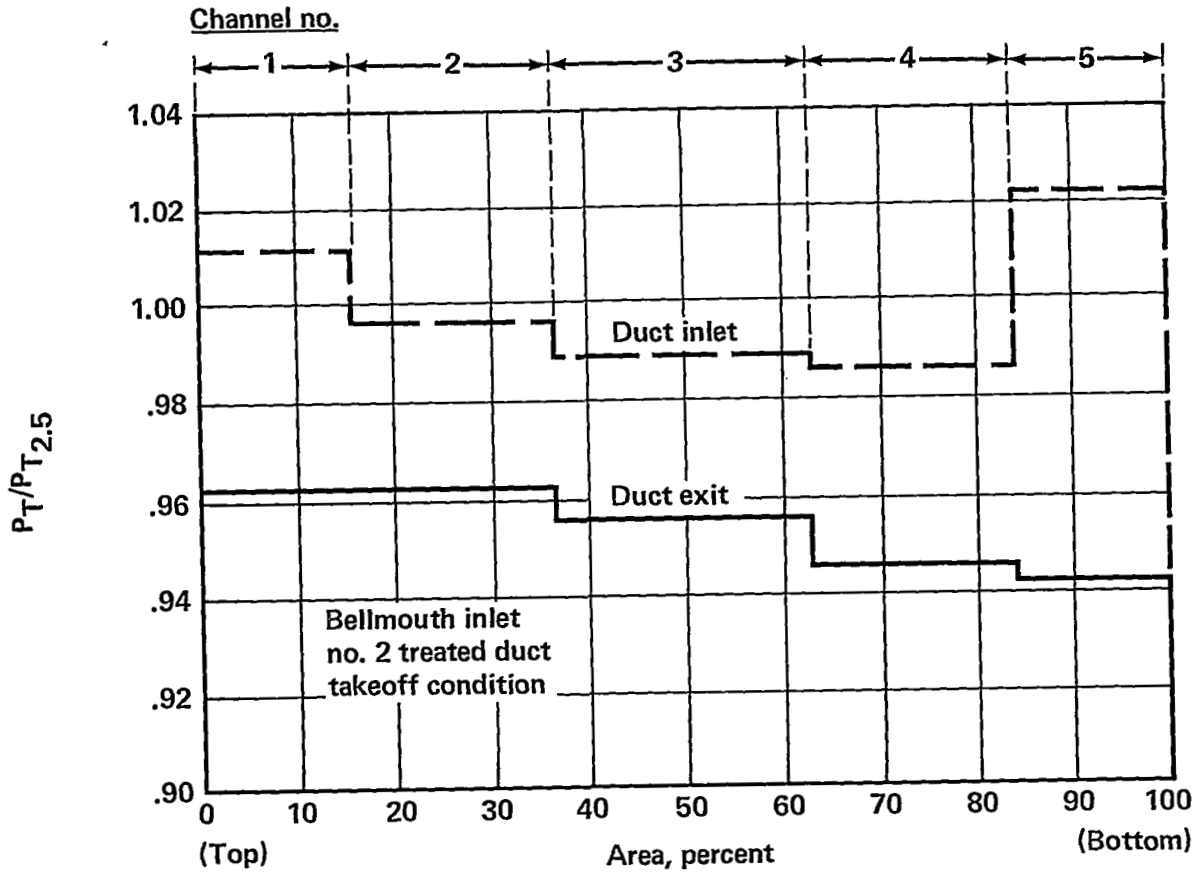

FIGURE 157.—TOTAL PRESSURE CIRCUMFERENTIAL DISTRIBUTION

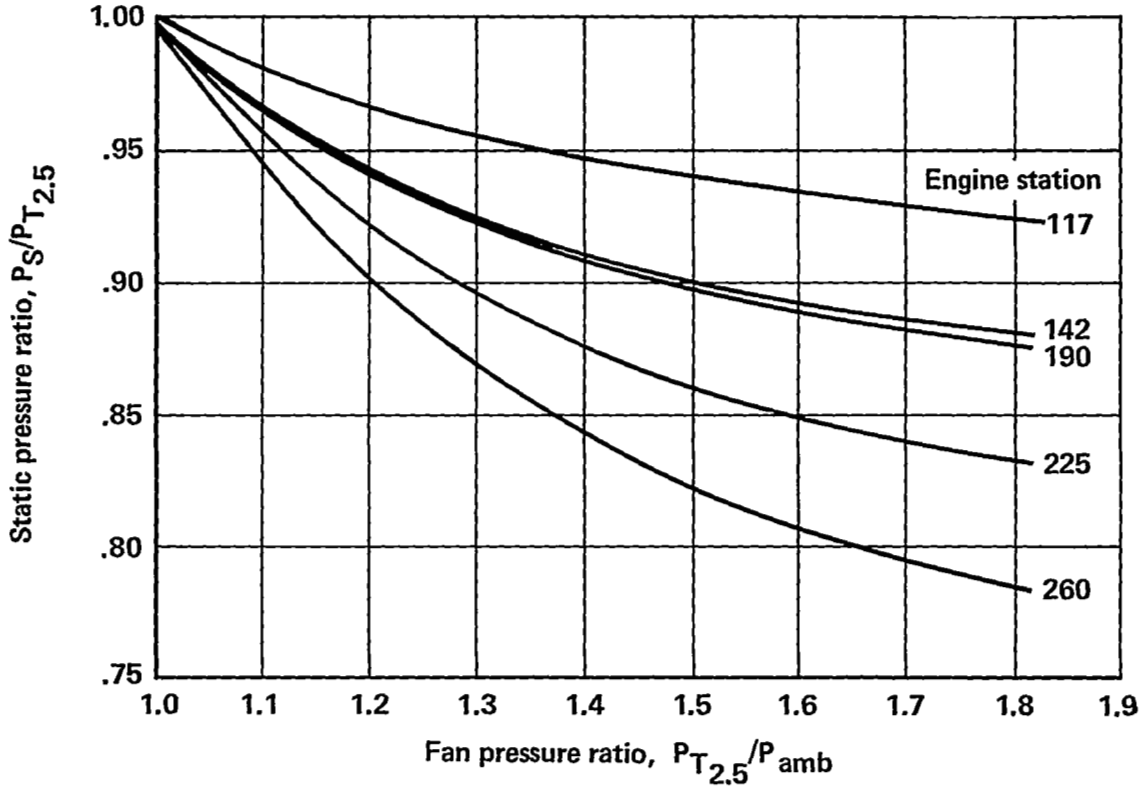

FIGURE 158.– DUCT INSIDE WALL STATIC PRESSURES, TREATED NACELLE NUMBER 2

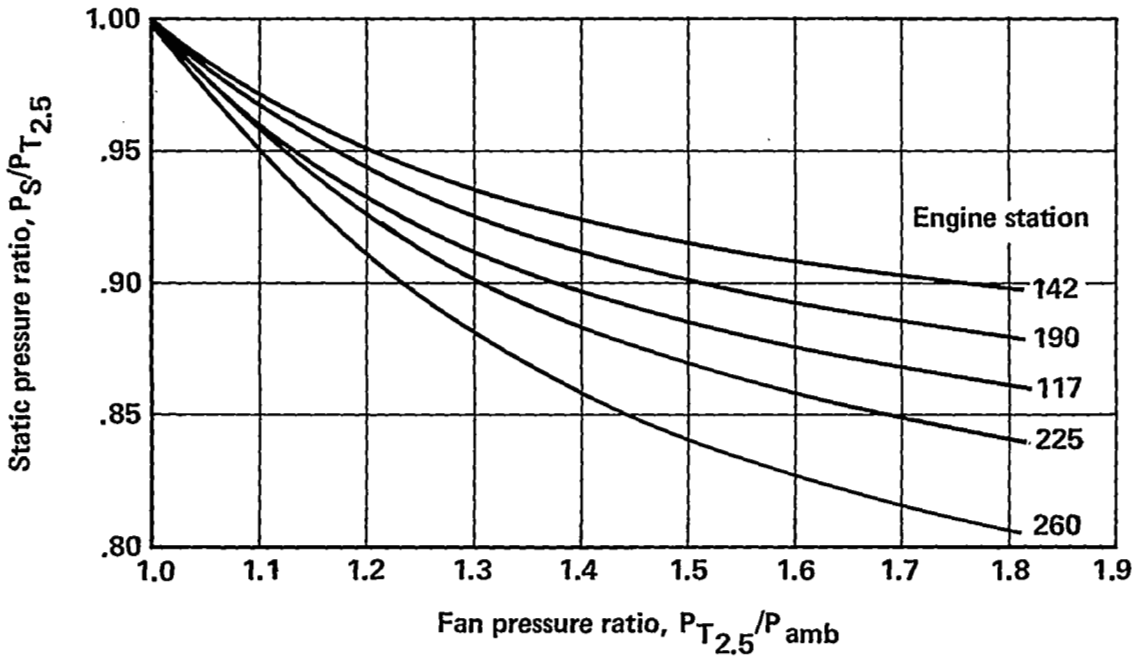

FIGURE 159.– DUCT OUTSIDE WALL STATIC PRESSURES, TREATED NACELLE NUMBER 2

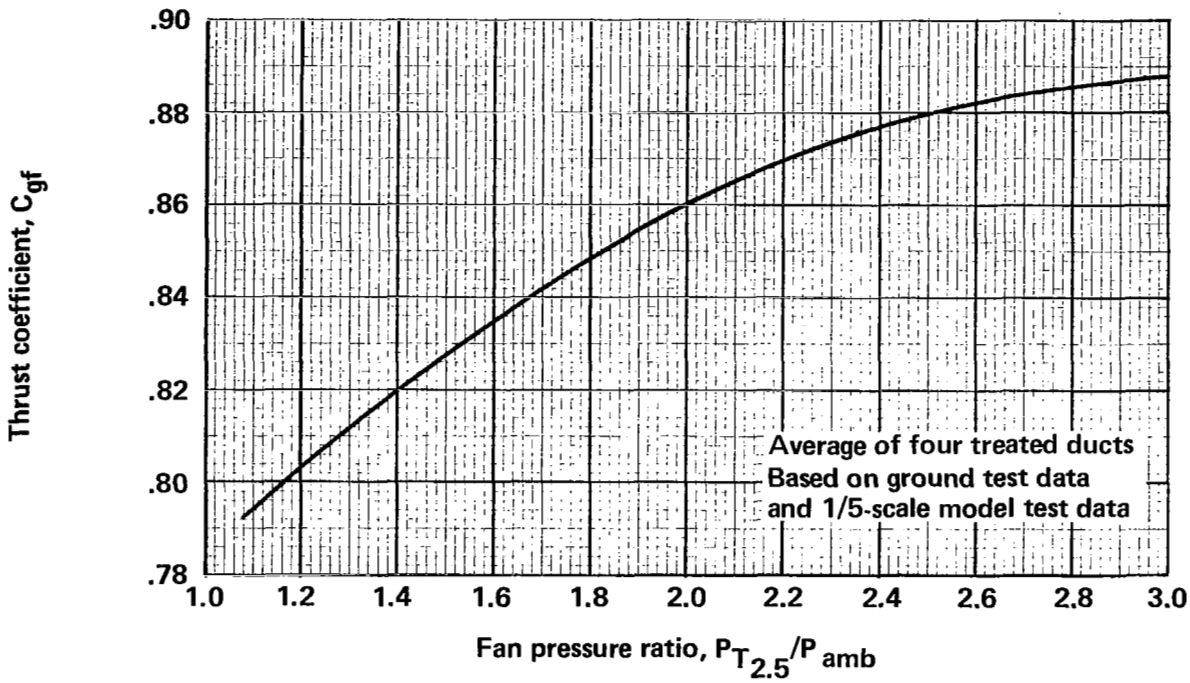

FIGURE 160.–FAN DUCT THRUST COEFFICIENT, TREATED DUCTS

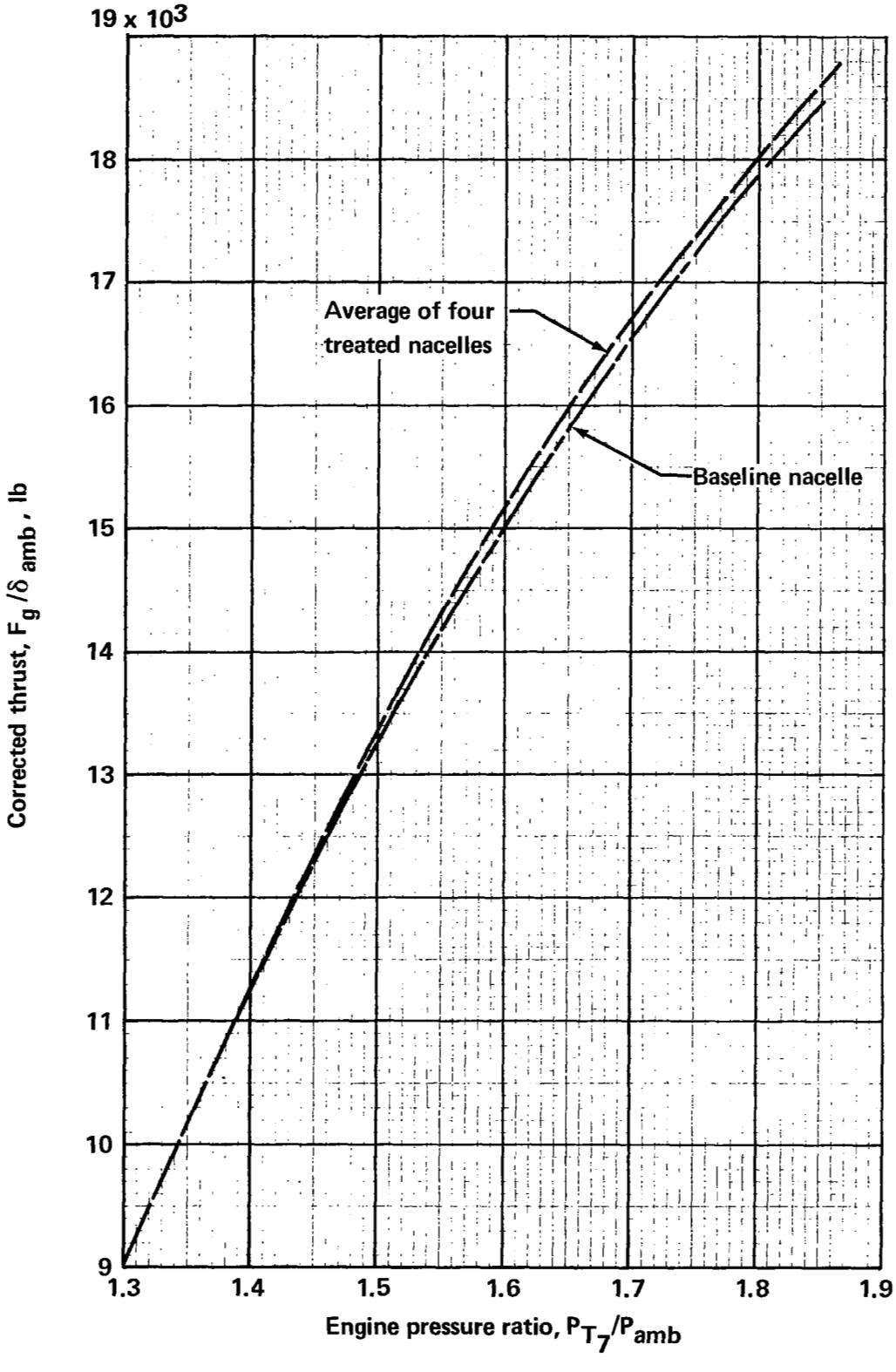

FIGURE 161.—THRUST COMPARISON—TREATED AND BASELINE NACELLES

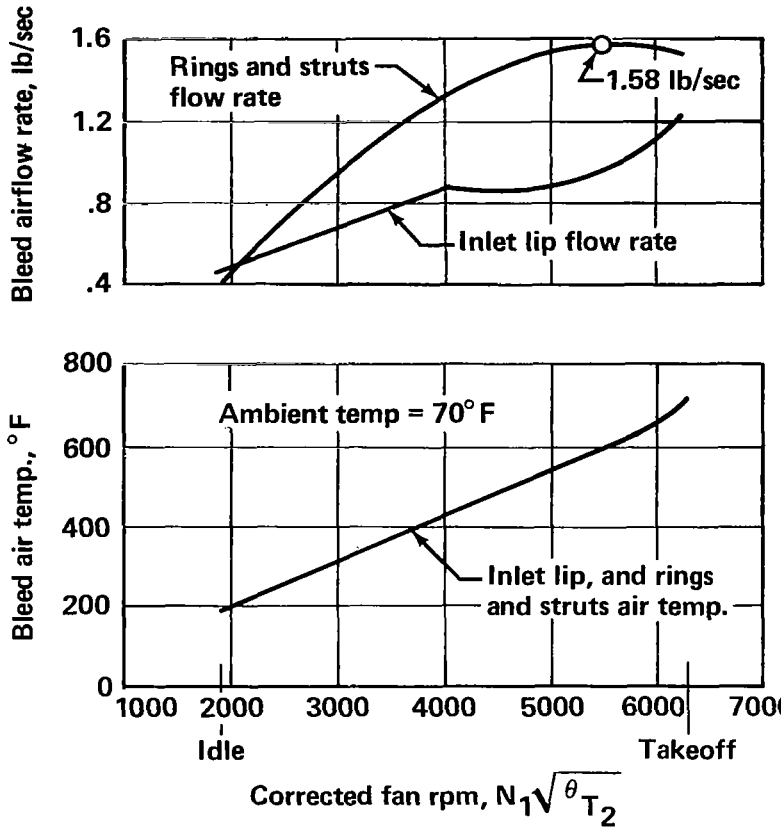

FIGURE 162.—TREATED INLET THERMAL ANTI-ICING—ENGINE BLEED AIRFLOW RATE AND TEMPERATURE

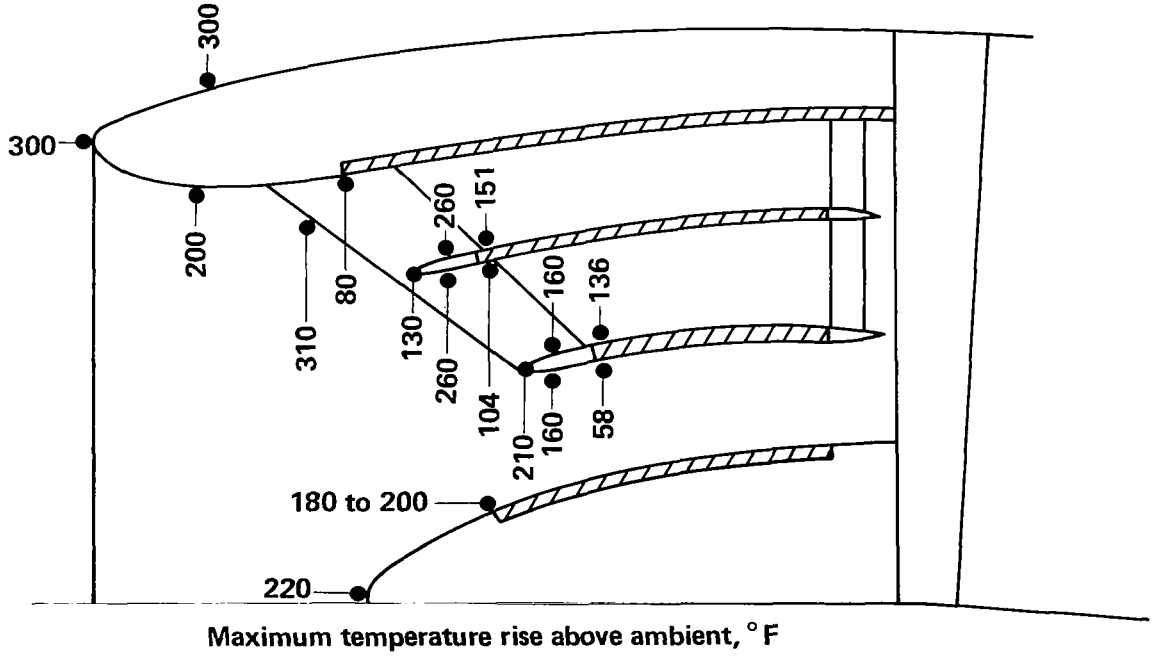

FIGURE 163.—TREATED INLET THERMAL ANTI-ICING—MAXIMUM SURFACE TEMPERATURES

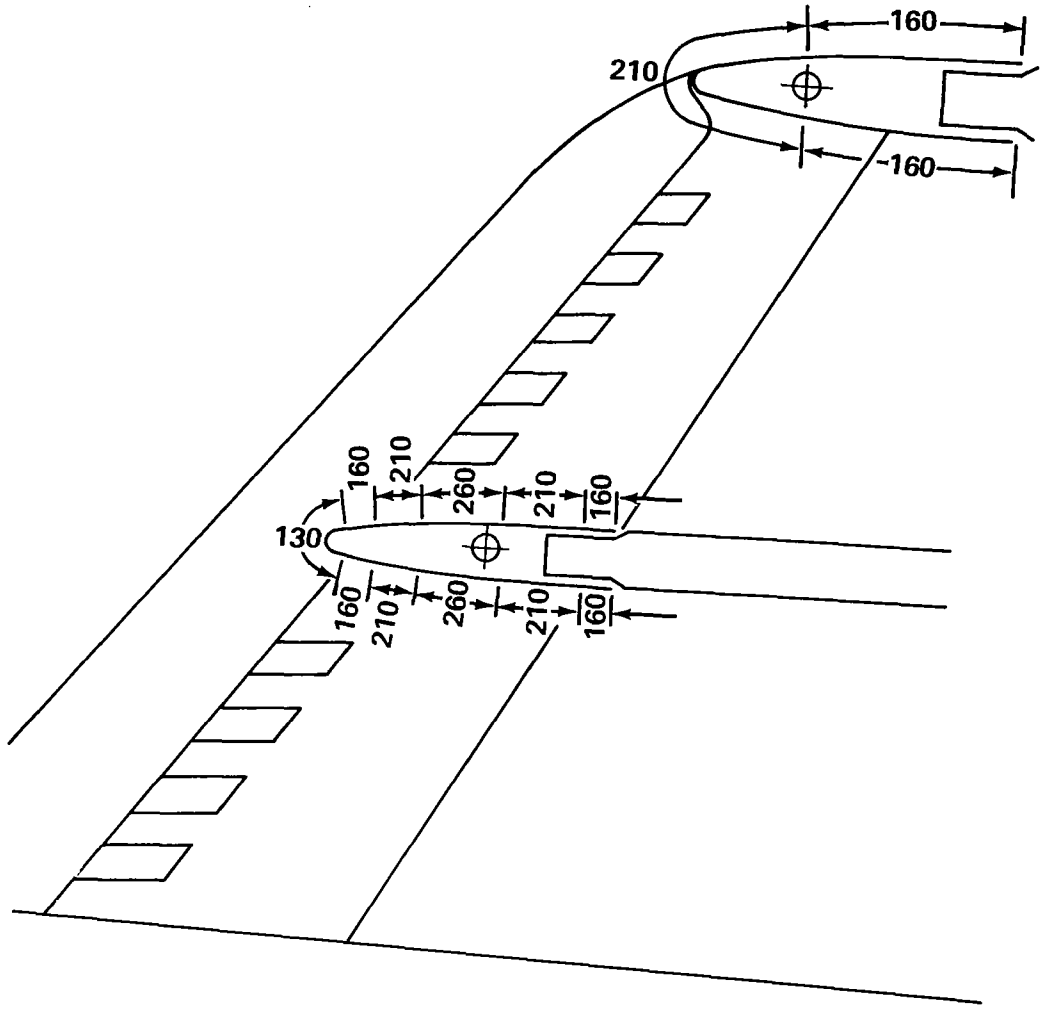

Maximum temperature rise above ambient, °F

FIGURE 164.—TREATED INLET THERMAL ANTI-ICING—RING SURFACE TEMPERATURES

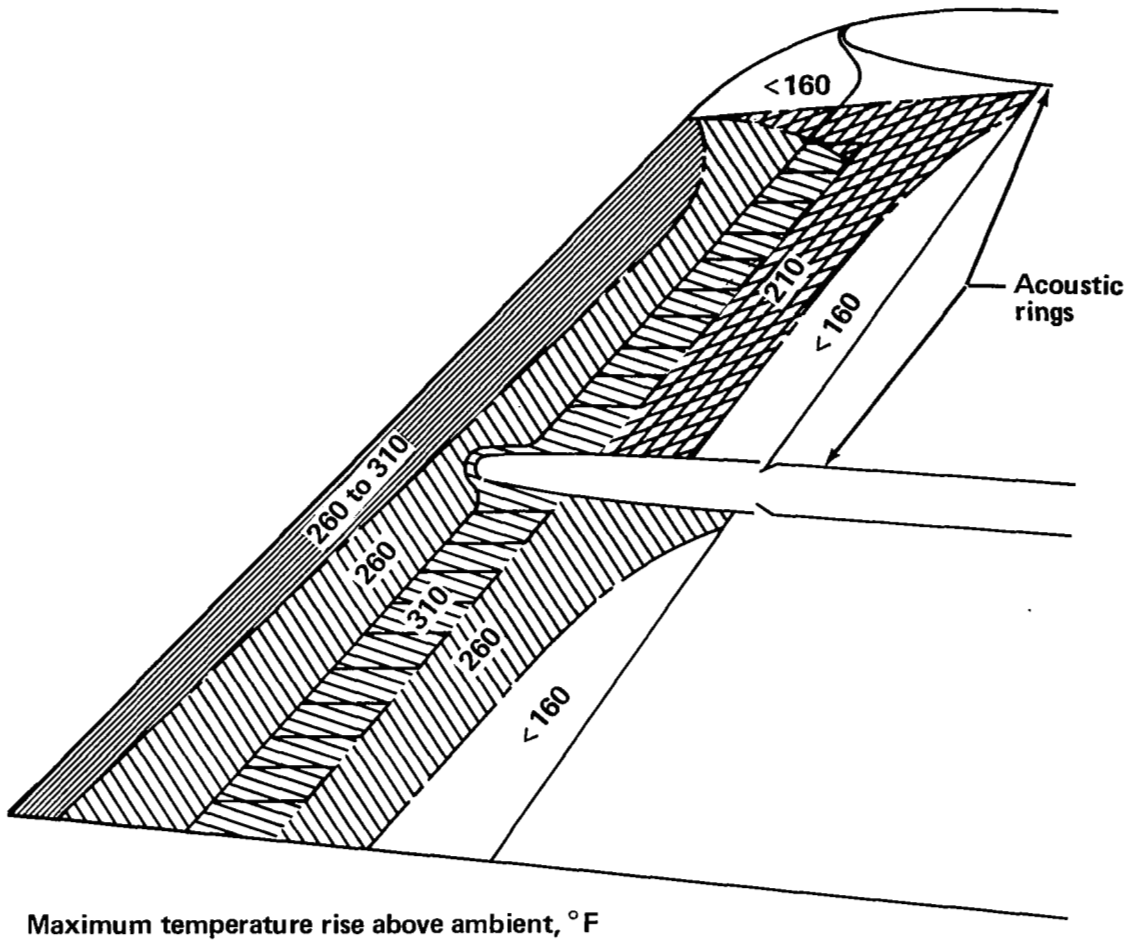

FIGURE 165.– TREATED INLET THERMAL ANTI-ICING–STRUT SURFACE TEMPERATURES